

Exploring the application of 2,5-furandicarboxylic acid as a monomer in high performance polymers : synthesis, characterization, and properties

Citation for published version (APA):

Wilsens, C. H. R. M. (2015). *Exploring the application of 2,5-furandicarboxylic acid as a monomer in high performance polymers : synthesis, characterization, and properties*. [Phd Thesis 1 (Research TU/e / Graduation TU/e), Chemical Engineering and Chemistry]. Technische Universiteit Eindhoven.
<https://doi.org/10.6100/IR783770>

DOI:

[10.6100/IR783770](https://doi.org/10.6100/IR783770)

Document status and date:

Published: 01/01/2015

Document Version:

Publisher's PDF, also known as Version of Record (includes final page, issue and volume numbers)

Please check the document version of this publication:

- A submitted manuscript is the version of the article upon submission and before peer-review. There can be important differences between the submitted version and the official published version of record. People interested in the research are advised to contact the author for the final version of the publication, or visit the DOI to the publisher's website.
- The final author version and the galley proof are versions of the publication after peer review.
- The final published version features the final layout of the paper including the volume, issue and page numbers.

[Link to publication](#)

General rights

Copyright and moral rights for the publications made accessible in the public portal are retained by the authors and/or other copyright owners and it is a condition of accessing publications that users recognise and abide by the legal requirements associated with these rights.

- Users may download and print one copy of any publication from the public portal for the purpose of private study or research.
- You may not further distribute the material or use it for any profit-making activity or commercial gain
- You may freely distribute the URL identifying the publication in the public portal.

If the publication is distributed under the terms of Article 25fa of the Dutch Copyright Act, indicated by the "Taverne" license above, please follow below link for the End User Agreement:

www.tue.nl/taverne

Take down policy

If you believe that this document breaches copyright please contact us at:

openaccess@tue.nl

providing details and we will investigate your claim.

Exploring the application of 2,5-furandicarboxylic acid as a
monomer in high performance polymers:
Synthesis, characterization, and properties.

PROEFSCHRIFT

ter verkrijging van de graad van doctor aan de Technische Universiteit Eindhoven, op
gezag van de rector magnificus prof.dr.ir. C.J. van Duijn,
voor een commissie aangewezen door het College voor Promoties, in het openbaar te
verdedigen op woensdag 21 januari 2015 om 16:00 uur

door

Carolus Henricus Radjindrenath Maria Wilsens

geboren te Tilburg

Dit proefschrift is goedgekeurd door de promotoren en de samenstelling van de promotiecommissie is als volgt:

voorzitter:	prof.dr.ir. J.C. Schouten
1 ^e promotor:	prof.dr. S. Rastogi
2 ^e promotor:	prof.dr.ir. H.E.H. Meijer
copromotor(en):	dr.ir. B.A.J. Noordover
leden:	prof.dr. R.P. Sijbesma
	prof.dr.ir. J.C.M. van Hest (Radboud University Nijmegen)
	prof. D. Haddleton (University of Warwick)
	prof.dr.dr.h.c. M. Möller (RWTH Aachen University)

“If we knew what it was we were doing, it would not be called research, would it?”

— Albert Einstein

A catalogue record is available from the Eindhoven University of Technology Library

ISBN: 978-90-386-3758-7

Content, layout and cover by: C.H.R.M. Wilsens

Printed by: Gildeprint Drukkerijen

The research described in this thesis forms part of the research programme of the Dutch Polymer Institute (DPI), project #739 “Melt processable Bio-based Aromatic Polymers”.

Contents

1. Introduction	1
1.1. From renewable resource to monomer	1
1.1.1. Aromatic monomers from sugars	2
1.1.2. Aromatic monomers from lignin.....	3
1.2. From monomer to polymer	5
1.2.1. Step-growth polymerization reactions	5
1.2.2. Condensation polymerization reactions	7
1.2.3. Synthesis of thermotropic polyesters.....	9
1.2.4. Designing thermotropic polyesters	11
1.2.5. Renewable monomers in thermotropic polyesters	12
1.3. From polymer to product.....	13
1.3.1. Fibers and films.....	13
1.3.2. Engineering plastics.....	14
1.3.3. Coatings and polymer glasses.....	14
1.4. Aim and scope of this thesis	15
1.5. Outline of this thesis	16
1.6. References	17
2. Aromatic thermotropic polyesters based on 2,5-furandicarboxylic acid and vanillic acid	21
2.1. Introduction.....	22
2.2. Experimental section.....	23
2.2.1. Materials	23
2.2.2. General acetylation procedure	24
2.2.3. Preparation of 4-acetoxybenzoic acid.....	24
2.2.4. Preparation of 4-acetoxy-3-methoxybenzoic acid.....	24
2.2.5. Preparation of 4,4'-diacetoxybiphenyl	25
2.2.6. Methods.....	25
2.3. Results and Discussion	26
2.3.1. Phase behavior of 2,5-FDCA/BP/BA system.....	26
2.3.2. Tuning the melting temperature of 2,5-FDCA based polymers.....	30
2.3.3. Comparing TFPs with scaled up experiments.....	34
2.4. Conclusions	37
2.5. References	38

3. Thermotropic polyesters from 2,5-furandicarboxylic acid and vanillic acid: Synthesis, thermal properties, melt-behavior, and mechanical performance	41
3.1. Introduction.....	42
3.2. Experimental section.....	43
3.2.1. Materials and monomer preparation.....	43
3.2.2. General polymerization procedure.....	44
3.2.3. Characterization methods.....	44
3.3. Results and discussion.....	46
3.3.1. Thermotropic polyester synthesis	46
3.3.2. Molecular weight build-up and reaction time	49
3.3.3. Thermal properties of the TLCPs	50
3.3.4. Melt behavior of the TLCPs	54
3.3.5. Influence of 2,5-FDCA and VA on the molecular mobility	57
3.3.6. Mechanical performance of the TLCPs.	59
3.4. Conclusions	61
3.5. References	62
4. Processing and performance of aromatic-aliphatic thermotropic polyesters based on vanillic acid	65
4.1. Introduction.....	66
4.2. Experimental section.....	68
4.2.1. General polymerization procedure.....	68
4.2.2. Processing of thermotropic polyesters	68
4.2.3. Characterization methods.....	68
4.3. Results and discussion.....	71
4.3.1. Synthesis and characterization of thermotropic polyesters.	71
4.3.2. Fiber spinning from the thermotropic melt.....	74
4.3.3. Effect of orientation on the thermal properties.....	77
4.3.4. Solvent casting for film preparation.....	80
4.3.5. Effect of processing methods on the molecular orientation.....	83
4.4. Conclusions	87
4.5. References	88

5. Influence of the 2,5-furandicarboxamide moiety on hydrogen bonding in aliphatic-aromatic poly(ester amide)s	89
5.1. Introduction.....	90
5.2. Experimental section.....	91
5.2.1. Materials and monomer preparation.....	91
5.2.2. Preparation of diacid chlorides	91
5.2.3. General model compound synthesis procedure.....	91
5.2.4. Synthesis of TAn.....	91
5.2.5. Synthesis of 2,5-TDCAn	92
5.2.6. Synthesis of 2,5-FDCAn.....	92
5.2.7. Synthesis of IAn.....	92
5.2.8. General polymerization procedure.....	92
5.2.9. Characterization methods.....	93
5.3. Results and discussion.....	94
5.3.1. Synthesis of the amide-ester model compounds.....	94
5.3.2. Analysis of the amide-ester model compounds in solution.....	95
5.3.3. Thermal analysis of the amide-ester model compounds.....	98
5.3.4. FTIR analysis of the amide-ester model compounds.....	99
5.3.5. Temperature resolved FTIR analysis of 2,5-FDCAn.....	101
5.3.6. Melt polymerization of the 2,5-FDCAn model compound	104
5.3.7. Comparison of p(2,5-FDCAn10) with p(IAn10) and p(2,5-TPDCAn10)	106
5.4. Conclusions	109
5.5. References	109
6. Synthesis, kinetics, and characterization of bio-based thermosets obtained through polymerization of a 2,5-furandicarboxylic acid-based bis(2-oxazoline) with sebacic acid.	111
6.1. Introduction.....	112
6.2. Experimental section.....	113
6.2.1. Materials	113
6.2.2. Preparation of N,N'-bis(2-chloroethyl)furan-2,5-dicarboxamide.....	114
6.2.3. Preparation of 2,5-bis(4,5-dihydrooxazol-2-yl)furan (2,5-FDCAox)	114
6.2.4. General melt polymerization procedure.....	114
6.2.5. Preparation of solvent-borne coatings.	114
6.2.6. Characterization methods.....	115
6.3. Results and discussion.....	116
6.3.1. Synthesis and characterization of 2,5-FDCAox.....	116
6.3.2. Polymerization of 2,5-FDCAox and IAox with Sebacic acid	117
6.3.3. Thermal properties of poly(ester amide)s	121

6.3.4.	Reaction mechanism of the branching reaction.....	122
6.3.5.	On-line monitoring of the branching reaction.....	123
6.3.6.	Influence of temperature and TPP on the branching reaction.....	127
6.3.7.	Thermal properties of the cured thermosets.....	129
6.3.8.	Preliminary coating performance of solvent-borne coatings.....	132
6.4.	Conclusions.....	132
6.5.	References.....	133
7.	Epilogue.....	135
7.1.	Conclusions, outlook, and technology assessment.....	135
7.1.1.	Application of 2,5-FDCA in melt-polycondensation reactions.....	135
7.1.2.	Development of renewable thermotropic polyesters.....	136
7.1.3.	Polymerization of protected 2,5-FDCA monomers.....	137
Appendix A	for chapter 3.....	139
	Variable temperature solid-state $^{13}\text{C}\{^1\text{H}\}$ CP/MAS and INEPT MAS NMR.....	139
Appendix B	for chapter 6.....	143
	FTIR and NMR data fitting procedure.....	143
Glossary	146
Summary		148
Curriculum Vitae		151
List of publications		152
Acknowledgements		154

Chapter 1

Introduction

1.1. From renewable resource to monomer

The application of renewable monomers for the synthesis of polymeric materials has gained significant attention over the last decades from both academia and industry. Driving factors stimulating this research are the projected depletion of commonly used fossil oil feedstock, the increasing demand of fossil oil-based materials, and the gradual increase of the oil prices.¹ Besides these practical and economic reasons, there is also a drive to develop renewable materials from a social and environmental perspective; the world-wide increase in pollution and greenhouse gas emissions, mainly resulting from the use of fossil oil-based fuels and materials, are causes for great concern among the human population and nations around the world.² The application of renewable and degradable materials in daily life can help to decrease both the pollution and the emission of greenhouse gases, thereby contributing to a clean and healthy environment.

Nature provides ample amounts of biomass every year, roughly 6 billion tons, that can be cultivated and used for human food, animal feed, and non-food applications.³ According to Okkerse and coworkers, this amount of biomass should be more than sufficient to function as a resource for mankind's demand for chemicals and materials.⁴ Furthermore, the application of biomass as a resource for the production of chemicals can yield structurally new materials, unattainable from fossil oil feedstock. In short, although an advance in technology is required, the development of materials from renewable resources can help to decrease mankind's dependency on fossil fuels.

Different classes of biopolymers are available for the production of chemicals or materials. Examples of such polymers are starch, lignin, cellulose, hemicellulose, and proteins. These biopolymers can be converted into different chemicals, which in turn can be chemically modified to yield other chemicals or materials. In general, two approaches are considered for the conversion of biomass into chemicals. The first approach involves the conversion of biomass into chemicals already used in industry. This approach is interesting from an industrial perspective, since these chemicals can be directly used in the existing petrochemical infrastructure. Examples of chemicals that can be produced via this approach are methanol, ethanol, ethylene, succinic acid, and glycerol.⁵⁻⁹ The second approach involves the development of new chemicals that can be used for the production of new materials. One important example of such a new renewable chemical is 2,5-furandicarboxylic acid (2,5-FDCA); recent reports indicate that the 2,5-FDCA based polycondensate poly(ethylene furanoate) is more rigid, has a slower chain mobility, has better barrier properties, and exhibits improved

mechanical properties, compared to its fossil oil-based counterpart poly(ethylene terephthalate).¹⁰⁻¹⁴ This example confirms that, although the development of new techniques and infrastructures are required for the production of these new chemicals, it is worthwhile to pursue their development.

In this thesis, the main focus lies on the application of renewable aromatic monomers such as 2,5-FDCA in polymers for demanding applications. In the next section, the origin and production of these renewable aromatic monomers are described in more detail.

1.1.1. Aromatic monomers from sugars

Sugars are an important class of carbohydrates that can be useful for the production of bio-based building blocks. Examples of sugars or monosaccharides are glucose, mannose, fructose, sucrose, and lactose. These monosaccharides are obtained after hydrolysis of cellulose, hemicellulose, or starch and can subsequently be converted into other chemicals or building blocks. In 2004, the U.S. Department of Energy (DOE) selected succinic acid, fumaric acid, malic acid, 2,5-FDCA, 3-hydroxypropionic acid, aspartic acid, glucaric acid, glutamic acid, itaconic acid, levulinic acid, 3-hydroxybutyrolactone, glycerol, sorbitol, and xylitol/arabinitol as the most promising sugar-based chemicals for industrial use.¹⁵ These fourteen platform chemicals were selected for their potential in the chemical industry and for the feasibility of their production processes. Furthermore, if required, these compounds can be converted into a larger list of chemicals or monomers.

The only aromatic compound in this list is 2,5-FDCA. This heterocyclic monomer can be derived from fructose, glucose, and cellulose.¹⁶⁻¹⁸ For example, the conversion of fructose into 5-(hydroxymethyl)furfural (HMF) can be performed via an acid-catalyzed dehydration reaction in supercritical acetone¹⁹, water with phase modifiers²⁰, or high boiling solvents²¹. In the next step, HMF is converted into 2,5-FDCA through an oxidation reaction in the presence of gold, cobalt, chromium, or platinum catalysts (Scheme 1.1).²²⁻²⁶ It should be noted that the two-step synthesis of 2,5-FDCA from fructose is not ideal, since HMF is not stable and degrades upon storage. Instead, the direct conversion of fructose into 2,5-FDCA in one pot is preferred.^{27,28} An alternative route to produce 2,5-FDCA without isolating the HMF intermediate is currently in use by the company Avantium which uses stable alkoxy-derivatives of HMF as feedstock.^{29,30}

2,5-FDCA has two carboxylic acid groups, which makes it a suitable monomer for polycondensation reactions with, for example, diols or diamines. Furthermore, the aromatic nature of the 2,5-furandicarboxylate moiety can be useful in the design of renewable rigid materials, having high glass transition temperatures and good thermal stability. Although the focus in literature lies on the development and optimization of production routes to obtain 2,5-FDCA in a pure form, HMF and furfural can also be

In nature, lignin is synthesized by the selective dehydrogenation of coniferyl alcohol, syringyl alcohol, or coumaryl alcohol, through coupling of carbon-carbon or carbon-oxygen bonds. The resulting branched polymer has a high aromatic content and therefore has a great potential to serve as a resource for the production of aromatic chemicals. In general, two routes are known to isolate these aromatics from lignin. The first route involves the selective degradation of lignin which yields complex aromatics, derived from *p*-hydroxyphenyl, guaiacyl, or syringyl with variable functional groups.^{32,33} Examples of these functional groups are aldehyde, alcohol, carboxylic acid, or allyl groups and the aromatic compounds can be mono, bi, or multifunctional. Figure 1.2 shows examples of possible aromatic hydroxycarboxylic acid monomers, obtained via this route.³¹ In this thesis, mostly *p*-hydroxybenzoic acid and vanillic acid are employed as lignin derived renewable aromatic monomers for the development of new polymers. These monomers are selected since they exhibit good thermal stability, which makes their application in melt polycondensation reactions at high temperatures possible. Furthermore, the rigid aromatic nature of these monomers can prove useful in the development of renewable rigid materials.

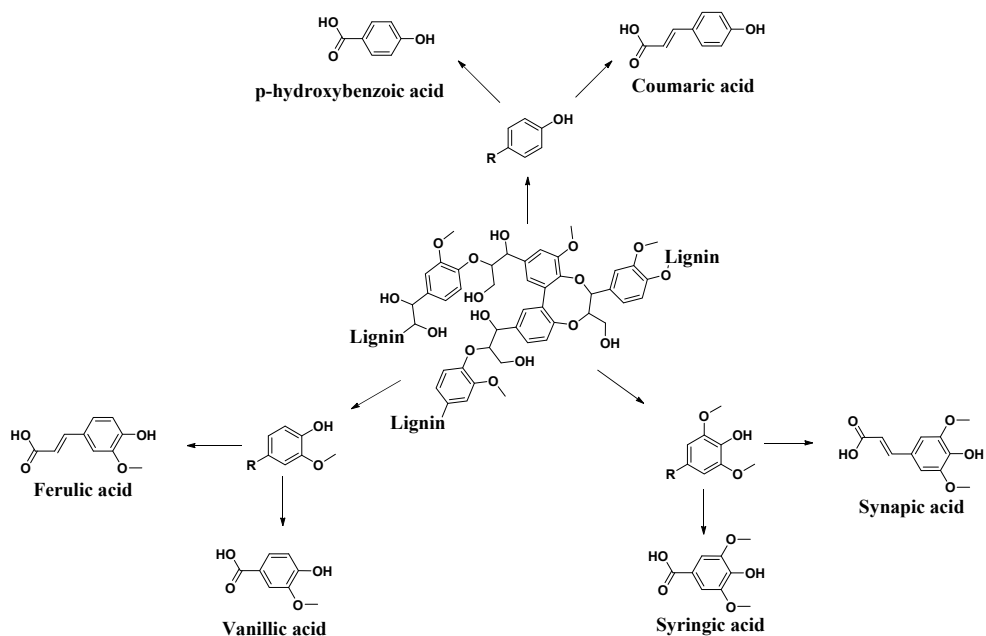


Figure 1.2. Different aromatic hydroxycarboxylic acid monomers that can be obtained from lignin. *N.b.* A representative chemical structure of lignin is shown in this figure since the composition of lignin varies from species to species.³¹

The second route involves the non-selective depolymerization of lignin, resulting in the breaking of both C-C and C-O bonds. An example of such a route has been described by Murray and coworker, who depolymerized lignin in the presence of

water, hydrogen, and a nickel catalyst, in a closed vessel at a temperature of 300 °C or higher.³⁴ The products obtained after such a non-selective depolymerization reaction are mostly phenols and BTX chemicals (i.e. benzene, toluene, and xylene) and can in turn be converted into other chemicals using existing technologies.³⁵⁻³⁷

1.2. From monomer to polymer

1.2.1. Step-growth polymerization reactions

In the previous section, the origins of the most important renewable aromatic monomers used in this thesis were described. In this section, the focus lies on the incorporation of these monomers into polymeric materials. The polymerization reactions employed in this thesis are step-growth polymerization reactions, such as polycondensation or polyaddition reactions. As is indicated by the term step-growth polymerization, the formation of polymer chains proceeds through the stepwise coupling reaction of bi- or multifunctional monomers. The reactions between these monomers result in the formation of dimers, trimers and longer oligomers, which in turn continue to react until a high molecular weight polymer is obtained (Figure 1.3).

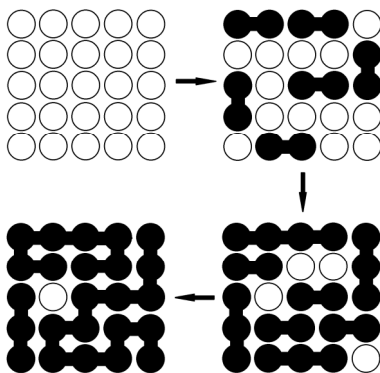


Figure 1.3. A schematic representation of different stages in a step-growth polymerization reaction. In this figure, the white dots represent bifunctional monomers, whereas the black dots are repeating units of dimers, trimers or longer oligomer chains.

As is shown by Carothers³⁸ and Flory,³⁹ the degree of polymerization, characteristic for the molecular weight of polymers synthesized via a step-growth polymerization reaction, can be calculated for linear polymers using the extent of reaction p and the stoichiometric ratio r of the monomers participating in polymerization (Equations 1.1 - 1.3). In equations 1.1 – 1.3, N_0 is the concentration of functional groups present at the start of the reaction, whereas N is defined as the concentration of functional groups at a specific moment during the reaction. Furthermore, N_{aa} is the concentration of bi-functional monomers with functionality AA, N_{bb} is the

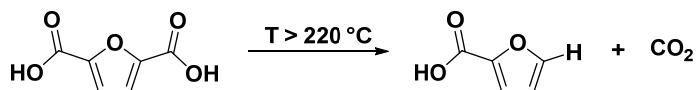
concentration of bi-functional monomers with functionality BB, and N_b is the concentration of mono-functional monomers having functionality B.

$$p = \frac{N_0 - N}{N_0} \quad (\text{Eq. 1.1})$$

$$r = \frac{N_{aa}}{N_{bb} + 2N_b} \quad (\text{Eq. 1.2})$$

$$\overline{X}_n = \frac{(1+r)}{1+r-2rp} \quad (\text{Eq. 1.3})$$

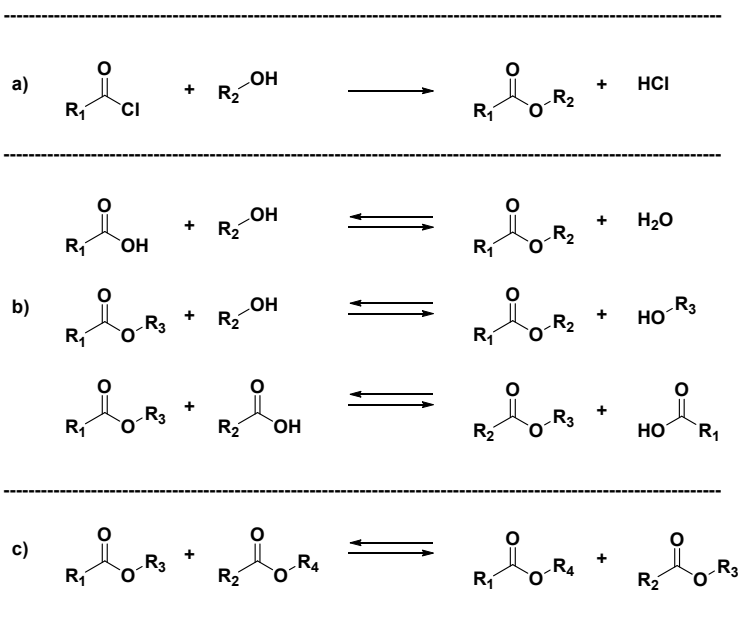
When the extent of reaction p and the stoichiometric ratio r are known, the number-average degree of polymerization, \overline{X}_n , can be calculated using equation 1.3. As is clear from equation 1.3, a large extent of reaction ($p \rightarrow 1$) and an equimolar stoichiometry of the reactive groups ($r = 1$) are essential to reach high \overline{X}_n . For this reason, it is important that the monomers used in such polymerization reactions are stable under the applied reaction conditions. For example, 2,5-FDCA is known to be unstable when processed at temperatures above 220-230 °C, resulting in the decarboxylation of the carboxylic acid groups (Scheme 1.2).^{40,41} The occurrence of this decarboxylation reaction during polymerization will generate carbon dioxide and 2-furancarboxylic acid. The latter will function as a mono-functional monomer, thus changing the stoichiometric ratio in the system. According to equation 1.3 such a deviation of the monomer stoichiometry severely limits the maximum attainable degree of polymerization and molecular weight during polymerization. For example, the polymerization of 2,5-FDCA and ethylene glycol can result in the degradation of part of the carboxylic acid groups of 2,5-FDCA, when the reaction is performed at too high temperatures. In the hypothetical case that 1%, 2.5%, or 5% of the carboxylic acid groups degrade during polymerization, the theoretically maximum attainable \overline{X}_n decreases from infinity to 201 ($M_n \sim 17,000$ g/mol), 81 ($M_n \sim 6,700$ g/mol), and 41 ($M_n \sim 3,400$ g/mol), respectively. To reflect, molecular weights (M_n) of at least 10,000-15,000 g/mol are required for practical processing purposes, for example for injection molding of poly(butylene terephthalate). The requirement of sufficient molecular weight demonstrates the importance of the absence of side-reactions during polymerization. Similarly, the purity of the used monomers is of crucial importance in these polymerization reactions to ensure an equimolar stoichiometry and to prevent unwanted side reactions.



Scheme 1.2. Decarboxylation of 2,5-FDCA occurring when processed at temperatures above 220 °C.

1.2.2. Condensation polymerization reactions

Several types of step-growth polymerization reactions are commonly employed for the preparation of linear polymers. The most important example of such a reaction is the condensation reaction. A condensation reaction generally involves the connection of two molecules while liberating a small molecule, called the condensate. Condensation reactions can be divided into non-reversible and reversible reactions. One example of a condensation reaction that is considered irreversible is the reaction between acid chlorides and alcohols or amines. Examples of reversible condensation reactions are the direct esterification reaction between an alcohol and a carboxylic acid, the alcoholysis reaction between an ester and an alcohol, and the acidolysis reaction between an ester and a carboxylic acid. Scheme 1.3 shows an overview of the condensation and exchange reactions commonly used for the preparation of polyesters.



Scheme 1.3. Examples of different step-growth reactions; a) the irreversible condensation reaction between an acyl chloride group and an alcohol forming an ester bond and hydrogen chloride, b) reversible esterification, alcoholysis, and acidolysis condensation reactions, and c) transesterification or ester exchange reaction occurring between two ester groups.

A straightforward reaction to use for the preparation of polymers in a solvent is an irreversible polycondensation reaction (Scheme 1.3a). In general, for such a polycondensation reaction, the polymerization proceeds as long as the polymer is soluble and the end-groups of the monomers do not undergo side reactions. The final

polymer can then be isolated via precipitation in a non-solvent after (near) full conversion is achieved. A common class of polymers synthesized via this route are aromatic polyamides, also known as aramids. A commercial example of a polymer synthesized via this route is poly(*p*-phenylene terephthalamide) (PPTA). This polymer is synthesized through the polymerization of *p*-phenylenediamine and terephthaloyl chloride in N-methylpyrrolidone.⁴² Commercially synthesized PPTA generally has a number average molecular weight (M_n) around 20,000 g/mol, whereas the weight average molecular weight (M_w) lies in the range between 40,000 and 50,000 g/mol.⁴² There are also examples of aromatic polyesters synthesized via this route, using solvents such as *o*-chlorobenzene, diphenyl ether or 1,1,2,2-tetrachloroethane.⁴³ However, in general, the solubility of aromatic polyesters is poor and molecular weight build-up is limited by the precipitation of the polymers during polymerization. In general, esterification, alcoholysis, and acidolysis melt-polycondensation reactions are more frequently used for the preparation of polyesters (Scheme 1.3b). Although these reactions are reversible, high molecular weight polymers can be synthesized via this method by the removal of the condensate, effectively pushing the equilibrium towards polymerization. The condensate can be removed via distillation at elevated temperatures and/or under reduced pressure, yielding molecular weights (M_n) well above 10,000 g/mol and polydispersity (PDI) values close to 2. Since these polymerization reactions are reversible, the molecular weight of the polymer is determined by the efficiency of the removal of the condensate. If required, the molecular weight of the final polymer obtained after the melt-polycondensation reaction can be increased further by performing a solid-state post condensation reaction, easily reaching M_w values in the range between 50,000 to 100,000 g/mol.⁴⁴ Another reaction that occurs in a polyester melt is the transesterification or ester exchange reaction (Scheme 1.3c). This ester exchange reaction can strongly influence the monomer distribution in polymers chains in a copolymerization reaction. For example, when a copolymerization is performed and the ester bonds in the copolymer are not equally reactive towards transesterification with other ester groups, different monomers can cluster into blocks resulting in a non-random distribution along the polymer chain.^{45,46} In contrast, a random copolymer is obtained when all ester bonds are equireactive towards transesterification. The distribution of the monomers along the polymer backbone can greatly affect the thermal properties, processability, and mechanical performance of the synthesized polymers.^{47,48} Therefore, it is of great importance to control the transesterification reaction and to control the distribution of the different comonomers along the polymer backbone. In this study, polyesters, poly(ester amide)s, and cross-linked poly(ester amide)s are developed. The synthesis of these polymers is performed using conventional melt-polycondensation or melt-transesterification reactions. In the next section, attention is

given to the synthesis and design of thermotropic polyesters, a special class of polyesters that are generally synthesized under demanding reaction conditions.

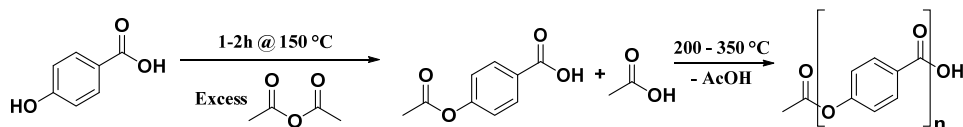
1.2.3. Synthesis of thermotropic polyesters

The liquid crystalline state, also known as the mesogenic state, was first discovered by Reinitzer⁴⁹ and Lehmann⁵⁰ in the late 19th century. These researchers observed that this phase exhibits a behavior characteristic of both liquids and solids; the liquid crystalline phase exhibits orientational order, reduced positional order, and has the ability to flow. For this reason, they called this state the mesogenic phase, which translates as the ‘in-between’ phase. The group of liquid crystalline polymers can be divided into two different classes; thermotropic polymers and lyotropic polymers. Polymers that exhibit the liquid crystalline state above the melting temperature of their crystals are called thermotropic polymers. Similarly, polymers that exhibit liquid crystalline behavior in solution are called lyotropic polymers. Examples of commercial lyotropic polymers are the Twaron® or Kevlar® polyamides and an example of thermotropic polymers are the Vectra® polyester series. Characteristic properties of these liquid crystalline polymers are low melt viscosities, excellent mechanical performance, excellent thermal properties, and good chemical resistance.

Thermotropic compounds are known to melt in three different liquid crystalline phases; the smectic phase, the nematic phase and the cholesteric phase. Polymer chains that reside in the smectic phase have both orientational and positional order. Often thermotropic polymers that exhibit a smectic phase have highly regular repeating units.⁵¹ The nematic phase is often less ordered resulting in molecules that only have directional order, but no long range positional order. The nematic phase is commonly observed in thermotropic polymers that contain different comonomers; no high degree of positional order can be maintained due to the irregularity the polymer backbone. The cholesteric phase resembles the nematic phase, but contains a chiral center that promotes periodic rotation of the chains into a helical pattern. For this reason, thermotropic polymers often exhibit this phase if they contain monomers that have chiral centers.⁵²

In general, thermotropic polyesters are synthesized via melt-polycondensation reactions. The most commonly used melt-polycondensation reaction for aromatic monomers was developed by Cottis^{53,54} and Duska⁵⁵. The method developed by these authors involves the dissolution of the aromatic diols, dicarboxylic acids, and hydroxy acids in acetic anhydride followed by the *in-situ* acetylation of the hydroxyl groups and consecutive polymerization through an acidolysis reaction (Scheme 1.4). In the first reaction step the acetic anhydride reacts with the aromatic alcohol groups, forming an acetate group and liberating one molecule of acetic acid. After one or two hours of reaction at temperatures around 150 °C, the temperature is gradually increased to promote the acidolysis reaction and the acetic acid is distilled off. Generally, the

polymerization is allowed to continue for several hours, while slowly increasing the reaction temperature and removing the liberated acetic acid. In the final stage of polymerization, vacuum is applied to remove the last traces of acetic acid and to push the reaction equilibrium towards polymerization.



Scheme 1.4. Acetylation reaction of *p*-hydroxybenzoic acid into *p*-acetoxybenzoic acid and its consecutive polymerization at elevated temperatures through an acidolysis reaction.

The final reaction temperature of the reaction step conducted under reduced pressure generally lies in the range of 300 to 350 °C, where the final reaction temperature depends on the melting temperature of the targeted polymer. One can imagine that all components participating in such a polymerization reaction have to be thermally stable at these reaction temperatures and should not be prone to undergo side reactions. Furthermore, to prevent cross-linking or oxidation reactions, these polymerizations are conducted in an inert, oxygen free, atmosphere. However, despite all efforts, side reactions such as the Fries rearrangement are known to occur in these polymerization reactions.^{56,57}

There are different variants known to the polymerization route developed by Cottis and Duska. For example, instead of performing the *in-situ* acetylation and polymerization, acetylated monomers can directly be polymerized at high temperatures. Another example is the polycondensation reaction performed in an high boiling, inert solvent, such as Marlotherm-S or Therminol.^{58,59} The benefits of using solvents during polymerization are the occurrence of less side reactions and a higher crystallinity of the formed polymer. Another variant of the reaction developed by Cottis and Duska is reported by Kricheldorf and coworkers, who used silylated dicarboxylic acids in combination with acetylated diols.⁶⁰

It should be noted that there are other, less demanding, methods available in literature to synthesize liquid crystalline polymers. Examples of solvent-based polymerizations involve the application of acyl chloride monomers, the direct esterification reaction of aromatic carboxylic acids and alcohols in the presence of triphenylphosphine and pyridine, and the *in-situ* activation and polymerization of aromatic carboxylic acid and alcohols in the presence of thionyl chloride and pyridine.^{59,60} However, as explained earlier, the preparation of aromatic polyesters via solvent-based techniques generally yields low molecular weight materials due to the poor solubility of the polymer in the used solvents. Furthermore, since the focus in this thesis lies on the preparation of polymers using melt-polymerization reactions, the development of thermotropic polyesters using this melt-polymerization reaction is evaluated in the next section.

1.2.4. Designing thermotropic polyesters

One important objective in the design of thermotropic polyesters is finding the balance between mechanical properties and convenient processing conditions. In general, thermotropic polyesters having a fully aromatic backbone exhibit excellent mechanical properties and can reach tensile moduli in the range of 50-100 GPa and tensile strengths in the range of 3-4 GPa for spun fibers.⁶¹ However, very often, these fully aromatic thermotropic polyesters have very high melting temperatures, which makes processing from the melt expensive or even impossible. Examples of such infusible polymers are poly(oxybenzoate), poly(4,4'-biphenol terephthalate), and poly(1,4-phenylene terephthalate).

In general, four typical approaches can be used to lower the melting temperatures of these infusible polyesters.⁶²⁻⁶⁶ The first method is through the addition of a linear comonomer during polymerization. The presence of this comonomer decreases the periodicity along the polymer backbone and reduces the melting temperature by inhibiting crystallization.⁶⁷ Ideally, the selected comonomer is linear to maintain the mesogenic character of the final polymers. Examples of linear mesogenic comonomers that can be used to lower the melting temperature *via* this approach are *p*-hydroxybenzoate, 4,4'-biphenol, and terephthalic acid.

The second approach to lower the melting temperature is to introduce a non-linear comonomer into the polymer backbone.⁶⁸ This approach is similar to the first route and lowers the melting temperature through inhibition of the crystallization. However, the addition of kinks or bends in the polymer backbone decreases the linearity of the chain and influences the liquid crystalline nature of the polymer. Commonly used kinked monomers include isophthalic acid, 2,5-thiophene, and *m*-hydroxybenzoic acid.⁶⁹ Another side effect of the introduction of kinks in the monomer backbone is that it tends to decrease the thermal stability of the polymer.⁷⁰ A special case of bended comonomers involve the so-called crankshaft monomers, such as 2,6-hydroxynaphthoic acid. The presence of these monomers in the polymer backbone results in a stepwise shift along the polymer backbone, limiting the formation of bends in the polymer chain.⁷¹

The third approach to lower the melting temperature is the incorporation of monomers with bulky side groups. Ideally, these side groups are located on linear monomers to maintain the linear character of the polymer chain. The presence of side groups such as phenylene rings, halogens, short aliphatic branches, or ether groups disturb the inter-chain packing and thereby limit crystallization. As is reported by Jackson⁷², the presence of these side groups does not seem to influence the fiber properties.

The fourth method to decrease the melting temperature is through the incorporation of aliphatic moieties in the polymer backbone. Examples of these aliphatic monomers

are suberic acid, sebacic acid, and ethylene glycol.^{73,74,75} This approach is by far the most effective in decreasing the melting temperature, but also results in a drastic loss of the mechanical performance of the obtained polymers.⁷⁶

1.2.5. Renewable monomers in thermotropic polyesters

According to the routes discussed in the previous section, the renewable aromatic monomers described in paragraphs 1.1.1 and 1.1.2 are expected to be good candidates to develop thermotropic polyesters that exhibit melting temperatures below their degradation temperature. As is shown earlier, *p*-hydroxybenzoic acid is potentially obtained from lignin and acts as a mesogen once incorporated into the polymer backbone. For this reason, *p*-hydroxybenzoic acid is an excellent monomer to use in the development of renewable thermotropic polyesters. However, as was also indicated previously, high molecular weight poly(oxybenzoate) is infusible and intractable, making processing from the melt impossible.

It is expected that the melting temperature of poly(oxybenzoate) can be decreased by the copolymerization of 2,5-FDCA, vanillic acid, or syringic acid. As is shown in the previous section, the copolymerization of kinked monomers is a proven method to lower melting temperatures or thermotropic polyesters. Since 2,5-FDCA has an angle of $\sim 123^\circ$ between its carboxylic acid groups it is anticipated that its presence in the polymer backbone introduces bends in the polymer chain, thereby hindering crystallization. Similarly, the presence of the methoxy side-groups of vanillic acid or syringic acid along the polymer backbone will disturb the inter-chain packing and limit crystallization. Although the side groups of vanillic acid and syringic acid are aliphatic, their backbones are aromatic and allow for the design of thermotropic polyesters having a fully aromatic backbone.

Another option to design renewable thermotropic polyesters is to perform a copolymerization of monomers that have a partially aliphatic backbone. Examples of aromatic-aliphatic monomers are coumaric acid, ferulic acid, synapic acid, or their hydrogenated counterparts such as 3-(4-hydroxyphenyl)propionic acid. Examples of applicable renewable monomers without aromatic rings are aliphatic acids, such as suberic acid and sebacic acid. As is explained earlier, the presence of aliphatic spacers is not desirable in polymers for high performance applications due to their low melting temperatures and poor mechanical performance. However, such a low melting temperature could be useful in a copolymerization with monomers that have a limited thermal stability.

More detail on the incorporation of the aforementioned renewable monomers into aromatic thermotropic polyesters is provided in chapter 2, whereas the synthesis of aromatic-aliphatic thermotropic polyesters is described in chapter 3 of this thesis.

1.3. From polymer to product

As is explained in the previous sections, the conversion of biomass to monomers and the polymerization of these monomers to prepare, for example, thermotropic polyesters, seems possible. However, one important prerequisite for these renewable polymers to be industrially viable is that their performance should be comparable to the performance of existing polymers used for similar applications. The following sections describe the targeted applications that can benefit from the rigid aromatic nature of the polymers developed in this thesis; application as high strength and high modulus fibers, application as engineering plastics, and applications as rigid coatings or polymer glasses.

1.3.1. Fibers and films

Thermotropic polymers are generally easy to process from the melt-phase. The origin of this ease in processing lies in the fact that, in the liquid crystalline melt, the polymer chains tend to orient in a more or less parallel fashion. The orientation of these polymer chains only occurs locally and results in what can be described as a domain with a preferred directional order. The directional order of such a domain can in turn be described using a vector, which is also known as the director. The thermotropic melt consists of many of these domains, and the director of each domain can point to any direction.⁷⁷ As a result, from a macroscopic viewpoint, the thermotropic melt does not have a net directional orientation, since the sum of the directors of all domains is zero. Although there is no net orientation in a thermotropic melt, one can imagine that these domains can easily be oriented into a desired direction (Figure 1.4). Besides the low energy involved to orient the thermotropic melt, the presence of these domains also explain the low melt-viscosity and shear thinning behavior of thermotropic polymer melts.⁷⁸ Additional benefits of processing from the liquid crystalline melt are low die swell, rapid solidification, and a good dimensional stability. The convenient processing from the liquid crystalline melt yields products that have a high degree of orientation. These anisotropic products often have a high tensile modulus and tensile strength due to the strong van der Waals interactions between the oriented chains. Examples of products that exhibit this high modulus and high strength are injection molded articles, fibers, films, and tapes.^{79-83,61} The processing and mechanical performance of the renewable thermotropic polyesters developed in this thesis are described and evaluated in chapter 4 of this thesis.

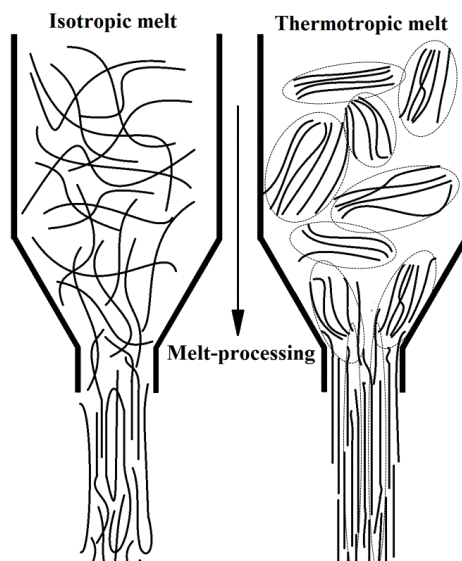


Figure 1.4. Schematic representation of the melt processing of an isotropic melt and a thermotropic melt. The different domains in the thermotropic polymer melt are indicated by the dashed circles.

1.3.2. Engineering plastics

In general, polycondensation polymers such as polyamides or polycarbonates are commonly used as engineering plastics. These polymers generally show a better mechanical and/or thermal performance compared to commodity plastics such as polyethylene, polypropylene, and polystyrene. One example of a polymer widely used as an engineering plastic is polyamide 4,6. This polymer has a melting temperature of 295 °C, a good heat resistance, and excellent abrasion resistance. The high crystallinity of this polymer, roughly 70%, also ensures a good mechanical performance above the glass transition temperature (T_g). Other examples of polycondensation polymers used as engineering plastics are poly(ethylene terephthalate) for the preparation of plastic bottles, and poly(butylene terephthalate) for injection molding purposes or for insulation. In chapter 5 of this thesis, the development of aromatic-aliphatic renewable poly(ester amide)s is described. In general such poly(ester amide)s exhibit high crystallinities, good thermal stability, and good performance at high temperature, making them interesting candidates for application as engineering plastics.

1.3.3. Coatings and polymer glasses

Step-growth polymers such as polyesters, polyurethanes or epoxy resins are commonly used in formulations for coatings. The wide variety of properties such as the functionality, rigidity, and hydrophilicity/hydrophobicity of monomers suitable for step-growth polymerization reactions makes them excellent build-blocks to tailor the

properties of coatings for the desired applications. For example, control over the T_g can be obtained by the addition of cyclic or aromatic comonomers during polymerization, resulting in a more rigid polymer chain having a higher T_g . Examples of monomers that have effectively been used to improve the T_g of coatings are isosorbide, 1,4-cyclohexane dicarboxylic acid, terephthalic acid, and 2,5-FDCA.^{84,85,86} In general, the preparation of thermosetting coatings proceeds in two steps. In the first step, a branched pre-polymer is synthesized, ideally with two or more reactive end-groups. This pre-polymer is then reacted with a curing agent to obtain a cross-linked network.⁸⁷ The cross-link density of the obtained polymer network is determined by the molecular weight of the pre-polymer, the functionality of the pre-polymer, the functionality of the cross-linker, and the ratio between the cross-linker and pre-polymer.⁸⁸ This route is generally applied for the preparation of solvent-borne coatings and thermally cured powder coatings. Another route to prepare coatings is the direct application of a thermoplastic elastomer onto a surface using either a solvent or melt based technique. Although this route is convenient since it does not require a curing reaction step, these coatings often suffer from poor performance due to the absence of a network structure. Another approach to prepare cross-linked polymer systems is *via* the *in-situ* polymerization and cross-linking of a monomer mixture.⁸⁹ Although this route can be applied for the preparation of coatings, this approach is generally preferred for the preparation of injection molded and fiber reinforced thermosets. Examples of commercially available resins prepared *via* this route are the CP resin series by Takeda Chemical Industries.⁹⁰ The reactive monomers used in this resin are bis(2-oxazoline)s, which form cross-linked poly(ester amide)s during the reaction with dicarboxylic acids.⁹¹ In chapter 6 of this thesis, the applicability of the aromatic monomer 2,5-FDCA in high T_g coatings or polymer glasses prepared *via* the *in-situ* polymerization and cross-linking reaction is evaluated.

1.4. Aim and scope of this thesis

The main motivation for the work presented in this thesis is the scientific curiosity to synthesize and characterize new polymers using renewable monomers. The objective of this study is to demonstrate the applicability of renewable, aromatic monomers in step-growth polymers that exhibit properties suitable for demanding applications, *e.g.* high strength and high modulus fibers. Furthermore, another objective of this study is to evaluate the performance of these renewable polymers and to show that renewable materials exhibit properties that are unattainable in standard petrochemical polymers. In order to compare the renewable polymers prepared in this study with their petrochemical counterparts, understanding of the involved chemistry, physics, and mechanical characterization is required. Therefore, to achieve the aforementioned objectives, a chain-of-knowledge approach was adopted, comprising the following steps:

- Monomer preparation and purification
- Design and preparation of polymers
- Chemical, thermal and physical characterization
- Polymer processing and mechanical characterization

The most important and relevant results obtained within the framework of this project are described in this thesis.

1.5. Outline of this thesis

This thesis consists of 7 chapters describing the application of 2,5-FDCA in step-growth polymers and the properties of the resulting polymeric materials. In chapter 2, the feasibility of incorporating 2,5-FDCA in fully aromatic, thermotropic polyesters via high temperature melt-polycondensation reactions up to 340 °C is discussed. Although the melt-synthesis of 2,5-FDCA based thermotropic polyesters is possible, the thermal stability of 2,5-FDCA limits the reaction temperature. Successful synthesis of the desired polymers is achieved through the addition of the comonomer vanillic acid. Preliminary up-scaling experiments are performed to determine the mechanical performance and processability of the polymers described in this chapter.

The application of 2,5-FDCA in thermotropic polyesters is explored further in chapter 3, where a low-temperature synthesis route is adopted to prevent thermal degradation of this monomer. The copolymerization of aliphatic dicarboxylic acids is performed to lower the melting temperature of the polymer and to allow the polymerization to proceed at reaction temperatures below 230 °C. Special attention is paid to the effect of the presence of 2,5-FDCA and vanillic acid in the polymer backbone on the thermal, physical and mechanical properties of the obtained polymers. The processing and performance of these renewable aromatic-aliphatic polymers is described in more detail in chapter 4. Compression molding, solvent casting and fiber spinning are performed on a series of thermotropic polymers and the effect of molecular weight and processing method on the mechanical and thermal performance is evaluated.

The application of thermally stable, amide-protected 2,5-FDCA monomers for the preparation of poly(ester amide)s is investigated in chapter 5. Special attention is paid to the properties of the 2,5-furandicarboxamide moiety and to its performance compared to the terephthalamide or isophthalamide moiety. In chapter 6, the application of the stable and rigid 2,5-furandicarboxamide moiety for the preparation of coatings or polymer glasses is investigated. These fully renewable and cross-linked polymers are obtained through the polymerization of a 2,5-FDCA based bis(2-oxazoline) monomer with dicarboxylic acids.

The final section of this thesis, chapter 7, highlights the most important results and conclusions described in chapters 2 to 6, together with suggestions for future research

in the field of renewable step-growth polymers. Furthermore, this chapter includes a technology assessment concerning the industrial relevance of the work performed.

1.6. References

- [1] Tsoskounogluc, M., Ayerides, G., Tritopoulou, E., *Energ. Policy*, **2008**, 36, 3797-3806
- [2] Olivier, J.G.J., Janssens-Maenhout, G., Muntean, M., Peters, J.A.H.W., *Trends in global CO₂ emissions: 2013 report*, **2013**, ISBN: 978-94-91506-51-2
- [3] Eggersdorfer, M., Meyer, J., Eckes, P. *FEMS Microbiol. Rev.*, **1992**, 103, 355-365
- [4] Okkerse, C., van Bekkum, H., *Green Chemistry*, **1999**, 1, 107-114
- [5] Brunschwig, C., Moussavou, W., Blin, J., *Progress in Energy and Combustion Science*, **2012**, 38, 283-301
- [6] Ten Dam, J., Hanefeld, U., *ChemSusChem*, **2011**, 4, 1017-1034
- [7] Bechthold, I., Bretz, K., Kabasci, S., Kopitzky, R., Springer, A., *Chem. Eng. Technol.*, **2008**, 37, 5, 647-654
- [8] Cheng, K-K., Zhao, X-B., Zeng, J., Zhang, J-A., *Biofuels, Bioproducts and Biorefining*, **2012**, 6, 302-318
- [9] Mathers, R.T., *Polymer Chemistry*, **2011**, 50, 1-15
- [10] Burgess, S.K., Leisen, J.K., Kraftschik, B.E., Mubarak, C.R., Kriegel, R.M., Koros, W.J., *Macromolecules*, **2014**, 47, 1383-1391
- [11] Ma, J., Pang, Y., Wang, M., Xu, J., Ma, H., Nie, X., *J. Mater. Chem.*, **2012**, 22, 3457-3461
- [12] Gomes, M., Gandini, A., Silvestre, A.J.D., Reis, B., *J. Polym. Sci. Part A: Polym. Chem.*, **2011**, 49, 3759-3768
- [13] Ma, J., Yu, X., Xu, J., Pang, Y., *Polymer*, **2012**, 53, 4145-4151
- [14] Dam, M.A., Gruter, G.M., Sipos, L., de Jong, E., Den Ouden, D., Society of Plastics Engineers-EUROTEC 2011 Conference Proceedings, Barcelona, Spain, November 14–15, **2011**.
- [15] Werpy, T., Petersen, G., Aden, A., Bozell, J., Holladay, J., White, J., Manheim, A., Eliot, D., Lasure, L., Jones, S., *Top Value Added Chemicals From Biomass. Volume 1- results of Screening for Potential Candidates from Sugars and Synthesis Gas*, Pacific Northwest National Laboratory, Richmond, **2004**, 1-69
- [16] Gandini, A., *Polym. Chem.* **2010**, 1, 245-251
- [17] Gandini, A., Belgacem, M.N., *Prog. Polym. Sci.*, **1997**, 22, 1203-1379
- [18] Gandini, A., Coelho, D., Gomes, M., Reis, B., Silvestra, A. *J. Mater. Chem.* **2009**, 19, 8656-8664
- [19] Bicker, M., Hirth, J., Vogel, H., *Green Chem*, **2003**, 5, 280-284
- [20] Román-Leshkov, Y., Chheda, J.N., Dumesic, J.A., *Science*, **2006**, 312, 1933-1937
- [21] Moreau, C., Belgacem, M.N., Gandini, A., *Top. Catal.*, **2004**, 385, 1-13
- [22] Gorbanev, Y.Y., Klitgaard, S.K., Woodley, J.M., Christensen, C.H., Riisager, A., *ChemSusChem*, **2009**, 2, 7, 675-675
- [23] Gupta, N.K., Nishimura, S., Takagaki, A., Ebitani, K., *Green Chem.*, **2011**, 12, 824-827
- [24] Taarning, E., Nielsen, I.S., Egeblad, k., Madsen, R., Christensen, C.H., *ChemSusChem*, **2008**, 1, 75-78
- [25] Casanova, O., Iborra, S., Corma, A., *J. Catal.*, **2009**, 265, 109-116
- [26] Zhou, H., Holladay, J.E., Brown, H., Zhang, C., *Science*, **2007**, 316, 1597-1600
- [27] Ribeiro, M. L., Schuchardt, U., *Catal. Commun.*, **2003**, 4, 83-86
- [28] Kröger, M., Prüße, U., Vorlop, K.-D., *Top. Catal.*, **2000**, 13, 237-242
- [29] Munoz de Diego, C., Schammel, W.P., Dam, M.A., Gruter, G.M., Method for the preparation of 2,5-furandicarboxylic acid and esters thereof, **2011**, WO2011043660.
- [30] Dam, M.A., Gruter, G.M., Munoz de Diego, C., Schammel, W.P., Method for the preparation of 2,5-furandicarboxylic acid and for the preparation of the dialkyl ester of 2,5-furandicarboxylic acid, **2010**, EP2486027.

- [31] Bozell, J.J., Holladay, J.E., Johnson, D., White, J.F., *Top Value Added Chemicals from Biomass, Volume II: Results of Screening for Potential Candidates from Biorefinery Lignin*, Pacific Northwest National Laboratory, Richmond, US, **2007**, 1-79
- [32] Singh, S., Varanasi, P., Blake, S., Renewable Aromatics from Lignocellulosic Lignin, **2014**, WO2014/089574
- [33] Roberts, V.M., Stein, V., Reiner, T., Lemonidou, A., Li, X., Lercher, J.A., *Chem. Eur. J.*, **2011**, 17, 5939-5948
- [34] Murray, A., Ryba, S., Lignin conversion process, **2012**, WO2012/174429 A1
- [35] Kloekhorst, A., Wildschut, J., Heeres, H.J., *Catal. Sci. Technol.*, **2014**, 4, 2367-2377
- [36] Deepa, A.K., Dhepe, P.L., *RSC Adv.*, **2014**, 4, 12625-12629
- [37] Zhang, J., Teo, J., Chen, X., Asakura, H., Tanaka, T., Teramura, K., Yan, N., *ACS Catal.*, **2014**, 4, 1574-1583
- [38] Carothers, W.H., *Chem. Rev.*, **1931**, 8, 353-426
- [39] Flory, P.J., *Chem. Rev.*, **1946**, 39, 137-197
- [40] Gruter, G.-J. M., Sipos, L., Dam, M.A., *Combinatorial Chemistry & High Throughput Screening*, **2012**, 15, 180-188
- [41] Drewitt, J.G.N., Lincoln, J., Improvements in Polymers, **1946**, Br. Patent, 621971,
- [42] Picken, S.J., Sikkema, D.J., Boerstael, H., Dingemans, T.J., van der Zwaag, S., *Liquid Crystals*, **2011**, 38, 1591-1605
- [43] Carfagna, C., *Liquid Crystalline Polymers*, Pergamon Press, Oxford, UK, **1994**
- [44] Vouyiouka, S.N., Karakatsani, E.K., Papaspyrides, C.D., *Prog. Polym. Sci.*, **2005**, 30, 10-37
- [45] Nicely, V.A., Dougherty, J.T., Renfro, L.W., *Macromolecules*, **1987**, 20, 573-578
- [46] Quach, L., Hornogen, E., Volksen, W., Economy, J., *J Polym Sci Part A: Polym Chem*, **1989**, 27, 775-784
- [47] Yang, D.K., Krigbaum, W.R., *J. Polym. Sci. Part B: Polym. Phys.*, **1989**, 27, 819-835.
- [48] Muramatsu, H., Krigbaum, W.R., *J. Polym. Sci. Part B: Polym. Phys.*, **1987**, 25, 2303-2314.
- [49] Reinitzer, F. *Monatsh. Chem.*, **1888**, 9, 421-441.
- [50] Lehmann, O., *Zeit. Phys. Chemie*, **1889**, 4, 462-472.
- [51] Krigbaum, W.R., Watanabe, J., Ishikawa, T., *Macromolecules*, **1983**, 16, 1271-1279
- [52] Chavan, N.N., *Materials Sciences and Applications*, **2011**, 2, 1520-1527
- [53] Cottis, S.G., Layton, R., Field, N.D., Injection moldable aromatic polyesters compositions and method of preparation, **1986**, US 4563508.
- [54] Cottis, S.G, Phosphite Bulk Polymerization, **1987**, US4639504.
- [55] Duska, J. J., Finestone, A. B., Maher, J. B., Aromatic polyesters, **1986**, US 4626557.
- [56] Fries, K., Pfaffendorf, W., *Ber. Dtsch. Chem. Ge.*, **1910**, 43, 212-219
- [57] Fries, K., Finck, G., *Ber. Dtsch. Chem. Ge.*, **1908**, 41, 4217-4282
- [58] Kricheldorf, H.R., Döring, V., *Polymer*, **1992**, 33, 5321
- [59] Bhowmik, P.K., Lenz, R. W., *J Polym Sci., Polym. Chem. Edn.*, **1994**, 32, 651
- [60] Han, H., Bhowmik, P.K., *Prog. Polym. Sci.*, **1997**, 22, 1431-1502
- [61] General brochure Vectran © **2008** Vectran®. Kururay America, Inc. Vectran® Division.
- [62] Ballauff, M., *Angewandte Chemie*, **1989**, 101, 261-276
- [63] Lin, J., Sherrington, D.C., *Advances in Polymer Science*, **1994**, 111, 177-219
- [64] Varshney, S.K., *J. Macromol. Sci., Rev. Macromol. Chem. Phys.*, **1986**, C26, 4, 551
- [65] Dobb, M.G., McIntyre, J.E., *Adv Polym Sci*, **1984**, 60/61, 61-98
- [66] Jackson, W.R., Jr., *Mol. Cryst. Liq. Cryst.*, **1989**, 169, 23-49

- [67] Demus D., Goodby, J., Gray G.W., Spiess H.-W., Vill V., *Handbook of liquid crystals Vol 3*, **1998**, Wiley-VCH Verlag GmbH
- [68] Chung, T.-S., *Polymer Engineering and Science*, **1986**, 26, 13, 901-919
- [69] Cai, R., Preston, J., Samulski, E.T. *Macromolecules*, **1992**, 25, 563-568
- [70] Shibaev, V.P., Lam, L., Windle, A.H., *Liquid Crystalline and Mesomorphic Polymers*, **1994**, Springer-Verlag, New York, US.
- [71] Collyer, A.A., *Liquid Crystal Polymers: From Structures to Applications*, **1992**, Elsevier Applied Science, Barking, UK.
- [72] Jackson, J., *The British polymer Journal*, **1980**, 154-160
- [73] De Ruijter, C., Bos, J., Boerstoel, H., Dingemans, T., *J Polym Sci Part A: Polym Chem*, **2008**, 46, 6565-6574.
- [74] Li, X.G., Huang, M.-R., Guan, G.-H., Sun, T., *Die Angewandte Makromolekulare Chemie*, **1995**, 227, 69-85
- [75] Li, X.G., Huang, M.-R., Guan, G.-H., Sun, T., *J. Appl. Polym. Sci.*, **1996**, 59, 1-8
- [76] Jackson, W.J., Kuhfuss, H.F., *J. Polym. Sci. Polym. Chem. Ed.*, **1976**, 14, 8, 2043-2058
- [77] De Gennes, P.G., Prost, J., *The physics of liquid crystals*, **1995**, Oxford University Press, UK.
- [78] Acierno, D., Collyer, A.A., *Rheology and Processing of Liquid Crystal Polymers*, **1996**, Chapman & Hall, London, UK.
- [79] Meijer, H.E.H., Lefevre, J., Felman, K., Tervoort, T.A., Smith, P., Giesbrecht, J.L., Polymer articles, and methods and dies for making the same, **2011**, US20110227247 A1
- [80] Muramatsu, H., Krigbaum, W.R., *Journal of Polymer Science Part B: Polymer Physics*, **1986**, 24, 1695-1711
- [81] Muramatsu, H., Krigbaum, W.R., *Macromolecules*, **1986**, 19, 2850-2855
- [82] Muramatsu, H., Krigbaum, W.R., *Journal of Polymer Science Part B: Polymer Physics*, **1987**, 25, 2303-2314
- [83] Lefèvre, J., Feldman, K., Giesbrecht, J., Smith, P., Tervoort, T.A., Meijer, H.E.H., *Journal of Polymer Science Part B: Polymer Physics*, **2012**, 50, 1713-1727
- [84] Noordover, B. A. J., Van Staalduinen, V. G., Duchateau, R., Koning, C. E., Van Benthem, R. A. T. M., Mak, M., Heise, A., Frissen, A. E., Van Haveren, J., *Biomacromolecules*, **2006**, 7, 3406-3416.
- [85] Van Haveren, J., Oostveen, E. A., Micciché, F., Noordover, B. A. J., Koning, C. E., Van Benthem, R. A. T. M., Frissen, A. E., Weijnen, J. G. J., *J. Coat. Technol. Res.* **2007**, 4, 177-186
- [86] Gubbels, E., Jasinska-Walc, L., Noordover, B.A.J., Koning, C.E., *Eur. Pol. J.*, **2013**, 49, 3188-3198
- [87] Misev, T. A., *Powder coatings - chemistry and technology*, **1991**, 1st ed: John Wiley & Sons, New York, US.
- [88] Richart, D. S., *Coating processes, powder technology*, in *Kirk-Othmer Encyclopedia of Chemical Technology*. **2001**, John Wiley & Sons, New York, US.
- [89] Culbertson, B., *Prog. Polym. Sci.*, **2002**, 27, 579-626.
- [90] Sano, Y., Arita, K., Masuda, I, Cross-linked polyesteramide from bis(2-oxazoline), **1984**, US 4,474,942.
- [91] Sano, Y., *J. Polym. Sci. Part A: Polym. Chem.*, **1989**, 27, 2749-2760

Chapter 2

Aromatic thermotropic polyesters based on 2,5-furandicarboxylic acid and vanillic acid

Abstract

In this chapter, the incorporation of 2,5-furandicarboxylic acid (2,5-FDCA) in fully aromatic thermotropic polyesters *via* a melt polycondensation reaction is explored. Special attention is given to the solubility of 2,5-FDCA in the monomer/oligomer melt to ensure the participation of 2,5-FDCA in the polymerization reaction. It is demonstrated that 2,5-FDCA can be incorporated in a copolymer together with 4,4'-biphenol (BP) and *p*-hydroxybenzoic acid (BA), yielding polymers with melting temperatures well above 300 °C. Since the thermal stability of 2,5-FDCA does not allow for processing at these temperatures, the copolymerization of vanillic acid (VA) is performed to perturb the polymer crystallization. It is demonstrated that the 2,5-FDCA and VA based thermotropic polyesters, obtained via this copolymerization method, exhibit melting temperatures between 240 and 300 °C. The relatively low melting temperatures of these polymers allows for their synthesis at mild reaction temperatures. Preliminary up-scaling experiments are performed to evaluate the molecular weight and performance of these aromatic thermotropic polyesters as a function of reaction temperature. It is shown that the molecular weight build-up of these polymers is hampered by the degradation of 2,5-FDCA, despite the application of decreased reaction temperatures. These results indicate that the processing temperatures have to be decreased further in order to fully eliminate degradation and side-reactions of 2,5-FDCA. Experimental techniques, such as polarization optical microscopy (POM), fourier-transform infra-red (FTIR) spectroscopy, differential scanning calorimetry (DSC), thermogravimetric analysis (TGA), and wide-angle x-ray diffraction (WAXD) are employed to monitor the polymerization reaction and to perform chemical, thermal and structural characterization of the synthesized polymers.

This chapter is partially based on Wilsens C.H.R.M., Noordover, B.A.J., Veld. M., Klop E.A., Rastogi, S. Liquid crystalline furandicarboxylic acid-based aromatic polyesters, **2013**, WO2013092667 and Wilsens, C.H.R.M., Noordover, B.A.J., Rastogi, S., *Polymer*, **2014**, 55, 2432-2439

2.1. Introduction

Over the last decades, extensive research has been performed to develop fully aromatic liquid crystalline (LC) polyesters. However, very often, thermotropic homopolyesters have high crystal-to-liquid crystal melting temperatures, making processing from the LC melt challenging and often unattractive from a practical perspective.¹ For this reason, the chemical structures of these polymers are modified to lower their melting temperatures, to decrease processing costs, and to prevent thermal degradation during processing.²⁻¹¹ As is described in chapter 1 of this thesis, these structural modifications involve the copolymerization of linear monomers, non-linear monomers, monomers with bulky side groups or flexible aliphatic monomers. Characteristic properties of these thermotropic polyesters are their excellent mechanical and thermal properties, chemical resistance, and ease of processing from their thermotropic melt. The numerous thermotropic polyesters developed over the years are extensively reviewed by Han and Bhowmik¹², Ballauff¹³, Windle¹⁴, and others.¹⁵⁻¹⁹

In this chapter, the copolymerization of aromatic bio-based moieties with *p*-hydroxybenzoic acid (BA) is investigated in order to decrease the melting temperature of the poly(oxybenzoate) backbone. The employed bio-based monomers are vanillic acid (4-hydroxy-3-methoxybenzoic acid, VA) and 2,5-furandicarboxylic acid (2,5-FDCA).²⁰ The copolymerization of small amounts of VA in thermotropic polyesters is known to increase the uniaxial deformation, mechanical properties, solubility and glass transition temperature of thermotropic polyesters based on poly(ethylene terephthalate) and BA.²¹⁻²³ The application of 2,5-FDCA in thermotropic polyesters has been reported in patent applications by Vriesema²⁴ and Fujioka²⁵. Vriesema demonstrated that the replacement of small amounts of terephthalic acid (TA) by 2,5-FDCA causes a decrease of the melting temperature while retaining the thermotropic behavior of the polymer. Fujioka copolymerized 2,5-FDCA and a phosphorous containing diol with BA to synthesize heat resistant thermotropic polyesters. Both of these inventions describe the application of 2,5-FDCA as a comonomer in poly(oxybenzoate)-based thermotropic polyesters. Although these reports demonstrate the feasibility of the incorporation of 2,5-FDCA into thermotropic polyesters, it should be noted that the crystal to LC transition temperature of their designed thermotropic polyesters exists only well above 300 °C. Although reports on the application of 2,5-FDCA as a monomer in thermotropic polyesters are limited, the use of other five membered heterocyclic rings such as pyridazine²⁶, thiadiazole²⁷, oxadiazole²⁸⁻³⁰, and imidazole³¹ in liquid crystals and liquid crystalline polymers is widely reported. Furthermore, the application of 2,5-thiophenedicarboxylic acid (2,5-TDCA), a heterocyclic monomer similar to 2,5-FDCA, is reported by Cai, Preston and Samulski³². These authors showed that the

replacement of TA with 2,5-TDCA in a thermotropic polyester resulted in a decrease of the melting temperature while maintaining the liquid crystalline nature of the polymer. Unlike furan³³, both the thiophene and oxadiazole moiety are of a mesogenic nature, allowing for the synthesis of non-linear structures exhibiting thermotropic melt-behavior.²⁹ Since the 2,5-furandicarboxylate moiety itself is not a mesogen, 4,4'-biphenol (BP) and BA are employed to ensure the thermotropic behavior of the polymers synthesized in this chapter.

It is acknowledged that 2,5-FDCA tends to undergo side reactions leading to increasingly discolored products at temperatures of 200 °C or higher.³⁴ As early as 1946, Drewitt and Lincoln³⁵ noticed that 2,5-FDCA is prone to decarboxylation and thus evolves CO₂ above 220 °C. Clearly, the decarboxylation and degradation of 2,5-FDCA limits the applicable reaction and processing temperatures. For this reason, the aim of this study is to investigate the viability of the heterocyclic 2,5-FDCA as a monomer in fully aromatic thermotropic polyesters. Considering the polymerization temperature as the limiting factor, in this chapter, a series of polymers containing 2,5-FDCA exhibiting LC behavior in the temperature window of 240 °C to 300 °C are synthesized and characterized.³⁶

The thin-film polymerization (TFP) method reported by Cheng et al.³⁷ is used to screen the incorporation of variable amounts of 2,5-FDCA into the poly(oxybenzoate) backbone and its influence on the evolution of the LC phase. The thin film polymerization is employed to study different monomer compositions to find compositions and reaction parameters suitable for the synthesis of a 2,5-FDCA based thermotropic polyester, without degradation of the monomers. To suppress the melting and polymerization temperatures, the copolymerization of bio-based vanillic acid with 2,5-FDCA is performed. The polymer composition and the polymerization reaction of the monomers are monitored as a function of time using high-temperature fourier-transform infra-red (FTIR) spectroscopy and polarization optical microscopy (POM). Analysis of the polymers with interesting compositions is performed using TGA and DSC. Lastly, preliminary up-scaling experiments are performed to evaluate the thermal properties and the processability of the thermotropic polyesters developed in this chapter.

2.2. Experimental section

2.2.1. Materials

p-Hydroxybenzoic acid, 4-hydroxy-3-methoxybenzoic acid, and zinc acetate (Zn(CH₃O)₂)₂ were obtained from Sigma. 4,4'-biphenol was purchased from TCI Europe. 2,5-Furandicarboxylic acid (99,5% purity, GC-MS) was ordered from Atomole (China). All monomers containing hydroxyl groups were acetylated and recrystallized at least once prior to

polymerization. All other chemicals were used as received unless mentioned otherwise. The monomers used in this study are shown in Figure 2.1.

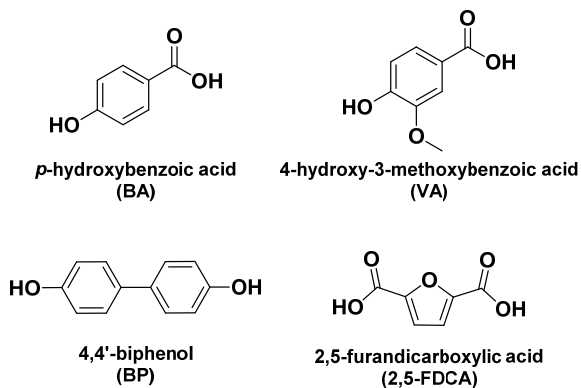


Figure 2.1. Structural formulas of the monomers used in this study.

2.2.2. General acetylation procedure

Ten grams of a monomer containing one or two hydroxyl groups were placed in a 100 mL round-bottom flask on a magnetic stirring plate. Acetic anhydride was added in a slight stoichiometric excess with respect to the hydroxyl groups together with a catalytic amount of H_2SO_4 . The mixture was heated to 80 °C and stirred for four hours. After cooling to 0 °C for one hour 200 mL water was added to the mixture and the solution was filtered. The crystals were washed with water and dried *in vacuo* at 40 °C overnight. All acetylated monomers were recrystallized at least once before usage in polymerization.

2.2.3. Preparation of 4-acetoxybenzoic acid

4-acetoxybenzoic acid was prepared from *p*-hydroxybenzoic acid (10 g, 72.4 mmol) and acetic anhydride (10 mL, 106 mmol) as described in the acetylation procedure. The resulting white powder was recrystallized twice from methanol to yield 8.44 g of product (64.7%). ^1H NMR (MeOD- d_4 , δ , ppm): 8.06 (d, J = 8.80 Hz, ArH, 2H), 7.21 (d, J = 8.80 Hz, ArH, 2H), 4.91 (s, CO-OH, 1H), 2.30 (s, O-CO-CH₃, 3H). ^{13}C NMR (MeOD- d_4 , δ , ppm): 170.57 (CH₃-CO), 169.00 (COOH), 155.97 (ArC-OAc), 132.27 (ArC-COOH), 129.49 (ArC), 122.90 (ArC), 20.95 (CO-CH₃).

2.2.4. Preparation of 4-acetoxy-3-methoxybenzoic acid

4-acetoxy-3-methoxybenzoic acid was prepared from 4-hydroxy-3-methoxybenzoic acid (10 g, 60.9 mmol) and 10 mL of acetic anhydride (106 mmol) as described in the acetylation procedure. The resulting slightly yellow powder was recrystallized twice from toluene to yield 9.34 g of product (72.9%). ^1H NMR (MeOD- d_4 , δ , ppm): 7.69 (d, J = 1.6 Hz, ArH, 1H), 7.64 (dd, J = 8.0 Hz and 1.6 Hz, ArH, 1H), 7.12 (d, J = 8.40 Hz, ArH, 1H), 3.86 (s, O-CH₃, 3H), 2.28 (s, CO-CH₃, 3H). ^{13}C NMR (MeOD- d_4 , δ , ppm): 170.20 (CH₃-C=O), 169.02 (COOH), 152.62 (ArC-OCH₃), 145.11 (ArC-OAc), 130.75 (ArC-COOH), 123.88 (ArC), 123.74 (ArC), 114.51 (ArC), 56.51 (O-CH₃), 20.46 (COCH₃).

2.2.5. Preparation of 4,4'-diacetoxybiphenyl

4,4'-dihydroxydiphenyl (10 g, 54 mmol) was acetylated as described in the general procedure to yield 11,2 g (77%) 4,4'-diacetoxybiphenyl after recrystallization from toluene. ¹H NMR (CDCl₃, δ, ppm): 7.55 (d, *J* = 8.4 Hz, ArH, 4H), 7.16 (d, *J* = 8.4 Hz, ArH, 4H), 2.33 (s, C=O-CH₃, 6H). ¹³C NMR (CDCl₃, δ, ppm): 169.4 (CH₃-C=O), 150.1 (ArC-OAc), 138.1 (ArC-ArC), 128.1 (ArC), 121.9 (ArC), 21.1 (CO-CH₃).

2.2.6. Methods

Thin-film polymerizations (TFP)s monitored by POM were conducted on a Zeiss Axioplan 2 Imaging optical microscope under crossed polarizers with or without a λ wave plate and CD achorplan objectives (20x or 32x Zoom). A THMS 600 heating stage connected to a Linkam TMS 94 control unit was mounted on the optical microscope. The monomers were dried overnight *in vacuo* at 40 °C, mixed and grinded twice before usage. It should be noted that all hydroxyl groups of the monomers used in polymerization were acetylated prior to polymerization. Samples were prepared by placing 2-5 mg of a monomer mixture in between two glass slides with a ring spacer, where the sample was placed on the top glass slide. Samples were heated from room temperature with 100 °C/min to the desired reaction temperature and all reactions were conducted under a N₂ flow. The reaction time (*t_r*) is set to 0 when the desired reaction temperature was reached. Calibration of the temperature was performed using the melting temperatures of well-known compounds. Temperature calibration showed a 20 °C ± 3 °C difference from the input temperature and all temperatures mentioned in this chapter are corrected values. The reactions were followed on-line and images were acquired every second. ATR-FTIR measurements were performed on a Bio-rad FTS6000 FTIR Spectrometer with an ATR-plate connected to a high temperature golden gate with a maximum temperature of 300 °C. Samples were measured by the placement of 2-5 mg sample onto the hot plate at a fixed reaction temperature and spectra were collected on-line with intervals of two seconds using a liquid nitrogen-cooled WB MCT detector with a resolution of 4 cm⁻¹. A cover was placed on the top of the ATR plate and was connected to N₂ flow to prevent evaporation and degradation of the monomers.

Wide-angle X-ray diffraction (WAXD) measurements were performed in transmission mode, on a Bruker AXS HI-STAR area detector, installed with P4 Diffractometer, using graphite-monochromated Cu K α radiation (λ = 0.154 nm) and a 0.5 mm collimator. The data was collected on both crude material and materials obtained from preliminary spinning experiments. The 2D data were corrected for detector non-uniformity and spatial distortion. Subsequently, background subtraction was performed and optionally the 2D data were transformed into a 1D profile via integration.

Thermal decomposition studies were performed on a TA instruments TGA Q500 machine under N₂ rich atmosphere. Samples were heated at 20 °C/min from 20 °C to 800 °C. Temperature calibration was performed using the Curie points of high-purity aluminum, nickel and perkalloy standards.

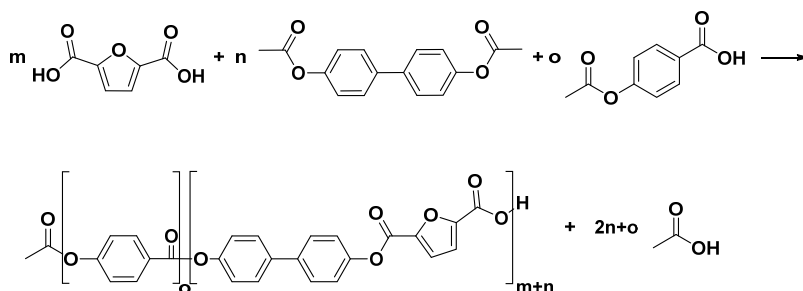
The thermal behavior of the samples was studied using a TA instruments Q1000 DSC. The apparatus was calibrated using indium and aluminum oxide. The normal heating and cooling-rates of the samples were 10 °C/min and measurements were performed under a N₂ rich atmosphere.

2.3. Results and Discussion

2.3.1. Phase behavior of 2,5-FDCA/BP/BA system

The thin-film polymerization (TFP) method, described by Cheng³⁷, was used to follow the influence of the copolymerization of 2,5-furandicarboxylic acid (2,5-FDCA) and 4,4'-dicatoybiphenyl (DABP) on the LC behavior during a polymerization of *p*-acetoxybenzoic acid (ABA). It should be noted that during the discussions in this chapter the abbreviations ABA and BA and DABP and BP are used. For clarification, ABA and DABP refer to the unreacted *p*-acetoxybenzoic acid and 4,4'-diacetoxybiphenyl monomers used for polymerization, whereas BA and BP refer to the *p*-oxybenzoate and 4,4'-biphenol moieties present in the polymer backbone, after polymerization. Similarly, acetylated vanillic acid (4-acetoxy-3-methoxybenzoic acid, AVA) and the 4-oxy-3-methoxybenzoate (VA) moiety are used in the discussion of the data.

The synthesis of polymers having different 2,5-FDCA, BP and BA compositions were monitored along a broad temperature range between 220 °C to 380 °C, and the morphological changes were monitored via polarization optical microscopy. Scheme 2.1 shows the reaction scheme of the polycondensation reaction occurring in the thin-film polymerization of 2,5-FDCA/DABP/ABA systems. During this reaction, polymerization proceeds through acidolysis condensation reactions, liberating acetic acid as the condensate. Figure 2.2 shows an example of the development of the morphology during the ongoing polymerization of the 2,5-FDCA/DABP/ABA 15/15/70 system at a reaction temperature of 300 °C. All micrographs were taken from the same area of the sample over time, under isothermal conditions. The micrographs show the typical morphological changes occurring during the synthesis of high melting, thermotropic polyesters. During this process, transformation of the isotropic phase to the LC phase ($t_r \sim 20s$) is observed, followed by the coalescence and homogenization of the LC phase ($t_r \sim 20-60s$) and crystallization ($t_r > 4 m$). Melting of the crystals formed during the synthesis of the 2,5-FDCA/BP/BA 15/15/70 copolymer is observed at 380 °C upon heating at 10 °C/min. Because of the rapid degradation of the monomers, a TFP to follow the development and morphology of the LC melt of the 2,5-FDCA/BP/BA 15/15/70 copolymer at 380 °C could not be performed.



Scheme 2.1. Reaction scheme of the acidolysis polycondensation occurring during a TFP of 2,5-FDCA, DABP, and ABA. *N.b.* The resulting polymer can be of a random or blocky nature.

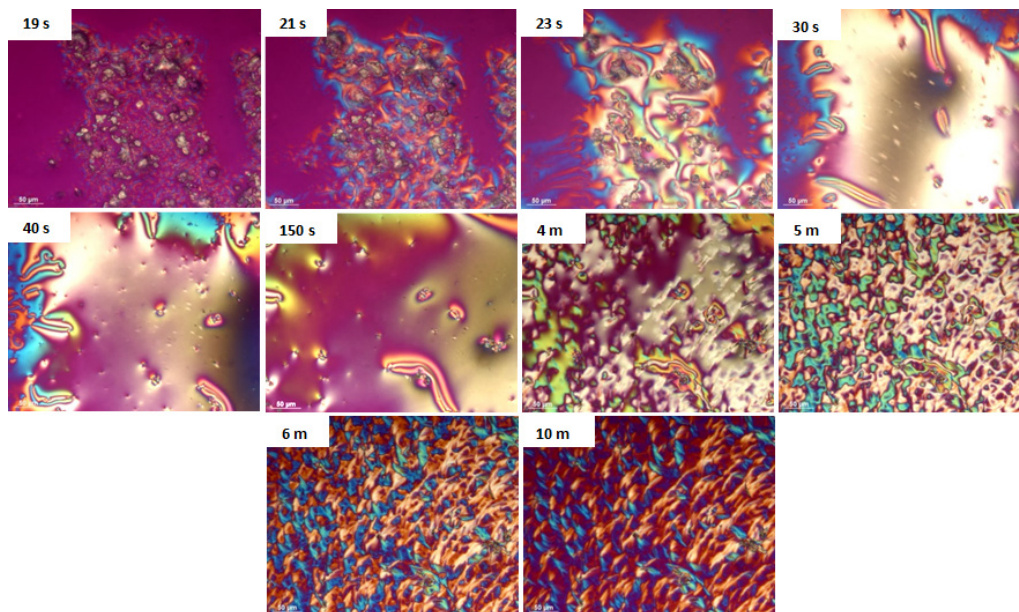


Figure 2.2. Optical micrographs showing the transitions from isotropic to the liquid-crystalline and to the crystalline phase during the TFP of the 2,5-FDCA/BP/BA 15/15/70 polymers at 300 °C. All micrographs were taken in between cross-polars and red wave plate. The mentioned time on the micrographs refers to the reaction time (t_r).

Figure 2.2 shows that the formation of the LC droplets occurs ($t_r = 19\text{-}23\text{s}$) prior to the full dissolution of the 2,5-FDCA crystals, indicating that the 2,5-FDCA is poorly soluble in the monomer/oligomer mixture. It is expected that the poor solubility of 2,5-FDCA allows the reaction to progress simultaneously with the dissolution of the 2,5-FDCA crystals, i.e. polymerization initiates on the surface of the 2,5-FDCA crystals. Hence, during polymerization, the crystals react and dissolve from the outside in. The participation of 2,5-FDCA in polymerization will thus be limited by the reaction temperature, by the availability of reactive groups, and by the surface to volume ratio of the 2,5-FDCA crystals.

Similar behavior was observed by Economy during a copolymerization of ABA with TA and BP.¹ This author showed that the poor solubility of TA resulted in the formation of domains with a oxybenzoate/4,4'-biphenol rich content. Rapid crystallization of the system prohibited the transesterification in the LC melt and resulted in a high degree of phase segregation of the monomers in the form of blocks in the final polymer. This slow dissolution behavior of TA was confirmed by Cheng *et al.*³⁸ during the TFP of ABA/DABP/TA systems.

It is expected that the polymers formed during the TFP of 2,5-FDCA/DABP/ABA systems exhibit a high degree of block formation, similar to the systems studied by Economy. The LC droplets formed in the initial phase of polymerization have an oxybenzoate/4,4'-biphenol rich composition, due to the unavailability of 2,5-FDCA in the liquid phase. The phase transformation from LC to crystal phase occurs once the 2,5-FDCA monomers have fully reacted. The blocky nature of the formed polymer is maintained since transesterification from the melt is prevented by the rapid crystallization (>4 m, Figure 2.2).

To follow the incorporation of the 2,5-FDCA monomer into the polymer backbone, a TFP was followed with time using ATR-FITR at 300 °C (Figure 2.3). The FTIR results show a rapid decrease of the signal for the CH₃ vibration band of the acetoxy end-group at 1376 cm⁻¹ (C=O-CH₃), the carbonyl stretch band of the acetoxy end-group at 1770 cm⁻¹, and carbonyl stretch band of the free acid group at 1703 cm⁻¹. This indicates that the concentration of the reactive end-groups decreases with polymerization. Simultaneously, the increase of the signal of the aromatic ester carbonyl stretch band at 1735 cm⁻¹ indicates that the aromatic ester groups are formed, thus polymerization occurs. The incorporation of 2,5-FDCA in the final polymer can be detected by the presence of bands at 943 and 1567 cm⁻¹ corresponding to the vibrations of the furan ring.³⁹

The presence of insoluble 2,5-FDCA crystals limits the polymerization rate at low reaction temperatures or in reactions with a very high 2,5-FDCA content. The time required for the 2,5-FDCA to fully dissolve and participate in the reaction increases with the increasing 2,5-FDCA concentrations and thus extends the reaction time. However, with the extended reaction times, the oxybenzoate/4,4'-biphenol rich blocks will have more time to build up molecular weight and will be able crystallize during polymerization. Figure 2.4a shows an example of the polymerization of the 2,5-FDCA/DABP/ABA 35/35/10 system at 280 °C where, due to the presence of undissolved 2,5-FDCA crystals, polymerization cannot be completed. When the polymerization is performed at 280 °C, the formation of an LC phase is visible after 120 seconds, but does not develop over the whole view area. Instead, the LC domains crystallize and the undissolved 2,5-FDCA crystals remain present ($t_r = 480$ s). When the same reaction is conducted at 300 °C, a full dissolution and simultaneous reaction

of the 2,5-FDCA monomers is achieved over time and the development of a homogeneous LC phase is observed (Figure 2.4b). On further polymerization (beyond $t_r = 180$ s) the LC phase transforms into the crystalline phase.

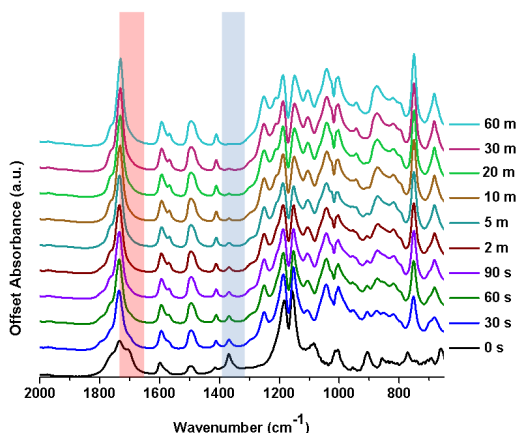


Figure 2.3. Overview of the ATR-FTIR spectra collected with increasing polymerization time between 2000 and 650 cm^{-1} , obtained during a TFP of the 2,5-FDCA/DABP/ABA 15/15/70 system at 300 $^{\circ}\text{C}$.

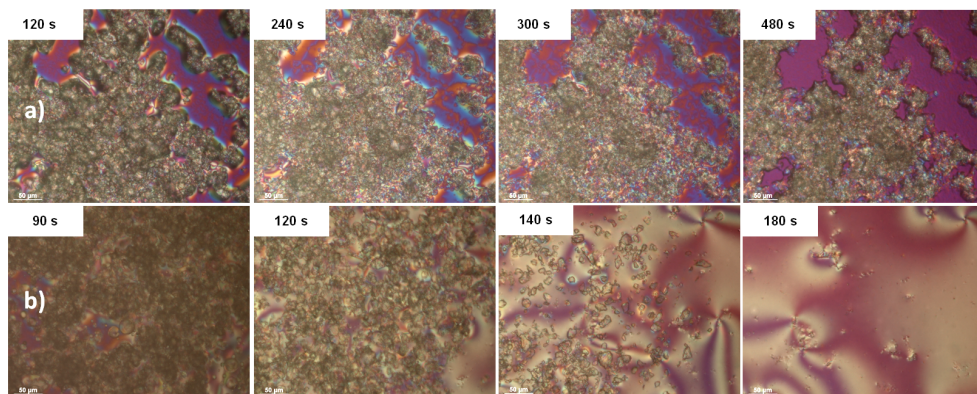


Figure 2.4. Optical micrographs showing the morphological changes of the LC phase formation during the TFP of the 2,5-FDCA/DABP/ABA 35/35/30 reaction system under isothermal condition at a) 280 $^{\circ}\text{C}$ and b) 300 $^{\circ}\text{C}$.

The effect of reaction temperature and composition on the LC layer formation and early precipitation in the 2,5-FDCA/DABP/ABA systems was determined, and is shown in a phase diagram as a function of 2,5-FDCA content (Figure 2.5). Region *I* in Figure 2.5 indicates the regime where a full dissolution and reaction of the 2,5-FDCA monomers occurs, while region *II* indicates the regime where crystallization occurs prior to the full reaction of the 2,5-FDCA monomers. Generally, the reaction temperature required to reach full conversion increases with the increasing 2,5-FDCA

concentration to a maximum of 330 °C for systems having 41 mol% or higher amounts of 2,5-FDCA. Apparently, the reaction temperature of 330 °C lies close enough to the melting temperature of 2,5-FDCA of 342 °C to allow rapid dissolution and reaction.⁴⁰

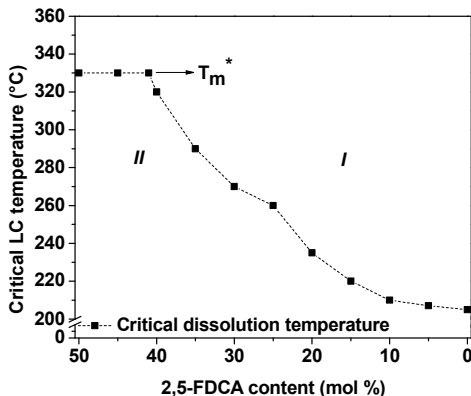


Figure 2.5. The increase of the critical dissolution/reaction temperatures as a function of the 2,5-FDCA content in the 2,5-FDCA/DABP/ABA systems. The ratio of 2,5-FDCA/DABP is kept equimolar. The T_m^* denotes the temperature where all visible 2,5-FDCA crystals are molten/dissolved at the start of the reaction, independent of the amount of 2,5-FDCA present in the system (>330 °C).

The 2,5-FDCA/BP/BA copolymers shows LC behavior along the whole range of compositions. However, the temperature required to observe the LC phase increases steadily from 200-210 °C for pure poly(oxybenzoate) to 340 °C for a 2,5-FDCA/BP/BA 40/40/20 copolymer. Above this temperature, the LC phase is observed, but if the reaction temperature is too low, crystallization from the isotropic melt occurs. For example, the LC phase is only observed above 360 °C during the synthesis of poly(4,4'-biphenylene 2,5-furanoate).

In the discussion of the data obtained thus far via the TFP, the effect of the thermal instability of the 2,5-FDCA monomer on the polymerization has been neglected. According to the Gruter³⁴ and Drewitt³⁵, it should be realized that the maximum polymerization temperature of 2,5-FDCA is 280 °C or lower, since severe discoloration occurs at 280 °C or higher. Preferably, reactions containing 2,5-FDCA should be conducted below 220 °C to fully prevent side reactions. According to Figure 2.5, only the 2,5-FDCA/BP/BA copolymer with ~30 mol% 2,5-FDCA or less can be synthesized at 280 °C or lower, without having the reaction mixture crystallizing prior to the full dissolution of the 2,5-FDCA monomers.

2.3.2. Tuning the melting temperature of 2,5-FDCA based polymers.

Since the high melting temperatures of the 2,5-FDCA/BP/BA copolymers do not allow molecular weight build-up, mainly due to rapid crystallization from the melt, 4-

acetoxy-3-methoxybenzoic acid (AVA) has been used as a comonomer during polymerization. It was anticipated that the presence of the methoxy group of VA perturbs the crystal lattice of the 2,5-FDCA/BP/BA copolymers and lowers the melting temperature. For this reason, systems where a small fraction of ABA was replaced by AVA were investigated using the TFP to determine the influence of AVA on the melting temperature. It is conclusively demonstrated that, on fixing the 2,5-FDCA/DABP content to 30 mol% and by varying the amount of AVA between 0 and 20 mol%, a series of polymers having thermotropic LC behavior can be obtained. Figure 2.6 shows an example of the morphological changes observed during the synthesis of a 2,5-FDCA/BP/BA/VA 15/15/60/10 copolymer at 300 °C.

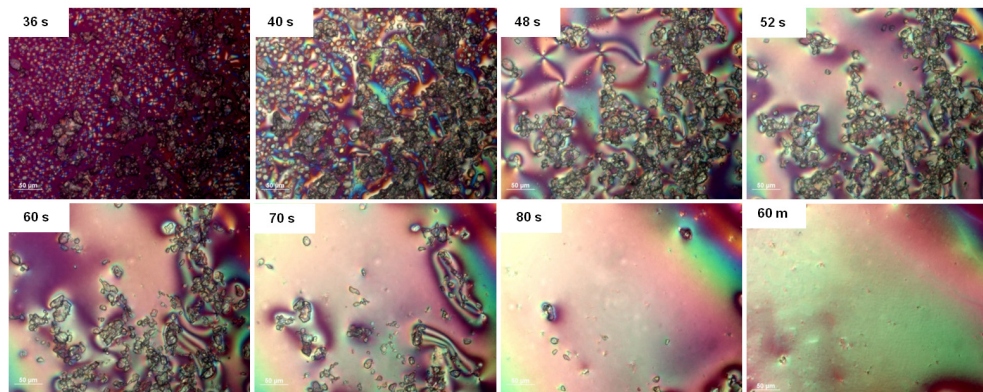


Figure 2.6. Optical micrographs showing formation of a stable LC melt in a TFP of the 2,5-FDCA/DABP/ABA/AVA 15/15/60/10 reaction system at 300 °C.

As is visible from Figure 2.6, the formation of the LC phase occurs prior to the complete dissolution of the 2,5-FDCA crystals. These observations are similar to the observations in the 2,5-FDCA/DABP/ABA 15/15/70 TFP, where 2,5-FDCA monomers are not distributed randomly along the polymer chains in the initial stage of polymerization. To recall, in the 2,5-FDCA/BP/BA 15/15/70 copolymers, the distribution of the monomers along the main chain is thought to be of a blocky nature due to rapid crystallization of the polymer chains during polymerization, preventing transesterification. However, the absence of crystallization during polymerization in the 2,5-FDCA/BP/BA/VA 15/15/60/10 copolymer allows for transesterification in the melt, promoting a random distribution of the monomers along the chain and limiting the block formation.

In Figure 2.6, with the increasing polymerization time, the LC drops coalesce rapidly and a typical Schlieren texture is formed while the 2,5-FDCA monomer dissolves and reacts. The LC phase is observed in full view of the optical micrograph after 2 minutes of reaction time. The LC melt does not show any phase transition within 60 minutes of reaction time and remains in the mobile melt phase. The absence of crystallization

allows for build-up of molecular weight by transesterification in the LC melt. Upon cooling at 10 °C/min, solidification of the sample is observed at 230-240 °C (T_c), while upon heating at 10 °C/min again, the crystal to LC transition is observed around 270-280 °C (T_m). Similar experiments are performed with the 2,5-FDCA/DABP/ABA/AVA 15/15/50/20 reaction system at different reaction temperatures. Similarly, the formation of a homogeneous LC phase is observed in this system and no crystallization occurs within 60 minutes of reaction time. The system shows crystallization at 200 °C upon cooling at 10 °C/min and on heating shows the transition from the crystalline to the LC phase at 240 °C. This data clearly indicates that AVA decreases the melting temperature of the 2,5-FDCA/DABP/ABA systems and provides opportunities for increasing the molecular weight in the LC phase at temperatures below 300 °C.

The thermal stability of the 2,5-FDCA/BP/BA/VA polymers containing 0% VA, 10% VA and 20% VA, synthesized through TFP at 300 °C, are evaluated by TGA. Figure 2.7 shows the thermograms of the analyzed polymers. The 2,5-FDCA/BP/BA/VA 15/15/70/0 copolymer shows an onset of weight loss (T_{ons}) at 475 °C, but partial weight loss of 5 wt% occurs around 350-370 °C. The partial weight loss of the polymer is likely to be a result of the limited thermal stability of the low molar mass component of the polymer that crystallizes during polymerization (as is detected in Figure 2.2). The introduction of VA into the 2,5-FDCA/BP/BA copolymer backbone decreases the onset temperature for thermal degradation from 475 °C to 411 °C. Furthermore, the polymers showed no weight loss for at least one hour at the isothermal temperature of 300 °C as observed by TGA.

DSC analysis of the different copolymers synthesized using the TFP at 300 °C is performed and the information from the second heating runs is depicted in Figure 2.8. It should be noted that the peak melting temperature (T_m) of the first heating run of the 2,5-FDCA/BP/BA/VA 15/15/70/0 copolymer is observed at 369 °C, but shifts to 330 °C during the second heating run. This shift is expected to be a result of the partial degradation, as observed in the TGA analysis. However, also the transesterification occurring upon melting of the sample in the DSC can lower the melting temperature observed in the second heating run. From the data shown in Figure 2.8, it is evident that the copolymerization of VA lowers the peak melting temperature, causes a broadening of the melting endotherm, and decreases the melt enthalpy (ΔH_{melt}) of the melting transition. Furthermore, the glass transition temperatures (T_g) of the copolymers containing AVA become more pronounced and shift to higher temperatures with the increasing VA content (Table 2.1). This increase of the T_g is likely to arise because of the distribution of methoxy groups along the backbone, limiting the rotational motion of the aromatic rings in the polymer chains.

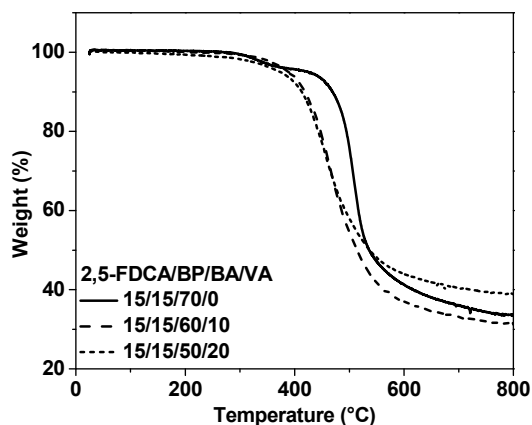


Figure 2.7. TGA thermograms showing a decrease of the weight loss temperature with the copolymerization of VA in 2,5-FDCA/BP/BA/VA 15/15/70/0, 15/15/60/10 and 15/15/50/20 copolymers synthesized via the TFP route at 300 °C.

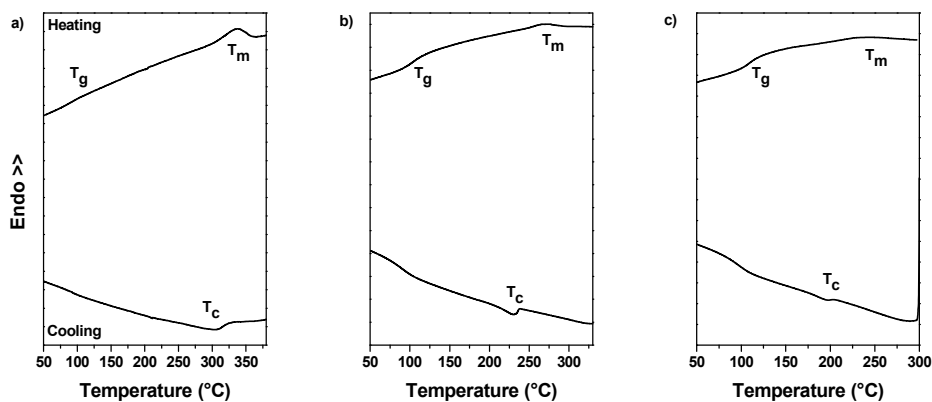


Figure 2.8. Second heating and cooling DSC traces showing the decrease of the melting temperature with the increasing amount of VA in the 2,5-FDCA/BP/BA/VA a) 15/15/70/0, b) 15/15/60/10 and c) 15/15/50/20 copolymers synthesized at 300 °C via the TFP method.

Table 2.1. Thermal data showing the influence of VA on the T_g , T_m , ΔH_{melt} and T_{ons} of 2,5-FDCA/BP/BA/VA copolymers.

AVA content	T_g^a (°C)	T_m^a (°C)	ΔH_{melt}^a (J/g)	T_m^b (°C)	T_{ons}^c (°C)
0 mol%	97	337	6.80	360-380	460
10 mol%	104	275	1.77	270-280	411
20 mol%	109	230	0.66	240-250	402

a) Obtained from the second heating runs in DSC experiments during heating and cooling at a rate of 10 °C/min, b) Obtained from optical microscopy experiments during heating and cooling at a rate of 10 °C/min, c) Obtained from TGA experiments with a heating rate of 20 °C/min.

2.3.3. Comparing TFPs with scaled up experiments.

Preliminary up-scaling experiments of the 2,5-FDCA/DABP/ABA/AVA 15/15/60/10 reaction system were performed on a 100 gram scale with maximum reaction temperatures (T_r) ranging from 260 °C to 340 °C. The polymerization was performed in a 500 mL three-neck round-bottom flask filled with a total of 100 gram of the 2,5-FDCA/DABP/ABA/AVA monomer mixture with a catalytic amount of $Zn(CH_3O_2)_2$. The mixture was heated slowly to 200 °C and the temperature was increased over time to the desired temperature of 260 °C, 280 °C, 300 °C, 320 °C or 340 °C over a period of 3 hours. Acetic acid was collected over of time and the reaction kept isothermal until more than 90% of the calculated amount of acetic acid had distilled off. Reduced pressure (<5 mbar) was applied to the system for one hour to remove the last traces of acetic acid. The final product was isolated from the hot reactor flask and ground after cooling.

Detailed molecular characterization could not be performed due to the insolubility of the synthesized polymers. However, the number average molecular weights and compositions could be estimated from the 1H NMR spectra, obtained after hydrolysis of the samples in MeOD/NaOD in D_2O 1:1 (Table 2.2). The polymer composition is obtained by taking ratio of the integrals corresponding to the protons of the different monomers. For the determination of the number average molecular weight (M_n), it was assumed that all polymer chains contain one acetoxy end-group and one free carboxylic acid group. To illustrate, Figure 2.9 shows the 1H NMR spectrum of the hydrolyzed polymer I listed shown in Table 2.2.

Table 2.2. Influence of the reaction temperature on the thermal properties and molecular weight build-up in 100 gram batch polymerization of 2,5-FDCA15/DABP15/ABA/AVA systems with varying amounts of AVA.

Entry	AVA feed composition (mol%)	T_r (°C)	T_n^a (°C)	T_{ons}^b (°C)	DP ^c	M_n^c (g/mol)
I	10	300	270	427	58	7,900
II	10	280	273	410	21	2,300
III	20	280	234	412	25	3,100

a) Determined using DSC analysis, b) Determined using TGA analysis, c) Estimated from 1H NMR spectroscopy of the product obtained after hydrolysis in a MeOD/NaOD in D_2O mixture.

As expected, attempts to perform the reactions at 320 °C and 340 °C yielded heavily discolored and thermally instable products. The reaction performed at 300 °C (Entry I, Table 2.2) yielded a dark brown polymer indicating that the 2,5-FDCA monomer did undergo (partial) degradation. Although degradation of 2,5-FDCA did occur during polymerization, the molecular weight calculated after degradation in MeOD/NaOD in D_2O is close to 8,000 g/mol. As expected, decreasing T_r to 280 °C led to a decrease in discoloration, but also limited the molecular weight build-up. For polymerizations performed at 280 °C, longer reaction times were required to evolve

acetic acid and resulted in some sublimation of monomer over time. Analysis of the sublimed product indicated the presence of 2,5-FDCA and its decarboxylated product 2-furancarboxylic acid. This indicates that the slow sublimation of 2,5-FDCA limits the molecular weight build-up observed at 280 °C. Furthermore, the 2-furancarboxylic acid formed upon decarboxylation of 2,5-FDCA acts as a chain stopper and limits the molecular weight build-up of the polymer further.

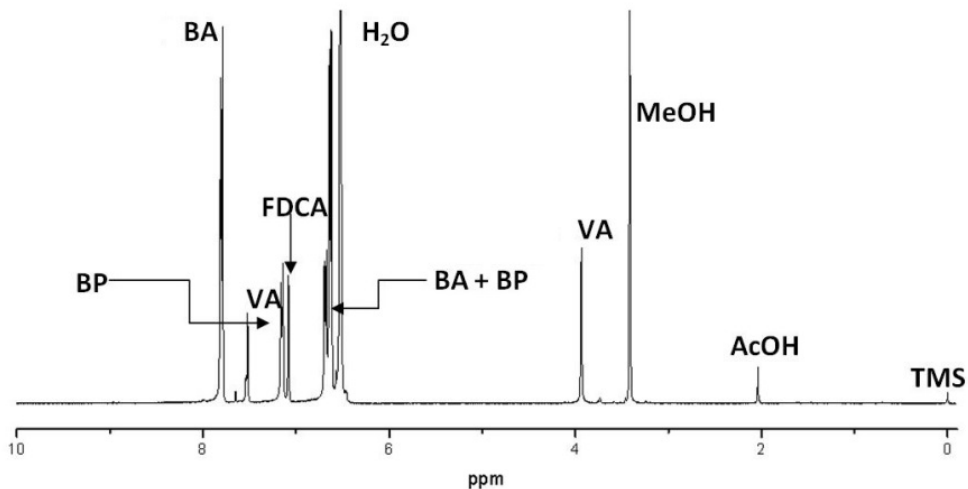


Figure 2.9. ^1H NMR plot of Entry I listed Table 2.2, hydrolyzed and measured in a 1:1 mixture of MeOD : 40%NaOD in D_2O .

Very mild discoloration occurred when the reaction was performed at 260 °C, but molecular weight build-up was not achieved, even after allowing the mixture to react for 20 hours. Similar to the reaction performed at a T_r of 280 °C, sublimation of monomers occurred on the inside of the reactor wall. It is known that the reaction kinetics in scaled-up experiments are significantly slower due to the less effective acetic acid removal compared to TFPs. In a TFP, a small amount of polymer is synthesized with a large surface to volume ratio, enabling the rapid removal of acetic acid and a rapid build-up of molecular weight. However, for the scaled up reactions the removal of the condensate is limiting the reaction rate, requiring a longer reaction time to build up molecular weight. Considering the poor dissolution and slow reaction behavior of 2,5-FDCA, the 2,5-FDCA sublimation and decarboxylation will be more severe in the scaled-up experiments. As observed in our experiments, increasing the reaction temperature does lead to an increase in reaction and dissolution kinetics and molecular weight build-up, but is again limited by the degradation and side reactions of the 2,5-FDCA at T_r above 300 °C. Thus to enhance the molar mass without degrading 2,5-FDCA the requisite is to perform polymerization at lower reaction temperatures.

Nonetheless, both the T_m and T_g of the products prepared in the large scale experiments (Table 2.2) agree well with the T_m and T_g of polymers obtained in the TFP. Furthermore, the 1D WAXD patterns of polymers I and III from Table 2.2 and the previously obtained polymer without vanillic acid show that the copolymerization of VA leads to a decrease of the crystalline fraction. As anticipated, the incorporation of AVA perturbs the crystal lattice of the 2,5-FDCA/BP/BA 15/15/70 copolymer, indicated by the broadening of the inter-chain diffraction peak at $20.1^\circ 2\theta$ ($d = 4.4 \text{ \AA}$) shown in Figure 2.10.

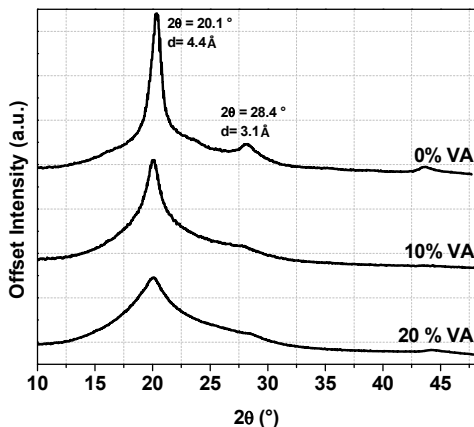


Figure 2.10. 1D WAXD patterns of the crude scaled-up polymers containing 0 mol% VA, 10 mol% VA (Entry I table 2.2) and 20 mol% VA (Entry III table 2.2).

Preliminary fiber drawing from the LC phase was performed by heating the polymers to 340°C on a hot plate and by pulling a strand by hand using tweezers (Figure 2.11). The 2D WAXD patterns of strands of polymer I and II are shown in Figure 2.12. The 2D WAXD fiber patterns of these polymers, though drawn in an uncontrolled way, show the presence of highly oriented chains and resemble the diffraction patterns of Vectran fibers spun from the commercial Vectra[®] polymer series.⁴¹

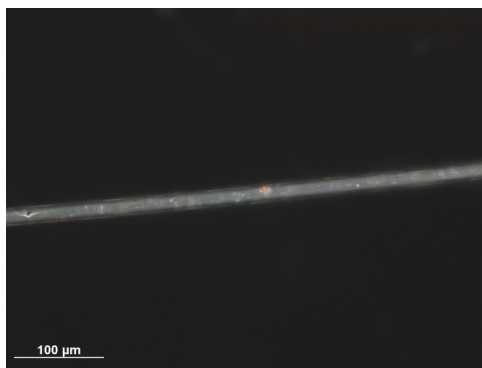


Figure 2.11. Optical micrograph in between cross-polars showing the smooth surface and birefringent nature of the hand drawn fiber of polymer I, obtained upon drawing at 340 °C

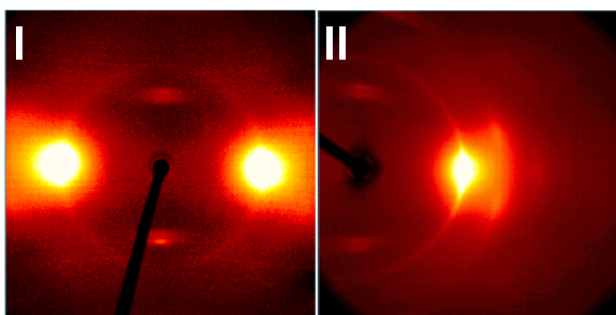


Figure 2.12. 2D WAXD patterns of hand-drawn fibers of polymers I and II, showing a high degree of orientation. The pattern of polymer II shows a higher crystallinity due to faster crystallization kinetics resulting from the lowered molecular weight compared to polymer I.

2.4. Conclusions

The thin-film polymerization is employed to successfully study the 2,5-FDCA incorporation in aromatic thermotropic polyesters. The 2,5-FDCA monomer shows a limited solubility and reactivity behavior in the melt, similar to terephthalic acid. The limited solubility requires extended reaction times or increased reaction temperatures to successfully dissolve the 2,5-FDCA monomer and incorporate it into the polymer backbone. However, the thermal stability of 2,5-FDCA limits the reaction temperature and reaction temperatures well below 300 °C are preferred. The copolymerization of AVA successfully decreases the melting temperature and indicates that there is a window for the synthesis of polymers containing 2,5-FDCA in a melt-polycondensation temperatures below 300 °C. The screening method adopted here has been helpful in identifying the monomer mixtures and reaction conditions that are required for up-scaling reactions. Molecular weight build-up in these up-scaling reactions was limited due to the decarboxylation of 2,5-FDCA during polymerization. In short, it can be concluded that, although 2,5-FDCA based thermotropic polyesters

can be synthesized in a small scale TFP, a significantly lower reaction temperature is required successfully synthesize 2,5-FDCA based thermotropic polyesters on a large scale.

2.5. References

- [1] Economy, J., *Mol. Cryst. Liq. Cryst.*, **1989**, 169, 1-22
- [2] Chung, R.S., Calundann, G.W., East, A. J., Liquid crystalline polymers and their applications, *Encyclopedia of Engineering Materials*, Vol. 2, Marcel Dekker Publisher, New York, **1989**, 65
- [3] Collyers, A. A., *Mater. Sci. Tech.*, **1989**, 5, 309
- [4] Jackson, W., *The British Polymer Journal*, **1980**, 12, 4, 154-162
- [5] Gray G.W., Spiess H., Vill V., *Handbook of liquid crystals Vol 3*, Wiley-VCH, ed by Demus D., Goodby, J., **1998**
- [6] Cottis, S.G., Economy, J., Nowak, B.E., US Patent 3 637 595, **1972**
- [7] Calundann, G.W., US Patent 4,067,854, **1978**
- [8] Rosenau-Eichin, R., Ballauff, M., Grebowicz, J., Fischer, E.W., *Polymer*, **1988**, 29, 518-525
- [9] Griffin, B.P., Cox, M.K., *The British Polymer Journal*, **1980**, 147-153
- [10] Kricheldorf, H.R., Erxleben, J., *Polymer*, **1990**, 31, 944-948
- [11] Jackson, W.J., Kuhfuss, H.F., *J. Polym. Sci., Polym. Chem. Ed.*, **1976**, 14, 2043-2058
- [12] Han, H., Bhowmik, P.K., *Prog. Polym. Sci.*, **1997**, 22, 1431-1502
- [13] Ballauff, M., *Angewandte Chemie*, **1989**, 101, 261-276
- [14] Windle, A.H., *Liquid Crystalline and Mesomorphic Polymers*, **1994**, Springer-Verlag, New York. Chapter 2, Ed. By Shibaev, V.P, and Lam, Lm,
- [15] Lin, J., Sherrington, D.C., *Advances in Polymer Science*, **1994**, 111, 177-219
- [16] Varshney, S.K., *J. Macromol. Sci., Rev. Macromol. Chem. Phys.*, **1986**, C26, 4, 551
- [17] Dobb, M.G., McIntyre, J.E., *Adv Polym Sci*, **1984**, 60/61, 61-98
- [18] Chung, T-S., *Polymer Engineering and Science*, **1986**, 26, 13, 901-919
- [19] Jackson, W.R., Jr., *Mol. Cryst. Liq. Cryst.*, **1989**, 169, 23-49
- [20] Shaikh, A., Janka, M. E., Lange, D. M., Morrow, M. C., Bowers, B. R., Parker, K. R. Partin, L.R. Jenkins, J. C., Moody, P., Shanks, T. E., Sumner, J.R., Charles E., US patent, 20120302772 A1, **2012**
- [21] Li, X.G, Huang, M.R., *Polym.-Plast. Technol. Eng.*, **2000**, 39(2), 317-331
- [22] Li, X.G., Huang, M.R., Guan, G-H., Sun, T., *Journal of Applied Polymer Science*, **1997**, 66, 2129-2138
- [23] Nagata M., *Journal of Applied Polymer Science*, **2000**, 78, 2474-2481
- [24] Vriesema, B. K., Miniaci, F., EU Patent 88200912.9, **1988**
- [25] Fujioka, Y., Mochizuki, M., Nagea Y, Japanese patent 2012122023 A, **2012**
- [26] Teoh M.M., Liu, S.L., Chung, T.S., *J. Polym. Sci., Part B: Polym. Phys.*, **2005**, 43, 2230-2242
- [27] Sato, M., Matsuoka, Y., Yamaguchi, I., *J. Polym. Sci., Part A: polym. Chem.*, **2007**, 45, 2998-3008
- [28] Guseva, M.A. et al., *Khimicheskie Volonka*, **1986**, 3, 13-15
- [29] Zafiroopoulos, N.A., Choi, E-J., Dingemans, T., Lin, W., Samulski, E.T., *Chem. Mater.*, **2008**, 20, 3821-3831
- [30] Dingemans, T.J. , Madsen, L.A., Zafiroopoulos, N.A., Lin, W., Samulski, E.T., *Phil. Trans. R. Soc. A.*, **2006**, 2681-2696
- [31] Pielartzik, H., 1988, EP 0 303 931 A2
- [32] Cai, R., Preston, J., Samulski, E.T. *Macromolecules*, **1992**, 25, 563-568
- [33] Seed, A.J., Hird, M., Styring, P., Gleeson, H.F., Mills, J.T., *Mol. Cryst. Liq. Cryst.*, **1997**, 299, 19-25
- [34] Gruter, G-J. M., Sipos, L., Dam, M.A., *Combinatorial Chemistry & High Throughput Screening*, **2012**, 15, 180-188

- [35] Drewitt, J.G.N., Lincoln, J., Br. Patent, 621971, **1946**, November 12
- [36] Wilsens, C.H.R.M., Rastogi, S., Veld, M.A.J., Klop, E.A., Noordover, B.A.J. WO 2013092667 A1, **2013**.
- [37] Cheng, S-X., Chung, T-S., Mullick, S., *Chemical Engineering Science*, **1999**, 54, 663-674
- [38] Cheng, S-X., Chung, T-S., *J. Polym. Sci., Part B: Polym. Phys.*, **2000**, 38, 2221-2331
- [39] Gandini, A., Silvestre, A.J.D., Neto, C.P., Sousa, A.F., Gomes, M., *J. Polym. Sci. Part. A: Polym. Chem.*, **2009**, 47, 295-298
- [40] Haworth, W.N., Jones, W.G.M., Wiggins, L.F., *J. Chem. Soc.*, **1945**, 1-4
- [41] Kalfon-Cohen, E., Marom, G., Weinberg, A., Wachtel, E., Migliaresi, C., Pegoretto, A., *Polym. Adv. Technol.*, **2007**, 18, 771-779

Chapter 3

Thermotropic polyesters from 2,5-furandicarboxylic acid and vanillic acid: Synthesis, thermal properties, melt-behavior, and mechanical performance

Abstract

In this chapter, the synthesis of low melting aliphatic-aromatic 2,5-furandicarboxylic acid (2,5-FDCA) based thermotropic polyesters that exhibit stable nematic melts up to 300 °C is addressed. It is demonstrated that the copolymerization of the renewable monomers 2,5-FDCA, suberic acid (SuA) and vanillic acid (VA) can be performed in the absence of degradation and side reactions through the application of low reaction temperatures. The chemical structures, molecular weights, phase transitions, thermal behavior, and mechanical performance of the synthesized polymers are studied using polarization optical microscopy, WAXD, DSC, TGA, DMTA, solid-state NMR spectroscopy, rheology, and tensile tests. It is shown that the incorporation of the rigid, aromatic 2,5-FDCA moiety enhances the formation of blocky copolymers, whereas the VA moiety tends to decrease the block formation. When combined, random thermotropic polyesters containing 2,5-FDCA and VA with high aromatic contents are obtained. Mechanical characterization shows that the performance of these polymers is correlated to their crystallinity. Surprisingly, a higher crystallinity results in ductile behavior, whereas a lower crystallinity results in a higher modulus, a higher stress at break, and a lower strain at break. Furthermore, it is demonstrated that the renewable 2,5-FDCA and VA moieties require more thermal energy to become mobile compared to the phenyl rings of *p*-hydroxybenzoic acid, hydroquinone, and 4,4'-biphenol.

This chapter is partially based on Wilsens, C.H.R.M., Verhoeven, J.M.G.A., Noordover, B.A.J., Hansen, M.R., Auhl, D., Rastogi, S., *Macromolecules*, **2014**, 47, 3306-3316.

3.1. Introduction

In the previous chapter of this thesis it was demonstrated that 2,5-furandicarboxylic acid (2,5-FDCA) can be used as a comonomer for the synthesis of fully aromatic poly(oxybenzoate) based thermotropic liquid crystalline polyesters (TLCP)s. However, it was also observed that the maximum reaction temperature applied during the synthesis of 2,5-FDCA based polymers *via* a melt polycondensation is limited by the thermal stability of 2,5-FDCA. The reaction temperatures required to synthesize fully aromatic polyesters with high molecular weights resulted in partial degradation of the 2,5-FDCA monomer and prevented extensive molecular weight build-up. From this data it is clear that a further suppression of the melting temperature is required to successfully incorporate 2,5-FDCA into the polymer backbone and to prevent degradation. In order to decrease the melting and reaction temperature during synthesis, the copolymerization of the aliphatic octanedioic acid (suberic acid, SuA) with the mentioned aromatic monomers is explored in this chapter.

Generally, examples of flexible spacers in thermotropic polyesters are aliphatic dicarboxylic acids or aliphatic diols such as ethylene glycol or its derivatives.¹⁻⁴ Especially the use of sebacic acid and suberic acid are of interest, since they can be obtained from bio-based feedstock such as vegetable oils and can be used to develop bio-based polymers^{5,6} and TLCPs.^{7,8} Furthermore, the presence of these aliphatic dicarboxylic acids drastically suppresses the melting temperature (crystal to liquid crystal transition) of the TLCPs. For example, Hsiue⁹ and colleagues reported the synthesis of TLCPs containing different amounts of sebacic acid, hydroquinone (HQ), and *p*-hydroxybenzoic acid (BA) via a melt polymerization. These polymers showed melting temperatures well below 200 °C, but the melting temperatures increased rapidly when the amount of sebacic acid was decreased. Though Hsiue reported the presence of a homogeneous liquid crystalline (LC) melt, the coexistence of both an isotropic melt and a LC melt in these polymers was reported by Dingemans¹⁰ and coworkers. The inhomogeneous structure of this polymer melt can be attributed to a non-random distribution of the monomers along the polymer backbone arising from clustering of monomers into blocks.^{11,12} Besides, Dingemans and coworkers also showed that the incorporation of one or two comonomers could enhance the stability of the LC melt. De Oca and coworkers¹³ reported the solvent based synthesis of bioresorbable TLCPs containing flexible aliphatic spacers, BA, 4,4'-sulfonyl *bis*(2-methylphenol), and vanillic acid (VA). These polymers showed low melting temperatures between 95 and 165 °C, while no isotropic melt was observed below 300 °C, indicating that the different monomers in these polymers are randomly distributed without forming any high melting blocks.

The influence of block formation on the processability and on the mechanical performance of thermotropic polyesters has been studied for many decades. For

example, the processing and rheology of different BA and 2-hydroxy-6-naphthoic acid-based copolymers has been studied extensively by Yang and Krigbaum.^{14,15} These authors showed that flow instabilities during processing of these copolymers are associated with the presence of crystallites having high melting temperatures, formed via transesterification in the melt. Furthermore, the mechanical performance of these spun materials greatly suffered from the presence of such crystals. Krigbaum and coworkers¹⁶ observed similar behavior for partially flexible TLCPs based on BA and poly(ethylene terephthalate) (PET).

It is clear that, in order to develop new 2,5-FDCA based thermotropic polyesters, an in-depth understanding of the role of the 2,5-FDCA moiety on the behavior of these materials is required.¹⁷ The influence of the rigid 2,5-FDCA moiety in aliphatic-aromatic thermotropic polyesters on the thermal properties, block formation and mechanical properties is not known to date. Therefore, this chapter reports on the synthesis and properties of new aliphatic-aromatic thermotropic polyesters containing 2,5-FDCA. Furthermore, copolymerizations with bio-based vanillic acid are performed to control block formation and to develop bio-based TLCPs with stable LC melts.

3.2. Experimental section

3.2.1. Materials and monomer preparation

Suberic acid, 1,4-diacetoxybenzene, and 4-hydroxy-3-methoxybenzoic acid were obtained from Sigma-Aldrich. The monomers 4,4'-diacetoxybiphenyl and *p*-acetoxybenzoic acid were obtained from TCI Europe and 2,5-furandicarboxylic acid (99.5%, GC-MS) was procured from Atomole (China). 4-hydroxy-3-methoxybenzoic acid was acetylated and recrystallized prior to use. 2,5-furandicarboxylic acid was purified through the recrystallization of the dimethyl 2,5-furandicarboxylate intermediate in methanol. The crystals were hydrolyzed in an aqueous NaOH solution, neutralized with an aqueous HCl solution, filtered and dried *in vacuo* overnight at 80 °C prior to usage. All other monomers were recrystallized at least once and dried *in vacuo* overnight prior to use. The structural formulas of the monomers used in this study are shown in Figure 3.1.

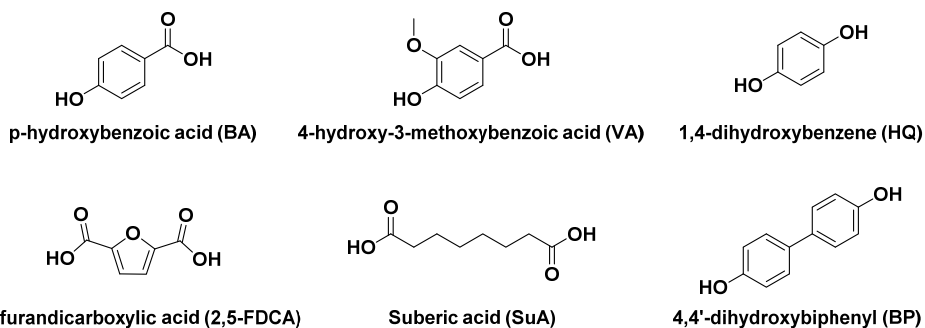


Figure 3.1. Chemical structures and abbreviations of the monomers used in this study.

3.2.2. General polymerization procedure

All polymerizations were performed in a 100 mL three-neck round bottom flask fitted with a mechanical stirrer. The monomer mixture, between 50 to 100 grams in total, was weighed together with 30-60 mg of $\text{Zn}(\text{CH}_3\text{CO}_2)_2$ in the round bottom flask. The monomers were dried *in vacuo* at 40 °C prior to usage to eliminate moisture. An oxygen poor atmosphere was created by flushing with Argon and applying reduced pressure for three times prior to the start of the reaction. The maximum reaction temperature used in this study is 230 °C for polymerizations using 2,5-FDCA and 260 °C for polymerizations without 2,5-FDCA. Acetic acid was distilled off for six to eight hours, after reaching the maximum reaction temperature. Reduced pressure was applied to the system for two to twelve hours after 90% of the calculated amount of acetic acid was collected. The final products were isolated from the reactor flask in the form of a crystalline solid or polymer melt.

3.2.3. Characterization methods

^1H and ^{13}C NMR spectroscopy was performed on a Bruker 400 MHz NMR spectrometer. Samples measured in NMR analysis were dissolved in HFIP, precipitated in methanol, and dried *in vacuo* at 40 °C prior to preparation for NMR measurements. All samples were measured in a mixture of deuterated chloroform and deuterated trifluoroacetic acid ($\text{CDCl}_3/\text{TFA}-d$) (50/50 v/v) and were referenced against tetramethylsilane (TMS). The compositions of the polymers were determined by taking the ratio between the resonance signals corresponding to the different monomers.

A Bruker AVANCE-III 500 spectrometer employing a double-resonance H-X probe for rotors with a 4.0 mm outside diameter was used to carry out $^{13}\text{C}\{^1\text{H}\}$ Inensitive Nuclei Enhanced by Polarization Transfer (INEPT) Magic-Angle spinning (MAS) and Variable-temperature (VT) solid-state $^{13}\text{C}\{^1\text{H}\}$ Cross-Polarization/MAS (CP/MAS) NMR experiments. These experiments utilized a MAS frequency of 10.0 kHz, a 5.0 μs $\pi/2$ pulse for ^1H and ^{13}C , TPPM decoupling during acquisition, and a CP contact time of 3.0 ms.¹⁸ The CP conditions were pre-optimized using L-alanine. The $^{13}\text{C}\{^1\text{H}\}$ INEPT MAS spectra were recorded using the refocused-INEPT sequence with a J-evolution period of $1/3J_{\text{CH}}$ or $1/6J_{\text{CH}}$ and assuming a $^1J_{\text{CH}}$ of 150 Hz, i.e., for a J-evolution time of $1/3J_{\text{CH}}$ the signals from CH and CH_3 groups are positive, while those of CH_2 are negative.^{19,20} The temperature was controlled using a Bruker temperature control unit in the range of 30 to 210 °C. The VT $^{13}\text{C}\{^1\text{H}\}$ CP/MAS and $^{13}\text{C}\{^1\text{H}\}$ INEPT MAS NMR spectra were recorded under isothermal conditions at selected temperatures whereas a heating rate of 2 °C/min was employed between temperatures. Reported temperatures are corrected for friction-induced heating due to spinning using ^{207}Pb MAS NMR of $\text{Pb}(\text{NO}_3)_2$ as a NMR thermometer.²¹

Molecular weights and polydispersity index (PDI) values were determined via 1,1,1,3,3,3-hexafluoroisopropanol (HFIP) size exclusion chromatography (SEC). This system is equipped with a Waters 1515 Isocratic HPLC pump, a Waters 2414 refractive index detector (40 °C), a Waters 2707 autosampler, and a PSS PFG guard column followed by 2 PFG-linear-XL (7 mm, 8 x 300 mm) columns in series at 40 °C. HFIP (Apollo Scientific Limited) with potassium trifluoroacetate (3 g L⁻¹) was used as an eluent at a flow rate of 0.8 ml min⁻¹. The molecular weights were calculated against poly(methyl methacrylate) standards (Polymer Laboratories, M_p

= 580 Da up to $M_p = 7.1 \times 10^6$ Da). SEC samples were filtered through a 200 μm filter prior to injection.

Melt morphologies of the synthesized polymers were determined on a Zeiss Axioplan 2 Imaging optical microscope under crossed polarizers and CD achorplan objectives (32x zoom). A THMS 600 heating stage connected to a Linkam TMS 94 control unit was mounted onto the optical microscope. Samples were prepared by placing a small amount of ground polymer in-between two glass slides and heating them at a heating rate of 50 $^\circ\text{C}/\text{min}$ to 250 – 300 $^\circ\text{C}$. The samples were then pressed in the melt and cooled to 50 $^\circ\text{C}$ at a cooling rate of 20 $^\circ\text{C}/\text{min}$. Optical micrographs were taken during the new heating run performed at a heating rate of 20 $^\circ\text{C}/\text{min}$ up to 350 $^\circ\text{C}$ or the degradation temperature.

The stability of the LC melt was followed using a TA Instruments ARG2 rheometer. Parallel plate geometry of a diameter of 25 mm and a sample diameter of 1 mm were used to study the temperature dependence of the apparent shear viscosity. A fixed strain (1.25%) and frequency (10 Hz) were chosen such that the experiments were performed in the linear viscoelastic regime. Data points were collected every 1 $^\circ\text{C}$ over the temperature range between 150 $^\circ\text{C}$ and 300 $^\circ\text{C}$ and a thermal expansion of 2.45 $\mu\text{m}/\text{K}$ for this geometry was taken into account. Prior to the collection of data points, the samples were allowed to relax for 15 minutes at the starting temperature of the experiments.

The thermal stability of the polymers was determined using thermogravimetric analysis (TGA) and was performed on a TA Instruments TGA Q500 in a nitrogen rich atmosphere. Samples were heated at 20 $^\circ\text{C}/\text{min}$ from 20 $^\circ\text{C}$ to 800 $^\circ\text{C}$.

The glass transition temperature (T_g) and the peak transition temperature from the crystalline to the LC phase (T_m) were determined by differential scanning calorimetry (DSC) using a TA Instruments Q1000 DSC. The normal heating and cooling-rates of the samples were 10 $^\circ\text{C}/\text{min}$ and measurements were performed under a nitrogen rich atmosphere.

Dynamic mechanical thermal analysis (DMTA) was performed on a TA Instruments DMA Q800. DMTA samples were prepared via compression molding at temperatures between 220 $^\circ\text{C}$ to 260 $^\circ\text{C}$ and were cut into rectangular shapes of 20 mm x 5 mm x 0.5 mm. All experiments were performed at a frequency of 1 Hz and at a heating rate of 2 $^\circ\text{C}/\text{min}$. Measurements were continued until the sample was molten or broken. The T_g values determined from DMTA analysis were obtained by taking the maximum value of the loss modulus during heating.

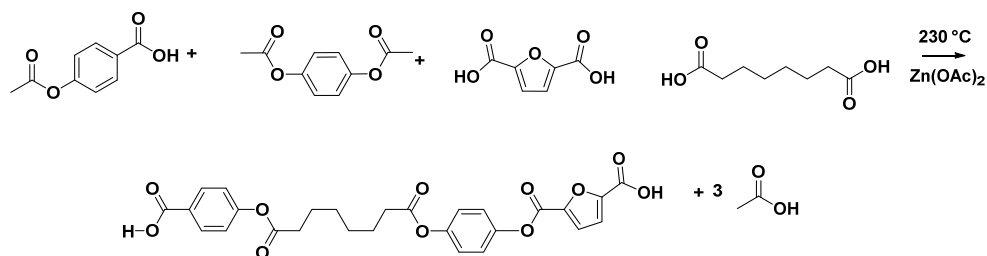
Wide-angle X-ray diffraction (WAXD) measurements were performed on a Rigaku Geigerflex Bragg-Brentano Powder Diffractometer using Cu K α radiation ($\lambda = 0.154$ nm), at 40 kV and 30 mA. The scans were performed with a 0.01 step in 2θ and a dwell time of 2s. Peak fitting was performed after background subtraction to determine the percentage of crystallinity.

Tensile test experiments were performed at a constant deformation rate of 5 mm/min using a Zwick 100 tensile apparatus and a load cell of 100 N, at room temperature. Samples were prepared via compression molding and cut into dog-bone shaped samples of 20 mm x 2 mm x 1 mm.

3.3. Results and discussion

3.3.1. Thermotropic polyester synthesis

A series of TLCPs with varying amounts of 2,5-FDCA and VA were synthesized according to the general polymerization procedure. Sets of polymers with three (3a-3b), four (4a-4f), and five (5a-5b) monomers were synthesized. Both polymers 3a and 3b contain BA, SuA, and HQ or 4,4'-biphenol (BP). In the synthesis of polymers 4a-4c, SuA was replaced with increasing amounts of 2,5-FDCA. For polymers 4d-4f, VA is added as the fourth monomer and no 2,5-FDCA was used. Polymer 5a and 5b contain both 2,5-FDCA and VA as additional monomers. Scheme 3.1 shows the acidolysis reaction occurring during the synthesis of polymer 4c.



Scheme 3.1. Acidolysis reaction occurring during the synthesis of the 2,5-FDCA containing TLCP 4c. *N.B.* The resulting polymer is a copolymer.

The composition of the polymers was estimated based on the monomer ratio determined by ¹H-NMR spectroscopy. Table 3.1 shows the polymer composition after polymerization, whereas the compositions weighed into the reactor are shown between brackets. No sublimation of monomers on the reactor wall was observed during the polymerizations except during the synthesis of polymers 5a and 5b. These polymers showed slow sublimation of 2,5-FDCA during the reduced pressure step. Because of this, the 2,5-FDCA content incorporated in these polymers is lower than weighed in the reactor. The sublimation of 2,5-FDCA during the synthesis of polymers 5a and 5b can be attributed to the extended reaction times required to build up molecular weight compared to, for example, polymer 4c. Sublimation of 2,5-FDCA during the synthesis of polymers 4a-4c was expected, but was not observed due to decreased amounts of 2,5-FDCA (4a, 4b) or rapid crystallization during synthesis (4c). Nonetheless, the compositions of the other polymers are in good agreement with the expected compositions.

Table 3.1. Compositions and molecular weight distributions determined for copolymers containing various amounts of BA, SuA, 2,5-FDCA and VA with HQ or BP as diols.

Entry	Diol	Composition (mole%) ^a				SEC	
		BA	SuA	2,5-FDCA	VA	M_n (g/mol)	PDI
3a	HQ 33 (33)	33 (33)	33 (33)	0 (0)	0 (0)	24,800	2.5
4a	HQ 34 (33)	34 (33)	29 (29)	3 (4)	0 (0)	10,700	2.2
4b	HQ 34 (33)	33 (33)	24 (24)	9 (8)	0 (0)	30,500	3.5
4c	HQ 32 (33)	33 (33)	18 (17)	17 (16)	0 (0)	27,100 ^b	6.8
4d	HQ 29 (30)	31 (30)	30 (30)	0 (0)	10 (10)	12,800	2.2
5a	HQ 28 (30)	33 (30)	16 (15)	12 (15)	11 (10)	63,400 ^b	5.1
3b	BP 34 (33)	32 (33)	32 (33)	0 (0)	0 (0)	8,200	2.7
4e	BP 31 (30)	30 (30)	30 (30)	0 (0)	9 (10)	28,500	2.1
4f	BP 26 (25)	24 (25)	26 (25)	0 (0)	24 (25)	14,600	2.4
5b	BP 29 (30)	32 (30)	17 (15)	10 (15)	11 (10)	12,000	2.3

a) Calculated by ¹H NMR analysis in CDCl₃/TFA-*d* 50/50. b) Partially soluble in the HFIP solvent.

It is well established that a decrease of the aliphatic content in aliphatic-aromatic polymers causes a rapid increase in melting temperature and a decrease in solubility.⁹ Furthermore, the formation of long aromatic blocks is enhanced in copolymers with decreasing aliphatic content. In this study, the influence of the non-linear aromatic 2,5-FDCA monomer on the formation of aromatic blocks along the main chain is determined. This effect is studied by gradually increasing the amount of 2,5-FDCA at the expense of SuA, for example, as is the case for polymers 3a and 4a-4c shown in Table 3.1.

The maximum amount of 2,5-FDCA that could be incorporated into the polymer backbone was 16 mole%, for systems with HQ as the diol comonomer. The limiting factor for the incorporation of higher amounts of 2,5-FDCA was the solidification of the reaction mixture at the chosen reaction temperature of 230 °C. The solidification of the reaction mixture inhibits the desired molecular weight build-up. Similar solidification problems were observed for systems containing a combination of 2,5-FDCA and BP. It is expected that higher amounts of 2,5-FDCA can be incorporated at higher reaction temperatures. However, an increase of the reaction temperature is known to result in partial degradation of the 2,5-FDCA monomer.^{22,23} For this reason, to prevent side reactions, the maximum temperature used in the synthesis of polymers containing 2,5-FDCA was set to 230 °C.

The PDI of the polymers increases with the incorporation of 2,5-FDCA, as is evident from the GPC traces of polymers 3a, 4b, 4c, and 5a shown in Figure 3.2. The GPC traces in Figure 3.2 clearly show that the increase in PDI arises from the presence of a high molecular weight tail. The replacement of SuA by 2,5-FDCA increases the aromatic content and apparently promotes the formation of less soluble, long aromatic sequences. It is expected that these aromatic sequences show a different

hydrodynamic volume during SEC analysis compared to the more soluble aliphatic sequences and elute at different times.²⁴ Another explanation for the high molecular weight tail in the SEC traces is the occurrence of a branching reaction during polymerization. Such branched chains should exhibit an improved solubility compared to linear chains. However, it is observed that the solubility of the polymers that elute a high molecular weight tail in fact decreases drastically, as is the case for polymers 4c and 5a. For this reason, it is expected that poorly soluble aromatic blocks are responsible for the observed high molecular weight tail and the increased PDI value. This dissolution behavior indicates that the replacement of flexible spacers with aromatic 2,5-FDCA enhances the block formation, similar to other aromatic monomers such as BA.

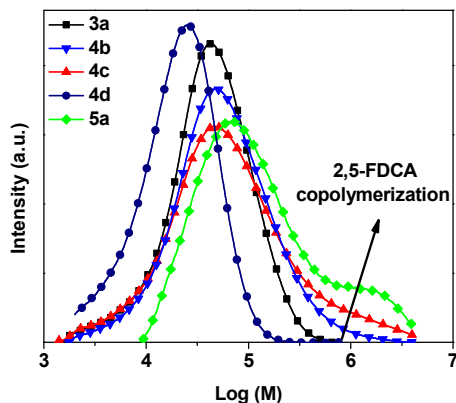


Figure 3.2. Overlay of the SEC traces of polymer 3a, 4b-4d and 5a showing the rise of a high molecular weight tail in 2,5-FDCA containing copolymers.

The samples containing VA show PDI values between 2.1 and 2.4 (e.g., SEC trace 4d in Figure 3.2), which is close to the theoretical PDI value of 2.0 expected for polycondensation polymers. The copolymerization of VA is known to lead to lower PDI values, as is reported by Li and coworkers²⁴ for copolymerizations of VA with PET and BA based TLCPs. The methoxy group of VA improves the solubility of the final polymer and is thought to be responsible for the decrease in PDI, as the solubility also affects the hydrodynamic volume in solution.²⁵ This implies that VA is able to increase the solubility of the aromatic blocks, while 2,5-FDCA only enhances the formation of aromatic blocks. In particular, the PDI of 2.3 for sample 5b is interesting since this sample contains 10 mole% of 2,5-FDCA and was expected to show a high molecular weight tail. This example clearly shows that the copolymerization of VA prevents the formation of poorly soluble aromatic blocks. However, other factors such as reactivity, solubility, and length of the mesogenic unit also affect the formation of aromatic sequences. For example, the addition of VA to polymer 4c decreases the PDI from 6.8 to 5.1 for polymer 5a. The high PDI of the

polymer 5a indicates that poorly soluble aromatic sequences are still present in this system. If the PDI values of the polymers 5a and 5b are compared, it appears that the choice of the diol also plays an important role in the formation of insoluble aromatic sequences (or blocks).

3.3.2. Molecular weight build-up and reaction time

Besides the formation of insoluble aromatic blocks, it was noticed that the composition of the polymers also influences the time required to build up molecular weight. During the synthesis of these polyesters, it was observed that the time required to build up molecular weight increases with the increasing amounts of VA and/or 2,5-FDCA. To probe this behavior, polymerizations were performed at 230 °C and samples were taken over time during the polycondensation step performed under reduced pressure. Figure 3.3 shows the molecular weight build-up over time for polymers containing BP as the diol. It can be seen that the molecular weight build-up for polymer 3b (having neither FDCA nor VA) is rather slow and levels off rapidly, which is due to solidification of the reaction mixture after 120 minutes. The addition of 10 mole% VA (4e) lowers the melting temperature, prevents the solidification of the reaction mixture, and allows for more extensive build-up of molecular weight. A number-average molecular weight (M_n) in excess of 20,000 g/mol is obtained within two hours of reaction under reduced pressure. The copolymerization of 25 mole% of VA (4f) proceeds significantly slower and a M_n of roughly 15,000 g/mol is obtained after seven hours of the reaction time. A similar increase in the reaction time was observed during the synthesis of polymer 4d, which required over six hours of synthesis under reduced pressure to obtain a M_n of 12,800 g/mol. For comparison, the application of two hours of reduced pressure during the synthesis of polymer 3a resulted in a molecular weight of 24,800 g/mol. For this reason, it is expected that the presence of the bulky methoxy group next to the acetic acid ester bond in the acetylated VA sterically hinders the ester exchange reaction occurring during polymerization. The slower incorporation of the VA monomer therefore requires an extended reaction time in order to obtain a higher molecular weight.

The reaction time required to build up molecular weight increased even further for systems containing both 2,5-FDCA and VA. For example, more than 10 hours were needed to build up a M_n of 12,000 g/mol during synthesis of the polymer 5b. In chapter 2 of this thesis it was demonstrated that 2,5-FDCA exhibits a poor dissolution behavior in the monomer/oligomers mixture at these reaction temperatures. Therefore, it is expected that both the slow reaction rate of VA and the slow dissolution of 2,5-FDCA are responsible for the increased reaction times required to build up molecular weight. Furthermore, these increased reaction times resulted in the

slow sublimation of 2,5-FDCA and might hamper the molecular weight build-up even further due to the generated stoichiometric imbalance.

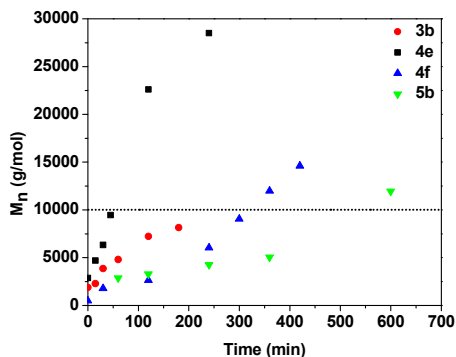


Figure 3.3. Number-average molecular weight build-up over time for systems containing BP with varying amounts of VA and 2,5-FDCA.

3.3.3. Thermal properties of the TLCs

The previous section showed that both 2,5-FDCA and VA influence the formation of aromatic sequences along the polymer chains. This variation of the chemical microstructure as a function of chemical composition is expected to influence both the melting behavior and the processability of these polymers. Thermogravimetric analysis (TGA), differential scanning calorimetry (DSC), polarization optical microscopy (POM), and dynamic mechanical thermal analysis (DMTA) were employed to identify the effect of the chemical composition and block formation on the thermal properties of the polymers (Table 3.2).

As is shown in Table 3.2, an onset temperature in the weight loss (T_{ons}) of 380 °C was found in TGA analysis for polymer 3a. An increase in T_{ons} to 405-410 °C was observed for the polymers containing 2,5-FDCA, which is thought to be the result of the increased aromatic content. Similarly, the replacement of diol from HQ to BP for the same monomer composition increases the T_{ons} by several degrees.

Figure 3.4 shows the second DSC heating curves of polymers 3a, 4b-4f, 5a and 5b. The polymer 3a, containing no 2,5-FDCA, shows a peak melting temperature (T_m) at 193 °C. The incorporation of 2,5-FDCA results in a decrease in T_m , but also to a broadening of the melting transition. For example, the incorporation of 17 mole% of 2,5-FDCA (4c) yields a polymer that shows a mobile liquid crystalline phase (T_{lc}) above 300 °C, as observed in POM. The DSC trace of polymer 4c shows the presence of a weak endotherm with a T_m at 165 °C (denoted with an * in Figure 3.4). This indicates that, although the peak melting temperature of this polymer decreases compared to polymer 3a, the melting range of this polymer increases resulting in an increase in T_{lc} from 210 °C (3a) to 300 °C (4c).

Table 3.2. Thermal data of TLCPs containing variable amounts of vanillic acid and 2,5-FDCA.

Entry	Composition			DSC		POM	DMTA	TGA
	Diol	VA	2,5-FDCA	T_g (°C)	T_m (°C) ^a	T_{lc} (°C) ^b	T_g (°C)	T_{ons} (°C)
3a	HQ	0	0	42	193	210	46	384
4a	HQ	0	3	43	184	205	47	384
4b	HQ	0	9	56	165	240	57	390
4c	HQ	0	17	-*	164	300	82	409
4d	HQ	10	0	45	126 ^d	150	47	370
5a	HQ	11	12	66	186	280	79	412
3b	BP	0	0	44	189	280	- ^c	410
4e	BP	9	0	63	191	220	67	402
4f	BP	24	0	63	148 ^d	210	63	406
5b	BP	11	10	73	145	170	82	406

a) Peak melting temperature, obtained from the second DSC heating run. b) Temperature where all crystals are molten and a liquid crystalline melt is obtained, determined using polarization optical microscopy. Thus the T_{lc} represents the end melting temperature determined from DSC as depicted by arrows in Figure 3.4. Melting refers to the crystal to liquid crystal transition. In all the polymers investigated in this publication, melting proceeds from crystal to liquid crystal where the liquid crystal to isotropic transition normally occurs close to or during thermal degradation (>300 °C). c) Not possible to compression mold samples due to a low melt-viscosity. d) Cold-crystallization is observed prior to melting. *Not observed.

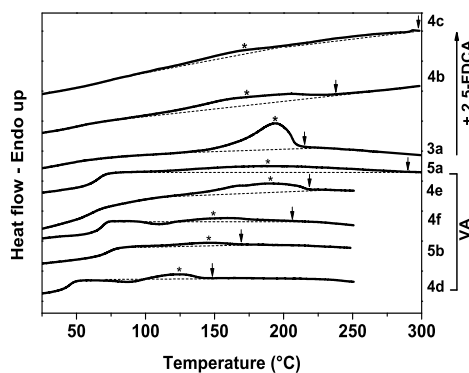


Figure 3.4. Second heating curves of polymers 3a, 4b-4f, 5a, and 5b, obtained during heating at 10 °C/min. The peak melting temperature T_m of the polymers is indicated with an *, whereas the arrows denote the T_{lc} as observed in polarization optical microscopy (POM). The dotted lines in the DSC traces are added to illustrate the temperature regions where melting of the polymers occur.

It is anticipated that long aromatic sequences present in polymer 4c can aggregate more easily in the melt resulting in crystallization upon cooling. However, the crystals

formed in such systems are non-periodic layer (NPL) crystallites rather than regular chain-folded crystals.²⁶ These NPL crystallites are formed when polymer chains with similar monomer sequences come in close contact, enabling chain stacking and local crystallization. The melting temperature of these crystals thus depends on both the composition of the polymer chains and on the chain length that participates in crystallization. It is anticipated that the chains with long aromatic sequences in polymer 4c are able to form NPL crystallites with high melting temperatures, whereas the flexible chains form crystallites with lower melting temperatures. For this reason, it is assumed that the endotherm observed below 200 °C, including the T_m at 164 °C, corresponds to the melting of crystallites containing the more flexible polymer chains. In contrast, the part of the transition between 200 and 300 °C corresponds with the melting of crystals containing more rigid polymer chains. Such a broad melting temperature range is characteristic for polymers that are of a blocky nature. A similar melting behavior was observed for polymers 3b and 5a, which showed a T_m in DSC at 189 °C and 186 °C respectively, but both showed a T_{ic} melt in POM above 280 °C.

Contrary to the effects observed when incorporating 2,5-FDCA, the copolymerization of VA results in a decrease of the melting temperature. For example, polymer 4d shows a weak melting endotherm between 90 and 140 °C and a thermotropic melt above this temperature. Similar melt behavior is observed for polymer 5b, which shows an LC melt above 170 °C. Such low T_m and T_{ic} are the characteristics for random polymers. As stated earlier, NPL crystals formed in these systems are a result of agglomeration or stacking of chains with similar sequences. The formation of these NPL crystals decreases with the increasing randomness in the monomer sequence distribution, yielding perturbed crystals with lower melting temperatures. Furthermore, it is anticipated that the steric hindrance of the methoxy groups of VA also decreases the ability of the polymer to crystallize. It should be noted that such perturbation of the crystallinity can only occur if the methoxy groups are distributed randomly along the polymer backbone. As observed earlier, this is clearly not the case for blocky polymer 5a, which also contains 10 mole% VA.

Polymers 4e and 4f show T_m values below 200 °C, but exhibit a T_{ic} above 210-220 °C. This indicates that these polymers are able to form NPL crystallites, but without the high melting temperatures observed for polymers 4c and 5a. It is likely that the length of the crystallizing aromatic blocks in these polymers is smaller than those in polymers 3b, 4c, and 5a, resulting in lowered melting temperatures. Therefore, the resulting melt behavior of these polymers is neither characteristic for a random nor a blocky polymer.

It should be noted that it is difficult to determine whether the polymers synthesized in this study are truly of a blocky nature or of a random nature. The determination of the chemical microstructure is normally performed via ¹³C NMR or ¹H NMR analysis. A

shift in aromatic protons or carbonyl resonances is expected for monomers with different neighbors and the chemical microstructure can be estimated with the ratio between these shifted signals.²⁴ Overlapping of signals observed in the NMR spectra, obtained in CDCl₃/TFA-*d* mixtures, did not allow us to determine the sequence distribution of the polymer synthesized in this study. Another route to determine the presence of species with different chemical microstructure is via solvent extraction. In this case, the polymer chains with different solubility can be extracted and analyzed separately. Extraction of the different phases in solvents such as boiling chloroform or toluene was also not successful. The poor solubility of the polymers in common solvents did not allow us to find a suitable solvent or solvent mixture to extract different polymer fractions. Furthermore, it is possible that polymers with a random chemical microstructure still contain blocks with long aromatic sequences. For example, as mentioned before, the exchange of flexible SuA for 2,5-FDCA in polymers 3a and 4c promotes the formation of large aromatic sequences, simply due to the increased statistics for aromatic monomers to have an aromatic neighbor.

Nonetheless, the data obtained so far indicates that polymers 3b, 4c, and 5a exhibit characteristic behavior expected for blocky polymers, whereas polymers 4d and 5b exhibit characteristic behavior of non-blocky polymers. Thus, in the following sections of this chapter the polymers 3b, 4c, and 5a will be considered to be blocky, whereas the polymers 4d and 5b will be considered to be random (or non-blocky).

It is expected that the non-blocky polymers have much lower crystallinities and show more pronounced glass transitions (T_g) in DSC and DMTA analysis. Indeed, this is the case when the T_g value of polymer 4c is compared to those of polymers 4d or 5b in Figure 3.4. Figure 3.5 shows the temperature dependent behavior of the storage (E') and loss (E'') moduli for the TLCPs, obtained by DMTA analysis. The decrease in the crystallinity and the melting temperature can clearly be detected for the non-blocky polymers 4d and 5b, indicated by the decrease in plateau modulus value above T_g and the rapid deterioration of the E' modulus at higher temperatures. As expected, the blocky polymers 4c and 5a have higher crystalline plateau modulus values above T_g and broader melt transitions. As already anticipated from the DSC analysis, polymers 4e and 4f show a partial blocky behavior; these polymers do show an onset of melting at low temperatures, but are mechanically more stable at higher temperatures.

Surprisingly, the copolymerization of vanillic acid does not seem to influence the T_g to a significant extent, for example, for polymers 3a ($T_g = 42$ °C, no VA, DSC) and 4d ($T_g = 45$ °C, 10% VA, DSC). In contrast, literature shows that the copolymerization of VA in PET and BA containing TLCPs did result in an increase in T_g with increasing VA content.²⁷ The copolymerization of 2,5-FDCA does increase the T_g of the polymers to values around 80 °C as is detectable by the shift of the peak value of E''

for polymers 4c, 5a and 5b. The shift in T_g is attributed to the increased aromatic content in these polymers.

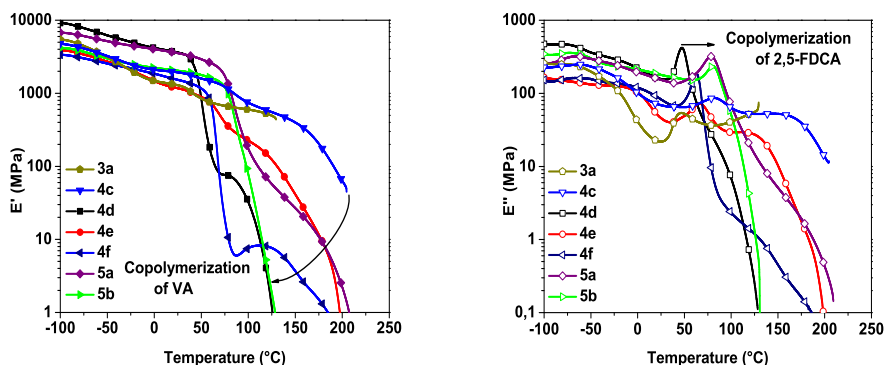


Figure 3.5. DMTA traces of left) E' and right) E'' of polymers 3a, 4c- 4f, 5a, and 5b, showing the effect of the copolymerization of VA and 2,5-FDCA on the T_g and melting behavior. The arrow in the E' versus temperature plot indicates the decrease in T_m and mechanical stability at higher temperatures upon copolymerization of VA. The arrow in the E'' versus temperature plot shows the increase of the T_g upon copolymerization of 2,5-FDCA.

3.3.4. Melt behavior of the TLCPs

It is well established that the homogeneity and the transition temperature of an LC phase are dependent on both the total amount of aromatic monomers in the polymer backbone and the chemical microstructure of the polymer chains. For example, Jackson reported the isotropization temperature for compounds with three and four oxybenzoate units connected with one acetic acid and one ethanol end-group.² The author showed that the isotropization temperature of the compound with three oxybenzoate units was 282 °C, while the compound with four oxybenzoate units showed no isotropization prior to degradation above 400 °C. For processing purposes, the stability of the LC melt is of great importance, since spinning from an entangled isotropic state leads to a loss of mechanical performance. Furthermore, in order to produce a highly oriented product, the presence of crystals is not desired. For these reasons, the occurrence of a homogeneous LC melt at the processing temperature is preferred.

The stability and the homogeneity of the LC melt of the synthesized polymers in this study are determined via polarized optical microscopy (POM). Upon heating at 20 °C/min, above 300 °C the formation and growth of isotropic droplets is observed in the LC melt for polymers 3a and 4a. Also blocky polymers 3b and 4b show a similar phase separation with the onset at 340-350 °C. However, none of these materials show a fully isotropic phase prior to degradation. The stability of the LC

melt of blocky polymers 4c and 5a is difficult to investigate due to the high melting temperatures of these polymers, and the rapid degradation of the polymer above 350 °C. Nevertheless, no phase separation of the melt is observed upon heating to and beyond the degradation temperature. Apparently, the increased aromatic content, due to the copolymerization of 2,5-FDCA, stabilizes the LC melt, even though these polymers are of a blocky nature.

For the polymers 4d and 5b, no phase transition from the LC phase to the isotropic phase is observed prior to degradation of the polymers. Instead, a threaded texture is observed over the whole temperature range. Also the partially blocky polymers 4e and 4f show no isotropization transition in POM. Apparently, a decrease in the ‘blockiness’ in these TLCPs improves the homogeneity of the LC melt. Figure 3.6 shows an example of the phase separation observed for polymer 3a upon heating (micrographs A and B) and the stable LC melt during heating for polymer 5b (micrographs C and D).

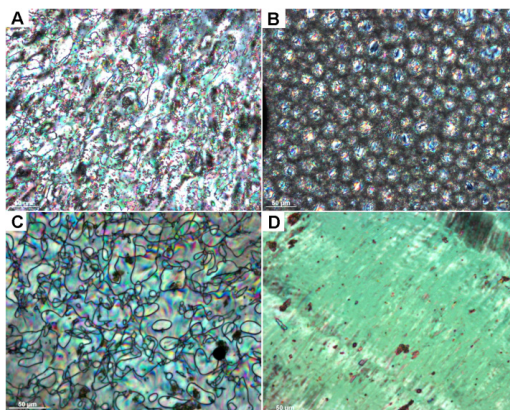


Figure 3.6. Optical micrographs, obtained between crossed polarizers during constant heating at 10 °C/min. The micrographs depict A) the LC phase of polymer 3a observed at 220 °C, B) the coexistence of the LC phase and the isotropic phase observed for polymer 3a at 300 °C, C) the LC phase of polymer 5b at 200 °C, and D) the LC phase of polymer 5b at 300 °C.

To obtain more information on the stability of the LC melt, rheological studies using plate-plate geometry as a function of temperature while heating up to 300 °C were performed on polymers 3a, 4d, 4e, and 5b. The complex viscosity curves of the melts thus obtained are depicted in Figure 3.7. The plate-plate configuration was chosen over a cone-plate configuration because it is easier to compensate for the thermal expansion occurring due to the wide temperature range of these experiments. Similar rheological experiments were performed by Gao and coworkers on polymers based on sebacic acid, HQ, and BA.²⁸ These authors showed that the transition from the crystalline to the nematic phase resulted in a decrease in viscosity, whereas the

transition from the nematic to the isotropic phase at higher temperatures increased the viscosity again. For some polymers in this study, the viscosity measured in the nematic phase falls below the transducer limit and might no longer be accurate (visible for polymer 5b in Figure 3.7). However, since only the dependence of the viscosity as a function of phase transitions is required for interpretation of the data, this data is used as a qualitative indicator.

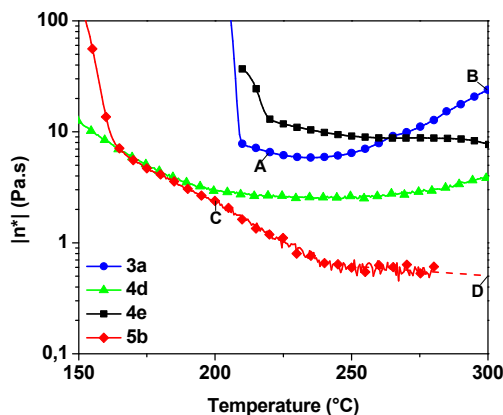


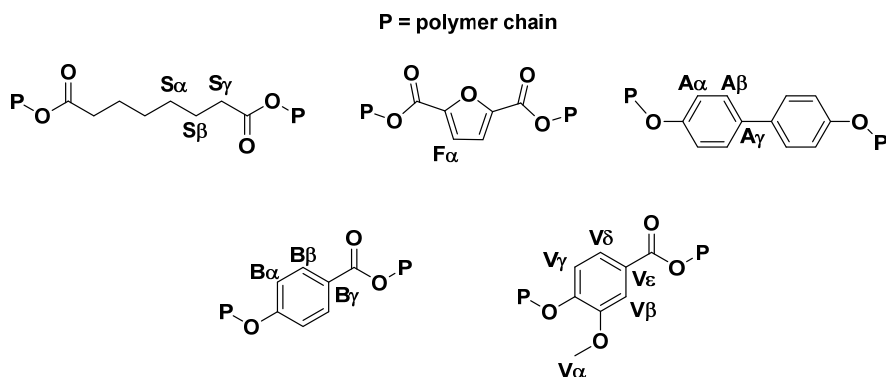
Figure 3.7. Complex viscosity versus temperature plot showing an increase in viscosity above 230 °C for polymer 3a, indicating that a phase transition is occurring. A continuous decrease in complex viscosity is observed for polymers 4d, 4e, and 5b, indicating that a higher mobility of the LC phase is achieved, but no phase transition is occurring. The letters A-D correspond to the temperatures where micrographs A-D in Figure 3.6 were taken for samples 3a and 5b.

From Figures 3.6 and 3.7 it can be seen that polymer 3a exhibits a stable nematic phase above its melting temperature. However, the increase in viscosity with temperature indicates the occurrence of a phase transition from the nematic to the isotropic phase. The POM micrograph of polymer 3a, taken at 300 °C (micrograph B, Figure 3.6), confirms the coexistence of the isotropic and the LC phase. Similar to our observation in POM, polymers 4e and 5b do not show the formation of the isotropic phase, and the viscosities of these polymers only decrease over temperature. Polymer 4d does show a slight increase in complex viscosity above 250 °C indicating that a slow phase transition, not observed in POM, might be occurring. However, other phenomena such as slow degradation, the formation of gaseous compounds, and cross-linking might also occur at these temperatures and can also affect the viscosity during these measurements. Nonetheless, this data clearly indicates that non-blocky polymers exhibit stable LC melts over a wide range of temperatures. Furthermore, this data also shows that bio-based thermotropic polyesters with high aromatic contents such as polymer 5b can be synthesized without exhibiting blocky behavior and with stable nematic melts up to 300 °C.

From the rheological data it is apparent that the polymers 3a, 4d, and 4e (without 2,5-FDCA) show the stable complex viscosity in the LC melt, whereas polymer 5b (with 2,5-FDCA) shows a continuous decrease in the complex viscosity over temperature. The difference in the rheological response of the polymer 5b could be attributed to the presence of 2,5-FDCA in the polymer. To investigate the cause of this difference, what follows, is the solid state NMR studies performed on these TLCs.

3.3.5. Influence of 2,5-FDCA and VA on the molecular mobility

Burgess and coworkers²⁹ recently showed that the furan ring exhibits much slower ring rotation/flipping in PEF compared to the phenyl ring in PET. In this study, Burgess correlated the slow ring flipping of the furan ring to the improved barrier properties. It is expected that similar slowed flipping kinetics of the 2,5-FDCA moiety occurs in 2,5-FDCA based TLCs and that the 2,5-FDCA ring requires more energy to become mobile. Furthermore, it was expected that the methoxy group limits the rotational motion of VA, causing VA to require a higher temperature to rotate freely too. To investigate this behavior, temperature-dependent solid-state $^{13}\text{C}\{^1\text{H}\}$ INEPT MAS and $^{13}\text{C}\{^1\text{H}\}$ CP/MAS NMR spectroscopy was performed on polymer 5b. Scheme 3.2 shows the structural formula of monomer residues present in polymer 5b and the labels of the corresponding carbon atoms, while Figure 3.8 summarizes the data obtained from the $^{13}\text{C}\{^1\text{H}\}$ CP/MAS NMR and the $^{13}\text{C}\{^1\text{H}\}$ INEPT MAS NMR measurements. The $^{13}\text{C}\{^1\text{H}\}$ INEPT NMR and $^{13}\text{C}\{^1\text{H}\}$ CP/MAS results of polymers 3a, 4c and 4d are provided in Appendix A (Figures A1 to A3).



Scheme 3.2. Labels of the carbon atoms in the structural formula of the monomer residues present in polymer 5b.

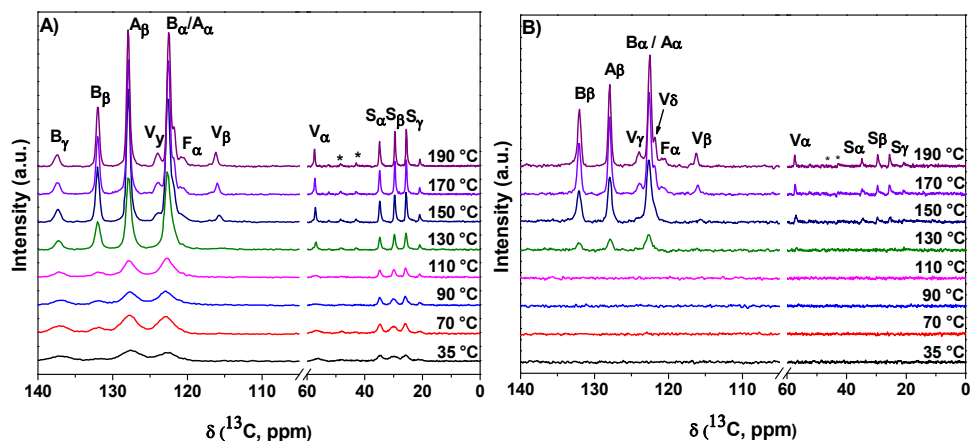


Figure 3.8. Temperature-dependent solid-state $^{13}\text{C}\{^1\text{H}\}$ CP/MAS NMR (A) and $^{13}\text{C}\{^1\text{H}\}$ INEPT MAS NMR (B) results showing the delayed mobility of the 2,5-furandicarboxylate and vanillic acid moieties occurring above 130 °C in polymer 5b. Signals are assigned according to Scheme 3.2 while the asterisks denote spinning sidebands. All experiments were recorded at 11.75 T (500.13 MHz for ^1H) using a MAS frequency of 10.0 kHz and ^1H decoupling during acquisition.

Figure 3.8b shows that no ^{13}C signals are observed in the $^{13}\text{C}\{^1\text{H}\}$ INEPT MAS NMR experiments below 130 °C, indicating that the polymer chains in sample 5b are rigid below this temperature; i.e., the polarization transfer from ^1H to ^{13}C via the J-coupling is inhibited due to large ^{13}C - ^1H dipolar couplings, leading to short, effective T_2 values.³⁰ Thus, the material can be described as crystalline and/or rigid amorphous. Upon heating to 130 °C, the ^{13}C resonances at 132.0 (B_β), 127.9 (A_β) and 122.6 ppm (A_α and B_β) start to rise. These signals appear due to the increased flexibility of the aromatic rings for BA and BP via rotational motion, which effectively averages the ^1H - ^{13}C dipolar couplings.³¹ This allows for an effective transfer via the J-coupling. The resonances at 57.4 (V_α), 34.9 (S_α), 29.5 (S_β), and 25.6 (S_γ) ppm, corresponding to the aliphatic carbons become apparent upon further heating to 150 °C. Simultaneously, a weak signal at 20.8 ppm corresponding to the aliphatic carbon of the acetoxy end-group rises. The $^{13}\text{C}\{^1\text{H}\}$ CP/MAS spectra of polymer 5b (Figure 3.8a) show a similar behavior as the $^{13}\text{C}\{^1\text{H}\}$ INEPT MAS NMR at low temperature; the peaks sharpen with increasing temperature and increase in intensity above the glass transition temperature.

As anticipated, the carbon signal of 2,5-FDCA moiety at 120.6 ppm (F_α) is not visible at 150 °C. At this temperature, the system is almost fully molten and all monomers can move freely. However, the F_α resonance only becomes visible at 170 °C, which is well above the melting temperature for this polymer (145 °C, DSC analysis, Table 3.2). Similarly, the rotational motion of the vanillic acid ring starts at 170 °C, indicated by the development of the signals at 123.9 (V_γ) and 121.8 (V_δ) ppm. This data shows that

both the 2,5-FDCA and the vanillic acid moiety require more thermal energy to become mobile in the LC melt phase. The delayed mobility in these two moieties might be the cause for the continuous decrease in the complex viscosity of polymer 5b as a function of temperature, see Figure 3.7.

The delayed mobility of the 2,5-FDCA moiety compared to regular phenyl based monomers is attributed to the energetic penalty of the dipole moment induced by the free electron pair of the oxygen heteroatom in the furan ring; thus it hinders rotational motion. Another possibility for the higher thermal energy requirement for the furan ring to become mobile is the melting of NPL crystals with different compositions, as is possible for blocky polymer 4c. However since polymer 5b is already molten before the furan moiety becomes mobile, this is not the case (see Appendix A for more information). This data clearly indicates that both VA and 2,5-FDCA become mobile at higher temperatures compared to the phenyl-based monomers such as BA and HQ (4c) or BP (5b). Similar changes in mobility as a function of temperature were observed for VA in polymer 4d (Figure A3, Appendix A), and for 2,5-FDCA in polymer 4c (Figure A2, Appendix A). As expected, polymer 3a did not show such behavior and only showed a gradual increase and sharpening of signals with increasing temperature (Figure A1, Appendix A). These molecular motions as a function of temperature can be correlated to the rheological response of these materials, see Figure 3.7. This information is interesting for future development and design of new bio-based thermotropic polyesters, containing 2,5-FDCA, vanillic acid, or other comparable bio-based monomers. The higher threshold in terms of the thermal energy required to become mobile can potentially contribute to the development of materials with an increased T_g value, a better dimensional stability at higher temperatures, and a better high temperature performance compared to polymers containing regular phenyl-based monomers.

3.3.6. Mechanical performance of the TLCs.

To determine the mechanical performance of these materials, tensile tests were performed on compression molded samples. All samples were compression molded at 10 °C above the temperature at which they were fully molten into the LC phase. WAXD was performed in reflection mode on the compression molded samples to determine the crystallinity (Table 3.3). Tensile tests were performed at room temperature (20 °C) at a constant stretching rate of 5 mm/min. Figure 3.9 and Table 3.3 show the characteristic tensile behavior observed for these polymers.

Table 3.3. Correlation between the mechanical performance and crystallinity of the compression molded samples. Standard deviations are displayed between brackets.

Entry	WAXD		Tensile tests	
	Crystallinity (%)	E-Modulus ^a (GPa)	Stress at break (MPa)	Strain at break (%)
4e	51.9 (0.4)	0.64 (0.07)	21.3 (2.9)	10.0 (2.42)
3a	49.5 (0.6)	0.50 (0.04)	17.4 (3.3)	15.14 (4.66)
5a	36.9 (0.1)	1.12 (0.11)	32.0 (6.4)	3.20 (0.70)
4c	36.6 (1.6)	1.22 (0.14)	50.8 (10.3)	7.38 (1.79)
4d	30.3 (0.3)	1.64 (0.10)	51.4 (4.0)	5.16 (0.75)
4f	—*	1.25 (0.12)	42.0 (5.6)	4.73 (0.95)
5b	—*	1.23 (0.10)	29.6 (5.2)	2.83 (0.61)

a) Calculated from tensile tests performed at 20 °C. The results are averaged from 10 tensile tests performed at 5 mm/min at RT of compression molded samples of 1 mm x 12 mm x 2 mm. * Polymers showed no diffraction peak after compression molding, only an amorphous halo.

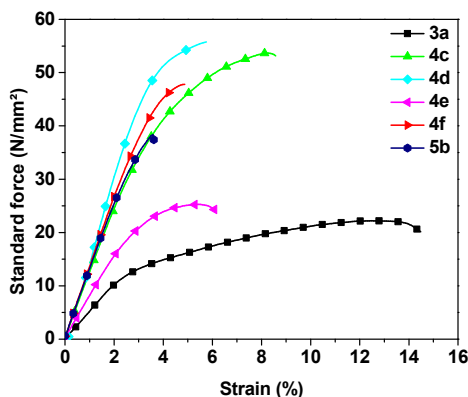


Figure 3.9. Characteristic tensile behavior of tensile tests the TLCPs synthesized in this study, performed at 5 mm/min at RT of compression molded samples of 1 mm x 12 mm x 2 mm.

In general, no yielding and low strain at break are anticipated in thermotropic polyester materials, since the LC domains do not allow for elongation due to a lack of entanglements. The polymers 4d, 4f and 5b, show this expected behavior for TLCPs. However, polymers 3a, 4c and 4e exhibit larger strain at break values. To recall, the polymers 4d, 4f and 5b are of non-blocky nature i.e. they are thought to exhibit a homogeneous distribution of monomers along the main chain. The non-blocky nature only allows the formation of small and defected NPL crystals. This becomes evident by the broad WAXD peak at $2\theta = 20^\circ$ and low crystallinity (4d) or absence of crystallinity (5b), as is shown in Figure 3.10. It is acknowledged that the rapid cooling of the non-blocky polymers limits crystallization in the isotropic samples even further, explaining the amorphous like diffraction patterns.

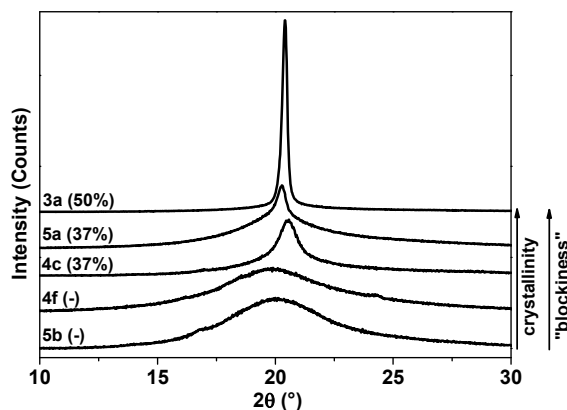


Figure 3.10. 1D WAXD diffractograms showing the difference in crystallinity (between brackets) and the width of the diffraction peak around 20° 2θ for the polymers 5b, 4f, 4c, 5a, and 3a. Polymers 5b and 4f do not show a distinct diffraction peak, which indicates that they are amorphous like, having short range structural correlation that cannot be easily detected by WAXD.

The polymers 3a, 4c and 4e are of a blocky nature, i.e. they exhibit a heterogeneous distribution of monomers along the main chain. This segregation promotes crystallization leading to the appearance of a sharper WAXD peak at $2\theta = 20^\circ$ (polymer 3a, Figure 3.10) and higher crystallinity (Table 3.3). The presence of non-crystalline domains between the crystalline segments likely act as a soft component that allow a larger strain at break. This is pronounced in polymer 3a, having the least amount of aromatic components. With the addition of 2,5-FDCA in polymer 4c i.e. with increasing amount of aromatic monomers, the polymer changes its ductile behavior to brittle and decreases in crystallinity from 50 to 37% while maintaining its blocky nature. This implies that the mechanical performance of these TLCPs is governed by both the aromatic content and the randomness of the distribution of monomers along the chain.

From these results, with the exception of the polymer 4e, it can also be concluded that the presence of vanillic acid promotes the homogeneous distribution of monomers and the presence of aromatic 2,5-FDCA enhances the modulus of the polymer.

3.4. Conclusions

Novel bio-based thermotropic polyesters containing 2,5-FDCA and vanillic acid were developed in this study. It is shown that 2,5-FDCA was successfully incorporated into the polymer backbone via the developed low-temperature synthesis route. Once 2,5-FDCA is incorporated in the chain it remains thermally stable. The incorporation of 2,5-FDCA as an additional aromatic component yields polymers that seem to be of a blocky nature. Furthermore, the T_g and T_m increase upon the replacement of the

flexible suberic acid moiety by the rigid 2,5-FDCA moiety. The increase in aromatic content also leads to an increase in mechanical performance of compression molded articles. Opposite to 2,5-FDCA, the copolymerization of vanillic acid appears to decrease the block formation in these TLCP, yielding polymers with a range of melting temperatures and stable LC melts. When combined, the application of 2,5-FDCA and VA can yield polymers that have a high aromatic content, low melting temperatures, and stable LC melts up to 300 °C. These polymers show overall low crystallinity and a good mechanical performance for compression molded samples. Furthermore, the 2,5-FDCA ring and the vanillic acid moiety require higher thermal energy to rotate the aromatic ring, which is anticipated to enhance the dimensional stability and high temperature performance of these polymers. Overall, it is concluded that, although 2,5-FDCA is unstable at temperatures above 250 °C and requires a low temperature synthetic route for successful incorporation in TLCPs, 2,5-FDCA is a viable monomer for use in aliphatic-aromatic thermotropic polyesters.

3.5. References

- [1] Liu, L., Lu, X., *Plast Rubber Comp*, **2002**, 21, 283-288
- [2] Jackson, W., *The British Polymer Journal*, **1980**, 12, 4, 154-162
- [3] Bello, P., Bello, A., Riande, E., Heaton, N.J., *Macromolecules*, **2001**, 34, 181-186
- [4] Kuhfuss, H., Jackson, W.J. Jr., **1974**, US patent 3 804 805
- [5] Jasinska-Walc, L.; Villani, M.; Dudenko, D.; van Asselen, O.; Klop, E.; Rastogi, S.; Hansen, M. R.; Koning, C. E. *Macromolecules*, **2012**, 45, 2796
- [6] Jasinska-Walc, L.; Dudenko, D.; Rozanski, A.; Thiyagarajan, S.; Sowinski, P.; van Es, D.; Shu, J.; Hansen, M. R.; Koning, C. E., *Macromolecules*, **2012**, 45, 5653
- [7] Zhang, M., CN101318892(A), **2008**.
- [8] Ayorinde, F.O., Osman, G., Shepard, R.L., Powers, F.T., *JAOCs*, **1988**, 65, 1774-1777
- [9] Hsiue, L.T., Ma, C.C.A., Tsai, H., *J Appl Polym Sci.*, **1995**, 56, 471-476
- [10] De Ruijter, C., Bos, J., Boerstool, H., Dingemans, T., *J Polym Sci Part A: Polym Chem*, **2008**, 46, 6565-6574.
- [11] Nicely, V.A., Dougherty, J.T., Renfro, L.W., *Macromolecules*, **1987**, 20, 573-578
- [12] Quach, L., Hornogen, E., Volksen, W., Economy, J., *J Polym Sci Part A: Polym Chem*, **1989**, 27, 775-784
- [13] De Oca, H.M., Wilson, J.E., Penrose A., Langton D.M., Dagger, A.C., Anderson, M., Farrar, D.F., Lovell, C.S., Ries, M.E., Ward, I.M., Wilson, A.D., Cowling, S.J., Saez, I.M., Goodby, J.W., *Biomaterials*, **2010**, 31, 7599-7605
- [14] Yang, D.K., Krigbaum, W.R., *Journal of Polymer Science Part B: Polymer Physics*, **1989**, 27, 1937-1851.
- [15] Yang, D.K., Krigbaum, W.R., *Journal of Polymer Science Part B: Polymer Physics*, **1989**, 27, 819-835.
- [16] Muramatsu, H., Krigbaum, W.R., *Journal of Polymer Science Part B: Polymer Physics*, **1987**, 25, 2303-2314.
- [17] Wilsens, C.H.R.M., Noorderover, B.A.J., Rastogi, S., *Polymer*, 2014, 55, 2432-2439
- [18] Bennett, A. E., Rienstra, C. M., Auger, C. M., Lakshmi, K. V., Griffin, R. G. *J. Chem. Phys.* **1995**, 103, 6951
- [19] G. Morris, R. Freeman, *J. Am. Chem. Soc.* **1979**, 101, 760-762.
- [20] D. P. Burum, R. R. Ernst, *J. Magn. Res.* **1980**, 39, 163-168.
- [21] Bielecki, A.; Burum, D. P., *J. Magn. Reson., Ser. A*, **1995**, 116, 215-220.

- [22] Gruter, G.-J. M., Sipos, L., Dam, M.A., *Combinatorial Chemistry & High Throughput Screening*, **2012**, 15, 180-188
- [23] Drewitt, J.G.N., Lincoln, J., Br. Patent, 621971, **1946**, November 12
- [24] Li, X.G., Huang, M.-R., Guan, G.-H., Sun, T., *Die Angewandte Makromolekulare Chemie*, **1995**, 227, 69-85
- [25] Nagata M., *Journal of Applied Polymer Science*, **2000**, 78, 2474–2481
- [26] Windle, A.H., Viney, C., Golombok, R., Donald, A.M., Mitchell, G.R., *Faraday Discuss. Chem. Soc.*, **1985**, 79, 55-72
- [27] Li, X.G., Huang, M.-R., Guan, G.-H., Sun, T., *J. Appl. Polym. Sci.*, **1996**, 59, 1-8
- [28] Gao, P., Lu, X.H., Chai, C.K., *Polymer Engineering and Science*, **1996**, 36, 22, 2771-2780
- [29] Burgess, S.K., Leisen, J.E., Kraftschik, B.E., Mubarak, C.R., Kriegel, R.M., Koros, W.J., *Macromolecules*, **2014**, 47, 1383-1391
- [30] Schmidt-Rohr, K.; Spiess, H. W. *Multidimensional Solid-State NMR and Polymers*, Academic Press: New York, **1994**.
- [31] Hansen, M. R.; Graf, R.; Spiess, H. W., *Acc. Chem. Res.* **2013**, 46, 1996–2007.

Chapter 4

Processing and performance of aromatic-aliphatic thermotropic polyesters based on vanillic acid

Abstract

In this chapter, the fiber spinning and performance of the vanillic acid based aliphatic-aromatic thermotropic polyesters, described in chapter three, is reported. It is demonstrated that the weight average molecular weight (M_w) of roughly 30 kg/mol is required in order to successfully perform fiber spinning on these polymers. The application of a polymer with lower M_w results in poor mechanical performance and fiber breakage during the winding process. Spinning polymers of sufficient molecular weight yields fibers having tensile moduli in the range of ~ 10 GPa and a tensile strength around ~ 150 - 200 MPa. These fibers retain their orientation up to temperatures in the range of 120 - 130 °C, after which they start to melt. FTIR and solid-state NMR experiments indicate that only the aromatic components are molecularly oriented during the spinning process. In contrast, the aliphatic moieties exhibit a high mobility, normally corresponding to a local isotropic motion. It is expected that the poor molecular orientation of the aliphatic moieties in these aliphatic-aromatic thermotropic polyester contribute to the low tensile modulus of the fibers, obtained after the spinning process.

4.1. Introduction

The synthesis, processing and performance of thermotropic polyesters has widely been investigated over the last decades. In general, their low melt-viscosity, the ease in processing, and the highly anisotropic products, obtained after melt-processing, has resulted in numerous publications and commercialization of several thermotropic polyesters.¹⁻⁸ Perhaps the most widely used thermotropic polyesters are the *p*-hydroxybenzoic acid (BA) and 6-hydroxy-2-naphthoic acid (NA) based copolymers, commercially known as the Vectra® series. Fibers having tensile moduli around 50 GPa and tensile strengths of over 1 GPa are readily obtained upon processing these polymers from the thermotropic melt. Furthermore, heat treatment of these fibers increases the mechanical performance further, yielding fibers with tensile moduli up to ~100 GPa and tensile strengths around 3 to 4 GPa. Generally, the increase in tensile modulus upon heat-treatment is attributed to the reorganization of the monomer sequences resulting in the formation of bigger and more perfect crystals. The improved tenacity of the fibers after heat-treatment is attributed to the occurrence of a post-condensation reaction, resulting in an increase of the molecular weight which facilitates a better stress transfer along the polymer chains.⁹

From these data, it becomes clear that a heat-treatment is advised for semi-crystalline fully aromatic thermotropic polyester fibers, in order to achieve the best mechanical performance. The application of such a heat-treatment is only possible when the fibers are dimensionally stable at the applied annealing temperatures, commonly in the range of 250-300 °C. For example, the application of such a heat-treatment is not possible for amorphous thermotropic polyesters or for thermotropic polyesters that have too low melting temperatures. An example of an amorphous fully aromatic thermotropic polyester, based on NA, terephthalic acid, and 4,4'-dihydroxy-2,2'-dimethyl-biphenyl, has been reported by Grasser and coworkers¹⁰. Although these polymers exhibited no melting or crystallization transition, fiber spinning from the thermotropic melt yielded fibers with tensile modulus in the range of 50 GPa and a tensile strength around 0.5 GPa.

A well-known example of aliphatic-aromatic thermotropic polyesters is the copolymer of poly(ethylene terephthalate) (PET) and BA. Depending on the processing temperature, processing of such copolymers containing 60 mole% BA from the thermotropic melt yields fibers having tensile moduli between 10-30 GPa.^{11,12} Another example of thermotropic fibers spun from aliphatic-aromatic polymers has been reported by Dingemans and coworkers.¹³ These authors reported the synthesis and preliminary fiber spinning results of polymers containing flexible suberic acid and sebacic acid spacers. These fibers exhibited a tensile modulus of 15 GPa and a tensile strength of 0.12 GPa. Although the presence of these aliphatic spacers drastically decreases the tensile performance, it is clear that fibers with promising tensile moduli

can still be obtained. The presence of these aliphatic spacers decreases the melting and processing temperatures of the thermotropic polymers, and allows for the incorporation of monomers that are thermally instable at high temperatures.

In the previous chapters of this thesis, a route to successfully design thermotropic polyesters containing 2,5-furandicarboxylic acid (2,5-FDCA) and vanillic acid into thermotropic polyesters was reported.^{14,15} In chapter 3 it was shown that the copolymerization of 2,5-FDCA as a replacement for flexible dicarboxylic acids can be used to increase the glass transition temperature (T_g) and melting temperature (T_m) of these thermotropic polyesters. Although it was proven that the synthesis of 2,5-FDCA based thermotropic polyesters is feasible, the reaction times required for sufficient molecular weight build-up were highly unpractical. To recall, it took more than 24 hours of processing under high vacuum to reach a number average molecular weight (M_n) of 10,000 g/mol during the synthesis of a copolymer containing only 16 mole% 2,5-FDCA. Furthermore, preliminary processing experiments performed on this polymer indicate that the molecular weight is too low for fiber spinning experiments. The spun fibers were extremely brittle and broke during the spinning process, because of their low molecular weight. In contrast, the synthesis of copolymers containing small amounts of vanillic acid could be performed significantly faster, yielding polymers with M_n values of 20 kg/mol within a few hours of reaction time. Moreover, the presence of vanillic acid was shown to (a) improve the monomer sequence distribution, (b) increase the stability of the thermotropic melt, (c) decrease the polymer melting temperature, and (d) improve the spinnability of thermotropic polyesters.¹⁶⁻¹⁸ Although the benefits of the copolymerization of vanillic acid are interesting from a chemical viewpoint, the low melting temperature of these polymers limits their application at high temperatures and does not allow for the processed products to undergo a heat-treatment step. These factors, mainly resulting from the presence of the aliphatic spacers, might limit the application of these fibers for practical purposes.

The effect of different processing routes on the mechanical performance of vanillic acid based renewable aliphatic-aromatic thermotropic polyesters are evaluated in this chapter. The used processing conditions are fiber spinning via melt-drawing, compression molding, and solvent casting. differential scanning calorimetry (DSC), dynamic mechanical thermal analysis (DMTA), wide-angle x-ray diffraction (WAXD), polarization optical microscopy (POM), Fourier-transform infra-red (FTIR), and solid-state NMR spectroscopy are used to characterize the processed products and to evaluate the performance of the aromatic-aliphatic thermotropic polyesters processed in this study.

4.2. Experimental section

4.2.1. General polymerization procedure

Thermotropic polyesters containing *p*-hydroxybenzoic acid (BA), vanillic acid (VA), suberic acid (SuA), and hydroquinone (HQ) were prepared using a 200 gram scale acidolysis melt-polycondensation reaction. The monomers were loaded into a 500 mL three-neck round bottom flask fitted with a mechanical stirrer, together with 50-100 mg of $\text{Zn}(\text{CH}_3\text{CO}_2)_2$ and the temperature was gradually increased to 260 °C. Acetic acid was distilled off and reduced pressure was applied to the system for eight to twelve hours after roughly 90% of the expected acetic acid was collected. A detailed description of the polymerization procedure can be found in chapter 3.

4.2.2. Processing of thermotropic polyesters

Solvent cast films of the polymers used in this study were prepared via dissolution of polymer samples in a 2:1 mixture (v/v) of chloroform/1,1,1,3,3,3-hexafluoroisopropanol (CHCl_3 /HFIP) at room temperature. The concentrations of the casting solutions were 1 g polymer per 3 mL solvent. Once the polymers were fully dissolved, the casting solutions were poured onto an aluminum plate and the films were allowed to dry at room temperature for 3 hours followed by drying *in vacuo* at 40 °C overnight. The prepared polymer films were slightly yellow/brown and transparent. A heat treatment and thorough drying of the samples was performed in a second drying step above the glass transition temperature (T_g) at 80 °C for 12 hours, to ensure the full removal of any residual solvent.

Compression molding of the polymers was performed using a P 300 E Collins compression mold. Samples were compression molded in sheets having a thickness of 0.5 mm or 1 mm at 10 °C above their melting temperature as observed in DSC analysis.

Small scale fiber spinning experiments were performed using a DSM Xplore MC15 twin-screw extruder. Prior to the processing, the polymers were dried *in vacuo* overnight at 80 °C. The dried polymer was loaded into the mini-extruder via a water-cooled hopper under a nitrogen rich flow to prevent degradation and depolymerization. SEC analysis was conducted on the spun fibers and no changes in molecular weight were observed before and after processing. Samples were mixed and extruded at a screw rotation speed of 50 rpm at 10 °C above their melting temperatures. The extrudate was quenched in a water bath located 1 cm from the extruder outlet and was wound on a bobbin having a diameter of 10 cm. Fiber were spun at different winding speeds to achieve different draw ratios. The fibers were dried *in vacuo* for 48 hours at room temperature prior to any measurement.

4.2.3. Characterization methods

Molecular weights and polydispersity index (PDI) values were determined *via* 1,1,1,3,3,3-hexafluoroisopropanol (HFIP) size exclusion chromatography (SEC). This system is equipped with a Waters 1515 Isocratic HPLC pump, a Waters 2414 refractive index detector (40 °C), a Waters 2707 autosampler, and a PSS PFG guard column followed by 2 PFG-linear-XL (7 mm, 8 x 300 mm) columns in series at 40 °C. HFIP (Apollo Scientific Limited) with potassium trifluoroacetate (3 g L⁻¹) was used as an eluent at a flow rate of 0.8 mL min⁻¹. The molecular

weights were calculated against poly(methyl methacrylate) standards (Polymer Laboratories, $M_p = 580$ Da up to $M_p = 7.1 \times 10^6$ Da). SEC samples were filtered through a 200 μm filter prior to injection.

The thermal stability of the polymers was determined using thermogravimetric analysis (TGA), which was performed on a TA Instruments TGA Q500 in a nitrogen rich atmosphere. Samples were heated at 10 $^\circ\text{C}/\text{min}$ from 20 $^\circ\text{C}$ to 600 $^\circ\text{C}$.

The T_g and the peak transition temperature from the crystalline to the LC phase (T_m) were determined by differential scanning calorimetry (DSC) using a TA Instruments Q1000 DSC. The normal heating and cooling rates of the samples were 10 $^\circ\text{C}/\text{min}$ and measurements were performed under a nitrogen rich atmosphere.

Dynamic mechanical thermal analysis (DMTA) was performed on a TA Instruments DMA Q800. DMTA samples were prepared via compression molding at temperatures between 160 $^\circ\text{C}$ to 180 $^\circ\text{C}$ and were cut into rectangular shapes of 20 mm x 5 mm x 0.5 mm. All experiments were performed at a frequency of 1 Hz and at a heating rate of 2 $^\circ\text{C}/\text{min}$. Measurements were continued until the sample was molten or broken. The T_g values determined from DMTA analysis were obtained by taking the maximum value of the loss modulus during heating. DMTA experiments on the fibers were performed after cutting them into strands of 25 mm.

Tensile test experiments were performed at a constant deformation rate of 5 mm/min using a Zwick 100 tensile apparatus and a load cell of 100 N at room temperature. Samples were prepared via compression molding and cut into dog-bone shaped samples of 20 mm x 2 mm x 1 mm. The spun fibers were loaded in the clamps after the fiber ends were pasted on a 3M sticky note to ensure fiber breakage occurred in the center of the fiber instead of breaking at the clamp position. Measurements resulting in fiber breakage at the clamp position were discarded to ensure repeatability of the tensile tests.

Morphologies of the synthesized polymers were determined on a Zeiss Axioplan 2 Imaging optical microscope under crossed polarizers and CD achorplan objectives (32x zoom). A THMS 600 heating stage connected to a Linkam TMS 94 control unit was mounted onto the optical microscope. Samples were prepared by placing a small amount of ground polymer in-between two glass slides. Optical micrographs were taken at various temperatures, while heating at a rate of 10 $^\circ\text{C}/\text{min}$.

Rheological experiments performed in the thermotropic melt were conducted using a TA Instruments ARG2 rheometer. Parallel plate geometry of a diameter of 25 mm and a thickness of 1 mm was used to identify the rheological response of the thermotropic melt. Experiments were performed in the linear viscoelastic regime at a fixed strain of 1.25%. Frequency sweeps were performed in the temperature range between 150 $^\circ\text{C}$ and 320 $^\circ\text{C}$. Prior to the data collection, the samples were allowed to relax for 15 minutes at the starting temperature of the experiments.

2D fiber patterns were taken at 40kV and 40mA, using a Bruker D8 equipped with GADDS, a 2-dimensional detector system using CuK_α radiation, and a wavelength of 1.54184 \AA . A parabolic Göbel mirror is used to provide a highly parallel beam whereby the $\text{K}\beta$ and Bremsstrahlung effect is suppressed. The measurements were performed in transmission mode with a sample to detector distance of 50 mm and an exposure time of 30 minutes. The

orientation parameter $\langle P_{2n}(\cos \varphi) \rangle_d$ was calculated via the procedure described by Mitchell and Windle.¹⁹ The azimuthal intensity $I(\varphi)$ at the maximum of the inter-chain diffraction peak ($2\theta = 21^\circ$) was taken. The orientation parameter $\langle P_{2n}(\cos \varphi) \rangle_d$ was then determined from an average of a Legendre polynomial, weighted against the azimuthal intensity scan using equations 4.1, 4.2 and 4.3. In this case, only the second order Legendre polynomial was taken into account, yielding $\langle P_{2n}(\cos \varphi) \rangle_m = -0.5$.

$$\langle P_{2n}(\cos \varphi) \rangle_d = \frac{\langle P_{2n}(\cos \varphi) \rangle}{\langle P_{2n}(\cos \varphi) \rangle_m} \quad (\text{Eq. 4.1})$$

$$\langle P_{2n}(\cos \varphi) \rangle = \frac{\int_0^{\pi/2} I(\theta, \varphi) P_{2n}(\cos \varphi) \sin \varphi \delta \varphi}{\int_0^{\pi/2} I(\theta, \varphi) \sin \varphi \delta \varphi} \quad (\text{Eq. 4.2})$$

$$\langle P_{2n}(\cos \varphi) \rangle_m = \frac{(2n)!}{(-1)^n 2^{2n} (n!)^2} = -\frac{1}{2} \text{ for the second term} \quad (\text{Eq. 4.3})$$

The order parameter reflects the contributions of the distribution of the director orientation throughout the bulk polydomain sample and the contributions of the director on a molecular level.²⁰ In short, the orientation parameter reflects the degree of anisotropy of the scattering of polymer chains, while assuming that these chains are infinitely long rigid rods. The values of $\langle P_{2n}(\cos \varphi) \rangle_d$ vary from 0, corresponding to a random chain orientation similar to the orientation of an isotropic liquid, to unity, corresponding to the perfect alignment of the polymer chains along the orientational axis.

FTIR spectroscopy studies were performed using a Varian 670IR spectrometer. Furthermore, one Specac FTIR GS12000 polarizer was placed above the condenser to polarize the light. The direction of the polarized light reaching the sample was changed by rotating the FTIR polarizer. All spectra were measured in the range of 4000 cm^{-1} to 650 cm^{-1} at a resolution of 4 cm^{-1} in transmission mode. For this purpose a SLIDE-ON ATR selenium crystal was used.

The solid-state NMR experiments were performed with Bruker Avance III spectrometer operating at 300.13 MHz ^1H Larmor-frequency. A 4mm MAS double-resonance probe was used in the experiments. The spinning speed of the rotor is set at 5 kHz in the ^{13}C CP/TOSS (cross-polarization total suppression of spinning sidebands) experiments, and 3 kHz in the SUPER (Separation of Undistorted Powder patterns by Effortless Recoupling) experiments²¹, which were used to obtain undistorted ^{13}C CSA (chemical shift anisotropy) patterns of the materials under MAS (magic angle spinning). The 90° pulse length in the experiments varies between 2.5 and $3 \mu\text{s}$ on both channels, corresponding to $\omega/2\pi = 83\text{-}100 \text{ kHz}$. The CW or TPPM schemes are applied for dipolar decoupling with the decoupling frequency of $\omega/2\pi = 83\text{-}100 \text{ kHz}$. Ramped-CP is used for the experiments with cross-polarization step. The ^{13}C chemical shifts were determined from the carbonyl signal ($\delta = 176.0 \text{ ppm}$) of glycine relative to tetramethylsilane (TMS).

For the study of the chain orientation in the drawn samples, the isotropic and oriented samples need to be distinguished and prepared. The isotropic samples were prepared by cutting the drawn samples to small pieces before putting them into the rotors, whereas the oriented samples were prepared by gluing the drawn samples aligned parallel to the fibre axis. For more details about the preparation of the oriented sample, see the publication of Yao and coworkers.²²

4.3. Results and discussion.

4.3.1. Synthesis and characterization of thermotropic polyesters.

Thermotropic polyesters containing 30 mole% *p*-hydroxybenzoic acid, 30 mole% suberic acid, 30 mole% 1,4-dihydroxybenzene, and 10 mole% vanillic acid were synthesized following the general polymerization procedure described in the experimental section (Figure 4.1). The copolymerization of 10 mole% vanillic acid was performed to ensure a random incorporation of the monomers along the polymer backbone and to reduce the melting temperature of the polymer. Table 4.1 shows an overview of the molecular weights, thermal transitions, and tensile performance after compression molding of polymers **I-III**.

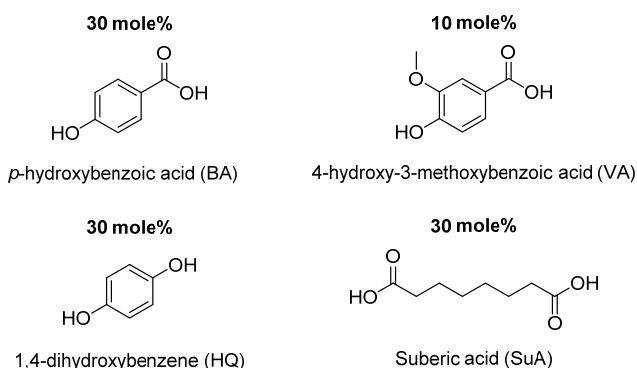


Figure 4.1. Chemical structures and composition of the monomers present in polymers **I-III** synthesized in this study.

Table 4.1. Molecular weights, thermal properties and mechanical performance of compression molded polymers **I-III**. Standard deviation values observed during tensile testing have been added in-between brackets.

Entry	SEC		DSC		DMTA	Tensile testing		
	M_w (kg/mol)	PDI (-)	T_g (°C)	T_m (°C)	T_g (°C)	E (GPa)	σ_{max} (MPa)	ϵ_{break} (%)
I	17.3	2.14	43.1	125.9	50.8	0.96 (0.13)	23.1 (2.88)	4.14 (2.17)
II	31.2	2.40	44.6	126.7	51.0	0.90 (0.05)	20.7 (2.21)	6.38 (0.85)
III	43.8	2.56	45.7	127.1	51.7	1.09 (0.12)	29.7 (2.49)	12.55 (0.35)

As is shown in table 4.1, the weight average molecular weight (M_w) of polymers **I**, **II**, and **III** are 17.3 kg/mol, 31.2 kg/mol, and 43.8 kg/mol, respectively. According to both DSC and DMTA analysis, the glass transition temperature (T_g) of these polymers increases with increasing molecular weight. This increase in T_g is likely a result from the decrease of the number of end-groups with an increase of the molecular weight. Similar to the T_g , the peak melting temperature (T_m) of these polymers increases slightly with increasing molecular weights.

The tensile modulus (E) and the maximum tensile stress (σ_{\max}) do not seem to be strongly influenced by the molecular weight of polymers **I-III** (Figure 4.2). In contrast, the strain at break (ϵ_{break}) increases slightly with increasing molecular weight. Although the ϵ_{break} increases with molecular weight, none of the polymers show strain hardening during uniaxial deformation. The absence of strain-hardening during deformation suggests that these liquid crystalline polymers are not or only loosely entangled.

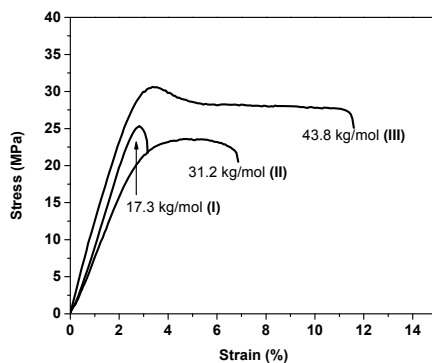


Figure 4.2. Characteristic stress-strain curves, obtained from the compression molded polymers **I, II** and **III**.

The viscoelastic response of polymer **III**, having the highest M_w of the three polymers, was investigated as a function of frequency at different temperatures (Figure 4.3). Prior to the evaluation of the data, it should be noted that caution should be taken when interpreting this rheological data; rheology on rigid liquid crystalline polyesters that have an inaccessible isotropic phase is generally complex due to the inability to remove the thermal and flow history of the sample.²³ Besides, continuous transesterification occurs in the polyester melt, possibly influencing the chemical microstructure of copolymers and thus changing the rheological response. These factors limit the repeatability of rheological experiments of thermotropic polyesters. In order to minimize errors from thermal and flow history, all samples were cut into discs with a diameter of 25 mm from the same compression molded sheet having a thickness of 1 mm. Furthermore, the samples were allowed to equilibrate for 15 minutes at the desired temperature prior the experiment.

From Figure 4.3 it can be seen that no rubber plateau region is detected for either G' or G'' up to 260 °C. Instead, G' and G'' decrease with decreasing angular frequency (ω) indicating that the measurements are performed in the terminal regime. The absence of a rubber plateau is commonly observed during frequency sweeps of semi-flexible thermotropic polyesters.²³⁻²⁵

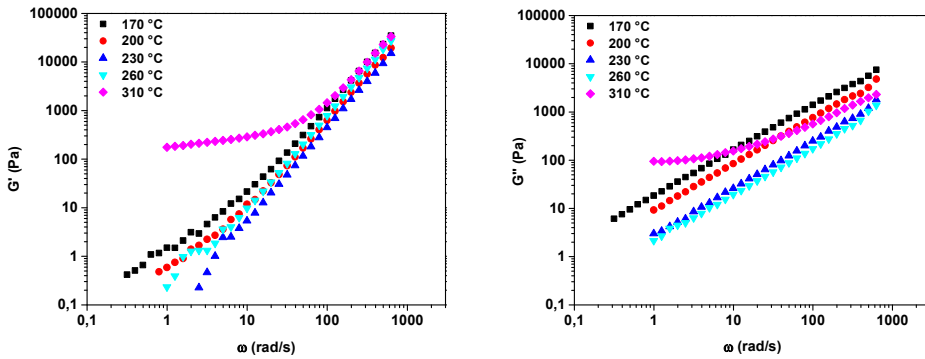


Figure 4.3. Elastic modulus G' (left) and viscous modulus G'' (right), observed during rheology experiments of polymer **III**, as a function of angular frequency ω performed at temperatures varying from 170 °C to 310 °C.

From the data in Figure 4.3 it is noticed that the data points of G' start to scatter at low ω values (<1 rad/s) at temperatures above 200 °C. The scattering in the data is believed to be a result of the G' values being too close to the transducer limits. However, it can be clearly seen that the decay of G' slowly levels off at low angular frequencies for measurements performed between 170 °C and 200 °C. Similarly, the slope of the $\log G''$ versus $\log G'$ plots does not follow the characteristic slope value of 2 expected for liquid crystalline polymers residing in the isotropic melt (Figure 4.4).^{24,26,27} Instead, an enhanced storage modulus is observed at low values, characteristic for the nematic phase. As is reported by Zhou and coworkers, this long relaxation tail at low oscillatory frequencies is a result of distortional elasticity related to the defect structure of the nematic phase.²³

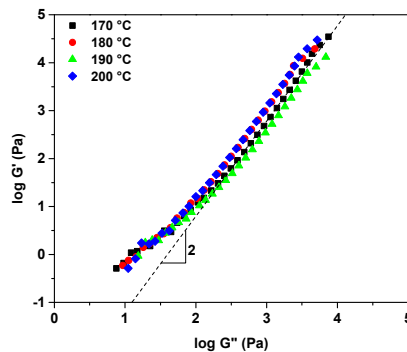


Figure 4.4. G'' versus G' plotted for frequency sweeps performed on polymer **III** at temperatures between 170 °C and 200 °C. It can be seen that the expected slope of 2 in the $\log G''$ versus $\log G'$ plot, characteristic for isotropic materials, is not followed at low moduli.

The rheological response of polymer **III** changes significantly at 300 °C or higher. A plateau value for both G' and G'' is observed at low ω values, indicating that the polymer cross-links at high temperature.

In general, from the rheology data it can be concluded that, although the thermal and flow history could not fully be erased, thermotropic polyester **III** exhibits the characteristic behavior for a nematic polymer melt. Furthermore, as is confirmed with polarization optical microscopy, polymers **I-III** show no isotropization transition prior to degradation and no side reactions up to 300 °C, which means that they have a broad temperature window for processing. In general, processing from the thermotropic melt is ideally performed at temperatures close to the melting temperature. At these temperatures, the viscosity of the polymer melt is sufficiently high to ensure good spinnability.

4.3.2. Fiber spinning from the thermotropic melt.

Spinning experiments were performed at 170 °C, since a good overall spinnability was observed for polymers **I-III** at this temperature. Small scale, single filament, fiber spinning experiments were performed on the polymers using a twin-screw extruder. Once extruded, the strand was quenched in a water bath and wound on a bobbin. The draw ratio was controlled by a variation of the winding speed. To ensure a high orientation of the fibers, the water bath was placed at 1 cm distance from the extruder outlet. Since the fiber is quenched once it touches the water surface, the drawing process takes place over the 1 cm in between the extruder outlet and the water bath. The average draw ratios of the fibers are calculated by dividing the cut-through area of the fiber by the area of the extruder outlet. The diameter of the fiber was calculated using the length and mass of the fiber and the density (1.21 g/mm³) of the non-oriented polymer.

The fibers obtained after spinning polymer **I** could not be wound since they were too brittle and broke during the winding process. This indicates that the molecular weight of this polymer is too low for uniaxial deformation. In contrast, polymers **II** and **III** could be easily spun at these conditions and were wound at varying draw ratios. Figure 4.5a shows an overview of the storage modulus (E') of the fibers of polymers **II** and **III** as a function of the draw ratio, obtained after DMTA analysis. Figure 4.5b shows the Young's modulus of the fibers of polymer **III** as determined via tensile testing. For comparison, the storage modulus observed in DMTA is added in Figure 4.5b.

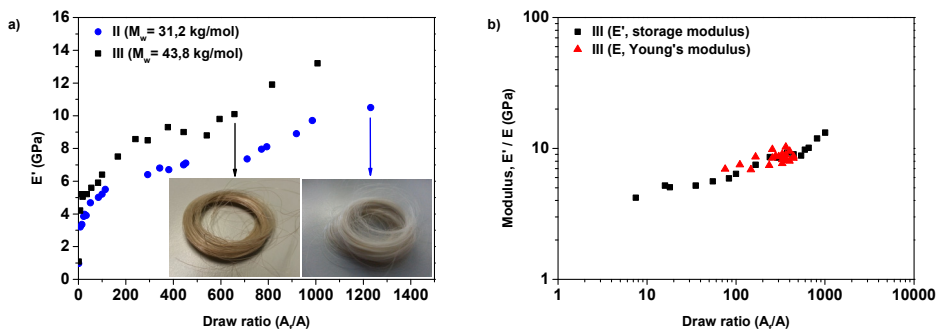


Figure 4.5. a) Storage modulus (E') versus draw ratio plot as observed in DMTA analysis for fibers spun from polymers **II** and **III**. Figures of the fibers, obtained after continuous spinning, are enclosed. b) Young's modulus as a function of the draw ratio of spun fibers from polymer **III** as determined via tensile testing. *N.b.* The experimental data points shown in this figure were obtained at room temperature.

As is depicted in Figure 4.5a, the modulus of the fibers made from both polymers increases with the draw ratio. Furthermore, fibers of polymer **III** exhibit higher storage moduli than polymer **II** when processed at the same conditions and draw ratio. This is probably a result from the difference in relaxation times of the oriented polymer chains prior to quenching in the water bath. As is suggested by Jackson and coworkers, processing of a thermotropic BA/PET based copolymer at increasing temperatures yields products with lower modulus, due to a faster relaxation of the polymers prior to quenching.²⁸ Similarly, the relaxation of polymer chains is also dependent on molecular weight, since relaxation and chain dynamics of short polymer chains is generally faster than long polymer chains. For this reason, it is anticipated that the slower relaxation during processing of polymer **III** facilitates the higher storage modulus.

Since the fibers spun from polymer **III** show better performance, tensile tests were performed on these fibers. In general, it is observed that fibers with a high draw-ratio exhibit a lower strain at break. This becomes evident when the tensile stress is plotted as a function of draw ratio for fibers that break between 2.5% and 3.5% strain, it can be seen that an increase in draw ratio results in an increase of the tensile strength (Figure 4.6).

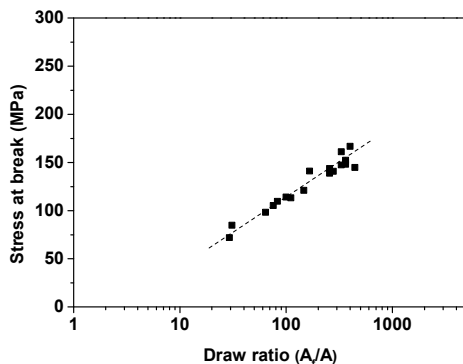


Figure 4.6. Stress at break versus draw ratio observed in tensile testing of spun fibers of polymer **III**, having a strain at break between 2.5 and 3.5%.

The fibers spun from polymer **III** were characterized using 2D wide-angle x-ray diffraction (WAXD) and their order parameter $\langle P_{2n}(\cos \varphi) \rangle_d$ was determined (Figure 4.7). The order parameter $\langle P_{2n}(\cos \varphi) \rangle_d$ is determined from an average of a Legendre polynomial, weighted against the azimuthal intensity scan as described in the experimental section. Figure 4.7a shows a characteristic 2D-WAXD fiber pattern and the corresponding azimuthal intensity scan taken at the maximum of the inter-chain diffraction peak at $2\theta = 21^\circ$. Figure 4.7b shows the orientation parameters $\langle P_{2n}(\cos \varphi) \rangle_d$ for fibers of polymer **III**, with varying draw ratios. In general, it can be seen that an increase of the draw ratio results in an increase of the orientation parameter. These results are in good agreement with the continuous increase of the storage/tensile modulus and the tensile strength of the fibers, which all increase with the draw-ratio. These data therefore suggest that a strong alignment and mechanical performance of these aliphatic-aromatic is only obtained at high draw ratios. Such a strong dependency of the mechanical performance on the draw ratio was also observed by Acierno and coworkers, during the spinning experiments of the BA/PET based thermotropic copolymers (60 mole% BA) at varying draw ratios and temperatures.¹¹

In general, these preliminary single-filament fiber spinning experiments show that these vanillic acid based thermotropic polyesters can easily be spun from the melt and their modulus, tensile strength, and orientation can be improved by increasing the draw ratio. Using the procedure reported in this study, fibers having tensile modulus >10 GPa and a tensile strength >150 MPa can be easily spun from polymer **III**. Although these values are promising, as is reported by Muramatsu and coworkers²⁹, optimization of the spinning procedure should be performed by controlling the processing temperature, the extrusion velocity, the geometry of die, the contraction

ratio inside the die, and the winding speed / draw ratio. However, this subject is beyond the scope of this study.

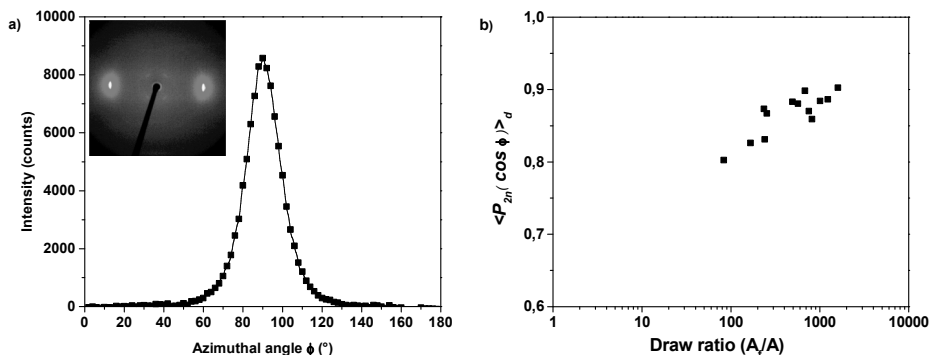


Figure 4.7. a) Characteristic WAXD pattern of the fibers developed in this study and the azimuthal density distribution of the oriented diffraction peak corresponding to the inter-chain distance taken at $2\theta = 21^\circ$ and, b) Order parameter $\langle P_{2n}(\cos \phi) \rangle_d$ as a function of draw ratio for fibers of polymer **III**.

4.3.3. Effect of orientation on the thermal properties.

In the previous section it was demonstrated that fibers can be readily spun from the thermotropic melt. The fibers, obtained after the spinning process, were characterized using DSC and DMTA analysis. Figure 4.8 shows an overview of the first heating run in the DSC analysis performed at $10^\circ\text{C}/\text{min}$ of the compression molded sample, the as spun fiber and the fiber after annealing at 100°C for 24 hours. It can be clearly seen that the spinning process does not influence the melting behavior of the polymer, as is indicated by the comparable enthalpy of the melting observed at 126°C for the compression molded sample (1.94 J/g) and the as spun fiber (2.08 J/g). This indicates that the crystallinity of the compression molded and the spun fibers are comparable. Although no changes in melting behavior are observed upon fiber spinning in DSC analysis, the performance of a heat-treatment (HT) results in a slight increase of the melt-enthalpy indicating a slightly higher crystallinity of the fiber after annealing at 100°C .

WAXD analysis was employed to identify the changes in crystallinity as a function of processing and annealing. In order to calculate the crystallinity, peak fitting of the inter-chain diffraction peak and the amorphous scattering was performed and the crystallinity was obtained by dividing the area of the diffraction peak at $2\theta = 21^\circ$ by the total area of the diffractogram. Following this procedure, a crystallinity of 31% is calculated for the compression molded sample of polymer **III**. In contrast, the heat-treated fibers show a crystallinity of $\sim 70\text{-}73\%$.

As is visible from the inset 2D WAXD fiber diffractogram in Figure 4.7a, there are no strong diffraction peaks in the diffractogram other than the inter-chain diffraction peak. It should be noted that a weak diffraction signal is observed at $2\theta \sim 8-9^\circ$, likely corresponding to the diffraction originating from the suberic acid spacer. However, the intensity of this signal is very low and can therefore not be used to determine the crystallinity of the fibers. For this reason, the oriented amorphous phase and the crystalline phase cannot be distinguished through WAXD analysis.³⁰ Nonetheless, when the results from WAXD and DSC analysis are combined, it can be concluded that fiber spinning results in a strong orientation of the amorphous phase, whereas annealing results in a significant increase of the crystallinity of the sample evident from the increase in melt enthalpy to 5.54 J/g from 2.09 J/g (Figure 4.8).

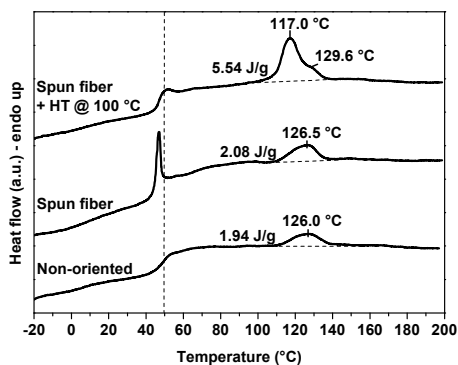


Figure 4.8. DSC heating runs of polymer **III** performed at 10 °C in the non-oriented state, the as-spun fiber, and the spun fiber after annealing for 24 hours at 100 °C (spun fiber + HT @ 100 °C). For the DSC experiments, a bundle of fibers having a draw ratio of 1500 was used.

According to DSC analysis, the glass transition of the spun polymers is not strongly influenced by the orientation of the fibers; the T_g of both the compression molded samples and the fibers lie in the range between 45 to 48 °C. According to the data shown in Figure 4.8, the as spun fiber exhibits a strong endotherm above T_g . This is thought to be a result of the release of stresses induced by the quenching step in the spinning process. In contrast to the DSC analysis, a clear increase of the glass transition temperature is observed for the oriented fibers when the thermal behavior is evaluated by DMTA analysis. As is shown in Figure 4.9, the peak in the loss modulus (E''), characteristic for the glass transition, increases by roughly 10 °C for the oriented and annealed sample (60.7 °C) compared to the compression molded sample (51.7 °C). Similarly, the T_g of the as-spun fibers increases by 3 to 10 °C compared to the compression molded samples, depending on the applied draw ratio of the fiber. This data clearly shows that, although not detectable in DSC analysis, an increased

orientation of the polymer chains causes an increase of the glass transition temperature.

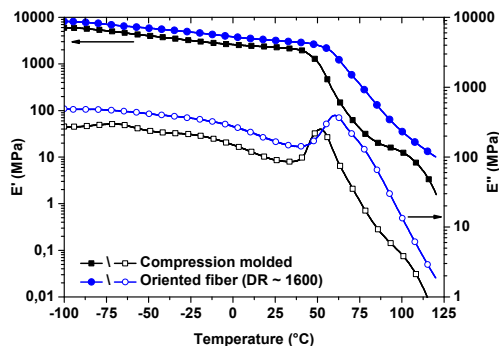


Figure 4.9. Temperature dependence of the storage (E') and loss (E'') moduli for the compression molded polymer **III** and a bundle of oriented fibers with an average draw-ratio of 1500.

Figure 4.10 shows the dependence of the orientation parameter $\langle P_{2n}(\cos \varphi) \rangle_d$ of a fiber with a draw ratio of 100 as a function of temperature (heating rate of $10\text{ }^\circ\text{C}/\text{min}$). For comparison, the first DSC heating trace of the same fiber is added. From Figure 4.10 it can be seen that the fiber relaxes slowly upon heating, resulting in a slight decrease in orientation. For example, the fiber has an orientation parameter of 0.81 at $20\text{ }^\circ\text{C}$ and the orientation parameter decreases to 0.79 upon heating to $100\text{ }^\circ\text{C}$. Upon further heating, melting starts to occur and a rapid loss of the orientation occurs. To illustrate this, an orientation parameter of 0.45 is found at $150\text{ }^\circ\text{C}$, indicating that the sample is fully molten and resides in a slightly ordered liquid crystalline melt.

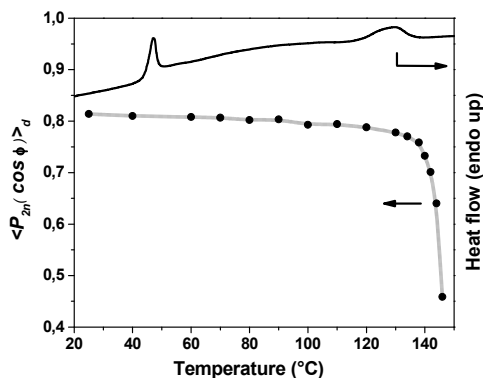


Figure 4.10. Orientation parameter $\langle P_{2n}(\cos \varphi) \rangle_d$ versus temperature plot, in combination with the first DSC heating run of the same fiber ($\text{DR} = 100$). Both experiments were performed at a heating rate of $10\text{ }^\circ\text{C}/\text{min}$.

It is clear from the thermal characterization of the fibers that, although these fibers retain their orientation above their glass transition, as anticipated, loss of the orientation occurs rapidly upon melting. This data implies that these fibers cannot be used at temperatures well above 100 °C. Furthermore, as is reported in the previous sections, a high temperature heat-treatment normally results in an increase of the molecular weight and crystallization by reorganization. As a result, the fibers subjected to such an annealing step generally exhibit higher melting temperatures, which in turn allows for their application at higher temperatures. As is shown by DSC and WAXD analysis, the application of a heat-treatment step at temperatures below the melting temperature of the fibers developed in this study does not significantly influence the melting temperature.

4.3.4. Solvent casting for film preparation

In order to investigate the effect of solvent based processing techniques on the mechanical properties, solvent cast films were prepared following the procedure reported in the experimental section. After drying the samples at 40 °C overnight *in vacuo*, the films of polymers **I** and **II** were extremely brittle and could not be used for mechanical testing. For polymer **I** this indicates that the molecular weight is too low for proper processing, similar to our observations of the melt processed products of this polymer. The brittle behavior of polymer **II** was unexpected since this polymer can easily be processed from the melt and yields highly oriented fibers. In contrast, polymer **III** could easily be solvent cast to form transparent films. As is shown in Figure 4.11, these films show no birefringence in polarized optical microscopy, indicating that they do not reside in the liquid crystalline phase (Figure 4.11, micrograph taken at 50 °C). Although it seems reasonable to assume that these films are amorphous, DMTA analysis shows a plateau for the E' modulus above T_g , indicating that these films are, in fact, semi-crystalline. As is visible from the micrograph taken at 90 °C in Figure 4.11, heating above the glass transition results in a further crystallization of the sample. This cold-crystallization behavior is confirmed in DSC analysis, as is shown in the heating trace of the solvent cast (SC) sample and the melt-crystallized (MC) samples, obtained at a heating rate of 10 °C (Figure 4.12). Further heating of the solvent cast film results in melting of the crystals and a slow reorganization of the polymer chains into the liquid crystalline melt, as is shown in Figure 4.11 for the micrographs taken at 120 °C and higher.

Although the very thin films prepared for polarized optical microscopy and DSC analysis were easily dried and contained no solvent, it was noticed that thick films prepared for mechanical testing contained some residual solvent after drying at 40 °C *in vacuo*. It is likely that this solvent is trapped during the drying process that is performed below the T_g of the polymer. Therefore, to ensure that the polymer is thoroughly dried prior to the performance of mechanical tests, the solvent cast films

were dried *in vacuo* at 80 °C overnight. Next, the tensile performance of the solvent cast films dried at 40 °C and 80 °C was evaluated. The solvent cast films dried at 40 °C were ductile and could be elongated more than 100% prior to failure. Since the modulus (~ 0.1 GPa) and yield point (~ 10 MPa) of these films are low it can be concluded that the solvent acts as a plasticizer, limiting the crystallization and improving the elongation at break. In contrast, the samples dried at 80 °C showed a tensile behavior very similar to the compression molded samples. The observed tensile modulus, stress at break and strain at break were 0.81 GPa, 29.7 MPa and 14.4% respectively, indicating that crystallization increases the stiffness, but also the brittle behavior of the sample. Such a brittle behavior is characteristic for aliphatic-aromatic semi-crystalline polyesters such as poly(butylene terephthalate) (PBT). Table 4.2 summarizes the tensile performance of products, obtained after processing of polymer **III** using the various methods evaluated in this study, including the solvent cast films. Similarly, Figure 4.13 gives an overview of the characteristic stress-strain curves observed for the products listed in Table 4.2.

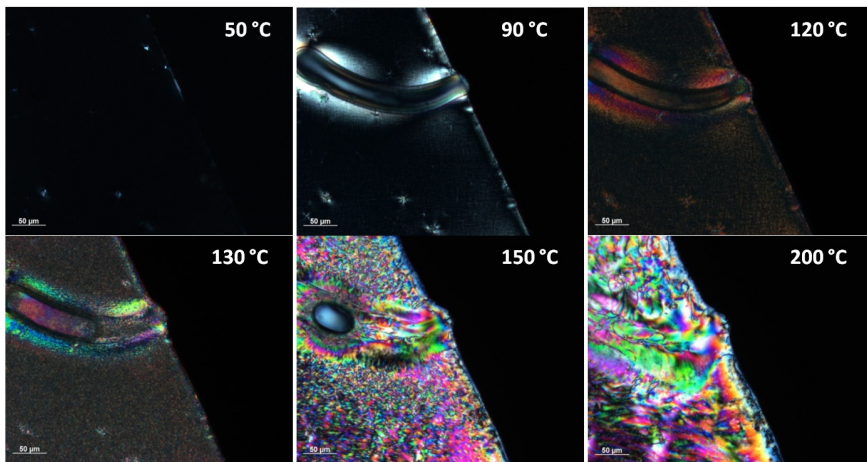


Figure 4.11. Optical micrographs taken between cross-polars of a solvent cast film of polymer **III**, during heating at 10 °C/min. The polymer film does not show birefringence and stays transparent below T_g . The film goes through cold-crystallization above T_g and transforms into a thermotropic melt at higher temperatures.

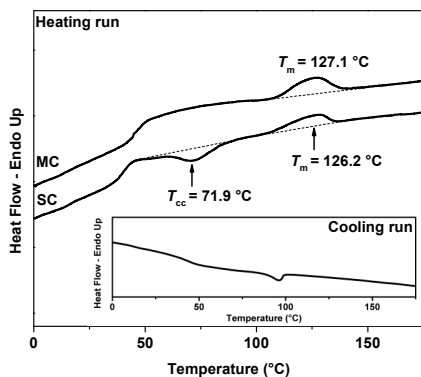


Figure 4.12. DSC heating run of a dried solvent-cast film (SC) and melt-crystallized film (MC) performed at a heating rate of 10 °C/min. The DSC trace observed during cooling at a rate of 10 °C/min of both samples were identical for the MC and SC samples. For this reason, only the cooling trace of the SC sample is embedded on the bottom of the Figure.

Table 4.2. Effect of processing method on the tensile performance of polymer III.

Processing method	Tensile tests		
	E (GPa)	σ_{\max} (MPa)	ϵ_{break} (%)
Solvent casting	0.11 (0.02)	9.69 (1.12)	114.5 (14.7)
Solvent casting + HT	0.81 (0.05)	29.7 (0.94)	14.4 (1.45)
Compression molding	1.09 (0.12)	29.7 (2.49)	12.6 (0.35)
Fiber spinning ^a	8.75 (0.77)	157 (32.5)	2.46 (0.83)

a) The draw ratio of the fibers reported in this table was 400.

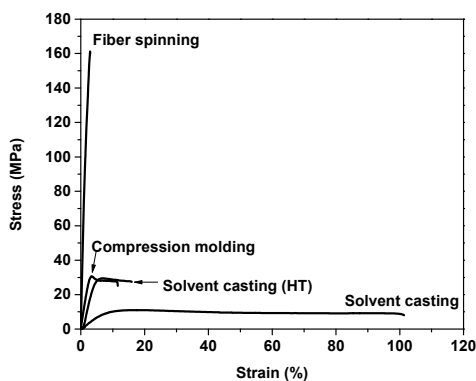


Figure 4.13. Characteristic stress-strain curves of the products of polymer III, obtained after processing through fiber spinning, compression molding or solvent casting. The latter is investigated before and after a heat-treatment step performed at 80 °C for 12 hours.

4.3.5. Effect of processing methods on the molecular orientation.

The effect of different processing methods on the mechanical performance of aliphatic-aromatic thermotropic polyesters was described in the previous sections. During the fiber spinning process, it was observed that rather high draw-ratios were required to improve the mechanical performance and to achieve a high degree of orientation in these samples. As reported by Jackson, the relaxation time of polymer chains decreases with chain stiffness.³¹ As a result, fibers spun from stiff, fully aromatic, thermotropic polyesters can be quenched or crystallized prior to relaxation of the polymer chains, achieving the desired high modulus fibers. As is reported by Acierno and coworkers, processing of alternating aliphatic-aromatic thermotropic polyesters is troublesome and yielded fibers with poor performance.³² This suggests that the presence of the aliphatic spacers decreases the relaxation times of the polymers and limits the orientation and performance of these thermotropic polyesters. In order to determine whether the aliphatic components in the aliphatic-aromatic thermotropic polyesters developed in this study orient during fiber spinning, polarized FTIR spectroscopy and solid-state NMR experiments were performed on the products, obtained after processing. Figure 4.14 shows the FTIR spectra between 1800-1350 cm^{-1} and 950-650 cm^{-1} of a solvent cast film (SC), a spun fiber lying perpendicular to the direction of the polarized light (F_{\perp}) and a spun fiber placed parallel to the direction of the polarized light (F_{\parallel}).

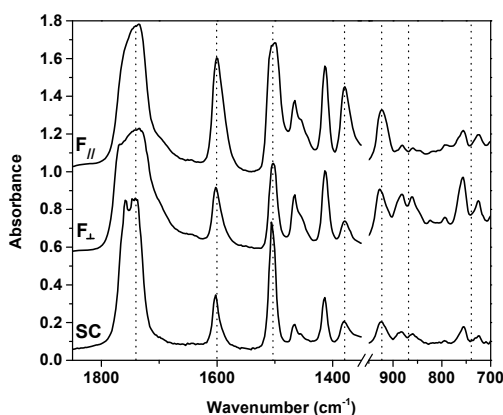


Figure 4.14. Polarized transmission FTIR spectra of polymer **III** recorded on a solvent cast film (SC), a spun fiber placed perpendicular to the orientation of the polariser (F_{\perp}) and the same fiber placed parallel to the orientation of the polariser (F_{\parallel}).

In the region between 1800 and 1350 cm^{-1} , characteristic bands corresponding to the carbonyl stretch vibrations (1736 and 1762 cm^{-1} , aromatic carbonyl and aliphatic carbonyl respectively), aromatic ring vibrations (1603 cm^{-1} , 1505 cm^{-1} , 1468 cm^{-1} and

1414 cm^{-1}), and the wag vibrations of the aliphatic carbons in the suberic acid moiety (1382 cm^{-1}) are observed. In the region between 950 and 650 cm^{-1} the characteristic aromatic C-H out of plane bending vibrations are detected at 885 and 755 cm^{-1} , together with the rocking vibrations of the aliphatic groups at 925 cm^{-1} .³⁰ As is reported by Kaito and coworkers, the intensity of a vibration band of oriented samples achieves a maximum when the transition moment direction of the vibration is parallel to the direction of the polarized light and increases further with increasing molecular orientation.³³ Similarly, the intensity is minimal when the transition moment direction of the vibration is perpendicular to the direction of the polarized light. Consequently, no differences are observed as a function of the direction of the polarized light in isotropic systems, as is the case for solvent cast films. As is seen in Figure 4.14, the intensity of the vibration bands at 1603, 1505, and 1382 cm^{-1} are significantly higher for the $F_{//}$ fiber compared to the F_{\perp} fiber. As expected, the vibration band corresponding to out of plane vibrations of the aromatic rings at 885 and 755 cm^{-1} are higher for the F_{\perp} fiber compared to the $F_{//}$ fiber. These data suggest that both the aromatic and the aliphatic chains are aligned along the spinning direction. As is shown in Figure 4.14, the vibration bands at 1468, 1414 and 925 cm^{-1} are not strongly influenced by a 90° rotation of the polarized light.

¹³C CP/TOSS NMR analysis was performed on the spun fibers of polymer **III** to compare molecular orientation of the polymer chains in the isotropic liquid crystalline phase and in the oriented liquid crystalline phase. Figure 4.15 shows the characteristic ¹³C CP/TOSS powder spectrum of polymer **III** taken at room temperature. The aliphatic and aromatic carbonyl resonances are observed at 172 and 164 ppm, respectively. Similarly, the signals of the aromatic rings of hydroquinone, *p*-hydroxybenzoic acid, and vanillic acid are observed in the region between 150 and 120 ppm. The resonances corresponding to the aliphatic carbon atoms are observed in the region between 60 and 20 ppm, where the resonance at 56 ppm corresponds to the methoxy carbon of vanillic acid and the resonances at 34, 30 and 26 ppm correspond to the carbon atoms in the suberic acid backbone. The signals of this ¹³C NMR spectrum are characteristic for this type of aliphatic-aromatic thermotropic polyesters.¹⁵

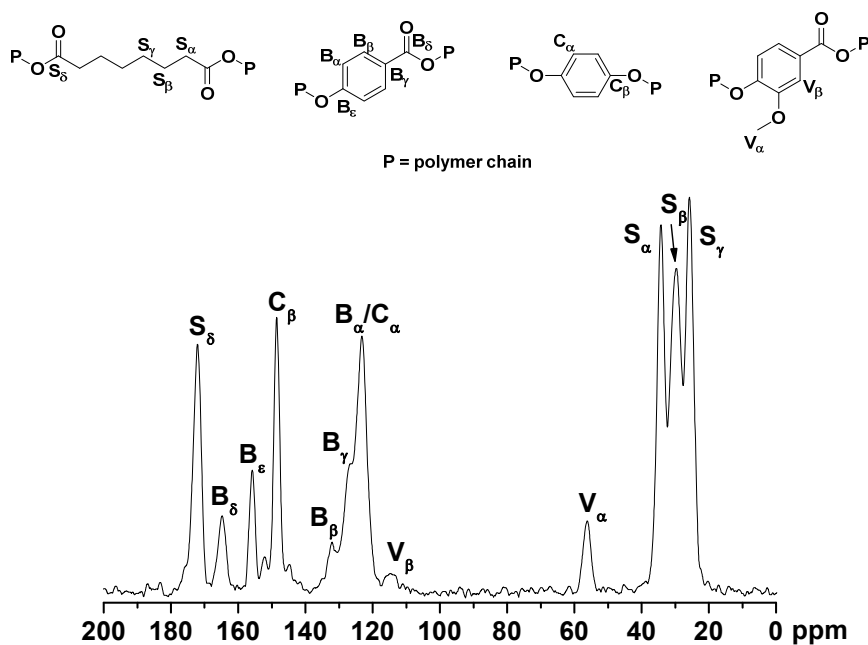


Figure 4.15. ^{13}C CP/TOSS powder NMR spectrum of polymer **III** in the region between 200 and 0 ppm.

To obtain more information on the differences in molecular orientation resulting from the fiber spinning process, 2D separation of undistorted powder patterns by effortless recoupling (SUPER) NMR experiments were performed on isotropically packed samples and oriented samples with the fibers packed parallel to the rotor axis.³⁴ Figure 4.16 shows the characteristic ^{13}C CSA patterns observed of the aliphatic carbonyl resonance at 172 ppm, the resonance of the aromatic carbon next to the alcohol group at 148 ppm, and the resonance of the aromatic carbon bearing a proton at 123 ppm. Similarly, the ^{13}C CSA patterns of the resonances corresponding to the aliphatic carbons atoms of suberic acid at 36, 30 and 24 ppm are displayed in Figure 4.16. It is clear that the ^{13}C CSA pattern of C_β (the isotropic chemical shift at 148 ppm) drastically sharpens after fiber spinning of the thermotropic polymer, indicating that the aromatic rings are strongly aligned upon fiber spinning. No significant changes are observed in the CSA line patterns of the carbonyl signal at 172 ppm and the aromatic carbon resonance at 122 ppm upon fiber spinning. It is thus highly likely that these groups are not oriented during fiber spinning.

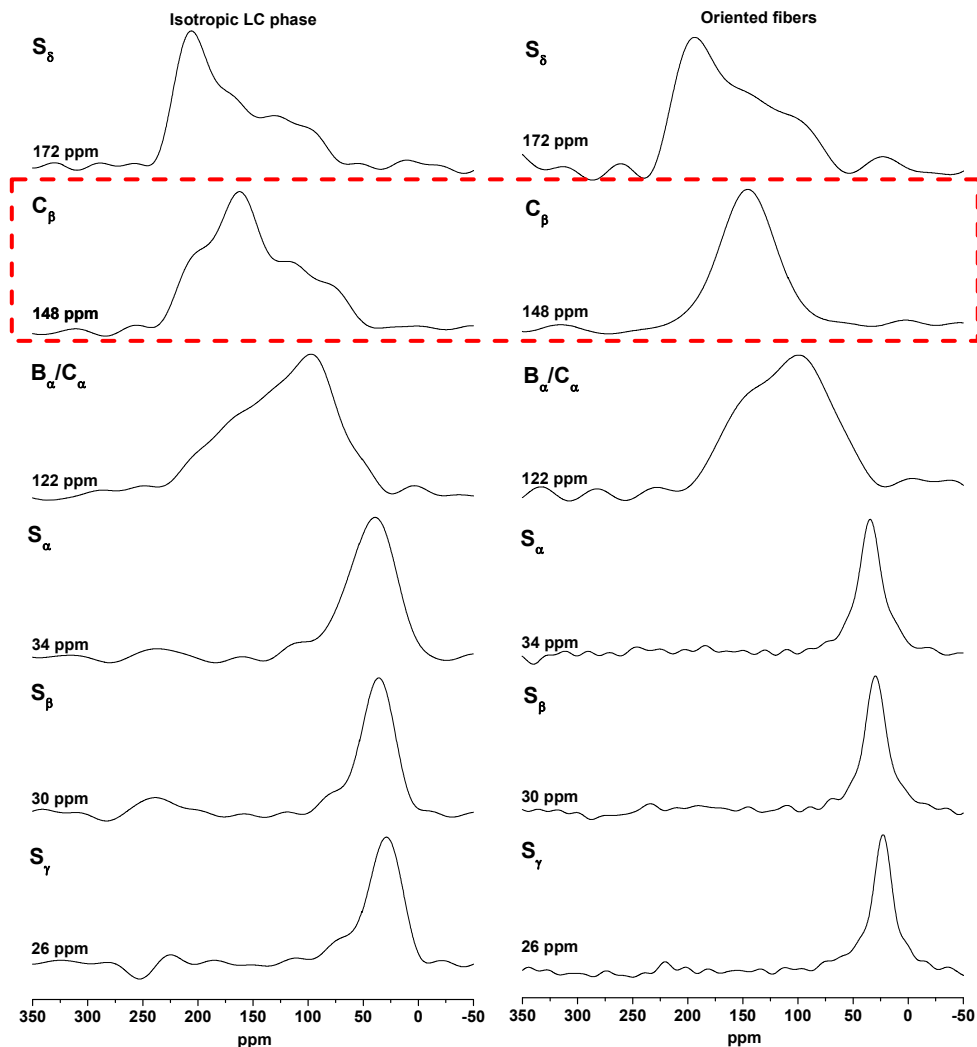


Figure 4.16. ^{13}C CSA line shapes extracted from different carbon signals observed in the 2D SUPER NMR measurements performed on a sample of polymer **III** packed as left) an isotropically packed LC powder and right) fibers aligned along the long axis of the rotor. Changes in line shape generally indicate either an improved orientation, or an increased mobility of the moiety in which the carbon atom resides.

The ^{13}C CSA patterns of aliphatic carbons of the suberic acid moiety all have a broad isotropic Lorentzian line shape and narrow upon fiber spinning. This narrowing of the lineshape cannot be attributed to the orientation of the groups induced by the fiber spinning process, but most likely is caused by the increased mobility of the groups during uniaxial deformation. To confirm this statement, ^{13}C T_1 relaxation measurements have been performed. These experiments indicate that the aliphatic

carbon atoms indeed exhibit very low relaxation times for both the non-oriented samples and the oriented fibers (~ 0.3 s). These results confirm that the sharpening of the CSA pattern of the aliphatic carbon atoms is a result from an increase in segmental mobility rather than an improved orientation.

In general, from the solid-state NMR analysis it is observed that only the aromatic rings are molecularly aligned upon fiber spinning. The aliphatic carbons of the suberic acid moiety show no molecular alignment upon fiber spinning. Instead, they exhibit a high mobility that normally corresponds to a local isotropic motion. In contrast to the NMR analysis, from the FTIR analysis it is observed that both the aromatic and aliphatic groups are oriented along the fiber direction. For this reason, it is concluded that, although the aliphatic moieties do align along the fiber axis, they are not subjected to strong restricted molecular orientation upon fiber spinning. These observations are in line with the observations of Acierno and coworkers³² who stated that the flexible spacers are more difficult to orient during fiber spinning from the thermotropic melt.

4.4. Conclusions

The synthesis and fiber spinning of aromatic-aliphatic thermotropic polyesters based on vanillic acid was performed and evaluated in this chapter. It is observed that these polymers require a M_w of at least 30 kg/mol to be successfully spun into fibers. In general, an increase in orientation, tensile modulus and tensile strength is observed with increasing molecular weight (M_w) and draw ratio of the fiber. FTIR and solid-state NMR experiments have been employed to demonstrate that only the aromatic components present in the polymer backbone undergo molecular alignment upon fiber spinning. It is expected that the poor molecular orientation of the aliphatic moieties in these aliphatic-aromatic thermotropic polyester contribute to the low tensile modulus of the fibers. Although fiber spinning is easily achieved at 170 °C and highly oriented fibers can be obtained, it is observed that these fibers are only dimensionally stable up to ~ 120 -130 °C. Above this temperature, melting starts to occur and the orientation of the samples is slowly lost. In general, this implies that these fibers cannot be used for demanding applications where high temperatures are required. Nonetheless, the developed concepts demonstrate that a random distribution of the monomers along the polymer chains facilitates an ease in deformation and provides better properties than when the monomers are alternately present in the polymer backbone, as is reported by Krigbaum and coworkers.³² In order to develop fully renewable thermotropic polyesters with good high temperature resistance, it is advised to decrease or eliminate the aliphatic content in the polymer backbone. Such a decrease in aliphatic content results in longer relaxation times of the polymer during processing, most likely yielding fibers with better mechanical performance. Furthermore, a decrease in aliphatic content allows for the development

of thermotropic polymers with higher melting temperatures that can be subjected to a high-temperature heat-treatment step, which will enhance their performance further.

4.5. References

- [1] Han, H., Bhowmik, P.K., *Prog. Polym. Sci.*, **1997**, 22, 1431-1502
- [2] Ballauff, M., *Angewandte Chemie*, **1989**, 101, 261-276
- [3] Windle, A.H., *Liquid Crystalline and Mesomorphic Polymers*, **1994**, Springer-Verlag, New York. Chapter 2, Ed. By Shibaev, V.P, and Lam, Lm,
- [4] Lin, J., Sherrington, D.C., *Advances in Polymer Science*, **1994**, 111, 177-219
- [5] Varshney, S.K., *J. Macromol. Sci. Rev. Macromol. Chem. Phys.*, **1986**, C26, 4, 551
- [6] Dobb, M.G., McIntyre, J.E., *Adv Polym Sci*, **1984**, 60/61, 61-98
- [7] Chung, T-S., *Polymer Engineering and Science*, **1986**, 26, 13, 901-919
- [8] Jackson, W.R., Jr., *Mol. Cryst. Liq. Cryst.*, **1989**, 169, 23-49
- [9] Warner, S.B., Lee, J., *J. Polym. Sci. Part B: Polym. Phys.*, **1994**, 32, 1759-1769
- [10] Grasser, W., Schmidt, H-W., Giesa, R., *Polymer*, 2001, 42, 8529-8540
- [11] Acierno, D., La Mantia, F.P., Polizzotti, G., *Macromolecules*, 1982, 15, 1455-1460
- [12] Economy, J., *Mol. Cryst. Liq. Cryst.* 1989, 169, 1-22
- [13] De Ruijter, C., Bos, J., Boerstoeel, H., Dingemans, T., *J Polym Sci Part A: Polym Chem*, **2008**, 46, 6565-6574.
- [14] Wilsens, C.H.R.M., Noorderover, B.A.J., Rastogi, S., *Polymer*, **2014**, 55 (10), 2432-2439
- [15] Wilsens, C.H.R.M., Verhoeven, J.M.G.A., Noorderover, B.A.J., Hansen, M.R., Auhl, D., Rastogi, S., *Macromolecules*, **2014**, 47 (10), 3306-3316
- [16] Li, X.G, Huang, M.R., *Polym.-Plast. Technol. Eng.*, **2000**, 39(2), 317-331
- [17] Li, X.G., Huang, M.R., Guan, G-H., Sun, T., *Journal of Applied Polymer Science*, **1997**, 66, 2129-2138
- [18] Nagata M., *Journal of Applied Polymer Science*, **2000**, 78, 2474-2481
- [19] Mitchell, G.R., Windle, A.H., *Developments in Crystalline polymers, Chapter 3: Orientation in liquid crystal polymers - 2*, edited by Basset, D.C., **1988**, Elsevier applied science publishers LTD, London, UK.
- [20] Ugaz, V., Burghardt, W.R., Zhou, W., Kornfield, J.A., *J. Rheol.*, **2001**, 45, 1029-1063
- [21] Liu, S. F.; Mao, J. D.; Schmidt-Rohr, K. *Journal of Magnetic Resonance*, **2002**, 155, 15-28.
- [22] Yao, Y. F.; Rastogi, S.; Xue, H. J.; Chen, Q.; Graf, R.; Verhoef, R., *Polymer*, **2013**, 54, 411-422.
- [23] Zhou, W-J., Kornfield, J.A., Ugaz, V., Burghardt, W.R., Link, D., Clark, N.A., *Macromolecules*, **1991**, 32, 5581-5593
- [24] Kim, S.S., Han, C.D., *Macromolecules*, **1993**, 26, 6633-6642
- [25] Somma, E., Nobile, M.R., *Journal of Rheology*, **2004**, 48, 1407,1422
- [26] Kim, S.S., Han, C.D., *J. Rheol.*, **1993**, 37, 847-866
- [27] Zhou, M., Han, C.D., *Macromolecules*, **2006**, 39, 232-242
- [28] Jackson, W.J., Kuhfuss, H.F., *J. Polym. Sci. Polym. Chem. Ed.*, **1976**, 14, 2043-2058
- [29] Muramatsu, H., Krigbaum, W.R., *J. Polym. Sci. Part B: Polym. Phys.*, **1986**, 24, 1695-1711
- [30] Karacan, I., *J. Appl. Polym. Sci.*, **2006**, 100, 142-160
- [31] Jackson, W.J., *Br. Polym. J.*, 1980, 12, 154-162
- [32] Acierno, D., La Mantia, F.P., Polizzotti, G., Ciferri, A., Krigbaum, W.R., Kotek, R., *J. Polym. Sci. Polym. Phys. Ed.*, **1983**, 21, 2027-2036
- [33] Kaito, A., Kyotani, M., Nakayama, K., *Macromolecules*, **1991**, 24, 3244-3249
- [34] Yao, Y., Jiang, S., Rastogi, S., *Macromolecules*, **2014**, 47, 1371-1382

Chapter 5

Influence of the 2,5-furandicarboxamide moiety on hydrogen bonding in aliphatic-aromatic poly(ester amide)s

Abstract

In this chapter, the effect of the protection of the thermally instable carboxylic acid groups of 2,5-furandicarboxylic acid (2,5-FDCA) through the formation of amide groups is investigated. A dimethyl 4,4'-((furan-2,5-dicarbonyl)bis(azanediyl))dibenzoate (2,5-FDCAn) model compound is synthesized and the properties of the 2,5-furandicarboxamide moiety are compared to its terephthalic acid (TA), 2,5-thiophenedicarboxylic acid (2,5-TDCA) and isophthalic acid (IA) analogues. Furthermore, the feasibility to perform a melt polycondensation reaction of these model compounds with different aliphatic diols is investigated. Solution NMR analysis indicates that the oxygen heteroatom in the furan ring functions as a hydrogen bond acceptor, resulting in the formation of intramolecular hydrogen bonds with the amide hydrogens in 2,5-FDCAn. It is anticipated that such intramolecular hydrogen bonds compete with the formation of intermolecular hydrogen bonds, which is generally considered to be the driving force for polyamide crystallization. As a consequence, 2,5-FDCAn exhibits a suppressed melting temperature, decreased crystallinity and an increased solubility compared to its TA, 2,5-TDCA and IA based counterparts. Furthermore, it is demonstrated that polymers containing the 2,5-furandicarboxamide moiety also exhibit an improved solubility and a decreased ability to crystallize. This implies that 2,5-furandicarboxamide based (macro)monomers are excellent, thermally stable candidates for application in rigid and amorphous polymers.

This chapter is partially based on Wilsens, C.H.R.M., Deshmukh, Y.S., Noordover, B.A.J., Rastogi, S., *Macromolecules*, **2014**, 47, 6196–6206.

5.1. Introduction

As was demonstrated in the previous three chapters, the incorporation of 2,5-FDCA into the backbone of a thermotropic polyesters is feasible while maintaining low reaction temperatures. However, as is shown in chapters two and three, the incorporation of 2,5-FDCA at such low temperatures requires the copolymerization of a flexible spacer such as suberic acid. The incorporation of such a flexible spacer suppresses the melting temperature of the polymer and ensures that molecular weight can be built up during a melt polycondensation reaction. Although it was demonstrated that it is possible to synthesize 2,5-FDCA based thermotropic polyesters via this route, it has to be noted that the reaction times required to build-up molecular weight are unrealistically high. Moreover, fiber spinning of this polymer proved impossible and yielded brittle products that could not be wound, indicating that the molecular weight is still too low for processing purposes. Besides, the high molecular mobility of the aliphatic spacers present in the thermotropic fibers is expected to decrease the stiffness of the polymer chains, yielding fibers having relatively low moduli compared to fully aromatic thermotropic polyester fibers.¹ It may be clear that it is preferred to develop fully aromatic thermotropic polyesters. For this reason, the thermal stability and properties of aromatic 2,5-FDCA based model compounds that might function as replacements for the 2,5-FDCA monomer in the synthesis of fully aromatic thermotropic polyesters is investigated in this chapter.

In literature, aliphatic or aromatic 2,5-FDCA based polyamides have been reported by Hopff and Krieger², Heertjes and Kok³, Grosshardt and coworkers⁴, and Mitiakoudis and Gandini⁵. In general, it is observed that polyamides containing 2,5-FDCA and aliphatic diamines have low crystallinities or are amorphous. This is in contrast to TA or isophthalic acid (IA) based polyamides, which often show high crystallinities and rapid crystallization. As stated by Gandini in 1993, the incorporation of 2,5-FDCA in polyamide materials has been described in literature, but an in-depth understanding is not yet obtained.⁶ Recently, Yeh and coworkers⁷ reported on the conformations and hydrogen bonding of furan-based polyamides, obtained via molecular dynamics (MD) simulations of the amorphous phase. These authors showed that hydrogen bonds in Nylons, such as Nylon 4,6, have longer lifetimes compared to 2,5-FDCA based polyamides, such as poly(hexamethylene furandicarboxamide). However, the 2,5-FDCA-based materials showed more van der Waals interactions, maintained more rigid structures, and showed slower weakening of hydrogen bonds upon heating.

From the findings summarized above, it is evident that the introduction of the furan ring in the polymer backbone drastically changes the polymer properties, allowing for the development of materials with novel properties. Therefore, the aim of this chapter is to gain more insight into the effect of the presence of the 2,5-furandicarboxamide moiety in the polymer backbone and to compare it to its TA, 2,5-

thiophenedicarboxylic acid (2,5-TDCA), and IA analogues. Ester-amide model compounds are prepared and studied after synthesis *via* a reaction of 4-methyl aminobenzoate and the acyl chloride of the different dicarboxylic acids. Melt polymerization of the synthesized model compounds with different diols is investigated in order to prepare and study 2,5-FDCA based poly(ester amide)s.

5.2. Experimental section

5.2.1. Materials and monomer preparation

Methyl 4-aminobenzoate, terephthaloyl chloride, isophthaloyl chloride, 2,5-thiophenedicarboxylic acid, triethyl amine, N-methylpyrrolidone, tetrahydrofuran, 1,10-decanediol, 1,8-octanediol, 1,6-hexanediol, 1,4-butanediol and 1,2-ethanediol were purchased from Sigma Aldrich. 2,5-furandicarboxylic acid was ordered from Atomole. All chemicals were used as received for model compound synthesis or dried *in vacuo* at 40 °C prior to polymerization.

5.2.2. Preparation of diacid chlorides

Terephthaloyl chloride and isophthaloyl chloride were used directly for model compound synthesis. The acid chlorides of 2,5-FDCA and 2,5-TDCA were prepared according to the following procedure. Dicarboxylic acid (1 eq.), thionyl chloride (2.2 eq.) and a catalytic amount of N,N-dimethylformamide (DMF) were loaded in a 50 mL round bottom flask equipped with a condenser under an inert Argon-rich atmosphere. The mixture was heated to 80°C for four hours under constant stirring while the evolving gas was led through a NaOH solution in water. After cooling down to 0 °C using an ice bath, vacuum was applied to the mixture for 30 minutes to remove residual SOCl₂. The acyl chloride was isolated as a crystalline solid and was dissolved in dry THF and immediately used for model compound preparation.

5.2.3. General model compound synthesis procedure

Methyl 4-aminobenzoate (10 grams, 66 mmol), triethylamine (5 mL) and dry THF (100 mL) were introduced into a round-bottom flask fitted with a condenser and magnetic stirrer. Dicarboxylic acid chloride (33 mmol) was dissolved in dry THF (50 mL) and added dropwise to the methyl 4-aminobenzoate / THF solution. The mixture was refluxed at 80 °C for 3 hours under constant stirring. The product was filtered using a Büchner filter and washed with acetone and water. Next, the product was stirred for half an hour in a saturated solution of NaHCO₃ in water, to removal any residual triethylamine hydrochloride salts formed during synthesis. Next, the product was filtered over a Büchner filter and dried *in vacuo* at 60 °C overnight. Finally the sample was recrystallized from NMP and dried *in vacuo* at 40 °C once more. Prior to the performance of analysis or polymerization reactions, the model compounds were dried *in vacuo* at 120 °C to remove water absorbed during storage.

5.2.4. Synthesis of TAn

Dimethyl 4,4'-(terephthaloylbis(azanediyl))dibenzoate (TAn) was obtained following the general synthesis procedure after reaction of terephthaloyl chloride (6.72 g, 33.0 mmol) with

methyl 4-aminobenzoate (10 g, 66.2 mmol). Yield 13.2 g (92%). ^1H NMR(LiCl/DMF-*d*₇) δ \ppm: 11.88 (s, 2H, NH), 8.53 (s, 2H, -TAH), 8.47 (d, $J = 8.8$ Hz, 4H, -ArH), 7.98 (d, $J = 8.8$ Hz, 4H, -ArH), 3.89 (s, 6H, -CH₃).

5.2.5. Synthesis of 2,5-TDCAn

Dimethyl 4,4'-((thiophene-2,5-dicarbonyl)bis(azanediyl))dibenzoate (2,5-TDCAn) was obtained following the general synthesis procedure after reaction of 2,5-TDCA chloride (2.00 g, 9.55 mmol) with methyl 4-aminobenzoate (2.90 g, 19.2 mmol). Yield 3.74 g (89%). ^1H NMR(LiCl/DMF-*d*₇) δ \ppm: 12.16 (s, 2H, NH), 9.20 (s, 2H, -TDCAH), 8.47 (d, $J = 8.8$ Hz, 4H, -ArH), 7.95 (d, $J = 8.8$ Hz, 4H, -ArH), 3.89 (s, 6H, -CH₃).

5.2.6. Synthesis of 2,5-FDCAn

Dimethyl 4,4'-((furan-2,5-dicarbonyl)bis(azanediyl))dibenzoate (2,5-FDCAn) was obtained following the general synthesis procedure after reaction of 2,5-FDCA chloride (2.44 g, 12.6 mmol) with methyl 4-aminobenzoate (4 g, 26.4 mmol). The mixture was left to stir at room temperature for three hours and the solution was precipitated in acetone prior to filtration. Yield = 3.80 g (68%). ^1H NMR(LiCl/DMF-*d*₇) δ \ppm: 12.37 (s, 2H, NH), 8.63 (d, $J = 8.4$ Hz, 4H, -ArH), 7.99 (d, $J = 8.8$ Hz, 4H, -ArH), 7.45 (s, 2H, -FuranH), 3.90 (s, 6H, -CH₃). ^{13}C NMR(LiCl/DMF-*d*₇) δ \ppm: 167.17 (O-C=O), 157.29 (NH-C=O), 149.89 (-FuranC), 145.03 (NH-ArC), 130.78 (ArC), 125.81 (-ArC-C=O), 121.14 (-ArC), 117.79 (FuranC), 52.52 (-CH₃).

5.2.7. Synthesis of IAn

Dimethyl 4,4'-((isophthaloyl)bis(azanediyl))dibenzoate (IAn) was obtained following the general synthesis procedure after reaction of isophthaloyl chloride (6.75 g, 33.1 mmol) with methyl 4-aminobenzoate (10 g, 66.2 mmol). Yield 12.89 g (90%). ^1H NMR(DMF-*d*₇) δ \ppm: 11.91 (s, 2H, NH), 8.73 (s, 1H, -IAH), 8.29 (dd, $J = 8.0$ Hz and 1.6 Hz, 2H, -IAH), 8.13 (d, $J = 8.8$ Hz, 4H, -ArH), 8.05 (d, $J = 8.8$ Hz, 4H, -ArH), 7.75 (t, $J = 8.0$ Hz, 1H, -IAH), 3.90 (s, 6H, -CH₃). ^{13}C NMR(DMF-*d*₇) δ \ppm: 167.18 (O-C=O), 166.68 (NH-C=O), 145.03 (NH-ArC), 136.26 (IA-C), 132.23 (IA-C), 131.37 (ArC), 129.94 (-ArC-C=O), 128.29 (IA-C), 126.07 (IA-C), 120.70 (-ArC), 52.66 (-CH₃).

5.2.8. General polymerization procedure

All polymerizations were performed in a 100 mL round-bottom flask fitted with a mechanical stirrer. Equimolar amounts of trimer and diol were weighed into the reactor together with 0.2 wt% Ti(IV)butoxide as a catalyst and Irganox 1330 as an anti-oxidant. The monomers were dried *in vacuo* prior to polymerization. The mixture was heated to temperatures between 200 °C to 240 °C, depending on the selected diol, and kept under this isothermal condition for one hour to allow for transesterification to occur and to distill methanol from the reaction mixture. NMP was added as a solvent in reactions containing the TA, 2,5-TDCA, and IA model compounds to promote their dissolution and participation in polymerization. The reaction temperature was kept at 200 °C for two hours to allow for transesterification with the diol to take place in polymerizations containing NMP. Reduced pressure was applied to the reactions in order to build up molecular weight, once the condensate and solvent (NMP and/or

methanol) were distilled off. The reaction temperature was slowly increased to 250 °C and the mixture was kept isothermal for 3 hours at 0.5 mbar, prior to isolation of the polymer. The obtained polymers were dissolved in DMF, precipitated from methanol and dried *in vacuo* at 40 °C for 24 hours followed by drying *in vacuo* at 120 °C for 48 hours. The infusible and poorly soluble polymers p(TAn10) and p(TDCAn10) were analyzed without purification.

5.2.9. Characterization methods

¹H, ¹³C NMR, and 2D Heteronuclear Multiple Bond Correlation (HMBC) experiments were performed on a Bruker 400 MHz NMR spectrometer. All samples were measured in DMF-*d*₇ or mixtures of DMF-*d*₇ with LiCl.

Molecular weights and polydispersity index (PDI) values were calculated from N,N-dimethylacetamide (DMAc) size exclusion chromatography (SEC) data. Measurements were performed on a Waters Alliance system equipped with a Waters 2695 separation module, a Waters 2414 refractive index detector (40 °C), a Waters 2996 photodiode array detector, a PSS GRAM guard column followed by 2 PSS GRAM columns in series of 100 Å (10 μm particles) and 3000 Å (10 μm particles) respectively at 60 °C. DMAc was used as an eluent at a flow rate of 1 mL min⁻¹. The molecular weights were calculated against polystyrene standards (Polymer Laboratories, M_p = 580 g/mol up to 7.1 x 10⁶ g/mol). Prior to SEC analysis, samples were filtered through a 0.2 mm PTFE filter (13 mm, PP housing, Alltech).

The thermal stability of the polymers was determined using thermogravimetric analysis (TGA) which was performed on a TA Instruments TGA Q500 in a nitrogen rich atmosphere. Samples were heated at 10 °C/min from 20 °C to 800 °C.

The glass transition temperatures (*T*_g) and the peak melting transition temperature (*T*_m) were determined by differential scanning calorimetry (DSC) using a TA Instruments Q1000 DSC. The normal heating and cooling rates of the samples were 10 °C/min and measurements were performed under a nitrogen rich atmosphere.

Melting temperatures were determined using a Zeiss Axioplan 2 Imaging optical microscope under crossed polarizers and CD achorplan objectives (32x zoom). A THMS 600 heating stage connected to a Linkam TMS 94 control unit was mounted onto the optical microscope. Samples were prepared by placing a small amount of polymer in-between two glass slides and heating them at a rate of 10 °C/min to their melting temperatures. Consecutive heating and cooling runs were performed and the melting temperatures were determined from the second and third run.

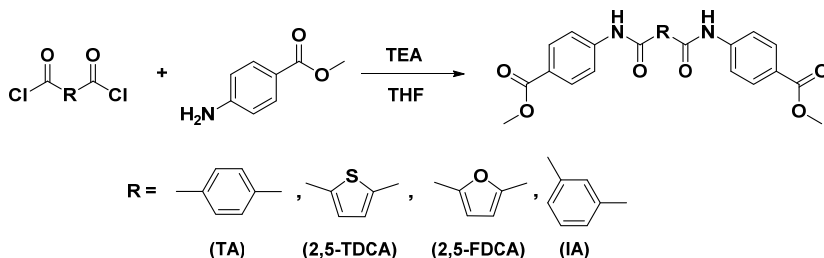
X-ray diffraction (XRD) measurements were performed on a Rigaku Geigerflex Bragg-Brentano Powder Diffractometer using Cu Kα radiation (λ = 0.154 nm), at 40 kV and 30 mA. The scans were performed with a 0.01 step in 2θ and a dwell time of 2s. Peak fitting was performed after background subtraction to determine the percentage of crystallinity. 2D diffraction patterns were obtain with a Bruker D8 discover with GADDS, a 2-dimensional detector system using Cu radiation, wavelength 1.54184 Å, at 40kV and 40mA. A Göbel mirror provides a highly parallel beam whereby the Kβ and Bremsstrahlung is suppressed. The measurements were performed in transmission mode with a sample to detector distance of 5 mm and an exposure time of 30 minutes.

Temperature resolved FTIR spectroscopy studies were performed using a Varian 670IR spectrometer. A THMS 600 heating stage connected to a Linkam TMS 94 control unit was mounted onto the FTIR spectrometer to control temperature. All spectra were measured in the range of 4000 cm^{-1} to 650 cm^{-1} at a resolution of 4 cm^{-1} in either Transmission or Attenuated Total Reflection (ATR) mode. For this purpose a SLIDE-ON ATR selenium crystal was used.

5.3. Results and discussion

5.3.1. Synthesis of the amide-ester model compounds

Four different model compounds have been synthesized by reacting 4-methyl aminobenzoate with TA, 2,5-TDCA, 2,5-FDCA, and IA, following the general synthesis route described in the experimental section (Scheme 5.1). The nomenclature of these compounds is chosen such that the initial part consists of the abbreviation of the central dicarboxylic acid followed by an “n” to indicate that they are connected to 4-methyl aminobenzoate. For example, the name of the dimethyl 4,4'-((furan-2,5-dicarbonyl)bis(azanediyl))dibenzoate compound is identified as 2,5-FDCAn.



Scheme 5.1. Chemical representation of the formation of the model compounds based on terephthalic acid (TA), 2,5-thiophenedicarboxylic acid (2,5-TDCA), 2,5-furandicarboxylic acid (2,5-FDCA) and isophthalic acid (IA).

The synthesis of the different model compounds was performed in solution with tetrahydrofuran (THF) / triethyl amine (TEA) as solvent. The TAn, 2,5-TDCAn and IAn compounds precipitated rapidly upon formation through the dropwise addition of the acyl chloride/THF solution to the 4-methyl aminobenzoate/THF/TEA solution. The 2,5-FDCAn compound remained in solution during synthesis and required precipitation from acetone prior to filtration and further purification. The solubility of 2,5-FDCAn in the reaction mixture was unexpected since aromatic amides generally show strong intermolecular hydrogen bonding interactions resulting in rapid crystallization and poor solubility. Since precipitation generally yields poorly defined crystals that can contain impurities such as the triethylamine hydrochloride salt formed during synthesis, the 2,5-FDCAn was thoroughly washed with acetone, water and a NaHCO_3 solution to ensure the full removal of such impurities. The high

purity and successful synthesis of 2,5-FDCAn was confirmed with electrospray ionization time-of-flight mass spectrometry (ESI-TOF MS) and NMR analysis. In short, all four model compounds were successfully isolated in a pure form and were recrystallized from NMP prior to analysis. The recrystallization in NMP was performed to ensure that all model compounds were crystallized according to the same procedure and to be able to compare their crystallization and thermal behavior.

5.3.2. Analysis of the amide-ester model compounds in solution

It is widely accepted that the carbonyl group of DMF is a strong hydrogen bond acceptor and helps to dissolve compounds that show weak hydrogen bonds.⁸ However, DMF is unable to dissolve compounds with strong intermolecular hydrogen bonds. In such compounds, the high efficiency of hydrogen bonding in the crystallized state is energetically favorable and is preferred over dissolution. This characteristic behavior is observed for both TAn and 2,5-TDCAn; dissolution in DMF occurs only at elevated temperatures, but crystallization occurs rapidly upon cooling. The addition of LiCl salt improved the solubility of the model compounds in DMF, allowing for ¹H NMR analysis. The effects of salts on the behavior of polyamide has been addressed in great detail in earlier publications where it was demonstrated that shielding of intermolecular hydrogen bonding improves the solubility of aliphatic amides in solution and suppresses the melting point in the solid state, ultimately yielding amorphous polyamides at room temperature.^{9,10}

The more sterically hindered 2,5-FDCAn and IAn compounds dissolve in DMF, in the absence of LiCl. It is expected that the non-linearity of these compounds limits the hydrogen bonding efficacy, resulting in an improved solubility compared to TAn and 2,5-TDCAn. To obtain more information on the effect of salt on the dissolution of these compounds, ¹H NMR analysis was performed on mixtures of 2,5-FDCA or IAn with different ratios of LiCl with DMF-*d*₇ as the solvent. As can be seen in Figure 5.1, the ¹H NMR spectrum of the 2,5-FDCAn compound in DMF-*d*₇ shows only two aromatic proton signals at 8.04 ppm and 7.55 ppm, whereas three aromatic resonances are expected; one singlet from the furan ring and two doublets from the benzoate groups. 2D-HMBC analysis confirmed that the correct structure was obtained after synthesis, but that the aromatic protons resonances of the methyl benzoate group overlap in DMF-*d*₇. Similarly, the resonances of the methyl benzoate of the IAn model compound in DMF-*d*₇ lie close together, although they do not overlap completely (Figure 5.1).

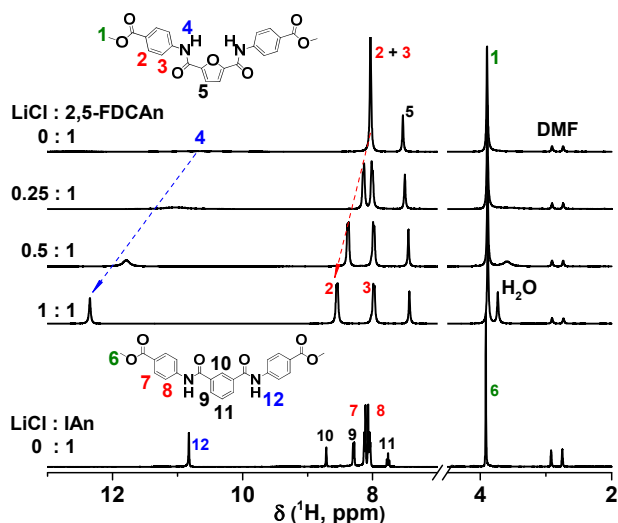


Figure 5.1. ^1H NMR spectra of the IAn model compound in $\text{DMF-}d_7$ and the 2,5-FDCAn model compound in $\text{DMF-}d_7$ with varying ratios of LiCl salt, showing the difference in aromatic resonances as a function of salt content. The arrows indicate the shift of the resonances with increasing LiCl concentration. *N.b.* although the resonances of 2,5-FDCAn split and the width and sharpness change upon the addition of LiCl salt, the integrals remain the same.

The addition of LiCl to the NMR mixtures results in the deshielding of the aromatic protons close to the ester bond (proton 2 for 2,5-FDCAn and proton 7 for IAn, Figure 5.1). This indicates that the interactions of the Li^+ and Cl^- ions with the amide motifs strongly influence the electron density of the 2,5-FDCAn and IAn compounds. Similarly, the amide protons of 2,5-FDCAn and IAn (protons 4 and 12, respectively) are deshielded upon the addition of LiCl. However, a distinct difference is observed in the shape and position of the amide proton resonances of 2,5-FDCAn and IAn. As is shown in Figure 5.1, the resonance corresponding to the 2,5-FDCAn amide protons (4) is very broad in the absence of LiCl, whereas the amide protons (12) of the IAn compound show a peak at 10.8 ppm. The peak at 10.8 ppm in the ^1H NMR spectrum of IAn in $\text{DMF-}d_7$ indicates that the amide protons are hydrogen bonded with the carbonyl group of DMF. The absence of such a resonance in the ^1H NMR spectrum of 2,5-FDCAn in $\text{DMF-}d_7$ indicates that the amide protons of 2,5-FDCAn are delocalized and undergo additional interactions compared to IAn.

As mentioned earlier, Yeh and coworkers⁷ investigated the furan-based polyamides via MD simulations of the amorphous phase. These authors showed that it is energetically favorable for 2,5-FDCA-based amides to reside in a planar and all-*trans* conformation, with the amide protons pointing towards the oxygen of the furan ring. It is reasonable to assume that this rigid, planar conformation enables interaction of the amide

protons with the oxygen heteroatom in the furan ring and potentially allows for intramolecular hydrogen bonding (Figure 5.2). The occurrence of such interactions implies that rotation of either the furan ring or the amide groups is accompanied by an energetic penalty, contributing to the rigid character of this moiety. Furthermore, the occurrence of such intramolecular interactions of 2,5-FDCAn is expected to compete with the formation of hydrogen bonds with DMF and explains the observed delocalized nature of the 2,5-FDCAn amide protons.

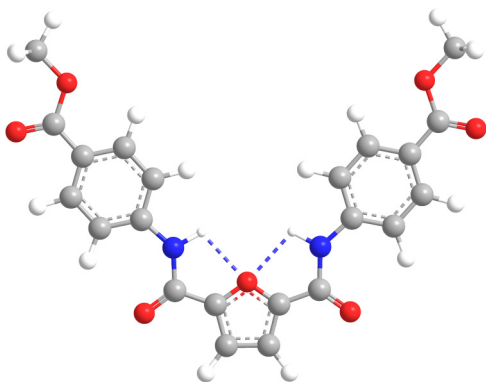


Figure 5.2. Molecular representation of the intramolecular hydrogen bonding, expected to occur in the all-*trans* conformation of the 2,5-FDCAn model compound. *N.b.* Although the all-*trans* conformation allows for the formation of two intramolecular hydrogen bonds, other conformations having one or no intramolecular hydrogen bonds are expected to be present in solution as well.

As is depicted in in Figure 5.1, the addition of LiCl to the 2,5-FDCAn/DMF-*d*₇ solution results in sharpening and deshielding of the amide proton signal of 2,5-FDCAn. This sharpening and deshielding of the amide proton resonance corresponds to the shielding of the amide groups by the Li⁺ and Cl⁻ ions, replacing the other inter- and intramolecular interactions in the 2,5-FDCAn/DMF-*d*₇ mixture. Correspondingly, the addition of LiCl to the IAn model compound mixture only deshields the amide proton resonance, but does not change the shape and width of the peak. This confirms that IAn only undergoes hydrogen bonding with DMF, and that the Li⁺ and Cl⁻ ions replace the hydrogen bonds with DMF.

It is observed that, although the LiCl was dried prior to use, some water was present in the DMF-*d*₇/LiCl mixtures. Water is known to influence the hydrogen bonding in DMF¹¹, which can also play a role in the solubility and hydrogen bonding of 2,5-FDCAn and IAn. However, the ¹H NMR spectrum of 2,5-FDCAn in DMF-*d*₇ / D₂O (97: 3) showed a delocalized amide proton resonance similar to the resonance of 2,5-FDCAn in pure DMF-*d*₇ (Figure 5.1). The effect of water on the interactions of 2,5-FDCAn could not be investigated further since 2,5-FDCAn did not dissolve in

mixtures with higher D₂O contents. Nonetheless, these data indicate that the changes in hydrogen bonding of 2,5-FDCAn in the presence of LiCl are to be attributed to the effect of LiCl rather than to the water present in the system.

5.3.3. Thermal analysis of the amide-ester model compounds

In general, the melting and crystallization of polyamide materials is governed by the formation of interchain or intermolecular hydrogen bonds. It is widely accepted that an increase in hydrogen bonding density in polyamides increases both the melting and crystallization temperatures. For this reason, it is expected that the melting temperatures (T_m) of the model compounds increases when the central dicarboxylic acid group becomes more linear, through a decrease in steric hindrance and an increase in the hydrogen bonding efficiency. However, as anticipated from the ¹H NMR data, interactions of the amide groups with the oxygen heteroatom of the furan ring might occur in 2,5-FDCAn. It is expected that these intramolecular interactions will decrease the formation of intermolecular hydrogen bonds and limit the crystallization of 2,5-FDCAn. Such poor crystallization would result in the formation of defected crystals and a concomitant suppression of the melting temperature. To investigate the effect of the hydrogen bonding on the thermal properties, thermogravimetric analysis (TGA), differential scanning calorimetry (DSC) and hot-stage polarization optical microscopy (POM) were employed to study the melting and crystallization behavior of 2,5-FDCAn and the other model compounds (Table 5.1).

Table 5.1. Thermal properties of the recrystallized model compounds TAn, 2,5-TDCAn, 2,5-FDCAn, and IAn.

Model compound	Bond angle ¹² (°)	T_m (°C) ^a	T_{ons} (°C) ^c
TAn	180	365	385
2,5-TDCAn	148	350	364
2,5-FDCAn	124	242 ^b	338
IAn	120	325	334

a) Observed in polarization optical microscopy upon heating at a rate of 10 °C / min. b) Confirmed with DSC analysis at a heating rate of 10 °C / min. c) Determined *via* TGA analysis.

As is summarized in Table 5.1, rapid thermal degradation occurs upon melting of TAn, 2,5-TDCAn, and IAn, as the T_m and the onset temperature for degradation (T_{ons}) values differ only slightly for these model compounds. For this reason, hot-stage polarization optical microscopy (POM) was employed to determine the T_m values of these compounds. Table 5.1 shows that the T_m decreases when the bond angle of the central dicarboxylic acid groups deviates from linearity, in the order TAn > 2,5-TDCA > IAn. As anticipated, 2,5-FDCAn has a substantially lower T_m compared to the other three model compounds. From the second heating and cooling DSC trace, shown in Figure 5.3, it is apparent that 2,5-FDCAn has a T_m of 242 °C and a peak crystallization

temperature (T_c) of 233 °C. The first heating run of 2,5-FDCAn in DSC shows a T_m at 269 °C with a melting enthalpy of 135.8 J/g, whereas the melt enthalpy of the second heating run is decreased to 72.7 J/g. The decrease in melting temperature and the melting enthalpy indicate that 2,5-FDCAn crystallized from solution is more perfect compared to melt crystallized 2,5-FDCAn.

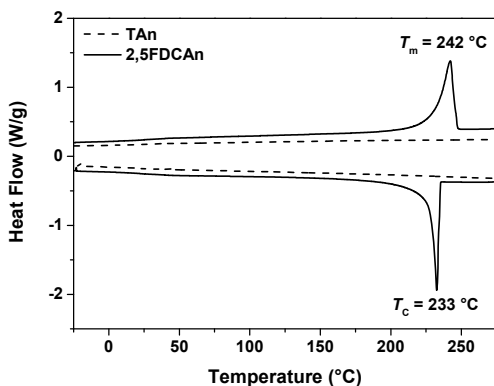


Figure 5.3. Second DSC heating run observed during heating at 10 °C / min for TAn and 2,5-FDCAn. Melting (242 °C) and crystallization (233 °C) are observed for the 2,5-FDCAn compound, whereas the TAn, 2,5-TDCAn and IAn model compounds do not melt below 300 °C.

Since the T_m of both 2,5-TDCAn and IAn lie well beyond 300 °C, it is concluded that the intermolecular hydrogen bonding of these compounds is not strongly affected by the steric hindrance of the central dicarboxylic acid motif (IA), nor by the presence of a five-membered ring with a heteroatom (2,5-TDCA). This implies that the low melting temperature of 2,5-FDCAn originates from either the rigid nature of the 2,5-furandicarboxamide moiety or from the interactions with the oxygen heteroatom in the furan ring. As is mentioned previously, the rigid nature of the 2,5-furandicarboxamide moiety and the intramolecular interactions in 2,5-FDCAn are likely to enhance each other's effect.

5.3.4. FTIR analysis of the amide-ester model compounds

The thermal analysis of the model compounds showed that, unlike the other model compounds, 2,5-FDCAn melts well below its degradation temperature. It is anticipated that this melt behavior originates from the perturbed intermolecular hydrogen bonding in 2,5-FDCAn, resulting in the formation of low-melting and defected crystals with poor hydrogen bonding. FTIR analysis was performed to obtain more information on the hydrogen bonding occurring in the different model compounds. Figure 5.4 shows the FTIR spectra in the regions between 3550 to 3150 cm^{-1} and 1850 to 1450 cm^{-1} , depicting the characteristic N-H stretch and C=O stretch

vibration bands of the model compounds, obtained upon recrystallization from NMP. The N-H stretch vibration region in the FTIR spectrum of 2,5-FDCAn shows bands at 3408 cm^{-1} and 3315 cm^{-1} , corresponding to the stretch vibrations of the free N-H groups and the hydrogen bonded N-H groups, respectively.¹³ Similar bands are observed for the other model compounds. However, these model compounds show a much weaker free N-H stretch vibration band compared to 2,5-FDCAn, indicating that solvent-crystallized 2,5-FDCAn has more unbound amide groups compared to the other model compounds.

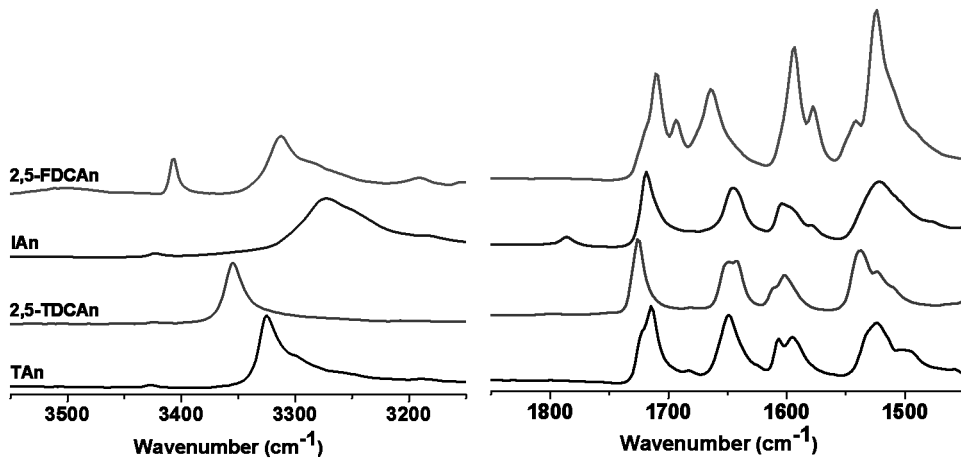


Figure 5.4. ATR-FTIR spectra of solvent-crystallized TAn, IAn, TDCAn, and 2,5-FDCAn taken at room temperature. The left side of the figure shows the region between 3550 cm^{-1} to 3150 cm^{-1} containing the N-H stretching vibrations. On the right side, the region between 1850 cm^{-1} and 1450 cm^{-1} showing the C=O stretch vibrations together with the combined amide two signal and the aromatic ring vibration signals is depicted. The differences of the N-H stretch and C=O stretch vibration bands of the free amide groups show that 2,5-FDCAn has a substantially higher fraction of non-hydrogen bonded amide groups compared to the other model compounds.

As is reported by Coleman and coworkers¹⁴, the width of the hydrogen bonded N-H stretch band reflects the distribution of the hydrogen bond strength. This indicates that the small width of the absorption corresponding to the hydrogen bonded N-H vibration of TAn (3325 cm^{-1}) and 2,5-TDCAn (3354 cm^{-1}) corresponds to the presence of regular hydrogen bonds with similar strengths and bond lengths. In other words, TAn and 2,5-TDCAn are of an ordered and crystalline nature. In contrast, both 2,5-FDCAn and IAn show a broad hydrogen bonded N-H stretch band at 3312 cm^{-1} and 2372 cm^{-1} respectively. This implies that the hydrogen bonds in these materials are not homogeneous and that these materials are less ordered.

Similar conclusions can be drawn on comparing the C=O stretch vibrations of 2,5-FDCAn to the other model compounds (Figure 5.4). The 2,5-FDCAn model

compound shows two C=O amide stretch vibrations at 1693 cm^{-1} and 1666 cm^{-1} , corresponding to the stretch vibration of the unbound carbonyl and stretch vibration of the hydrogen bonded carbonyl, respectively. Since the band corresponding to the unbound carbonyl stretch vibration is more dominantly present in the FTIR spectrum of 2,5-FDCAn, it is concluded that the other model compounds have a more optimal hydrogen bonding after recrystallization from NMP.

5.3.5. Temperature resolved FTIR analysis of 2,5-FDCAn

Temperature-resolved transmission FTIR was performed on 2,5-FDCAn to obtain more information on the changes in hydrogen bonding upon heating and melting. The sample was heated at a rate of 10 $^{\circ}\text{C}/\text{min}$ to the desired temperature. FTIR spectra were collected after the sample was kept isothermal for one minute. Heating was performed to a maximum temperature of 275 $^{\circ}\text{C}$ and melting of 2,5-FDCAn was observed at 273 $^{\circ}\text{C}$. This melting point is in accordance with the T_m observed in DSC (269 $^{\circ}\text{C}$) for solution-crystallized 2,5-FDCAn. Figure 5.5 shows the FTIR spectra, obtained at room temperature (RT), just below melting at 240 $^{\circ}\text{C}$, in the melt at 275 $^{\circ}\text{C}$, during isothermal crystallization at 240 $^{\circ}\text{C}$ and cooled to RT.

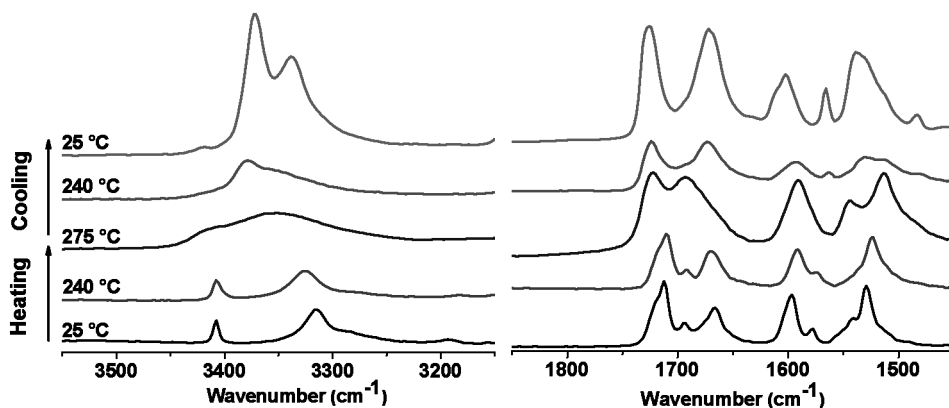


Figure 5.5. Temperature-resolved FTIR spectra, obtained during heating and melting of solvent-crystallized 2,5-FDCAn and during cooling back to room temperature. The left side of the figure shows the region between 3550 cm^{-1} to 3150 cm^{-1} , encompassing the N-H stretching vibrations. On the right side, the region between 1850 cm^{-1} and 1450 cm^{-1} is depicted, showing the C=O stretch vibrations, the amide II signals and the aromatic ring vibration signals.

The FTIR spectrum in Figure 5.5 taken at room temperature (transmission mode) is comparable to the spectrum of 2,5-FDCAn shown in Figure 5.4 (ATR mode) and shows the N-H stretch vibration bands at 3408 cm^{-1} and 3315 cm^{-1} . It is observed that the band corresponding to the N-H stretch of the hydrogen bonded amides shifts to 3325 cm^{-1} and broadens after heating to 240 $^{\circ}\text{C}$. The broadening is the anticipated result of the weakening of the hydrogen bonds due to the increase in vibrational

energy. The presence of both N-H stretch vibration bands, though broad, suggests the presence of weak hydrogen bonding in the melt. Three bands at 3420 cm^{-1} , 3373 cm^{-1} , and 3340 cm^{-1} appear upon crystallization at $240\text{ }^{\circ}\text{C}$ and strengthen upon cooling to room temperature. Similarly to in the FTIR spectra of TAn, 2,5-TDCAn and IAn model compounds, the band at 3420 cm^{-1} of melt-crystallized 2,5-FDCAn corresponds to the free N-H stretch vibration. The N-H stretch vibration can be considered to consist solely of the stretching motion and is, in other words, an isolated mode which is not sensitive to differences in conformations.^{13,15} This indicates that both bands at 3373 cm^{-1} and 3340 cm^{-1} are to be attributed to the N-H stretch motion of hydrogen bonded N-H groups. Since both bands are narrow and well-resolved, it can be concluded that melt-crystallization of 2,5-FDCAn results in the formation of crystals containing two different, yet well-defined, types of hydrogen bonds. These hydrogen bonds could correspond to the previously observed inter- and intramolecular interactions occurring in 2,5-FDCAn.

Similarly, the carbonyl region shows a change of hydrogen bonding upon melting. Three peaks can be identified in the carbonyl (C=O) region at room temperature for solution-crystallized 2,5-FDCAn in Figure 5.5. The C=O stretch band of the ester is located at 1713 cm^{-1} , whereas the C=O stretch vibrations of the amide are found at 1666 cm^{-1} (hydrogen bonded) and 1693 cm^{-1} (free amide). Upon melting, the hydrogen bonded amide carbonyl stretch disappears, while the intensity of the non-hydrogen bonded carbonyl stretch vibration increases. Furthermore, the ester C=O stretch vibration shifts to 1722 cm^{-1} upon melting. This again confirms that the order in the system is lost above the melting temperature, as expected. Upon cooling and crystallization, the ester C=O stretch vibration remains at 1722 cm^{-1} indicating that no hydrogen bonding interactions with the ester carbonyl are occurring in melt-crystallized 2,5-FDCAn. The shift of the resonance of the hydrogen bonded amide C=O band for solvent-crystallized 2,5-FDCAn (1665 cm^{-1}) to melt-crystallized 2,5-FDCAn (1672 cm^{-1}), confirms the decrease in hydrogen bonding strength in melt-crystallized 2,5-FDCAn. Unlike the observations in the N-H stretch vibrations, only one band is observed for the hydrogen bonded C=O amide group. The absence of a second hydrogen bonded C=O band in the amide region could indicate that the C=O of the amide group is involved in only one type of hydrogen bonding. Although the FTIR data provides no conclusive proof for the occurrence of intramolecular interactions in 2,5-FDCAn, the presence of two hydrogen bonded amide N-H stretch vibration bands and the presence of only one hydrogen bonded C=O vibration stretch signal likely indicate that one of the N-H stretch vibration bands originates from the interactions of the amide protons with the oxygen atom in the furan ring.

The bands corresponding to the “free” N-H stretch vibration (3408 cm^{-1}) and the “free” C=O stretch vibrations (1693 cm^{-1}) are smaller for melt-crystallized 2,5-

FDCAn compared to the solvent-crystallized 2,5-FDCAn, indicating that solvent-crystallized 2,5-FDCAn contains more free amide groups. In the case of the N-H stretch vibration of the free amide, the shift in vibration mode for solution-crystallized 2,5-FDCAn (3315 cm^{-1}) and melt-crystallized 2,5-FDCAn (3340 cm^{-1}) indicates that the hydrogen bond strength and crystal perfection decreases upon melting of 2,5-FDCAn. A similar shift is observed for the C=O stretch vibrations of solvent crystallized and melt-crystallized 2,5-FDCAn. This apparent contradiction is expected to originate from the difference in sample preparation; Solution-crystallized 2,5-FDCAn consists of smaller crystals with a higher surface area per volume compared to melt-crystallized 2,5-FDCAn crystals. Hence, the molecules at the surface of the crystals are unable to undergo optimal hydrogen bonding interactions, which will increase the fraction of non-hydrogen bonded amide groups and explains the difference of the “free” N-H stretch vibration bands. This possibility is supported on comparing the WAXD patterns of the solvent-crystallized and the melt-crystallized 2,5-FDCAn, shown in Figure 5.6.

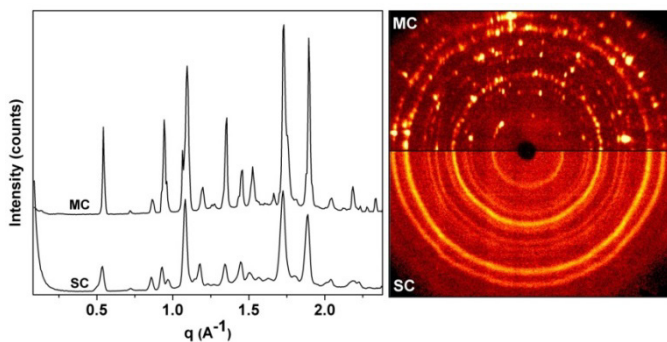


Figure 5.6. Characteristic 1D (left) and 2D (right) WAXD spectra of solution-crystallized and melt-crystallized 2,5-FDCAn (labeled SC and MC respectively). The uniform powder diffraction of solvent-crystallized 2,5-FDCAn corresponds to the diffraction from single crystals, whereas the diffraction peaks of melt-crystallized 2,5-FDCAn originate from scattering of larger crystals.

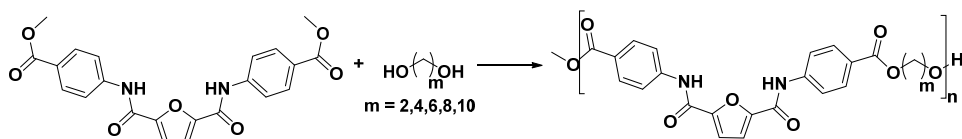
The diffraction rings observed in the 2D diffractogram of the solvent-crystallized 2,5-FDCAn correspond to the powder diffraction pattern originating from well-defined crystallites. In contrast, the diffraction peaks observed in the 2D diffractogram of the melt-crystallized 2,5-FDCAn is characteristic for diffraction of an ensemble of crystallites oriented in all directions. Although a decrease in crystal area per volume ratio is anticipated from the FTIR data in the melt-crystallized sample, it should be kept in mind that the crystal growth of melt-crystallized 2,5-FDCAn is also promoted through nucleation on the surface of the used glass capillary. Nonetheless, in solution-crystallized 2,5-FDCAn, the increase in diffraction intensity in the q range below 0.1 \AA^{-1} ($d > 62,8\text{ \AA}$) indicates the presence of long range order between crystallites

sedimented from solution. The absence of such a diffraction signal in melt-crystallized 2,5-FDCAn suggests that, similar to our observations in FTIR, the order of the crystals decreases upon crystallization from the melt. Furthermore, besides a slight shift of the diffraction peaks upon melting, likely a result from the decrease in crystal perfection, it is concluded that the crystal structure of 2,5-FDCAn does not change significantly upon melting.

5.3.6. Melt polymerization of the 2,5-FDCAn model compound

TGA analysis of the synthesized model compounds shows that all model compounds degrade upon melting, except 2,5-FDCAn. TGA analysis on 2,5-FDCAn showed that no significant weight loss is observed under isothermal conditions below 280 °C. This indicates that the melt of 2,5-FDCAn is stable, which allows for its use as a monomer in a melt polycondensation reaction. In contrast, Drewitt and Lincoln¹⁶ and Gruter and coworkers¹⁷ have reported that the parent 2,5-FDCA tends to discolor and decarboxylate at reaction temperatures above 200 to 220 °C, limiting its processing and reaction temperatures.

Polymerization of the 2,5-FDCAn model compound (Scheme 5.2) was performed according to the general polymerization procedure as described in the experiments section. Table 5.2 shows an overview of the thermal data, molecular weights and PDI values of the different polymers, obtained after polymerization with aliphatic diols containing 2, 4, 6, 8 or 10 methylene groups. For convenience, the nomenclature chosen for the polymers synthesized in this study consist of the name of the model compound, followed by the number of methylene units of the diol in the polymer backbone. For example, the polymer obtained after polymerization of 2,5-FDCAn and 1,10-decanediol is named p(2,5-FDCAn10).



Scheme 5.2. Schematic presentation of the polymerization reaction between 2,5-FDCAn and the different diols used in this study.

Table 5.2. Thermal data, number-average molecular weights and PDI values of the 2,5-FDCAn-based polymers containing aliphatic spacers with 2, 4, 6, 8 or 10 methylene groups.

Entry	DSC ^a		TGA ^b	SEC ^c	
	T_g (°C)	T_m (°C)	T_{ons} (°C)	M_n (kg/mol)	PDI
p(2,5-FDCAn2)	-	$>T_{deg}$	363	6.0	3.90
p(2,5-FDCAn4)	138.3	260 ^e	374	9.6	2.44
p(2,5-FDCAn6)	131.5	^d	364	13.4	2.45
p(2,5-FDCAn8)	118.5	^d	372	28.7	2.21
p(2,5-FDCAn10)	117.8	^d	377	34.8	2.03

a) DSC analysis performed with heating and cooling rates of 10 °C / min. b) Observed in TGA analysis performed at a heating rate of 10 °C / min. c) Observed in DMAc-SEC analysis performed against PPMA standards. d) Not observed during the second heating DSC run. e) Observed in hot-stage polarization optical microscopy during the first heating run.

As is listed in Table 5.2, a melt polycondensation of 2,5-FDCAn with aliphatic spacers with 6 methylene units or more yields polymers having molecular weights above 10,000 g/mol. Crystallization of the reaction mixture occurred during the reaction step under reduced pressure and hindered further molecular weight build-up in polymerizations where 1,2-ethanediol or 1,4-butanediol are used as the diol. As is shown in Table 5.2, the PDI of p(2,5-FDCAn2) lies close to 4, which is expected to originate from the crystallization during polymerization. The other polymers show PDI values between 2 and 2.5, which are expected for polymers synthesized via a melt transesterification reaction.

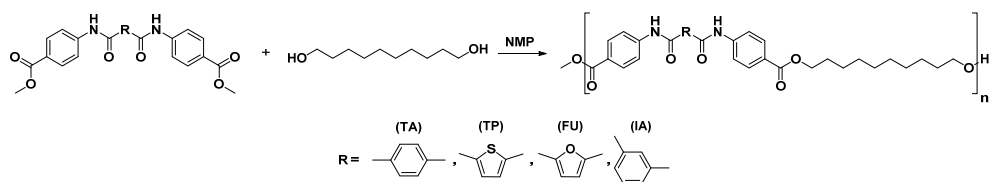
The glass transition temperatures of the 2,5-FDCAn based polymers lie between 117 °C and 138 °C, as observed in DSC analysis. These relatively high glass transition temperatures are attributed to the presence of the rigid aromatic 2,5-FDCAn moiety along the main chain. No melting or crystallization was observed for p(2,5-FDCAn6), p(2,5-FDCAn8), and p(2,5-FDCAn10) at heating and cooling rates of 10 °C/min. However, upon performing DSC analysis at 1 °C/min, weak cold crystallization and melting is observed at 248 °C, 241 °C, and 210 °C for the polymers having 6, 8 and 10 methylene spacers, respectively. The melting temperature of p(2,5-FDCAn4) could not be determined using DSC, since gas was produced above its melting temperature. This is thought to be a result of the degradation or evaporation of the low molecular weight compounds present in this polymer. Still, melting was visually observed at 260 °C in hot-stage polarization optical microscopy performed at a heating rate of 10 °C/min. No crystallization was observed for this polymer upon cooling and during the second heating run. In general, this indicates that these materials are poorly crystalline and only exhibit slow crystallization rates. The poor crystallization of the

2,5-FDCAn based poly(ester amide)s developed in this study is similar to the crystallization behavior observed for 2,5-FDCA-based polyamides reported in literature.⁴

Crystallization of 2,5-FDCAn based polymers is more easily detected during DSC heating and cooling runs of lower molecular weight 2,5-FDCAn based polymers. For example, p(2,5-FDCAn10) was synthesized with a M_n of 9,600 g/mol (PDI = 2.53) and showed a melting endotherm at 205 °C in DSC at a heating rate of 10 °C/min. Correspondingly, WAXD indicated that this sample had a degree of crystallinity of 19.9%. Similarly, p(2,5-FDCAn8) with a M_n of 10,700 g/mol (PDI = 1.72) shows a melting endotherm at 208 °C in DSC analysis and a degree of crystallinity of 25.5%, according to WAXD analysis. In contrast, the WAXD diffractograms of the p(2,5-FDCAn10) and p(2,5-FDCAn8) reported in Table 5.2 only show amorphous scattering in WAXD when measured after heating and cooling at a heating rate of 10 °C/min. These DSC and WAXD experiments indicate that both the crystallization rate and the total percentage of crystallinity increase with decreasing molecular weights. This data suggests that the crystallization of these 2,5-FDCAn based polymers is highly diffusion dependent. It is assumed that the perturbed intermolecular hydrogen bonding observed in 2,5-FDCA also occurs in 2,5-FDCAn based polymers and is responsible for the slow crystallization rate and the overall low degree of crystallinity.

5.3.7. Comparison of p(2,5-FDCAn10) with p(IAn10) and p(2,5-TDCA10)

To compare the properties of the 2,5-FDCAn based polymers with the properties of their TA, 2,5-TDCA and IAn analogues, polymerization of the TAn, 2,5-TDCA and IAn with 1,10-decanediol was attempted (Scheme 5.3). However, the synthesis of these materials in the absence of a solvent proved impossible due to the infusibility of the model compounds at the used reaction temperatures. Instead, NMP was used as solvent to promote transesterification in the early stage of polymerization. The NMP was distilled off upon the application of reduced pressure over the reaction mixture and rapid crystallization of p(2,5-TDCA10) and p(IAn10) polymers occurred. The polymers were isolated from the reactor flask and used for analysis without further purification. The addition of NMP to the TAn and 1,10-decanediol reaction mixture did not result in the dissolution of the TAn and prevented polymerization. Neither the addition of more NMP, nor the increase in the reaction temperature resulted in the formation of the p(TAn10) polymer. Instead, a brown, infusible and insoluble product was obtained. Table 5.3 shows the thermal data, the molecular weights, PDI, and the crystallinity of the other polymers, obtained *via* DSC, TGA, DMAc-SEC, and WAXD analysis, respectively.



Scheme 5.3. Schematic representation of the polymerization reaction between the different model compounds and 1,10-decanediol used in this study.

Table 5.3. Thermal data, number-average molecular weights and PDI values of the 2,5-TDCAn, IAn, and 2,5-FDCAn based polymers containing 1,10-decanediol as aliphatic diol.

Entry	DSC		TGA	SEC		WAXD
	T_g (°C)	T_m (°C)	T_{ons} (°C)	M_n (kg/mol)	PDI (-)	Crystallinity (%)
p(2,5-TDCAn10)	a	a	371	20.1	1.82	69.9
p(IAn10)	114.8	219.9 ^b	374	16.8	2.4	38.7
p(2,5-FDCAn10)	117.8	n.o.	377	34.8	2.03	c

a) No transitions observed in DSC analysis. b) Cold crystallization observed prior to melting. c) Amorphous scattering observed in WAXD.

It is observed that all products shown in Table 5.3 have an onset of degradation around 370-375 °C, similar to the onset of degradation of the other 2,5-FDCAn based polymers shown in Table 5.2. It is reasonable to assume that the thermal stability of these polymers is limited by the presence of the aliphatic spacers, which is less stable compared to the aromatic moieties. The molecular weights of the polymers in Table 5.3 are determined using DMAc-SEC analysis and show that all polymers have number-average molecular weights of more than 10,000 g/mol. Polymer p(2,5-TDCAn10) did not melt prior to degradation, and showed no T_g transition in DSC analysis, indicating that it is highly crystalline. A crystallinity close to 70% was obtained after peak fitting of the WAXD spectrum of p(TDCAn10). Such behavior is expected for polymers having 2,5-TDCAn or TAn moieties, since the corresponding model compounds also have high melting temperatures and very strong intermolecular hydrogen bonds. However, it should be noted that the crystallinity observed for the 2,5-TDCAn polymer is likely enhanced by the crystallization occurring during polymerization; The infusible nature of this polymer results in a rapid crystallization during synthesis and molecular weight build-up takes place in the solid state. As a result, the polymer crystals are subjected to an extensive annealing step, improving the crystallinity and the crystal perfection.

In contrast, p(IAn10) does show a T_g at 115 °C, which is slightly lower than the T_g of 118 °C observed for p(2,5-FDCAn10). Furthermore, p(IAn10) shows cold-crystallization at 187 °C and melting at 220 °C during heating (Figure 5.7). No crystallization is observed during cooling of p(IAn10) at 10 °C/min, indicating that

crystallization is slightly hindered in this polymer. Nonetheless, WAXD analysis of the p(IAn10) polymer, obtained after the cold-crystallization process, indicates that its crystallinity is $\sim 40\%$ (Figure 5.8). This example indicates that the p(IAn10) polymer crystallizes at an enhanced rate and has a higher crystallinity than the p(2,5-FDCAn10) polymer.

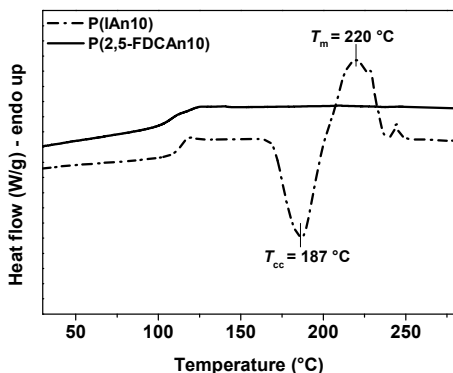


Figure 5.7. Second DSC heating run observed during heating at $10\text{ }^{\circ}\text{C}/\text{min}$ for p(IAn10) and p(2,5-FDCAn10). Cold-crystallization ($187\text{ }^{\circ}\text{C}$) and melting ($220\text{ }^{\circ}\text{C}$) are observed for p(IAn10), whereas the p(2,5-FDCAn) does not show any melt or crystallization transitions in DSC analysis.

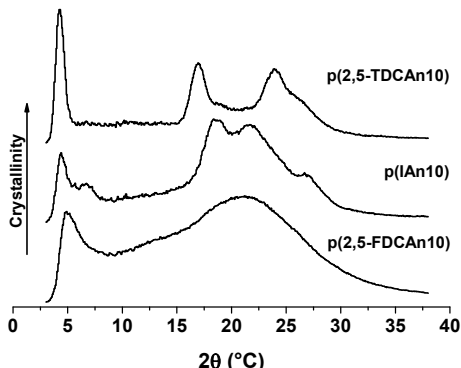


Figure 5.8. WAXD diffractograms of p(2,5-FDCAn10), p(IAn10), and p(2,5-TDCAn10). The amorphous diffraction observed for p(2,5-FDCAn10) is characteristic for the 2,5-FDCA based poly(ester amide)s synthesized in this study.

To recall, the crystallization behavior of these poly(ester amide)s is greatly affected by the molecular weight. Therefore it might be possible that the enhanced crystallization of the p(IAn10) polymer originates from the simple fact that this material has a lower molecular weight than the p(2,5-FDCAn10) polymer. However, when the crystallinity of a p(2,5-FDCAn10) polymer having a molecular weight of $9,6\text{ kg/mol}$ ($\sim 20\%$) is compared to the crystallinity of the p(IAn10) having a molecular weight of 16.8

kg/mol (~40 %), it may be clear that the difference in crystallization behavior is not attributable to the molecular weight difference of these polymers. Therefore, it is concluded that p(IA_n10) has faster crystallization kinetics than p(2,5-FDCAn₁₀). Furthermore, this data confirms that the poor crystallization of 2,5-FDCAn based polymers originates from the inability of the 2,5-furandicarboxamide moiety to crystallize and not from the steric hindrance from the non-linear 2,5-FDCA group, which would otherwise also be present in IA-based polymers.

5.4. Conclusions

Four different ester-amide model compounds containing TA, 2,5-TDCA, 2,5-FDCA and IA were successfully synthesized through reaction of 4-methyl aminobenzoic acid with the corresponding diacid chloride. It is shown that intermolecular hydrogen bonding is weaker in the ester-amide model compound containing 2,5-FDCA (2,5-FDCAn) compared to the other model compounds, resulting in a suppression of the melting temperature. It is anticipated that the presence of the oxygen heteroatom in the 2,5-FDCA ring acts as a hydrogen bond acceptor and perturbs the formation of intermolecular hydrogen bonds. The low melting temperature of 2,5-FDCAn allows for its application in melt polycondensation reactions at temperatures up to 280 °C, whereas free 2,5-FDCA is too thermally instable to be processed above 220 – 230 °C. Polymers having molecular weights above 10,000 g/mol can readily be obtained via a melt polycondensation of 2,5-FDCAn with aliphatic diols. where the synthesis is performed at 250 °C. Cold crystallization is observed for polymers with molecular weights below 10,000 g/mol, whereas polymers with higher molecular weights show thermal behavior characteristic for poorly crystalline polymers. In contrast to the 2,5-FDCA based model compound, the presence of more optimal hydrogen bonding in the TA, 2,5-TDCA and IA based model compounds does not allow melt polycondensation reactions without the use of solvents.

5.5. References

- [1] Warner, S.B., Lee, J., *J. Polym. Sci. Part B: Polym. Phys.*, **1994**, 32, 1759-1769
- [2] Hopff, H., Krieger, A., *Makromol. Chem.*, **1961**, 47, 93-113
- [3] Heertjes, P.M., Kok, G.J., *Delft Progress Reports, Series A*, **1974**, 1, 59-63
- [4] Grosshardt, O., Fehrenbacher, U., Kowollik, K., Tubke, B., Dingenouts, N., Wilhelm, M., *Chemie Ingenieur Technik*, **2009**, 81, 11, 1829-1835
- [5] Mitiakoudis, A., Gandini, A., *Macromolecules*, **1991**, 24, 830, 835
- [6] Gandini, A., Belgacem, M.N., *Prog. Polym. Sci.*, **1997**, 22, 1203-1379
- [7] Yeh, I.-C., Rinderspacher, B.C., Andzelm, J.W., Cureton, L.T., La Scala, J., *Polymer*, **2014**, 55, 166-174
- [8] Zhang, C., Ren, Z., Liu, L., Yin, Z., *Molecular Simulations*, **2013**, 39, 11, 875-881
- [9] Harings, J.A.W., Deshmukh, Y.S., Hansen, M.R., Graf, R., Rastogi, S., *Macromolecules*, **2012**, 45, 5789-5797

- [10] Deshmukh, Y.S., Graf, R., Hansen, M.R., Rastogi, S., *Macromolecules*, **2013**, 46, 7086-7096
- [11] Lei, Y., Li, H., Pan, H., Han, S., *J. Phys. Chem. A.*, **2003**, 107, 1574-1583
- [12] Cai, R., Preston, J., Samulski, E.T., *Macromolecules*, **1992**, 25, 563-568
- [13] Skrovanek, D.J., Howe, S.E., Painter, P.C., Coleman, M.M., *Macromolecules*, **1985**, 18, 1676-1683
- [14] Coleman, M.M., Lee, K.H., Skrovanek, D.J., Painter, P.C., *Macromolecules*, **1986**, 19, 2149-2157
- [15] Moore, W.H., Krimm, S., *Biopolymers*, 1976, 15, 2439-2464
- [16] Drewitt, J.G.N., Lincoln, J., Br. Patent, 621971, **1946**, November 12
- [17] Gruter, G-J. M., Sipos, L., Dam, M.A., *Combinatorial Chemistry & High Throughput Screening*, **2012**, 15, 180-188

Chapter 6

Synthesis, kinetics, and characterization of bio-based thermosets obtained through polymerization of a 2,5-furandicarboxylic acid-based bis(2-oxazoline) with sebacic acid

Abstract

The synthesis of renewable 2,5-furandicarboxylic acid-based cross-linked poly(ester amide)s is described in this chapter. These poly(ester amide)s are obtained after polymerization of 2,5-bis(4,5-dihydrooxazol-2-yl)furan (2,5-FDCAox) with sebacic acid (SeA). It is demonstrated that the 2,5-FDCAox monomer is more susceptible to participate in a branching reaction than the 1,3-bis(4,5-dihydrooxazol-2-yl)benzene (IAox) monomer. This preference of 2,5-FDCAox to form branched or cross-linked chains is attributed to the increased nucleophilicity of the 2,5-furandicarboxamide group formed during polymerization, resulting from intramolecular hydrogen bonding with the furan oxygen heteroatom. As a result, the application of 2,5-FDCAox in polymerizations allows for the development of fully renewable polymer glasses or coatings, without the requirement of a catalyst. However, when preferred, it is demonstrated that triphenyl phosphite (TPP) can be used to accelerate the branching reaction further and to reduce the curing times of the cross-linked poly(ester amide)s synthesized in this study. Overall it can be concluded that the decreased curing times and the good thermal properties make 2,5-FDCA-based bis(2-oxazoline) monomers interesting candidates for the preparation of fully renewable cross-linked poly(ester amide)s.

6.1. Introduction

In the previous chapter it was demonstrated that, in contrast to 2,5-furandicarboxylic acid (2,5-FDCA), the 2,5-furandicarboxamide moiety is stable at temperatures well above 250 °C. Furthermore, the occurrence of intra-molecular hydrogen bonding limits crystallization and increases the solubility of 2,5-FDCA based polyamides or poly(ester amide)s. The work reported in chapter 5 demonstrates that 2,5-furandicarboxamide based monomers can be employed to suppress crystallization and melting temperatures, and to improve the solubility of polymer chains. In this chapter, the versatility of the 2,5-furandicarboxamide moiety is demonstrated by the development of renewable polymer glasses via the ring opening polyaddition reaction of 2,5-bis(4,5-dihydrooxazol-2-yl)furan with aliphatic dicarboxylic acids.

The synthesis, ring-opening, and polymerization of oxazoline groups has been a topic of study for many years, as is indicated by the early communications of Wenker¹, Fry², and Goldberg³ published more than 60 years ago. The interest in these oxazoline rings originates from their ability to undergo ring-opening addition reactions with species bearing labile protons, such as carboxylic acids, thiols, phenols, amines, and amides.⁴ For this reason, these versatile compounds are used as monomers in addition or step growth reactions such as cationic polymerizations, enzymatic polymerizations or thermally initiated melt polymerizations.⁴⁻⁸ Furthermore, bis(2-oxazoline)s have been used for chain extension of polymers and end-capping or modification of polymers and for introducing functionalities along the polymer backbone.⁹⁻¹²

Especially thermally initiated melt polymerizations or chain extension reactions are of interest for industrial purposes due to the absence of solvents and solvent recovery systems. Besides the synthesis of linear polymer chains, these melt-polymerizations allow for the production of cross-linked polymers in one reaction step. As reported by Sano^{13,14}, cross-linked poly(ester amide)s can be obtained through a triphenylphosphite (TPP) catalyzed melt-polymerization of bis(2-oxazoline)s with dicarboxylic acids. Néry and coworkers¹⁵ reported no detectable branching or cross-linking in systems synthesized in the absence of TPP, indicating that this catalyst is essential for the production of cross-linked polymers via this route. This suggests that the degree of cross-linking, occurring during polymerization of bis(2-oxazoline)s and dicarboxylic acids, can be tailored by using TPP as a catalyst.

Recently, the interest in the development and production of renewable materials such as 2,5-furandicarboxylic acid (2,5-FDCA) has increased significantly. Many examples of the application of 2,5-FDCA as a monomer in polycondensation reactions have been reported over the last years.¹⁶ Examples of the synthesis of 2,5-FDCA based polyesters have been reported by Moore and Kelly¹⁷⁻¹⁹, Gubbels and coworkers,²⁰ and Gandini and coworkers,^{21,22}. These 2,5-FDCA based polyesters generally exhibit different properties compared to their petroleum based analogues. For example, as is

reported by Burgess and coworkers, poly(ethylene 2,5-furandicarboxylate) (PEF) has an improved glass transition temperature, improved mechanical properties, reduced oxygen permeability and reduced chain mobility compared to poly(ethylene terephthalate).²³ Also, 2,5-FDCA based polyamides show properties deviating from the properties of its petroleum based analogues. For example, the low crystallinity observed for 2,5-FDCA based polyamides are in contrast to both the high crystallinities and crystallization rates observed in terephthalic acid based polyamides.²⁴⁻²⁷ Furthermore, 2,5-FDCA based polyamides exhibit more van der Waals interactions, maintain more rigid structures, and show slower weakening of hydrogen bonds upon heating compared to nylon 4,6, as was recently reported by Yeh and coworkers.²⁸ These reports clearly show that the presence of the furan ring in a polymer backbone yields materials with properties that are rather different from polymers containing phenyl based monomers such as terephthalic acid or isophthalic acid (IA).

Although the synthesis of a 2,5-FDCA based bis(2-oxazoline) monomer has been described in literature²⁹, no reports were found concerning its use as a monomer in melt-polymerization. Therefore, this chapter reports on the synthesis of 2,5-bis(4,5-dihydrooxazol-2-yl)furan (2,5-FDCAox) and on the application of 2,5-FDCAox in polymerization with sebacic acid (SeA). The behavior of 2,5-FDCAox in such polymerization is compared to that of its isophthalic acid based counterpart, 1,3-bis(4,5-dihydrooxazol-2-yl)benzene (IAox). The branching and cross-linking reactions occurring during the bulk-polymerization of 2,5-FDCAox with SeA are investigated using FTIR spectroscopy and the reaction parameters required for the development of renewable polymer glasses are determined. Lastly, 2,5-FDCA based polymer glasses and coatings are prepared and their thermal properties are evaluated.

6.2. Experimental section

6.2.1. Materials

2,5-Furandicarboxylic acid (2,5-FDCA) was obtained from Atomole, China (>99,5 wt%, GC-MS). Sebacic acid (SeA), 2-chloroethylamine hydrochloride, triphenylphosphite (TPP), thionyl chloride, sodium hydroxide, and potassium hydroxide were purchased from Sigma. Irganox 1330 antioxidant was a kind gift from Ciba Specialty Chemicals. 1,3-bis(4,5-dihydrooxazol-2-yl)benzene (IAox) was purchased from TCI Europe. Deuterated dimethyl sulfoxide (DMSO-*d*₆, 99.9% atom D) was acquired from Cambridge Isotope Laboratories. Methanol, dichloromethane (dried over Al₂O₃), N,N-dimethylformamide (DMF) and N-methyl-2-pyrrolidone (NMP) were obtained from Biosolve. All chemicals were used as received, unless stated otherwise.

6.2.2. Preparation of N,N'-bis(2-chloroethyl)furan-2,5-dicarboxamide

2,5-furandicarboxylic acid (16.4 g, 0.105 mol) was reacted with an excess of thionyl chloride (27.5 mL, 0.23 mol), in the presence of a catalytic amount of DMF (100 μ L) in a 250 mL three-neck flask at 80 °C for four hours. A condenser was connected to the flask to allow refluxing of thionyl chloride and the reaction was conducted under an argon rich atmosphere. The released gaseous SO₂ and HCl were passed through an aqueous NaOH solution, neutralizing the hydrochloric acid. After 4 hours of reaction time, the mixture was cooled with an ice-bath followed by the application of reduced pressure for 30 minutes to remove any residual thionyl chloride. The 2,5-furandicarboxylic acid chloride was dissolved in anhydrous dichloromethane (150 mL) and dropwise added to an aqueous solution of 2-chloroethylamine hydrochloride (24.4 g, 0.21 mol) and NaOH (16.4 g, 0.41 mol) under vigorous stirring. After 2 hours of reaction time, the organic phase was distilled off using reduced pressure and the water phase was filtered. The product, N,N'-bis(2-chloroethyl)furan-2,5-dicarboxamide, was obtained as white powder and was dried overnight under reduced pressure at 40 °C. Yield = 25.3 g (86.4%). ¹H NMR (400 MHz, DMSO-*d*₆, δ , ppm): 7.19 (s, 2H, furan), 3.75 (t, *J* = 6.0 Hz, 4H, ClCH₂), 3.60 (d, *J* = 6.0 Hz, 4H, NCH₂).

6.2.3. Preparation of 2,5-bis(4,5-dihydrooxazol-2-yl)furan (2,5-FDCAox)

N,N'-bis(2-chloroethyl)furan-2,5-dicarboxamide (15.00 g, 0.054 mol) and NaOH (4.8 g, 0.12 mol) were dissolved in 50 mL methanol in a 250 mL round-bottom flask, and were allowed to reflux for 4 hours. During the reaction white crystals precipitated. The formed product was isolated using filtration and washed with water prior to drying *in vacuo* overnight at 40 °C. Yield = 8.98 g (81.1%). ¹H NMR (400 MHz, DMSO-*d*₆, δ , ppm): 7.13 (s, 2H, furan), 4.35 (t, *J* = 9.6 Hz, 4H, NCH₂), 3.92 (t, *J* = 9.6 Hz, 4H, OCH₂). ¹³C NMR (400 MHz, DMSO-*d*₆, δ , ppm): 155.4 (O-C=N), 144.8 (O-C=C), 115.9 (C-C=C), 68.0 (CH₂-O), 55.0 (CH₂-N). Elemental analysis for C₁₀H₁₀N₂O₃, observed (calculated): C = 58.25% (58.19%), H = 4.89% (4.82%), and N = 13.59% (13.58%).

6.2.4. General melt polymerization procedure.

Reaction mixtures were prepared by weighing and grinding 2,5-FDCAox (1.0 to 2.5 eq), SeA (1 eq), Irganox 1330 (1 wt%), and TPP (0 to 7 wt%) using a mortar and pestle. Samples prepared for DMAc-SEC and DSC analysis were loaded into 1 mL glass vials and immersed in an oil-bath at the desired temperature of 160 °C for the desired reaction time (0 – 60 minutes) prior to analysis. Samples prepared for DMTA analysis were preheated to 160 °C for one minute until a clear casting liquid was obtained. The casting liquid was then poured onto a Teflon film and cured in an oven at 200 °C under a nitrogen rich atmosphere for 10 minutes to one hour.

6.2.5. Preparation of solvent-borne coatings.

2,5-FDCA (2.25 eq) was cured with SeA (1 eq) in the presence of 5 wt% TPP using the following procedure. A solution of 2,5-FDCAox (139.3 mg, 0.675 mmol), sebacic acid (60.7 mg, 0.3 mmol) and triphenylphosphite (10 mg, 5 wt%) was prepared in 0.6 mL N-Methyl-2-Pyrrolidone at 100 °C. This solution was subsequently applied to Q-panels, preheated in an oven at 200 °C, using a coating applicator frame with a spacing of 120 μ m. The coatings were

cured by heating the coated panels in an oven at 200 °C for 1 hour under a nitrogen rich atmosphere.

6.2.6. Characterization methods

^1H NMR and ^{13}C NMR spectroscopy was performed on a 400 MHz Bruker AVANCE-III spectrometer. Samples were prepared by dissolving 5–10 mg of monomer or polymer in 0.5 - 1 mL deuterated dimethyl sulfoxide (DMSO-*d*₆) and were referenced against tetramethylsilane (TMS).

Cross polarization total sideband suppression (CP/TOSS) ^{13}C NMR experiments were performed at room temperature on a 300 MHz Bruker AVANCE-III spectrometer. These experiments utilized a rotational frequency of 5.0 kHz. Experiments were performed using a ^1H 90° pulse, followed by a contact time of 1000 μs , and a TOSS sequence to remove sidebands. The 90° pulse was 4 μs and the 180° pulse was 8 μs . The pulse power, used during contact, was 4 dB (1000 μs) and 1 dB during decoupling (2.5 μs). The number of scans and recycle delay were 2000 and 2 s, respectively.

N,N-Dimethylacetamide size exclusion chromatography (DMAc-SEC) was performed on a Waters Alliance system equipped with a Water 2413 refractive index detector (40 °C), a Waters 2695 separation module, a Waters 2996 photodiode array detector, a PSS GRAM guard column followed by two PSS GRAM columns in series of 100 Å (10 μm particles) and 3000 Å (10 μm particles) at 60 °C. DMAc was used at a flow rate of 1 mL/min and molecular weights were calculated against polystyrene standards (Polymer Laboratories, $M_p = 580$ Da up to $M_p = 7.1 \times 10^6$ Da). Polymer samples prepared in a concentration of 5 mg/mL and were filtered through a 0.2 μm PTFE filter (13 mm, PP housing, Alltech) prior to injection.

Thermal stability of the materials synthesized in this study was evaluated using thermogravimetric analysis (TGA). Experiments were performed on a TA Instruments TGA Q500 in a nitrogen rich atmosphere. Samples were heated from 20 to 800 °C, at a heating rate of 10 °C/min.

Differential scanning calorimetry (DSC) was performed using a TA Instruments DSC Q100. Two heating and cooling runs were performed -50 °C to 220 °C at 10 °C/min and the glass transition temperatures were determined from the second heating run.

Dynamic mechanical thermal analysis (DMTA) was performed using a TA Instruments Q800. Samples were prepared by mixing and grinding the desired ratio of 2,5-FDCAox to SeA powder prior to the addition of 5 wt% TPP and 1 wt% Irganox 1330. The mixtures were heated to 160 °C until a clear casting liquid was obtained (generally 30 seconds to 1 minute under mild stirring). The formed liquid was poured on a Teflon film and cured in an oven at 200 °C for 10 minutes to one hour under a nitrogen atmosphere. The polymer films were reshaped into rectangles of 20 mm x 5 mm and were measured in the DMTA from -50 °C to 225 °C at a heating rate of 2 °C/min, a frequency of 1 Hz, and an amplitude of 10 μm . If required, the samples were kept under isothermal conditions at 200 °C to follow the curing process of the sample. Glass transition temperatures were calculated from the maximum in the $\tan \delta$ trace, obtained during heating of the sample.

Attenuated Total Reflection (ATR) Fourier transform infrared spectroscopy (FTIR) was performed using a Bio-Rad FTS6000 equipped with an Golden Gate, Int. Line WB MCT

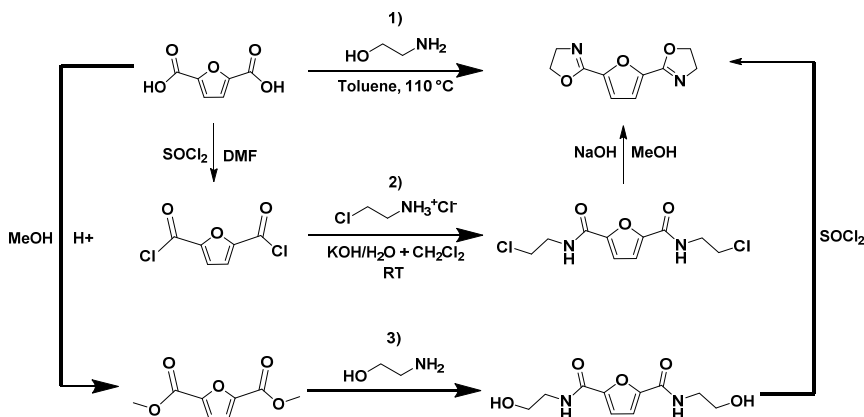
detector, and KRS-5 polarizer. Polymerization and curing reactions were monitored *on-line* for one hour at the desired reaction temperature between 150°C and 230 °C. Spectra were collected every two seconds in the range between 4000 to 650 cm⁻¹ with a spectral resolution of 4 cm⁻¹.

Coating thicknesses of the solvent-borne coatings were measured using a magnetic induction coating thickness gauge (LD0400 by Thermimport Quality Control). Reverse impact tests were performed by dropping a weight of 1 kg from a controlled height of 100 cm on the backside of the coated panels and the pencil hardness test was performed by scratching the coatings with pencils of increasing hardness. Chemical resistance was determined by the acetone double rub test in which the material is rubbed back and forth (double rubs) by an acetone drenched cloth 100 times.

6.3. Results and discussion

6.3.1. Synthesis and characterization of 2,5-FDCAox

In general, three synthetic routes are found in literature for the preparation of bis(2-oxazoline)s from dicarboxylic acids. As reported by Li and coworkers, bis(2-oxazoline)s from IA, 2,5-thiophenedicarboxylic acid, and 2,5-furandicarboxylic acid can be synthesized *via* the direct reaction of these dicarboxylic acids with β -amino alcohols in refluxing toluene for 24 hours through water deprivation (route 1, Scheme 6.1).²⁹ Although this method comprises only one reaction step, up-scaling is tedious due to the requirement of large amounts of solvents. Furthermore, purification of the reaction products is required, making this reaction route unattractive for the synthesis of large amounts of 2,5-FDCAox.



Scheme 6.1. Synthetic routes to obtain 2,5-FDCAox from 2,5-furandicarboxylic acid.

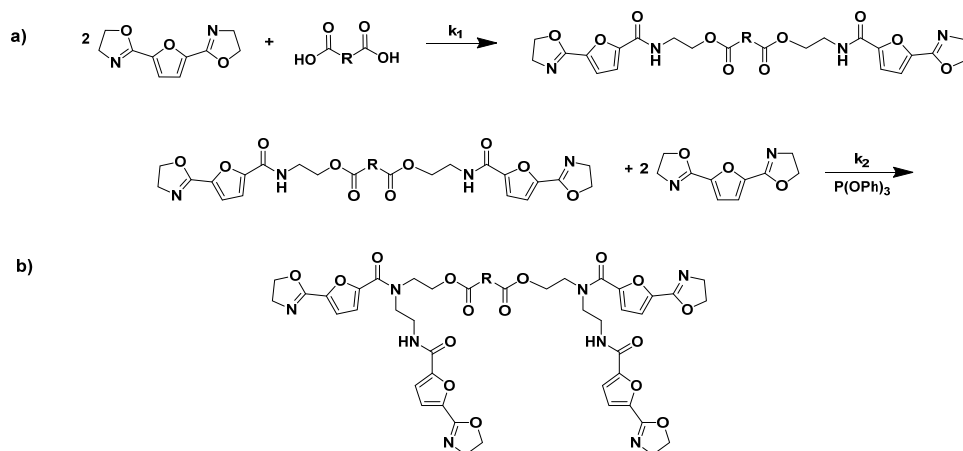
The second route (route 2, Scheme 6.1) describes the synthesis of 2,5-FDCAox through the conversion of 2,5-FDCA to the diacid chloride via reaction with thionyl chloride, followed by reaction with chloroethylamine hydrochloride, and consecutive

ring closing in methanol.⁸ The reaction products, obtained after synthesis via this route, were easily isolated by filtration and required no additional purification.

The bis(2-oxazoline) synthesized via the third route (route 3, Scheme 6.1) is obtained after the esterification of the 2,5-FDCA in methanol under acidic conditions, followed by the reaction with ethanolamine, and ring closure in thionyl chloride.³⁰ In contrast to the products formed in route 2, additional purification of the *N,N'*-bis(2-hydroxyethyl)furan-2,5-dicarboxamide intermediate was required to remove residual ethanolamine prior to performing the ring closing reaction step. For the convenient large scale synthesis, route 2 was used for the preparation of the 2,5-FDCAox monomer used in this chapter.

6.3.2. Polymerization of 2,5-FDCAox and IAox with Sebacic acid.

As is well known from literature, the ring-opening polymerization of a bis(2-oxazoline) with a dicarboxylic acid results in the formation of a linear poly(ester amide) as is shown in Scheme 6.2a. Furthermore, as is reported by Sano^{13,14}, the amide group formed in this ring-opening addition reaction can subsequently react with a 2-oxazoline group in the presence of TPP, forming a tertiary amide and a new secondary amide group (branching reaction, Scheme 6.2b). Generally, the reaction rate of the reaction between a 2-oxazoline ring and carboxylic acid (k_1) is significantly faster than the rate of the branching reaction (k_2) in the absence of TPP. Nonetheless, if the reaction constant k_2 is not zero, tertiary amides are, inevitably, formed during polymerization. These tertiary amides act as branching points in the polymer backbone, and eventually result in the formation of a cross-linked system.



Scheme 6.2. Thermally initiated ring-opening addition reactions occurring during the reaction of 2,5-FDCAox and a dicarboxylic acid. The formation of a linear chain through the reaction of 2,5-FDCAox with a carboxylic acid group is shown in reaction scheme 6.2a, whereas the branching reaction is shown in reaction scheme 6.2b.

The reaction kinetics involved during the polymerization of bis(2-oxazoline)s and dicarboxylic acids can be described using differential equations (6.1) – (6.3). To obtain these differential equations, it is assumed that both reactions are irreversible and second order¹³, that the 2-oxazoline groups are equireactive¹⁵, and that the secondary amides are equireactive. In differential equations (6.1) - (6.3), the unreacted (2-oxazoline) bulk concentration is denoted as [OX] in mol kg⁻¹. Similarly, the bulk concentrations of the formed ester groups, secondary amide groups, and tertiary amide groups are denoted as [Ester], [Sec. Amide], and [Tert. Amide] respectively in mol kg⁻¹.

$$\frac{\delta[\text{Acid}]}{\delta t} = -\frac{\delta[\text{Ester}]}{\delta t} = -\frac{\delta[\text{Sec.Amide}]}{\delta t} = -k_1 [\text{Acid}][\text{OX}] \quad (\text{eq. 6.1})$$

$$\frac{\delta[\text{OX}]}{\delta t} = -k_1 [\text{Acid}][\text{OX}] - k_2 [\text{Sec. Amide}][\text{OX}] \quad (\text{eq 6.2})$$

$$\frac{\delta[\text{Tert.Amide}]}{\delta t} = k_2 [\text{Sec. Amide}][\text{OX}] \quad (\text{eq 6.3})$$

To study the rates of these reactions occurring during polymerization, the 2-oxazoline conversion was monitored during the polymerization of an equimolar mixture of 2,5-FDCAox and sebacic acid (SeA) at 160 °C. The monomers were mixed in the solid state and heated for a fixed reaction time (t_r) using a salt bath. After cooling back to room temperature, the obtained polymers were dissolved in deuterated dimethylsulfoxide (DMSO- d_6) and analyzed using ¹H NMR analysis. To compare the reaction rate of 2,5-FDCAox with the commercially available bis(2-oxazoline) monomer derived from isophthalic acid (1,3-bis(4,5-dihydrooxazol-2-yl)benzene, IAox), the polymerizations of equimolar mixtures of IAox and SeA were performed under the same conditions.

The 2-oxazoline conversion was calculated from the ¹H NMR spectra of the products, obtained after polymerization for t_r varying from 1 to 15 minutes. First, the fraction of unreacted 2-oxazoline groups was obtained after dividing the value of the integral of the CH₂N resonance (4.35 ppm) by the value of the integral of the resonance of the furanic protons (7.13 ppm). Next, the conversion was calculated via subtraction of the 2-oxazoline fraction from 1.00 and translation to percentages. A correction for the number of protons was performed prior to the subtraction. Similarly, the fraction of unreacted 2-oxazoline groups in the IAox polymerization was calculated using the resonance of CH₂N proton at 4.35 ppm and the aromatic proton at 8.30 ppm. The 2-oxazoline conversion as a function of reaction time was used for data fitting with differential equations (6.1) – (6.3). The data fitting was performed using non-linear

regression, yielding reaction constants k_1 and k_2 , as is shown in Figure 6.1. A detailed description of the data fitting procedure is supplied in Appendix B.

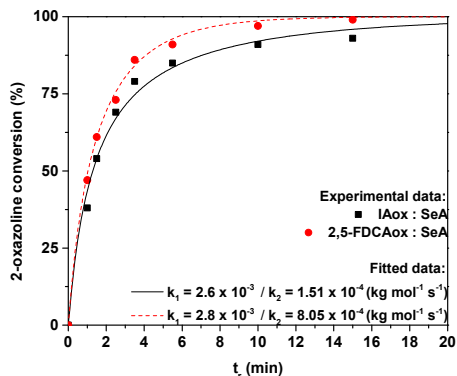


Figure 6.1. Conversion of 2-oxazoline groups over time during melt-polymerization of equimolar mixtures IAox and SeA (squares) or 2,5-FDCAox and SeA (circles) at 160 °C, as calculated from the ^1H NMR spectra. The theoretical curves and reaction constants found after data fitting are shown for the IAox (continuous line) and 2,5-FDCAox (dotted line) systems.

No accurate fit of the experimental data could be found without taking the k_2 reaction constant in account, indicating that the branching reaction also proceeds during polymerization in the absence of TPP and cannot be neglected. This is in contrast to the observations of Néry and coworkers, who found no detectable branching in the model reaction between IAox and dodecanoic acid.¹⁵ It is expected that the absence of branching in the model reaction reported by Néry is a result from the low viscosity of their system. In contrast, the viscosities of the reaction mixtures reported in this study increase rapidly as the polymerization reaction proceeds, limiting diffusion and likely promoting the formation of branches.

From the experimental data shown in Figure 6.1 it can be clearly seen that the 2,5-FDCAox monomer is consumed faster during polymerization with SeA than the IAox monomer. The observed k_1 reaction constant found after data fitting for the polymerization of the system containing IAox ($k_1 = 2.6 \times 10^{-3} \text{ kg mol}^{-1} \text{ s}^{-1}$) and 2,5-FDCAox ($k_1 = 2.8 \times 10^{-3} \text{ kg mol}^{-1} \text{ s}^{-1}$) are comparable, suggesting that both oxazoline-functional monomers have a comparable reactivity towards carboxylic acid groups. Furthermore, from Figure 6.1 is observed that the k_2 reaction constant observed in the polymerization of 2,5-FDCAox with SeA is roughly 5 times larger ($8.05 \times 10^{-4} \text{ kg mol}^{-1} \text{ s}^{-1}$) than the k_2 reaction constant found in the polymerization of IAox with SeA ($1.51 \times 10^{-4} \text{ kg mol}^{-1} \text{ s}^{-1}$). This indicates that branching is occurring at an enhanced rate in the polymerization of 2,5-FDCAox with SeA.

The results obtained in the ^1H NMR analysis suggest that branching occurs at a higher rate in the polymerization of 2,5-FDCAox with SeA than in the polymerization of

IAox with SeA. It is anticipated that this increased tendency to form branched polymer chains results in an accelerated increase of the weight-average molecular weight (M_w) during polymerization. Furthermore, this branching reaction is generally accompanied by an increase in the PDI, until the polymer starts to cross-link and becomes insoluble. To investigate the effect of this branching reaction on the M_w and PDI, DMAc-SEC analysis was performed on the polymers obtained after polymerization of equimolar mixtures of 2,5-FDCAox with SeA and IAox with SeA at 160 °C. Figure 6.2a shows an overview of the M_w and PDI obtained for the 2,5-FDCAox and IAox based systems. Figure 6.2b and 6.2c show the SEC chromatograms of the polymers formed at variable reaction times during the polymerization of the 2,5-FDCAox and IA based systems, respectively.

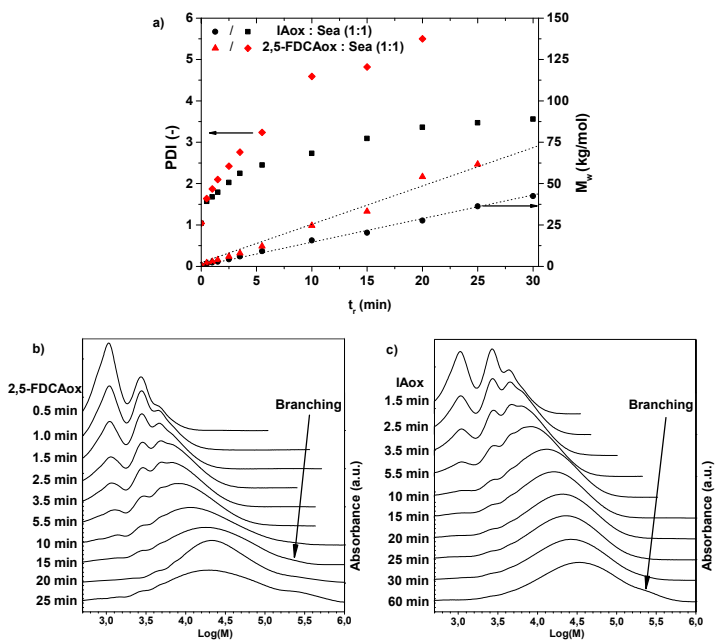


Figure 6.2. Changes of the weight-average molecular weight (M_w) and PDI over time during the polymerization of 2,5-FDCAox with SeA and IAox with SeA in an equimolar ratio performed at 160 °C, as observed in DMAc-SEC analysis. Figure 6.2a shows an overview of changes in the M_w and PDI during polymerization, whereas Figures 6.2b and 6.2c show changes in the DMAc-SEC chromatograms observed over time for the systems containing 2,5-FDCAox and IAox respectively. The dotted lines in Figure 6.2a are added to guide the eye.

From Figure 6.2a, it can be seen that both the M_w and PDI increase faster during the polymerization of 2,5-FDCAox with SeA compared to the polymerization of IAox with SeA. For example, a M_w of 33.2 kg/mol and a PDI of 4.8 is achieved in the polymerization of 2,5-FDCAox with SeA after 15 minutes of reaction time. In

contrast, the IA based polymer has only reached a M_w of 20.4 kg/mol and a PDI of 3.1 after 15 minutes of polymerization. Such a difference in molecular weight corresponds well to the difference in 2-oxazoline consumption observed in the ^1H NMR analysis.

From Figure 6.2b, it can be seen that branching of the polymer chains is occurring in the polymerization of 2,5-FDCAox with SeA, as is detected by the elution of a high molecular weight fraction in the DMAc-SEC chromatogram for polymers having a t_r of 10 minutes or longer. This high molecular weight fraction, characteristic for branched chains formed through chain coupling, is indicated by the black arrow in Figure 6.2b. Interestingly, the continued branching occurring during polymerization results in the formation of a cross-linked and insoluble polymer after 25 minutes of reaction time. In contrast, the polymer obtained after 60 minutes of polymerization of IAox with SeA is fully soluble in the DMAc solvent, indicating that the polymer is not cross-linked. However, the presence of a high molecular weight fraction is detected after 60 minutes of polymerization, indicating that branching does occur over time (Figure 6.2c).

These observations are in good agreement with the observations from ^1H NMR analysis; branching does occur during the polymerization of IAox with SeA, but at a lower rate than in polymerizations involving 2,5-FDCAox.

6.3.3. Thermal properties of poly(ester amide)s

The thermal properties of the polymers, obtained after one hour of polymerization, were evaluated using DSC analysis. The samples were measured at a heating and cooling rate of 10 °C / min and the second heating runs are depicted in Figure 6.3. It is observed that the glass transition temperature (T_g) of the 2,5-FDCA based polymer is roughly 5 °C higher than the T_g of the IA based polymer. This difference in T_g is attributed to the cross-linked nature of the 2,5-FDCA based polymer, as is confirmed by the broad temperature range of the glass transition. Furthermore, the 2,5-FDCA based polymer shows no melting transitions prior to degradation, similar to other 2,5-FDCA based polyamides and poly(ester amide)s reported in chapter 5 and in literature.^{16,26} It should be noted that, even though 2,5-FDCA based polyamides generally do not exhibit crystallization or melting, the cross-linked nature of the 2,5-FDCA based poly(ester amide) synthesized in this study is expected to limit crystallization and melting even further. In contrast, the IAox based polymer shows a peak melting temperature at 105 °C, which is in agreement with the melting range between 110 to 115 °C reported in literature.⁷

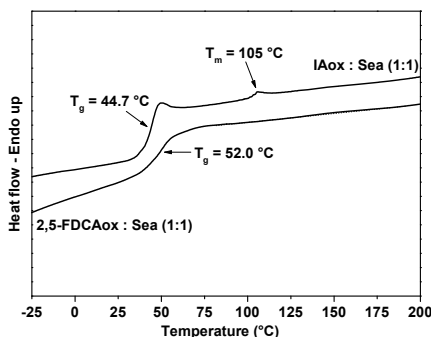
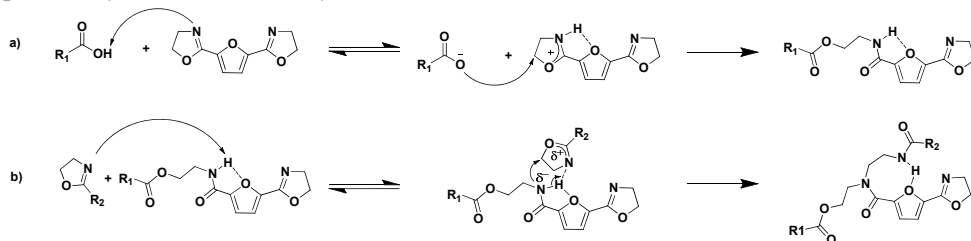


Figure 6.3. Second heating DSC curves of the polymers, obtained after one hour of polymerization of equimolar 2,5-FDCAox : SeA and IAox : SeA reaction mixtures at 160 °C.

6.3.4. Reaction mechanism of the branching reaction

In general, thermally initiated ring-opening addition reactions of a 2-oxazoline groups are reported to proceed through the reaction of a nucleophile bearing a labile proton, such as carboxylic acids, thiols or aromatic phenols.^{2,3} The presence of this labile proton is considered to be crucial for the ring-opening reaction, since it interacts with the nitrogen atom in the 2-oxazoline ring. The resulting electron deficiency makes the the 2-oxazoline ring susceptible for a nucleophilic attack on the carbon next to the oxygen atom. This reaction route explains the high reactivity of the 2-oxazoline ring towards carboxylic acids; the carboxylic acid group donates a proton to the 2-oxazoline ring, followed by a nucleophilic attack of the carboxylate anion on the carbon next to the oxygen atom in the protonated 2-oxazoline ring (Scheme 6.3a).¹⁵ This mechanism also explains the low reactivity of the reaction between amide groups and 2-oxazoline rings occurring in the branching reaction; the amide group is a poor nucleophile due to the resonance stabilization with the carbonyl group. This resonance stabilization results in a significantly reduced nucleophilic attack of the nitrogen atom of the amide group, compared to the nucleophilic attack of the previously described carboxylate anion.



Scheme 6.3. Schematic representation of the weakening of the amide N-H bond via intramolecular hydrogen bonding occurring during the reaction of a furancarboxamide group with a 2-oxazoline ring.

In the polymerizations studied thus far, it was observed that branching occurs at an enhanced rate in systems containing 2,5-FDCAox compared to systems containing IAox. It is thought that the increased rate of branching observed in the polymerization of 2,5-FDCAox with SeA is a result of the intra-molecular hydrogen bonding occurring in 2,5-FDCA based polyamides.³¹ This intra-molecular hydrogen bond is formed through the interaction of the free electron pairs of the oxygen atom of the furan ring with the proton of the amide group. As a result, the N-H bond of the amide group weakens and the nitrogen of the amide group becomes more electron rich and thus becomes a better nucleophile (Scheme 6.3b). The increased nucleophilic nature of the amide group enhances its reactivity towards 2-oxazoline rings and explains the increased branching rate occurring in the polymerization of 2,5-FDCAox with SeA. For this reason, the increased rate of branching observed in the polymerizations involving 2,5-FDCAox is attributed to the presence of the furan(di)carboxamide groups rather than to a difference in reactivity of the 2-oxazoline groups in 2,5-FDCAox and IAox.

6.3.5. *On-line* monitoring of the branching reaction.

In the previous section it was demonstrated that 2-oxazoline rings have an increased reactivity towards furan(di)carboxamide moieties. As observed, this branching reaction proceeds in the absence of triphenyl phosphite (TPP), resulting in the formation of a cross-linked product after already 25 minutes of polymerization of 2,5-FDCAox and SeA in an equimolar ratio at 160 °C. Although this branching reaction is highly interesting for the development of renewable 2,5-FDCAox based thermosets, chemical analysis of the formed cross-linked products is challenging due to their insoluble nature. For this reason, polymerization reactions of 2,5-FDCAox with SeA were monitored *on-line* using ATR-FTIR spectroscopy, to obtain more insight into the effect of the reaction temperature and the triphenylphosphite (TPP) concentration on the rate of branching and on the total curing time.

The left hand side of Figure 6.4 shows the characteristic FTIR spectra between 1800 and 800 cm^{-1} , obtained during a polymerization of 2,5-FDCAox with SeA (ratio = 2.25 : 1) at 200 °C in the absence of TPP (Figure 6.4a) and containing 5 wt% TPP (Figure 6.4b). The changes in intensity of different vibrations, normalized on the intensity of the aliphatic CH_2 stretch vibration at 2932 cm^{-1} , are shown on the right hand sides of Figures 6.4a and 6.4b. It should be noted that the excess of 2,5-FDCAox, used in these polymerization reactions, was chosen to promote the cross-linking of the system and to obtain a densely cross-linked material at full conversion.

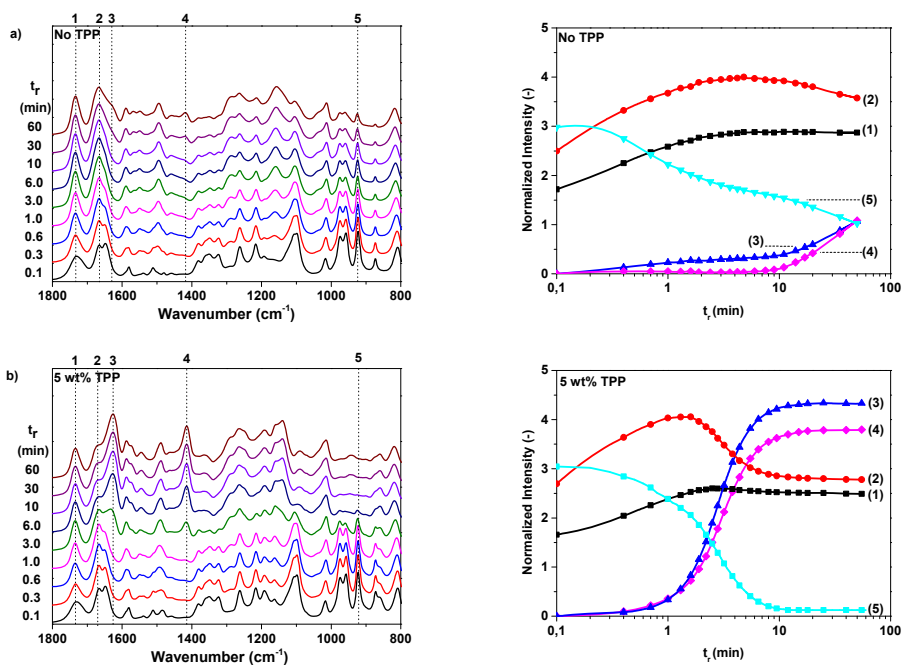


Figure 6.4. Characteristic FTIR spectra between 1800 and 800 cm⁻¹ obtained during the polymerization of 2,5-FDCAox with SeA (ratio = 2.25 : 1) at 200 °C containing (a) no TPP and (b) 5 wt% TPP. The right two figures show the changes in intensity of the ester carbonyl stretch vibration at 1734 cm⁻¹ (1, —■—), the secondary amide carbonyl stretch vibration at 1667 cm⁻¹ (2, —●—), and the tertiary amide carbonyl stretch vibration at 1625 cm⁻¹ (3, —▲—). Furthermore, band 4 at 1417 cm⁻¹ (—◆—) and band 5 at 922 cm⁻¹ (—▼—) are attributed to the bend vibrations of the CH₂ groups adjacent to the tertiary amide group and the ring vibrations of the 2-oxazoline ring, respectively. *N.b.* the intensity of the vibration bands are normalized against the intensity of the CH₂ stretch vibration at 2932 cm⁻¹. The rapid decrease in intensity of the bands corresponding to the 2-oxazoline groups and the simultaneous rise of the intensity of the signals originating from the secondary and tertiary amide groups confirm that the 2-oxazoline groups react with both acid groups and secondary amide groups.

From the FTIR spectra shown in Figure 6.4a, it can be seen that the bands corresponding to the carbonyl stretch vibration of the carboxylic acid group at 1734 cm⁻¹ (band 1), the C=N stretch vibration of the oxazoline ring at 1637 cm⁻¹, and the vibration of the oxazoline ring at 922 cm⁻¹ (band 5) are present at the start of the reaction. The intensity of the carbonyl stretch vibration increases slightly during the first eight minutes of the reaction, indicating that the groups are converted into ester bonds. Furthermore, a simultaneous decrease in intensity of the C=N stretch vibration band at 1637 cm⁻¹ occurs in the first eight minutes together with an increase in intensity of the secondary amide carbonyl stretch vibration at 1667 cm⁻¹ (band 2). The rise of band 2 with the simultaneous decrease in 2-oxazoline C=N stretch

vibration band confirms that the reaction between the 2-oxazoline groups with carboxylic acid groups results in the formation of secondary amide groups.

After 8 minutes of reaction time, no changes are detected in the intensity of band **1**, indicating that all carboxylic acid groups are successfully converted into ester groups. However, band **2** and band **5** decrease slowly over time together with the C=N stretch vibration at 1637 cm^{-1} , indicating that the 2-oxazoline concentration is decreasing. As expected, the band of the carbonyl stretch vibration of the tertiary amide at 1625 cm^{-1} (band **3**) and the band of the bend vibrations of the CH_2 groups adjacent to the tertiary amide groups at 1417 cm^{-1} (band **4**) rise simultaneously with the decrease in intensity of vibration bands **2**, **5**, and the band at 1637 cm^{-1} . The simultaneous rise of bands **3** and **4** and the decrease in band **1** indicate that the concentration of tertiary amides is increasing and thus, branching and cross-linking is taking place in the system. Since vibration **5** is still present after 60 minutes of reaction time, it can be concluded that a full conversion of the 2-oxazoline moieties was not obtained. For this reason, it is expected that the cross-linking will continue with the extension of the reaction time. Nonetheless, from the FTIR data shown in Figure 6.4a it can be concluded that no catalyst is required to enable the formation of branched and cross-linked structures during polymerization of 2,5-FDCAox and SeA.

As can be seen in differential equation (6.1), the concentration of secondary amide groups is only dependent on the reaction of the 2-oxazoline rings with carboxylic acid groups. During the branching reaction, a 2-oxazoline ring reacts with a secondary amide forming a new secondary amide together with a tertiary amide. This implies that the concentration of secondary amides should remain constant after the full conversion of the carboxylic acid groups. However, as can be seen in Figure 6.4, the intensity of band **2** slowly decreases over time even after the carboxylic acid groups have reacted into ester groups. It is likely that this change in intensity is a result of the decrease of the C=N vibration band at 1637 cm^{-1} which partially overlaps with the C=O stretch vibration of the secondary amide, band **2**.

Similar changes in intensity for band **1** to **5** are observed for the TPP catalyzed system shown in Figure 6.4b. However, the decrease of the intensity of band **5** and the rise of band **3** and **4** is significantly faster than in the non-catalyzed system. Furthermore, the intensities of bands **3** and **4** are much higher after 60 minutes of reaction in the presence of TPP, indicating that the concentration of tertiary amides is higher in the TPP catalyzed system than in the non-catalyzed system. This clearly indicates that TPP increases the k_2 branching reaction constant. No changes in FTIR spectra are observed after 10 minutes of reaction time, indicating that the reaction is close to full conversion. This high conversion of the 2-oxazoline groups is confirmed by the low intensity of band **5** after 60 minutes of reaction time. Overall, from the data shown in Figure 6.4, it can be concluded that TPP can be successfully used to enhance the

branching and cross-linking reaction of 2,5-FDCA further and to reduce the reaction or curing times.

Cross polarization total sideband suppression (CP/TOSS) ^{13}C NMR spectroscopy was performed on the product, obtained after polymerization of 2,5-FDCAox with SeA for 60 minutes at 200 °C in the presence of 5 wt% TPP, to confirm that polymerization had successfully taken place. The CP/TOSS spectra of the reaction mixture before and after polymerization are shown in Figure 6.5a and 6.5b, respectively. It is observed that resonance O_a (69.2 ppm), corresponding to the methylene carbon next the oxygen atom in the unreacted 2-oxazoline ring, has decreased significantly after one hour of reaction. This confirms that the 2-oxazoline concentration has significantly decreased after one hour of polymerization and that almost full conversion is obtained. Furthermore, the presence of resonances C_a (ester carbonyl carbon, 173.5 ppm), F_a (the furan C-H carbon, 120.7 ppm), O_c (methylene carbon next to the secondary amide group, 38.5 ppm), and O_d (methylene carbon next to the ester group, 65.0 ppm) indicate that the ring-opening addition reaction between the 2-oxazoline rings and the carboxylic acid groups has successfully taken place. The presence of the tertiary amides formed during the branching reaction can be detected by the presence of resonances O_e (methylene carbon next to the tertiary amide group, 46.9 ppm) and F_e (furan carbon of a furan ring connected to a tertiary amide group, 115.9 ppm).

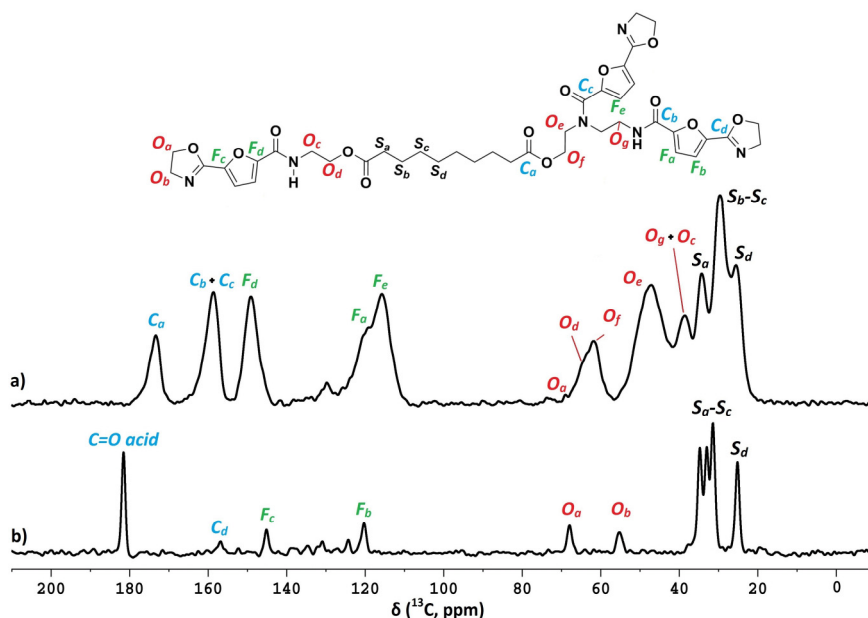


Figure 6.5. CP/TOSS ^{13}C NMR spectra obtained a) after and b) before polymerization of 2,5-FDCAox with SeA (ratio = 2.25 : 1) containing 5 wt% TPP for one hour at 200 °C.

As can be seen in Figure 6.5, the area of the resonance O_e (46.9 ppm) is larger than the resonances O_d (65.0 ppm) + O_f (62.1 ppm) and O_g + O_e (38.5 ppm), indicating that the concentration of tertiary amides is larger than that of the secondary amides. Although the CP/TOSS spectra do not allow for quantitative analysis of the signals, such an excess of tertiary amides groups is expected for polymerizations using a large excess of 2,5-FDCAox. According to differential equations (6.1) to (6.3), polymerization will continue until all 2-oxazoline groups have reacted, indicating that, at full conversion, all oxazoline groups have reacted into secondary or tertiary amide groups. Therefore, the concentration of tertiary amides at full conversion should be equal to the excess of 2-oxazoline groups added at the start of the reaction, since the maximum concentration of amide groups is equal to the starting concentration of carboxylic acid groups.

Overall, based on the CP/TOSS NMR data shown in Figure 6.5, it can be concluded that both the expected secondary and tertiary amides are present in the system, thus, polymerization in the presence of TPP yields the expected cross-linked product.

6.3.6. Influence of temperature and TPP on the branching reaction

To obtain more insight in the effect of the reaction temperature and the catalyst loading on the branching reaction, polymerizations of 2,5-FDCAox with SeA (ratio = 2.25 : 1) were monitored *on-line* using FTIR spectroscopy. Experiments were performed at different reaction temperatures and at different TPP loadings. The observed change in intensity of the vibration band at 1417 cm^{-1} , indicative for the concentration of branches, during polymerizations at different temperatures is shown in Figure 6.6a (no TPP) and Figure 6.6b (5wt% TPP).

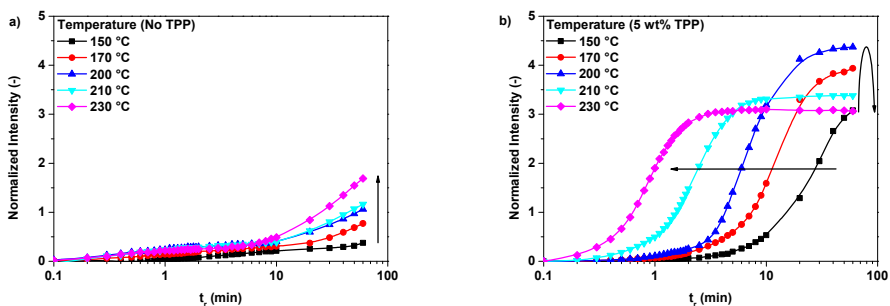


Figure 6.6. Changes in intensity of the vibration band at 1417 cm^{-1} during the polymerization of 2,5-FDCAox with SeA (ratio = 2.25 : 1) at different reaction temperatures containing a) no TPP and b) 5wt% TPP. *N.B.* The intensity of the vibration band at 1417 cm^{-1} is normalized against the intensity of the CH_2 stretch vibration at 2932 cm^{-1} .

From the data in Figure 6.6a it can be seen that the intensity of the vibration band at 1417 cm^{-1} increases faster with increasing reaction temperature, indicating that the

branching reaction is accelerated by an increase of the reaction temperature. However, it is clear from the low intensity of the vibration band at 1417 cm^{-1} that the reaction does not reach full conversion within one hour of reaction time. For this reason it is concluded that, although the increase of the reaction temperature promotes the formation of branches, full conversion is only obtained after polymerization for several hours (over 6 hours at $200\text{ }^{\circ}\text{C}$). It should be noted that sublimation of 2,5-FDCAox was observed in polymerizations performed above $200\text{ }^{\circ}\text{C}$, making the performance of experiments at temperatures above $200\text{ }^{\circ}\text{C}$ troublesome due to the continuous change in stoichiometry during the ongoing reaction.

Similarly, the rate of branch formation increases with increasing reaction temperature in systems containing TPP, as is shown in Figure 6.6b. As expected, the rate of branching is significantly higher in systems catalyzed by TPP; full conversion is reached within 5 minutes of reaction time, as is observed for the TPP catalyzed polymerizations performed at $230\text{ }^{\circ}\text{C}$. The maximum intensity of the normalized absorbance signal of the vibration band at 1417 cm^{-1} decreases for polymerizations performed above $200\text{ }^{\circ}\text{C}$. This decrease is attributed to the slow sublimation of 2,5-FDCAox occurring at these temperatures, effectively decreasing the maximum number of cross-links at full conversion. For this reason, further polymerizations of 2,5-FDCAox are conducted at $200\text{ }^{\circ}\text{C}$ or lower.

To investigate the effect of the TPP concentration on the branching reaction, experiments were performed at $200\text{ }^{\circ}\text{C}$ (2,5-FDCAox to Sea ratio of 2.25 to 1) with various TPP loadings (Figure 6.7a). Similar to the increase of the reaction temperature, the increase of the TPP concentration accelerates the formation of branches. To obtain information regarding the effect of TPP on the reaction constants k_1 and k_2 , differential equations (6.1) - (6.3) were fitted to the data shown in Figure 6.7a using a non-linear regression and the results are depicted in Figure 6.7b.

It should be noted that no information was available on the final concentrations of the reactive groups after 60 minutes of polymerization, making it impossible to convert the normalized intensity signal, obtained from FTIR, to bulk concentration values required for accurate data fitting. For this reason, reaction constants k_1 and k_2 were calculated using different conversion factors. The conversion factor is defined as the normalized intensity signal divided by the bulk concentration, assuming that correlation between the intensity observed in FTIR spectroscopy and the bulk concentration is linear. Detailed information on the data fitting process is supplied in Appendix B. In this manuscript, a conversion factor of 0.95 is used to convert the normalized intensity to the bulk concentration. This conversion factor was chosen since the concentrations, obtained after conversion of the normalized intensity, correspond to the theoretical bulk concentrations expected after reaching full

conversion. A detailed description and justification for the conversion factor determination procedure is supplied in Appendix B.

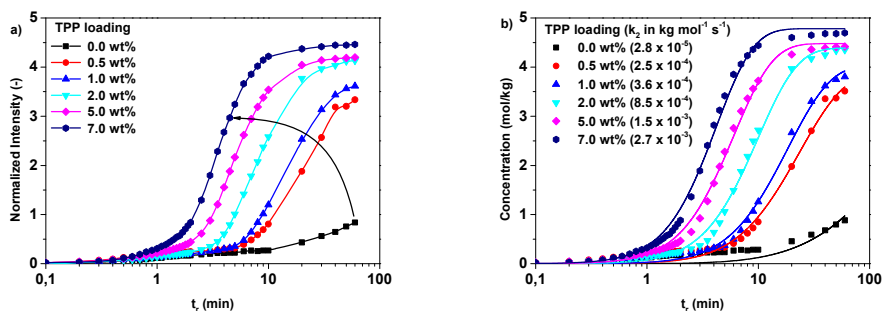


Figure 6.7. Changes in normalized intensity of the vibration band at 1417 cm^{-1} during the polymerization of 2,5-FDCAox with SeA (ratio = 2.25 : 1) at different TPP loadings performed at $200\text{ }^{\circ}\text{C}$ (Figure 6.7a). The fit, obtained after non-linear regression of the data shown in Figure 6.7a, is shown in Figure 6.7b (conversion factor = 0.95). A detailed description of the data fitting process is supplied in Appendix B.

Figure 6.8 shows the k_1 and k_2 values, obtained after fitting of the data using a conversion factor of 0.95. The effect of the addition of TPP on the k_1 and k_2 reaction constants was similar, independent of the selected conversion factor; the addition of TPP increases the k_2 reaction constant, whereas it does not seem to influence the k_1 reaction constant to a great extent. This observation is in good agreement with the statement of Sano, who concluded that TPP catalyzes the branching of IAox, whereas the k_1 reaction constant increased only with a factor 1.3 in the presence of 1 wt% TPP.¹³

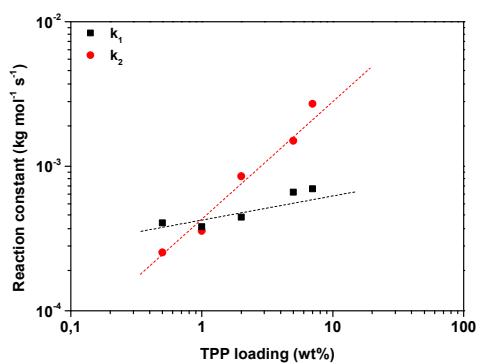


Figure 6.8. Changes in the observed reaction constants k_1 and k_2 found after fitting of the FTIR data (conversion factor = 0.95), obtained during polymerizations of 2,5-FDCAox with SeA (ratio = 2.25 : 1) at $200\text{ }^{\circ}\text{C}$ with varying TPP loadings. *N.b.* The dotted lines are added to guide the eye.

6.3.7. Thermal properties of the cured thermosets.

In the previous section, it was demonstrated that the addition of TPP can be used to selectively accelerate the branching reaction occurring in the polymerization of 2,5-FDCAox with SeA. Furthermore, the addition of this catalyst decreases the reaction and curing time, facilitating the synthesis of renewable polymer glasses and coatings within reasonable reaction times. In order to investigate the thermal properties of the polymer synthesized via this route, DMTA analysis was performed on cured glasses and the glass transition temperatures were determined from the peak in the $\tan(\delta)$ trace. Figure 6.9 shows the characteristic behavior of systems of a) IAox : SeA (2.25 : 1) and b) 2,5-FDCAox : SeA (2.25 : 1) containing 5 wt% TPP. The samples were cured for 10 minutes in an oven preheated to 200 °C prior to the DMTA analysis to prevent breaking of the samples above T_g during the DMTA experiment.

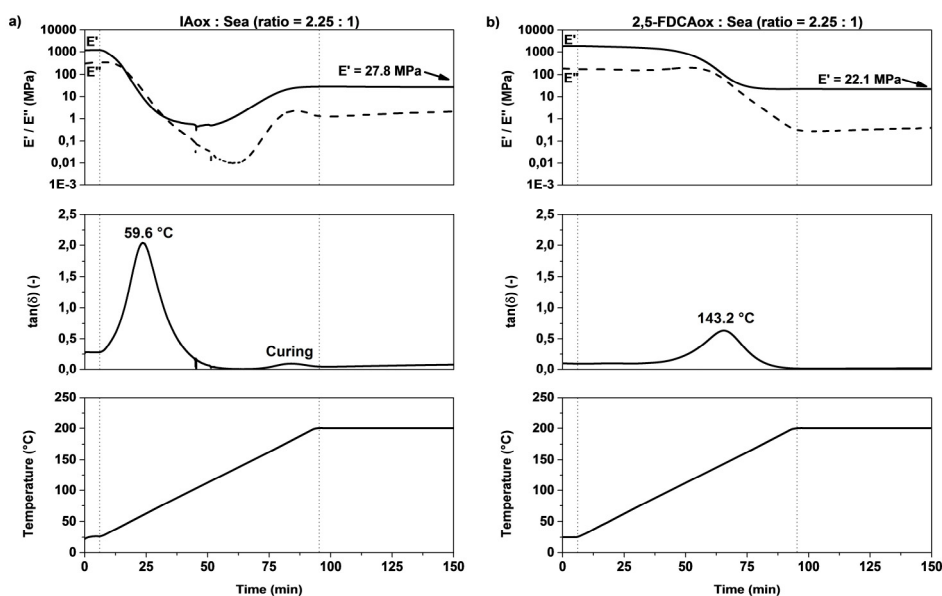


Figure 6.9. Variation of the temperature, $\tan(\delta)$, E' , and E'' during a heating (2 °C / min) and isothermal curing (200 °C, 60 min) as observed in the DMTA analysis in TPP (5 wt%) catalyzed systems of a) IAox : SeA (ratio = 2.25 : 1) and b) 2,5-FDCAox : SeA (ratio = 2.25 : 1). *N.b.* both systems were heated until a clear casting liquid was obtained, which was poured on a Teflon film and cured at 200 °C for 10 minutes prior to DMTA analysis.

From the data shown in Figure 6.9, it can be clearly seen that the IAox based polymer, formed after 10 minutes of curing, is slightly cross-linked, as is indicated by the low storage modulus (E') of 0.53 MPa above the T_g (59.6 °C). Such a low storage modulus above T_g corresponds to a high molecular weight between entanglements and indicates that the system is not densely cross-linked. As expected, the curing process continues after heating to 120 °C and higher, as is indicated by the gradual increase of

both the storage and loss moduli as these temperatures. No changes in storage and loss modulus are observed after 30 minutes of curing (thus after 90 minutes of the DMTA experiment), indicating that the cross-linking reaction is complete.

The DMTA analysis of the polymer, obtained after heating, casting and curing the 2,5-FDCAox and SeA mixture (ratio = 2.25 : 1) for 10 minutes in the presence of 5 wt% TPP, shows a T_g at 143.2 °C and a plateau modulus (E') of 22.01 MPa. This increased glass transition temperature, compared to the glass transition temperature of the IAox based polymer, indicates that the 2,5-FDCAox based polymer is more densely cross-linked after 10 minutes of reaction time. Furthermore, no significant increase of the plateau modulus is observed upon further heating to temperatures above the T_g followed by curing under isothermal conditions for 60 minutes at 200 °C.

For both systems, obtained after 60 minutes curing at 200 °C, a second heating run was performed at 2 °C/min to determine the T_g of the fully cross-linked polymers. The T_g of the IAox based polymer (155.1 °C) was comparable with the T_g of the 2,5-FDCAox based polymer (156.3 °C), indicating that the fully cross-linked materials have comparable glass transition temperatures. Although the thermal properties of the fully cured systems are comparable, the DMTA experiments indicate that the cross-linking in the 2,5-FDCAox polymerization with SeA in the presence of TPP proceeds significantly faster than for the IAox based system. It should be noted that, although the exact mechanism of the TPP catalysis is unknown, the application of 2,5-FDCAox in polymerization in the presence of TPP drastically reduces the curing times compared to similar polymerizations containing IAox as bis(2-oxazoline) monomer.

DMTA experiments were performed on polymers with varying 2,5-FDCAox to SeA ratios to determine if there is a correlation between the concentration of tertiary amide groups and the glass transition temperature. The polymers were cured for 60 minutes at 200 °C prior to the DMTA analysis to ensure that the samples were fully cross-linked. Furthermore, FTIR analysis was performed on different spots of the samples, obtained after DMTA analysis, and the normalized intensity of the vibration band at 1417 cm^{-1} was calculated following the FTIR analysis procedure. Figure 6.10 shows the normalized intensity signal, obtained from FTIR, plotted against the glass transition temperatures found via DMTA analysis for the different polymer glasses.

It can be seen that the normalized intensity varied slightly over the surface of the cured samples, indicating that the thermosets are probably not homogeneously cured. Nonetheless, it is clearly demonstrated that the normalized intensities, obtained from FTIR analysis, increase linearly with the increasing T_g of the polymers. These data suggest that the increase in glass transition temperature is directly correlated to the increase in the bulk concentration of tertiary amides and thus to the concentration of branches and cross-links.

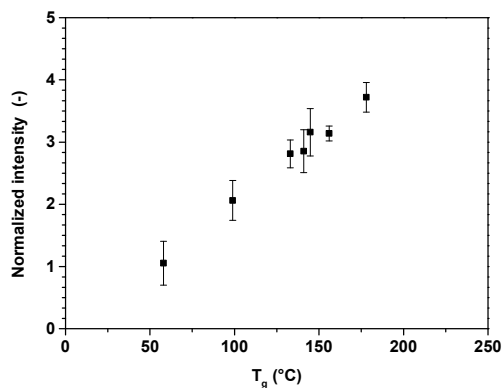


Figure 6.10. T_g values (°C) calculated from the maximum in the $\tan(\delta)$ trace, obtained from a DMTA heating run performed at 2 °C/min, versus the normalized intensity of the vibration band at 1417 cm^{-1} observed in FTIR analysis of cured systems having varying 2,5-FDCA to SeA ratio's.

6.3.8. Preliminary coating performance of solvent-borne coatings.

Solvent-borne coatings were prepared using NMP as a solvent and were cured at 200 °C, as is described in the coating procedure in the experimental section. The coatings had a thickness of approximately 35 μm . No changes were observed in the coatings after acetone double rub tests, in which the coatings are rubbed back and forth 100 times with a cloth drenched in acetone. The acetone resistance of the coatings confirms the cross-linked nature of these materials. Furthermore, the coatings were soft, as became evident from the pencil hardness test (2H). This indicates that the materials were not densely cross-linked, which was confirmed through FTIR analysis; the coatings showed an average normalized intensity of 1.6 (the vibration at 1417 cm^{-1}) corresponding to a T_g around 80 °C, as follows from the data shown in Figure 6.10. This indicates that the solvent-borne coatings show a lower cross-link density than the free standing films prepared from bulk, which showed a T_g close to 150 °C.

Although the coatings were not densely cross-linked, they exhibit ductile deformation and showed no crazing or cracking when subjected to rapid deformation during reverse impact testing. These preliminary coating results indicate that these 2,5-FDCA based poly(ester amide)s are good candidates for application in both thermally cured and solvent-borne polymer glasses and coatings.

6.4. Conclusions

In this work, the synthesis of a 2,5-furandicarboxylic acid (2,5-FDCA) based bis(2-oxazoline) monomer and its polymerization with sebacic acid (SeA) is reported. 2,5-bis(4,5-dihydrooxazol-2-yl)furan (2,5-FDCAox) was successfully isolated after

reaction of 2,5-FDCA with thionyl chloride, followed by reaction with chloroethylamine hydrochloride, and ring closure in methanol. It is demonstrated that the branching reaction occurs more rapidly in the polymerization of equimolar mixtures of 2,5-FDCAox with SeA than in the polymerizations of equimolar mixtures of 1,3-bis(4,5-dihydrooxazol-2-yl)benzene (IAox) with SeA. This enhanced rate of cross-linking in the 2,5-FDCAox based system is attributed to the increased nucleophilicity of the 2,5-furandicarboxamide resulting from intra-molecular hydrogen bonding, causing an enhanced reactivity towards 2-oxazoline rings. FTIR analysis has successfully been employed to monitor this branching reaction *on-line* and to determine the effect of the reaction temperature and the triphenyl phosphite (TPP) concentration on the polymerization. It is shown that TPP can be successfully used to accelerate the branching reaction and to reduce the curing times of the cross-linked poly(ester amide)s synthesized in this study. Furthermore, it is demonstrated that, also in the presence of TPP, the branching reaction proceeds significantly faster in 2,5-FDCAox based systems than in IAox based systems. Although the reaction and curing times vary when using different bis(2-oxazoline) monomers, the glass transition temperatures of the fully cured materials are comparable. Furthermore, preliminary coating studies indicate that these fully renewable 2,5-furandicarboxylic acid based cross-linked poly(ester amide)s are interesting candidates for application in coatings or polymer glasses. Overall, it can be concluded that the decreased curing times and the thermal properties make the 2,5-FDCA based bis(2-oxazoline) monomers interesting candidates for the preparation of fully renewable cross-linked poly(ester amide)s.

6.5. References

- [1] Wenker, H., *J. Am. Chem. Soc.*, **1938**, 60, 2152-2153
- [2] Fry, E.M., *J. Org. Chem.*, **1950**, 15, 802-806
- [3] Goldberg, A.A., Kelly, W., *J. Chem. Soc.*, **1948**, 1919-1926
- [4] Culbertson, B.M., *Prog. Polym. Sci.*, **2002**, 27, 579-626
- [5] Du Prez, F.E., Goethals, E.J. and Hoogenboom, R., Cationic Polymerizations, in Handbook of Polymer Synthesis, Characterization, and Processing (eds E. Saldívar-Guerra and E. Vivaldo-Lima), **2013**, John Wiley & Sons, Inc., Hoboken, NJ, USA. doi: 10.1002/9781118480793.ch8
- [6] Lustoň, J., Kronek, J., Böhme, F., *J. Polym. Sci. Part A: Polym. Chem.*, **2006**, 44, 343-355
- [7] Lustoň, J., Kronek, J., Markus, O., Janigová, I., Böhme, F., *Polym. Advan. Technol.*, **2007**, 18, 165-172
- [8] Aoi, K., Okada, M., *Prog. Polym. Sci.*, **1996**, 21, 151-208
- [9] Baier, A., Böhme, F., Vogel, R., Martin, H., Leistner, D., *Die Angewandte Makromolekulare Chemie*, **1995**, 228, 117-129
- [10] Taylan, E., Küsefoğlu, S.H., *J. Appl. Polym. Sci.*, **2012**, 124, 3229-3235
- [11] Inata, H., Matsumura, S., *J. Appl. Polym. Sci.*, **1987**, 33, 3069-3079
- [12] Lustoň, J., Böhme, F., Komber, H., Pompe, G., *J. Appl. Polym. Sci.*, **1999**, 72, 1047-1053
- [13] Sano, Y., Arita, K., Masuda, I, US patent 4,474,942, **1984** to Takeda Chemical Industries Ltd.
- [14] Sano, Y., *J. Polym. Sci. Part A: Polym. Chem.*, **1989**, 27, 2749-2760

- [15] Néry, L., Lefebvre, H., Fradet, A., *Macromol. Chem. Phys.*, **2003**, 204, 1775-1764
- [16] Gandini, A., Belgacem, M.N., *Prog. Polym. Sci.*, **1997**, 22, 1203-1379
- [17] Moore, J.A., Kelly, J.E., *Polymer*, **1979**, 20, 627-628
- [18] Moore, J.A., Kelly, J.E., *J. Polym. Sci.: Polym. Chem. Ed.*, **1978**, 16, 2407-2409
- [19] Moore, J.A., Kelly, J.E., *Macromolecules*, **1978**, 11, 568-573
- [20] Gubbels, E.; Drijfhout, P.J., Posthuma-van Tent, C.; Jasinska-Walc, L., Noordover, B.A.J., Koning, C.E., *Progress in Organic Coatings*, **2014**, 77, 277-284
- [21] Gandini, A., Silvestre, A.J.D., Neto, C.P., Sousa, A.F., Gomes, M., *J. Polym. Sci. Part A: Polym. Chem.*, **2009**, 47, 295-298
- [22] Gomes, M., Gandini, A., Silvestre, A.J.D., Reis, B., *J. Polym. Sci. Part A: Polym. Chem.*, **2011**, 49, 3759-3768
- [23] Burgess, S.K., Leisen, J.K., Kraftschik, B.E., Mubarak, C.R., Kriegel, R.M., Koros, W.J., *Macromolecules*, **2014**, 47, 1383-1391
- [24] Hopff, H., Krieger, A., *Makromol. Chem.*, **1961**, 47, 93-113
- [25] Heertjes, P.M., Kok, G.J., *Delft Progress Reports, Series A*, **1974**, 1, 59-63
- [26] Grosshardt, O., Fehrenbacher, U., Kowollik, K., Tubke, B., Dingenouts, N., Wilhelm, M., *Chemie Ingenieur Technik*, **2009**, 81, 11, 1829-1835
- [27] Mitiakoudis, A., Gandini, A., *Macromolecules*, **1991**, 24, 830, 835
- [28] Yeh, I-C., Rinderspacher, B.C., Andzelm, J.W., Cureton, L.T., La Scala, J., *Polymer*, **2014**, 55, 166-174
- [29] Li, W.J., Qiu, S.X., *J. Heterocyclic Chem.*, **2010**, 47, 1340-1343
- [30] Lustoň, J., Kronek, J., Kleinova, A., Janigová, I., Valentová, H., Nedbal, J., *J. Polym. Sci. Part A: Polym. Chem.*, **2012**, 50, 19, 3936-3943
- [31] Wilsens, C.H.R.M., Deshmukh, Y.S., Noordover, B.A.J., Rastogi, S., *Macromolecules*, **2014**, 47, 6196-6206.

Chapter 7

Epilogue

7.1. Conclusions, outlook, and technology assessment

The scope of this project was to explore and evaluate the application of renewable aromatic monomers such as 2,5-furandicarboxylic acid (2,5-FDCA) in polymers with properties suitable for demanding applications. As explained in the introductory chapter, examples of the targeted properties involve high glass transition temperatures for a good performance at elevated temperatures, thermotropic melt behavior for the preparation of highly anisotropic products, and high crystallinity in combination with high melting temperatures for a good dimensional stability at elevated temperatures. Beside these properties targeted for the polymers developed in this study, the focus of this thesis was to develop these polymers *via* melt polymerization reactions. The application of melt polymerization reactions is preferred to avoid the requirement of expensive (toxic) solvents during processing and thereby reduce potential processing and production costs. This chapter highlights the most important findings, obtained within the framework of this project, and evaluates their industrial relevance. Furthermore, recommendations are provided for future research or for improvement of the findings reported in this thesis.

7.1.1. Application of 2,5-FDCA in melt-polycondensation reactions

In general, it can be stated that the copolymerization of 2,5-FDCA in thermotropic polyesters can be employed to control polymer properties. For example, a control over the glass transition temperature and the melting temperature of fully aromatic thermotropic polyesters can be obtained through a variation in the 2,5-FDCA and vanillic acid content in the polymer backbone. Following this approach, rigid renewable thermotropic polyesters with melting temperatures ranging from 240 °C to 360 °C can be synthesized. The synthesis of these polymers can be performed in existing polymerization vessels, used for the industrial production of high melting thermotropic polyesters, since the polymerization procedures are identical. The potential of these polymer compositions and properties was recognized by the industrial partners involved in this project, and a patent application has been filed on these renewable aromatic thermotropic polymers.

However, a reoccurring challenge observed during melt polymerization reactions of 2,5-FDCA is its degradation during polymerization. As was demonstrated in chapters 2 and 3 of this thesis, 2,5-FDCA can only be incorporated into a polymer backbone when polymerization reactions are performed at 230 °C or lower. Processing of 2,5-FDCA at higher temperatures inevitably results in severe discoloration of the polymer melt and decarboxylation of the carboxylic acid groups. Besides, the 2-furancarboxylic

acid, formed upon decarboxylation of 2,5-FDCA, will function as a chain-stopper in polycondensation reactions and limit the molecular weight build-up. For this reason, it is not advisable to use 2,5-FDCA as a monomer in any synthesis reaction performed at temperatures above 230 °C.

As is demonstrated in chapter 3 of this thesis, 2,5-FDCA can be incorporated into the backbone of thermotropic polyesters when conducting the polymerization reaction at or below 230 °C. It was observed that the introduction of 2,5-FDCA into the polymer backbone improves the rigidity of the polymer chain at elevated temperatures. This improved rigidity can potentially be employed to design renewable polymers having high glass transition temperatures and good dimensional stability at elevated temperatures. The synthesis of the 2,5-FDCA based aliphatic-aromatic thermotropic polyesters reported in chapter 3 has been taken up into a separate patent application.

Although the properties of the 2,5-FDCA based thermotropic polyesters described in chapters 3 are highly interesting, the large scale synthesis might prove challenging. Beside the limitations originating from the thermal instability of 2,5-FDCA, it was observed that the time required to build-up molecular weight in systems containing 2,5-FDCA was unrealistically long. To illustrate, it takes over 24 hours of reaction time to synthesize a 2,5-FDCA based aliphatic-aromatic thermotropic polyester in a molecular weight around 10,000 g/mol on a 50 gram scale. It should be realized that the less effective acetic acid removal in up-scaled systems would elongate the reaction times further, making the batch-wise production of such polymers too tedious and expensive for industrial purposes.

In short, the application of 2,5-FDCA in the melt-synthesis of thermotropic polyesters is highly interesting from an academic viewpoint, but the application of such polymers for industrial purposes is discouraged.

7.1.2. Development of renewable thermotropic polyesters

In this thesis, we have tried to design renewable thermotropic polyesters using renewable aromatic monomers. However, as is concluded from the previous section, the used monomers should be stable at temperatures well above the employed reaction temperatures. In contrast to 2,5-FDCA, vanillic acid shows an excellent thermal stability and is easily incorporated into the polymer backbone. The random distribution of the methoxy group in the vanillic acid moiety along the polymer chain limits crystallization of polymer chains. Moreover, the copolymerization of vanillic acid was shown to promote the random distribution of the monomers along the polymer backbone, limiting crystallization further. As a result, thermotropic polymers containing vanillic acid showed low crystallinities, good solubility and stable nematic melts above their melting temperatures.

The synthesis and performance of the aliphatic-aromatic vanillic acid based thermotropic polyesters has been investigated in chapters 3 and 4 of this thesis. As is

shown in these chapters, vanillic acid based aliphatic-aromatic thermotropic polyesters could be synthesized in good molecular weights (>40 kg/mol) on a 200 gram scale synthesis within reasonable reaction times. As was stated earlier, the synthesis and processing conditions of these polymers are identical to the industrially synthesized thermotropic polyesters such as the Vectra series. Therefore, these materials can be prepared using the current industrial infrastructure. Furthermore, the excellent processability of these materials from their thermotropic melts and the promising properties of the processed fibers indicate the potential industrial relevance of these materials. To recall, fibers spun from polymers containing 10 mole% vanillic acid showed tensile moduli in the range of 10 GPa and tensile strengths in the order of 150 - 200 MPa. It is realized that the spinning equipment used (e.g. spin hole diameter and die inflow geometry) and spinning conditions applied, were rather basic and far from optimal. Therefore improvement in properties under improved processing is to be expected. But first another issue requires attention:

As is reported in chapter 4, it was observed that only the aromatic components present in these aliphatic-aromatic thermotropic polyesters are molecularly oriented during the fiber spinning process. In contrast, the aliphatic moieties exhibit a high mobility, normally corresponding to a local isotropic motion. This indicates that the orientation of these aliphatic segments during the melt drawing process is challenging and possibly explains the relatively low stiffness of the fibers. For this reason, it is expected that the performance of these vanillic acid based thermotropic polyesters can be improved significantly by decreasing or fully eliminating the aliphatic content.

It may be clear that the development of renewable thermotropic polyesters for demanding applications is feasible when employing thermally stable and rigid monomers such as vanillic acid. For this reason, it is recommended that further research is conducted on the development of such polymers and the application of other renewable aromatic or rigid monomers should be explored. Examples of monomers that could prove useful for this purpose are lignin based monomers described in the introductory chapter or the protected 2,5-FDCA based monomers described in chapters 5 and 6.

7.1.3. Polymerization of protected 2,5-FDCA monomers

As was evaluated in chapters 5 and 6, the application of monomers containing the 2,5-furandicarboxamide moiety yields polymers with highly unexpected properties. For example, the presence of this moiety in the polymer backbone results in the formation of intra-molecular hydrogen bonds. These hydrogen bonds can limit crystallization in poly(ester amide)s, yielding poorly crystalline or amorphous polymers. Although this clearly limits the application of such polymers as engineering plastics, it allows for the development of rigid transparent materials with high glass transition temperatures. Possible applications of such materials lie in the field of coatings, composites, or

adhesives. However, it should be noted that such amide based amorphous polymers are likely to absorb water, limiting their application in humid environments. As is demonstrated in chapter 6 of this thesis, the intra-molecular hydrogen bonding of the 2,5-furandicarboxamide moiety catalyzes the branching reaction of this amide group with 2-oxazoline rings. As a result, polymerization of 2,5-FDCA based bis(2-oxazoline) monomers with bio-based carboxylic acids yields fully renewable cross-linked polymers. These polymers can be applied as coatings or as free standing films with high glass transition temperatures and good thermal stability.

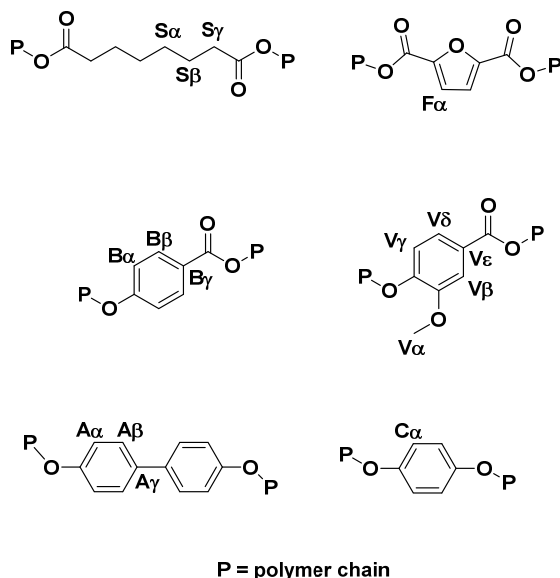
In general, the preparation of renewable coatings *via* 2-oxazoline polyaddition reactions is an interesting topic for future research. As is demonstrated for the 2,5-FDCA monomer, the presence of the oxygen heteroatom significantly increases the reaction rate during polymerization, allowing for the preparation of renewable coatings with shortened curing times. It is anticipated that 2,5-FDCA is not the only renewable monomer that exhibits such an enhanced reactivity, since many renewable monomers contain oxygen or nitrogen heteroatoms which can possibly facilitate similar intra-molecular hydrogen bonds. Furthermore, the polymerization of these bis(2-oxazoline) monomers already proceeds at 150 °C, which allows the application of monomers with a poor thermal stability. For these reasons, it is expected that the development of renewable cross-linked polymers *via* the bis(2-oxazoline) polyaddition reactions can yield new and interesting materials and should be pursued.

Lastly, if the development of 2,5-FDCA based thermotropic polymers via melt-polymerization reactions should be desired, it is recommended that the application of macromonomers containing the 2,5-furandicarboxamide moiety is considered. The protection of the carboxylic acid groups of 2,5-FDCA through reaction with amines yields macromonomers with a significantly increased thermal stability. These stable monomers might be suitable for application in fully aromatic thermotropic poly(ester amide)s that require synthesis temperatures close to 300 °C or higher. The improved thermal stability, increased solubility and decreased crystallinity of the macromonomers containing the 2,5-FDCA moiety might allow for the development of new high molecular weight thermotropic polymers for high performance applications, otherwise unattainable through the direct polymerization of 2,5-FDCA.

Appendix A for chapter 3

Variable temperature solid-state $^{13}\text{C}\{^1\text{H}\}$ CP/MAS and INEPT MAS NMR

Temperature-dependent solid-state $^{13}\text{C}\{^1\text{H}\}$ Inensitive Nuclei Enhanced by Polarization Transfer (INEPT) Magic-Angle spinning (MAS) and Variable-temperature (VT) solid-state $^{13}\text{C}\{^1\text{H}\}$ Cross-Polarization/MAS (CP/MAS) NMR measurements have been performed to follow the molecular changes during heating of polymers 3a, 4c, 4d, and 5b described in chapter 3. Scheme A1 shows the structural formulas of the monomer residues present in these polymers and the labels of the corresponding carbon atoms. Figure A1 shows the overlay of the $^{13}\text{C}\{^1\text{H}\}$ CP/MAS and $^{13}\text{C}\{^1\text{H}\}$ INEPT MAS NMR measurements performed as a function of temperature for polymer 3a in the region between 140 and 0 ppm. Below the glass transition temperature of the polymer ($<35\text{ }^\circ\text{C}$), broad peaks are observed in the $^{13}\text{C}\{^1\text{H}\}$ CP/MAS NMR spectrum (Figure A1a) with moderate intensity, indicating that the polymer chains reside in a rigid amorphous or crystalline phase. Upon heating to temperatures above T_g , the ^{13}C resonances assigned to \mathbf{S}_α , \mathbf{S}_β , \mathbf{S}_γ , \mathbf{B}_α , \mathbf{B}_β , and \mathbf{C}_α become sharper and the signal intensities increase due to more favorable CP conditions. Interestingly, no significant change of the carbons close to the carbonyls (\mathbf{B}_γ) is observed. This suggests that the motion of the aromatic moieties is restricted to the rotation of the phenyl rings (not shown). Heating of the polymer above the onset of melting leads to a further sharpening of the peaks, while \mathbf{B}_γ decreases in intensity ($>150\text{ }^\circ\text{C}$) as can be seen in Figure A1a. The increased intensity of the ^{13}C signals in the molten phase can be explained by the high mobility of the phenyl rings and aliphatic carbons in the oriented nematic phase. The effective T_2 relaxation time of these carbons and protons increases upon melting and signals start to rise in the $^{13}\text{C}\{^1\text{H}\}$ INEPT MAS NMR spectra shown in Figure A1b at $150\text{ }^\circ\text{C}$ and higher. Upon further heating the intensity of the $^{13}\text{C}\{^1\text{H}\}$ INEPT MAS NMR spectra increases, indicating that a larger fraction of the polymer resides in the mobile liquid crystalline phase.



Scheme A1. Labels of the carbon atoms in the structural formulas of monomer residues present in polymer 3a.

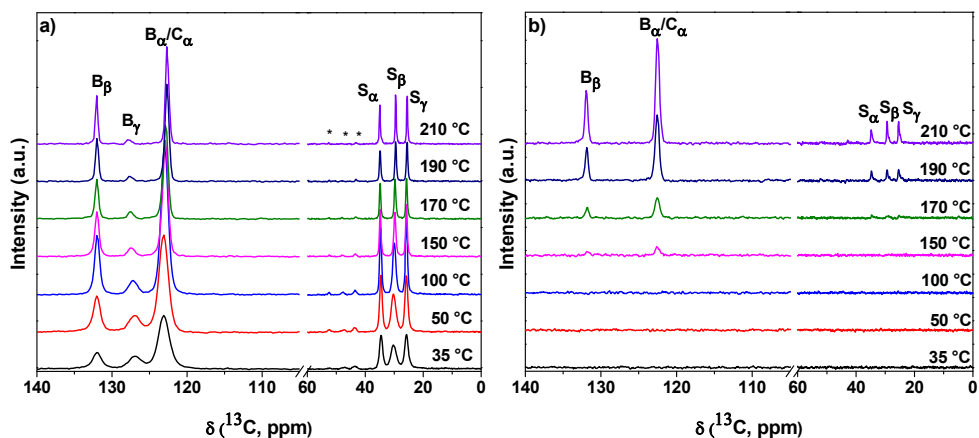


Figure A1. Temperature-dependent solid-state $^{13}\text{C}\{^1\text{H}\}$ CP/MAS NMR (a) and $^{13}\text{C}\{^1\text{H}\}$ INEPT MAS NMR (b) results obtained for sample 3a in the region between 140 and 0 ppm. Signals denoted with an * are spinning sidebands. All experiments were recorded at 11.75 T (500.13 MHz for ^1H) using a MAS frequency of 10.0 kHz and ^1H decoupling during acquisition.

Figure A2 shows the $^{13}\text{C}\{^1\text{H}\}$ CP/MAS and $^{13}\text{C}\{^1\text{H}\}$ INEPT MAS NMR spectra of polymer 4c, which shows the same signal sharpening above T_g (< 80 °C) as observed for polymer 3a (see Figure A1). An increase in the flexibility of the phenyl rings and aliphatic spacers is clearly visible above T_g in the $^{13}\text{C}\{^1\text{H}\}$ CP/MAS NMR spectra indicated by the sharpening and increase of the ^{13}C signals (Figure A2a). The onset of

melting is observed above 150 °C, which can be identified by the rise in resonance signals in the $^{13}\text{C}\{^1\text{H}\}$ INEPT MAS NMR spectra. Interestingly, the $^{13}\text{C}\{^1\text{H}\}$ CP/MAS NMR spectra obtained above 170 °C show the rise of a peak at 120.7 ppm, corresponding to the aromatic carbons (\mathbf{F}_α) of the 2,5-FDCA-moiety. The \mathbf{F}_α resonance is also visible in the $^{13}\text{C}\{^1\text{H}\}$ INEPT MAS NMR experiments above 190 °C, indicating a fraction of the 2,5-FDCA moieties becomes mobile at much higher temperatures compared to the other aromatic rings (Figure A2b). Moreover, we anticipate that the 2,5-FDCA moiety is unable to perform full rotations at temperatures below 190 °C due to the dipole moment that is induced upon rotation of the furan ring. For this reason it is expected that a higher thermal energy is required for the furan ring to rotate, compared to phenyl rings of HBA and HQ. Another possibility is that the mobile fraction observed at temperatures between 150 °C and 190 °C corresponds to the melting of crystals containing flexible chains. As observed by GPC and DSC analysis, polymer 4c is of a blocky nature and crystals with high melting temperatures are expected to contain higher amounts of aromatic 2,5-FDCA than flexible suberic acid. Melting of these crystals requires a higher temperature compared to the melting of crystals containing the more flexible suberic acid, thus requiring higher temperatures to for the \mathbf{F}_α signal to become visible.

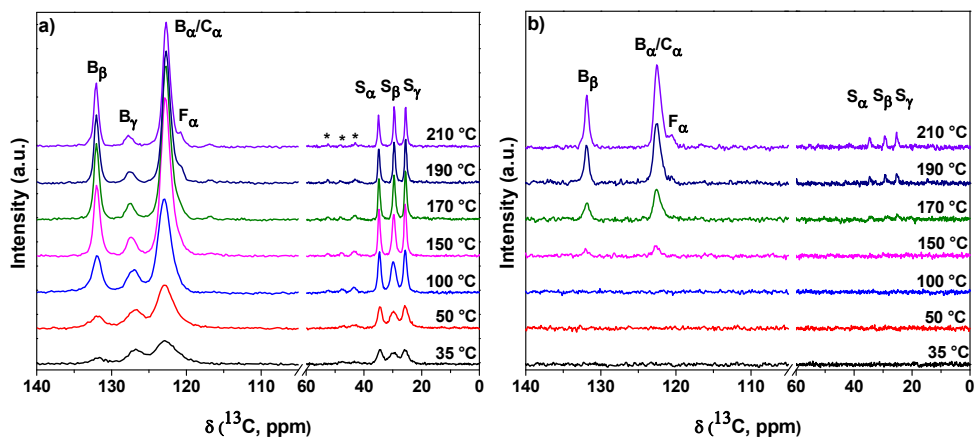


Figure A2. Temperature-dependent solid-state $^{13}\text{C}\{^1\text{H}\}$ CP/MAS NMR (a) and $^{13}\text{C}\{^1\text{H}\}$ INEPT MAS NMR (b) results obtained for sample 4c. Signals are assigned according to Scheme A1 while the asterisks denote spinning sidebands. All experiments were recorded at 11.75 T (500.13 MHz for ^1H) using a MAS frequency of 10.0 kHz and ^1H decoupling during acquisition.

Figure A3 shows the temperature-dependent solid-state $^{13}\text{C}\{^1\text{H}\}$ CP/MAS and $^{13}\text{C}\{^1\text{H}\}$ INEPT MAS NMR spectra for polymer 4d, containing 10 mole% vanillic acid. The rise of the ^{13}C signals at 57.1 ppm (\mathbf{V}_α), 116.1 ppm (\mathbf{V}_β) and 152.4 ppm (\mathbf{V}_γ)

indicate the presence of vanillic acid. Some peaks of the vanillic acid partially overlap with the peaks of HQ and HBA, e.g., the ^{13}C resonance at 127.0 ppm. It can further be seen that the intensity of the $^{13}\text{C}\{^1\text{H}\}$ CP/MAS NMR spectra decreases upon heating above the glass transition temperature (Figure A3a). This can be attributed to cold-crystallization of the sample, as also observed in DSC analysis. Flexibility of the phenyl rings and aliphatic spacers in this polymer occur already at 90 °C, which is close to the onset of melting. Interestingly, only the methoxy group of VA ($\mathbf{V}\alpha$) becomes mobile at 90 °C, while the phenyl ring of VA ($\mathbf{V}\beta$ and $\mathbf{V}\gamma$) becomes mobile at 110 °C and higher as is visible in both the $^{13}\text{C}\{^1\text{H}\}$ CP/MAS and $^{13}\text{C}\{^1\text{H}\}$ INEPT MAS NMR experiments in Figure A3a and A3b. In fact, it is expected that the presence of the methoxy group of VA hinders the rotational motion of the VA phenyl ring and restricts its motion. Interestingly, since the mobile methoxy group does not affect the mobility of its neighboring groups, it can be concluded that the T_m decreasing effect of vanillic is can only be attributed to the sterical hindrance of the methoxy group that inhibits crystallization.

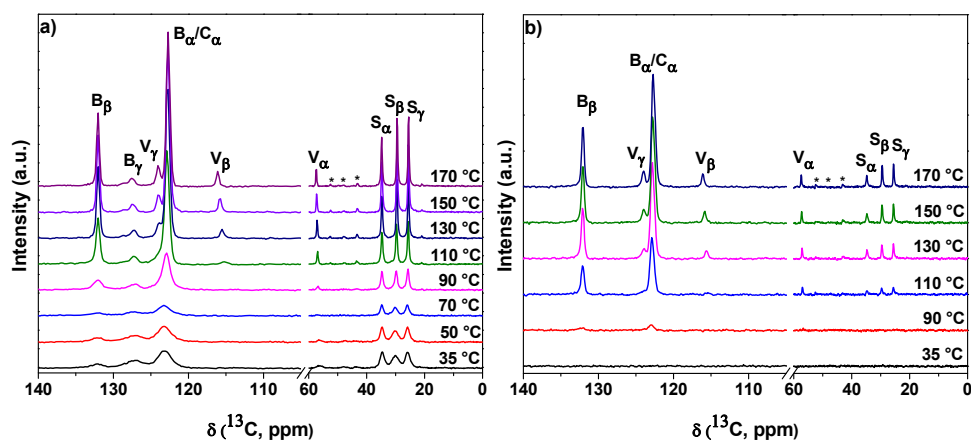


Figure A3. Temperature-dependent solid-state $^{13}\text{C}\{^1\text{H}\}$ CP/MAS NMR (a) and $^{13}\text{C}\{^1\text{H}\}$ INEPT MAS NMR (b) results obtained for sample 4d. Signals denoted with an asterisk are spinning sidebands, whereas the assignment follows that of Scheme S1. All experiments were recorded at 11.75 T (500.13 MHz for ^1H) using a MAS frequency of 10.0 kHz and ^1H decoupling during acquisition.

Appendix B for chapter 6

FTIR and NMR data fitting procedure

For the data fitting process described in the sections “Polymerization of 2,5-FDCAox and IAox with Sebacic acid” and “Influence of the reaction temperature and TPP loading on the branching reaction” in chapter 6, a Matlab script was used containing the differential equations (6.1) to (6.3) as described in the original manuscript. The starting bulk concentrations of the reactive groups at $t_r = 0$ min were calculated in mol/kg by taking the monomer ratio and molar masses of the 2,5-FDCAox and SeA into account. For the equimolar systems of 2,5-FDCAox and SeA and IAox and SeA, the starting concentrations of the reactive groups were 4.89 mol/kg and 4.78 mol/kg, respectively. For the 2,5-FDCAox and SeA polymerization in a ratio of 2.25 to 1, the used starting concentrations were 6.75 mol/kg (2,5-FDCAox) and 3.00 mol/kg (SeA). The concentration of the ester, amide and tertiary amide groups were set to 0 mol/kg at the start of the reaction. Next, the experimental data, either the oxazoline concentration or the tertiary amide concentration, was loaded into the program and fitted to the differential equations (6.1) to (6.3) through a non-linear regression.

In order to fit the FTIR data, the intensity of the vibration bands has to be converted to concentration in mol/kg. However, since the extent of the reaction is unknown after 60 minutes of reaction, no information on the exact concentration is available and thus the concentration of the reactive groups cannot be calculated. Therefore, in order to obtain a value for the bulk concentration, the authors have used a conversion factor to linearly convert the intensity to bulk concentrations. The conversion factor is defined as the normalized intensity signal divided by the bulk concentration, assuming that the correlation between the intensity observed in FTIR spectroscopy and the bulk concentration is linear.

It was observed that the signal corresponding to the vibration of the unreacted 2-oxazoline ring at 922 cm^{-1} was very small or not detectable in systems polymerized at $200\text{ }^\circ\text{C}$ in the presence of $>5\text{ wt}\%$ of TPP. This indicates that the polymerization was close to full conversion. For this reason, it was assumed that 100% conversion was reached in these systems, and the theoretical bulk concentration of tertiary amides (3.75 mol/kg) was used to calculate the conversion factor (yielding a value of 0.95). Nonetheless, to ensure that the FTIR data was interpreted correctly, other conversion factors were also taken into account. Figure B1 shows the calculated k_1 and k_2 reaction constants as a function of various conversion factors.

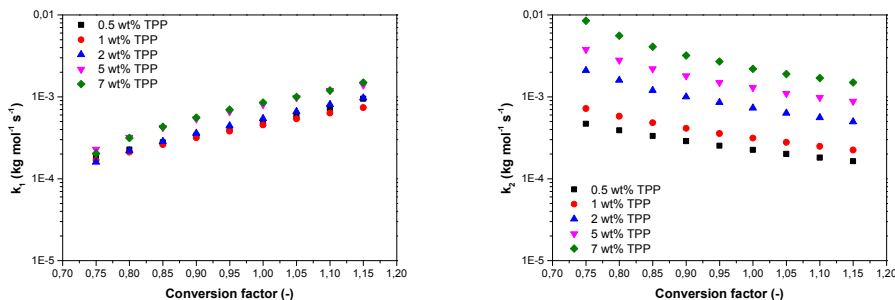


Figure B1. Effect of the conversion factor on the k_1 (left) and k_2 (right) reaction constants found after data fitting of polymerizations containing different TPP concentrations.

From the data in Figure B1 it can be seen that both the k_1 and k_2 reaction constants vary with one order of magnitude as a function of the conversion factor. Furthermore, from the data shown in Figure B1 it is clear that, independently of the selected conversion factor, the k_1 constant does not vary significantly as a function of TPP loading. In contrast, the k_2 reaction constant varies with at least one order of magnitude as a function of the TPP loading. As is shown in Figure B2, the k_2 reaction constant increases roughly at least with one order of magnitude when increasing the TPP loading from 0.5 wt% to 7 wt%, and increases even further with decreasing conversion factors. From this data it is concluded that TPP can be used to selectively enhance the branching reaction occurring between amide groups and 2-oxazoline rings.

The residuals after data fitting of the experimental data, using different conversion factors, were evaluated to determine the accuracy of the fit. The residuals of these fits can generally be used to evaluate the ability of the fit to describe the experimental data. To be more specific, a residual of 0.00 corresponds to a fit that describes the experimental data perfectly. Similarly, a high residual indicates that the found fit is poor and deviates drastically from the experimental data.

Figure B3 shows the residuals obtained after fitting the experimental data using different conversion factors. It can be seen that the residuals are lowest at conversion factors between 0.9 and 0.95, indicating that these conversion factors yield the most accurate fit. For this reason, and for the reasons described earlier, the authors use 0.95 as conversion factor for the data analysis described in chapter 6.

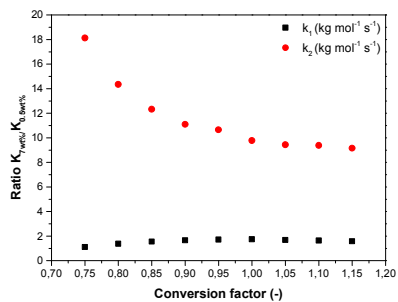


Figure B2. Ratio of the k_1 and k_2 reaction constants after increasing the TPP content from 0.5 wt% to 7 wt%, as a function of the conversion factor.

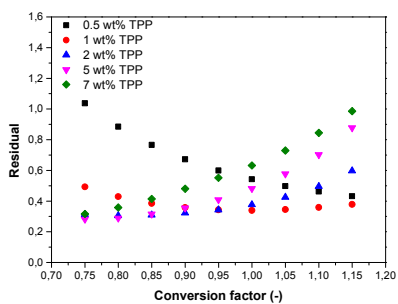


Figure B3. Residuals of the fit as a function of the conversion factor and the TPP concentration.

Glossary

Abbreviations and symbols

2,5-FDCA	2,5-furandicarboxylic acid
2,5-FDCAox	2,5-bis(4,5-dihydrooxazol-2-yl)furan
2,5-TDCA	2,5-thiophenedicarboxylic acid
ABA	<i>p</i> -acetoxybenzoic acid / 4-acetoxybenzoic acid
ATR	attenuated total reflection
AVA	4-acetoxy-3-methoxybenzoic acid
BA	<i>p</i> -hydroxybenzoic acid / 4-hydroxybenzoic acid
BP	4,4'-biphenol
CHCl ₃	chloroform
CP/MAS	cross-polarization/magic-angle spinning
CP/TOSS	cross-polarization/total suppression of spinning sidebands
CSA	chemical shift anisotropy
DABP	4,4'-diacetoxybiphenyl
DMAc	N,N-dimethylacetamide
DMF	N,N-dimethylformamide
DMSO	dimethylsulfoxide
DMTA	dynamic mechanical thermal analysis
DOE	Department of Energy
DSC	differential scanning calorimetry
E'	storage modulus (Pa)
E''	loss modulus (Pa)
ESI-ToF-MS	electron spray ionization time of flight mass spectrometry
FTIR	Fourier-transform infra-red
G'	elastic modulus (Pa)
G''	viscous modulus (Pa)
HFIP	1,1,1,3,3,3-hexafluoroisopropanol
HMBC	heteronuclear multiple bond correlation
HMF	5-hydroxymethylfurfural
HQ	hydroquinone / 1,4-dihydroxybenzene
IA	isophthalic acid
IAox	1,3-bis(4,5-dihydrooxazol-2-yl)benzene
INEPT	insensitive nuclei enhanced by polarization transfer
k _x	reaction constant of reaction x (kg mol ⁻¹ s ⁻¹)
LC	liquid crystalline
LiCl	lithium chloride
M _n	number average molecular weight (g/mol)
M _w	weight average molecular weight (g/mol)
NaHCO ₃	sodium bicarbonate

NMP	N-methyl-2-pyrrolidone
NMR	nuclear magnetic resonance
N_x	concentration of functional group x
p	extent of reaction
PBT	poly(butylene terephthalate)
PDI	polydispersity index (-)
PEF	poly(ethylene furanoate)
PET	poly(ethylene terephthalate)
POM	polarization optical microscopy
r	monomer ratio
SeA	sebacic acid
SEC	size-exclusion chromatography
SuA	suberic acid
SUPER	separation of undistorted powder patterns by effortless recoupling
TA	terephthalic acid
T_c	peak crystallization temperature (°C)
TEA	triethyl amine
TFP	thin-film polymerization
T_g	glass transition temperature (°C)
TGA	thermogravimetric analysis
THF	tetrahydrofuran
TLCP	thermotropic liquid crystalline polyester
T_m	melting temperature / peak melting temperature (°C)
TMS	tetramethylsilane
T_{ons}	onset degradation temperature (°C)
T_r	reaction temperature (°C)
t_r	reaction time (s / min / h)
TPP	triphenyl phosphite
VA	vanillic acid / 3-methoxy-4-hydroxybenzoic acid
WAXD	wide-angle x-ray diffraction
ω	angular frequency (rad/s)
\bar{X}_n	number average degree of polymerization
$Zn(CH_3CO_2)_2$	zinc acetate
ΔH_{melt}	melt enthalphy (J/g)

Summary

Exploring the application of 2,5-furandicarboxylic acid as a monomer in high performance polymers: Synthesis, characterization, and properties.

The application of renewable monomers for the synthesis of polymeric materials has gained significant attention over the last decades. Examples of driving factors promoting this research are the projected depletion of commonly used fossil oil feedstock, the gradual increase of the oil prices, and the increasing pollution and green-house gas emissions resulting from the increase in consumption of fossil based materials. In short, the development of renewable materials may prove beneficial from an economic and an environmental viewpoint. However, for these renewable materials to be industrially viable, one important demand is that their performance should be comparable or, preferably, superior to their fossil fuel based counterparts. This study therefore focuses on the development of renewable materials with high performance properties and aims to demonstrate the unique features of these materials. Examples of the targeted high performance properties are the presence of a thermotropic melt for the production of high modulus and high strength fibers, or a good temperature resistance for applications in coatings. In order to achieve the previously mentioned properties, this thesis focuses on the application of the rigid aromatic monomer 2,5-furandicarboxylic acid (2,5-FDCA). The aromatic nature of this monomer is expected to contribute to the development of rigid polymer chains that have high glass transition temperatures and exhibit a thermotropic melt.

The feasibility to incorporate 2,5-FDCA in fully aromatic thermotropic polyesters *via* a melt polycondensation is investigated in chapter 2. A thin-film polymerization route is adopted to screen and monitor the polymerization process and track the morphological changes occurring during the reaction. During these screening studies it was observed that 2,5-FDCA shows a limited thermal stability, since rapid decarboxylation and discoloration occurs when the monomer is processed above 230 °C. Furthermore, 2,5-FDCA exhibits a poor solubility in the monomer/oligomer melt, requiring reaction temperatures well above its degradation temperature to promote polymerization. Using the screening method, it is demonstrated that the melting temperature of these aromatic thermotropic polyesters can be decreased through the copolymerization of vanillic acid. The presence of vanillic acid in the polymer backbone perturbs the crystalline structure of the resulting copolyesters and yields polymers with melting temperatures well below 300 °C. The decreased melting temperatures allow for melt synthesis at lower reaction temperatures, which limits the

thermal degradation of 2,5-FDCA during polymerization. However, although it is demonstrated that the polymerization can successfully be performed on a small scale (<100 mg), the partial degradation of 2,5-FDCA could not be fully avoided during reactions performed on a larger scale.

In chapter 3, a route is developed to successfully synthesize thermotropic polyesters on up to a 200 gram scale, through the copolymerization of the aliphatic suberic acid monomer. This aliphatic monomer acts as flexible a spacer between the rigid aromatic segments resulting in a drastic decrease of the melting temperature, while maintaining the thermotropic behavior of the polymer melt. These decreased melting temperatures allow for the polymerization at temperatures at which no degradation of 2,5-FDCA occurs, yielding 2,5-FDCA based thermotropic polyesters having number-average molecular weights well above 10,000 g/mol. Interestingly, both the renewable 2,5-FDCA and vanillic acid moieties require more energy to become mobile in the melt as observed through temperature-dependent solid-state NMR spectroscopy. These results indicate that these renewable monomers can be used to design materials that have superior high temperature chain rigidity compared to their fossil fuel based counterparts.

In chapter 4, the processing and mechanical performance of the developed thermotropic polyesters is evaluated. The properties of polymers with varying molecular weights are evaluated after compression molding, extrusion followed by melt-drawing, and solvent casting. It is demonstrated that these materials are easily processed from the melt, but do not exhibit the tensile modulus and tensile strength required for demanding applications, for example in ropes, sails, or protective clothing. Instead, a tensile modulus of approximately 10 GPa and a tensile stress between 150 to 200 MPa is observed for these materials. Wide-angle x-ray diffraction, solid-state NMR spectroscopy and FTIR analysis have been employed to demonstrate that, although a high orientation parameter is observed, only the aromatic components are molecularly oriented. In contrast, the aliphatic components are not subjected to strongly restricted molecular orientation upon processing. For this reason, it is anticipated that the tensile performance of these renewable thermotropic polyesters can be enhanced by decreasing or eliminating the aliphatic content.

As concluded from chapters 3 and 4, the application of 2,5-FDCA in melt-polymerizations is hampered by its limited thermal stability and therefore requires the copolymerization of aliphatic components. Therefore, the application of thermally stable aromatic 2,5-furandicarboxamide based macromonomers in polymerizations is investigated in chapter 5. In this chapter, it is demonstrated that the 2,5-furandicarboxamide moiety is capable of undergoing both inter and intra molecular

hydrogen bonding. As a result, crystallization of polymers containing this moiety is drastically suppressed, often resulting in an amorphous behavior of the polymers. Interestingly, these polymers can be successfully synthesized during a melt polycondensation reaction, whereas polymers containing the terephthalamide, 2,5-thiophenedicarboxamide, or isophthalamide counterparts are semi-crystalline and cannot be synthesized in the absence of solvents.

In chapter 6, the rigid amorphous nature of polymers containing the 2,5-furandicarboxamide moiety is employed to synthesize high T_g polymer glasses using oxazoline ring-opening addition chemistry. It is demonstrated that the developed polymer glasses or coatings exhibit glass transition temperatures of up to 175 °C, depending on the cross-link density. Furthermore, although the performance of the 2,5-FDCA based coatings is comparable to the performance of the commercially available isophthalic acid based coatings, it is observed that curing times are significantly reduced in the 2,5-FDCA based systems. The excellent thermal stability and the enhanced curing kinetics of these 2,5-furandicarboxamide based compounds make them an interesting choice as monomers in melt polymerization reactions and for application in coatings, films or composites.

Overall, from the data reported in this thesis, it is concluded that 2,5-FDCA is a viable monomer for application in high performance polymers. However, the direct application of 2,5-FDCA in melt polycondensation reactions is not attractive due to its limited thermal stability. As a result, 2,5-FDCA can only be incorporated in the targeted performance polyesters at relatively low reaction temperatures. In contrast, initial investigations of amide-protected 2,5-FDCA macro-monomers show promise for application in polymerizations. For this reason, it is suggested to continue to investigate the application of these 2,5-furandicarboxamide based monomers in thermotropic polyesters, coatings, and composites. Overall, it is concluded that the application of this renewable aromatic monomer has potential and, if used correctly, yields polymers with unique properties.

Curriculum Vitae

Carolus (Karel) Wilsens was born on 5th of August 1987 in Tilburg, The Netherlands. After finishing pre-university secondary educations (VWO) in 2005 at the Theresialyceum in Tilburg, he studied Chemical Engineering at Eindhoven University of Technology. In 2011 he graduated under supervision of prof. dr. Cor Koning, dr. Andreas Heise, and dr. ir. Gijs Habraken in the field of N-carboxyanhydride ring opening polymerization in the Polymer Chemistry group (SPC). In Februari 2011 he started a PhD project under the supervision of prof. dr. Sanjay Rastogi, prof. dr. ir. Han Meijer and dr. Bart Noorderover at the Eindhoven University of Technology. This PhD project was initiated by Teijin Aramid and became part of the research program of the Dutch Polymer Institute in 2012 (DPI, #739, BIOLcp). The main results of his PhD research are presented in this dissertation. Since November 2014, he is employed at Maastricht University.

List of publications

Publications:

- "Processing and performance of aromatic-aliphatic thermotropic polyesters based on vanillic acid." C.H.R.M. Wilsens, Y.S. Deshmukh, Y. Yao, B.A.J. Noorderover, S. Rastogi, H. Meijer, *Polymer*, submitted.
- "Synthesis, kinetics, and characterization of bio-based thermosets obtained through polymerization of a 2,5-furandicarboxylic acid-based bis(2-oxazolone) with sebacic acid." C.H.R.M. Wilsens, E. Gubbels, N.J.M. Wullems, Y. Yao, B.A.J. Noorderover, S. Rastogi, *Polymer Chemistry*, submitted.
- "Self-Assembling Process of Macromolecules having Oxalamide Groups and their Nucleation Efficiency in Poly (hydroxyalkanoates)." Y.S. Deshmukh, P. Ma, C.H.R.M. Wilsens, M.R. Hansen, R. Graf, S. Rastogi, *ACS Macro Letters*, submitted.
- "Influence of Methylene Segment Length on Crystal Packing, Chain Dynamics, and Thermal Properties of Poly(amide-aramid)s." Y.S. Deshmukh, C.H.R.M. Wilsens, R. Verhoef, M.R. Hansen, D. Dudenko, R. Graf, E. Klop, S. Rastogi, *Macromolecules*, under revision.
- "Effect of the 2,5-furandicarboxamide moiety on hydrogen bonding in aliphatic-aromatic poly(ester-amides)." C.H.R.M. Wilsens, Y.S. Deshmukh, Y. Yao, B.A.J. Noorderover, S. Rastogi, *Macromolecules*, **2014**, 47, 6196–6206.
- "Thermotropic polyesters from 2,5-furandicarboxylic acid and vanillic acid: Synthesis, thermal properties, melt-behavior, and mechanical performance." C.H.R.M. Wilsens; J.M.G.A. Verhoeven; B.A.J. Noorderover; M.R.Hansen; D. Auhl; S. Rastogi, *Macromolecules*, **2014**, 47, 3306-3316.
- "Aromatic thermotropic polyesters based on 2,5-furandicarboxylic acid and vanillic acid." C.H.R.M. Wilsens; B.A.J. Noorderover; S. Rastogi, *Polymer*, **2014**, 55, 2432-2439
- "Optimization of N-carboxyanhydride (NCA) polymerization by variation of reaction temperature and pressure." G.J.M. Habraken; C.H.R.M. Wilsens; C.E. Koning; A. Heise., *Polymer Chemistry*, **2011**, 2(6), 1322-1330.

Patent applications:

- "(2-oxazolonyl)-furan based polyamides" Wilsens, C.H.R.M., Wullems, N.J.M., Gubbels, E., Noorderover, B.A.J., Rastogi, S., Filed, November **2014** (CUN3017)
- "Thermotropic polymers based on 2,5-furandicarboxylic acid." Wilsens, C.H.R.M., Noorderover, B.A.J., Rastogi, S., Filed November **2013**

- *“Nucleating agents for polyesters and polyolefins.”*
Rastogi, S., Deshmukh, Y.S., Auhl, D., Bernaerts, K.M., Wilsens, C.H.R.M., Harings, J.,
Filed August **2013**
- *“Liquid crystalline furandicarboxylic acid-based aromatic polyesters.”*
Wilsens C.H.R.M., Noordover, B.A.J., Veld. M., Klop E.A., Rastogi, S.,
WO2013092667, **2013**
- *“Oxalamide-based nucleating agents for biopolymers and method for crystallization of biopolymers.”*
Deshmukh, Y.S., Ma. P., Wilsens C.H.R.M., Rastogi, S.,
WO2013120793, **2013**
- *“Nucleating agents for polypropylene and polypropylene copolymers.”*
Ma. P. Deshmukh, Y.S., Wilsens, C.H.R.M., Rastogi, S.,
WO201356565, **2013**

Awards and prizes:

- *DPI invention award* – DPI annual meeting, November 2014
- *Lecture award for the best chemistry workshop* - Dutch Polymer Days 2014, March 2014
- *Second poster award* – DPI annual meeting, November 2013

Acknowledgements

Four years of hard work, summarized in this thesis. A thesis of which I am proud and four years for which I am grateful. Proud for seeing the results of many collaborations materialize into publications and patents. Grateful for the possibility to work with all the colleagues and friends I have met and made over the years. I would like to dedicate these last pages to express my gratitude to everyone who contributed to this thesis.

Firstly, I would like to thank Sanjay Rastogi, Han Meijer, and Bart Noordover for the guidance and the help they gave me over the years. Sanjay, thank you for giving me the possibility to work with you. I have thoroughly enjoyed all the discussions, conferences, lunches, coffees, car travels, and laughs we had. I have learned a lot from you, both on a professional and a personal level. Thank you. Han, although you were only involved in the last part of my project, I highly appreciate your input and time dedicated to improving this thesis. Every time we had a meeting, you ensured that I learned something new. Bart, thank you for being my daily supervisor. Your patience, discussions and feedback were of great value for me! I hope we are able to continue to work together in the future!

I would like to thank the members of my defense committee, Rint Sijbesma, Jan van Hest, Dave Haddleton, and Martin Möller, for taking the time to read and evaluate my thesis. Your feedback and your critical reviews have definitely improved the quality of this thesis.

Special thanks to all my colleagues from SKT, SPC, and SPM. I have had a great time and would like to thank you all. However, I owe a special thanks to certain colleagues and friends; Mark, Benny, Erik, Martin, Pim, Marco, Julien, Geert, Judith, Nino, and Lily. I enjoyed all the collaborations, discussions, fun, beer, coffee, squash, fitness, and dinners we had together (delete where not applicable)! You made my time here at the TU/e both educational and fun! Further thanks to Gijs, Inge, Bahar, Rafiq, Piming, Tamara, Maria, Timo, Jan, Marjolijn, Pleunie, Caroline, Anne, Pauline, Peter, Bob, Han, Yanwu, Mohammad, and Yingyuan, for all the help during my stay. Furthermore, I would like to thank Peter Albers and Michiel de Beer for the refreshing coffee breaks, work related discussions and the (more frequent) non-work related discussions.

Besides working solely at the TU/e, I had the pleasure to perform part of my work with the Maastricht Science Programme. Fred Offerein and Yvonne van der Meer, thank you for giving me the opportunity to collaborate with this new group! Dietmar Auhl, Jules Harings, Katrien Bernaerts, and Stefaan de Wildeman, thank you for all the discussions we had and the insights you gave me during these discussions. Yogesh,

I would like to thank you in particular. We have been collaborating already for many years, but your experience and knowledge still amazes me. I hope that your significant contribution to this thesis may be clear from the ongoing list of publications we have written over the years. Thank you for being my colleague and friend!

Special thanks to the Dutch Polymer Institute for financial support and the members from the Bio-Inspired cluster for all discussions and other contributions. Special thanks to Daan van Es, Jacco van Haveren, Rutger Knoop, Shanmugam Thiyagarajan, Willem Vogelzang, Carmen Boeriu, Vincent van der Vlist, Gerrit Eggink, and Peter Nossin, for their input, discussions, and presentations during the TA-BIO review meetings and “umbrella” meetings.

Similarly, I would like to thank the people from Teijin Aramid, who were involved with the start and initial financing of this project. Jan Roos, Johan Boelee, Bert Gebben, Enno Klop, Ulrike Jacobi, Martijn Veld, Rene Verhoef, Annika Tikkel, Aart Klinkhamer, and Evert Meijrink, thank you for the discussions, measurements, and help with my project!

I would like to thank Michael Ryan Hansen, Robert Graf, and Yefen Yao for your help regarding the solid-state NMR measurements performed during our collaborations. We would not have progressed this much without your help!

Although I have had a great deal of help on a professional level, I owe thanks to all my friends and family who have supported me on a personal level during my PhD; Michiel, Ele, JJ, Wenya, Marieke, Daan, Jeroen (2x), Peter, Steef, Simone, Mark, Laura, Tim, and Maryam. Thank you for all the good times! Pap, Mam, Saskia, Jeroen, Imara, en Jori, bedankt voor alle steun! Jullie rotsvaste vertrouwen, goede zorgen (+lekkere eten!), open discussies en huiselijke warmte waren precies wat nodig was om energie bij te tanken na een week werken. Flynt, vandaag de dag is het als volwassene moeilijk te verantwoorden waarom je in het weekend speelt met lego, maar met jou in de buurt heb ik een goed excuus! Ton, Tineke, Marc, en Rick, mijn dank gaat ook naar jullie uit; jullie hebben me altijd thuis laten voelen, al vanaf de eerste keer dat ik over de vloer kwam! Als laatste wil ik Marly bedanken. Ik heb helaas de ruimte niet om mijn dank uit te schrijven in dit boekje, maar weet dat deze thesis hier niet had gelegen als ik jou niet had. Bedankt voor alles!